



UNIVERSITY OF
LEICESTER

ROLE OF C-PEPTIDE IN THE VASCULATURE

**Thesis submitted for the degree of Doctor of Philosophy
at the University of Leicester**

By

Zahraa Jawad Al-isawi

**Department of Cardiovascular Sciences (Renal Group)
College of Life Sciences**

January 2019

ROLE OF C-PEPTIDE IN THE VASCULATURE

Zahraa J. Al-isawi

Abstract

Subjects with diabetes are at high risk of developing long-term complications, including cardiovascular diseases. Recent data suggest that diabetes maybe a dual hormone deficiency disease in which secretion of both insulin and C-peptide is insufficient. Insulin is supplemented as part of treatment regimes, while altered C-peptide levels remain untreated. Herein, the potential beneficial effect of C-peptide replacement on vascular system health was investigated. Using cultured human endothelial cells (EAhy926), incubation with 5nM C-peptide resulted in an upregulation of protein expression of endothelial nitric oxide synthase, suggesting a direct regulatory effect for C-peptide on normal endothelial cell function. This was associated with stimulatory effects of key intracellular signalling pathway MAP kinase (ERK1/2). This ERK1/2 activation in EA.hy926 cells was not associated with cell growth or increased protein content.

In apoptotic endothelial cells, C-peptide exerted a moderate stimulatory effect on microparticle generation as a measure of endothelial cell function. This effect was restored close to normal level by treating the cells with pertussis toxin suggesting that C-peptide acted through a G-protein coupled receptor. C-peptide-derived miroparticles analysed by flow cytometry demonstrated CD31 and CD105 expression as well as superficial phosphatidylserine. Further confirmation of the vesicle morphology and size range was performed using electron microscopy and nanoparticle tracking analysis. Preliminary investigation of potential biological significance of these MPs did not reveal obvious effects on endothelial apoptosis level as assessed by Caspase-3 cleavage, or their inflammatory status as evaluated by the expression of intercellular adhesion molecule 1 and E-selectin adhesion molecules, and Interleukin-8 secretion. However, proteomic analysis of C-peptide-mediated MPs highlighted the possibility of selective packaging of biomolecules within these vesicles.

The proposed protective effect of C-peptide on the vascular system was also investigated *in vivo*. Administration of C-peptide subcutaneously in type 1 diabetic rats attenuated von willebrand factor overexpression in aortic intima of these animals. Furthermore, C-peptide treatment retarded collagen deposition in the vascular wall suggesting an important role for C-peptide in extracellular matrix remodelling. Therefore, in contrast to the older views that portrayed C-peptide as an inert molecule with no bioactivity, the data presented in this study support an active role for C-peptide in the vasculature.

Keywords: diabetes, C-peptide, endothelial dysfunction, microparticles

Acknowledgments

‘All praises and gratitude to the Almighty’

Firstly, I would like to express my sincere gratitude to my supervisor **Prof Nigel Brunskill**; I would like to thank you for giving me encouragement and support during my PhD journey, and for allowing me to grow my confidence as an independent researcher. I also owe a huge debt of gratitude to my supervisor **Dr Alan Bevington** who, without his guidance and encouragement, my thesis might never have seen the light of day.

Very special thanks are due to **Dr Ravinder Chana** for his constant support and encouragement – Ravi, I will always remember how you would give me those hopeful words every morning: “It’s a lovely day!” I am thankful to **Dr Nima Abbasian** for providing advice and technical support.

I would also like to thank my PRP members, **Prof Jonathan Barratt** and **Dr Peter Topham** for their insightful feedback and constructive criticism.

It is a pleasure to acknowledge with sincere thanks **Dr Kees Straatman** for helping with image analysis – Dr Kees, you are one of the best people I have met in Leicester. Thanks to **Natalie Allcock** for assisting with TEM, **Dr David Moore** and **Prof Kevin West** for assessing the histological sections.

Particular thanks go to **Prof Andrea Copper** and **Dr John Pearl** for providing unlimited access to their flow cytometry facility – thank you, John, for inviting me to the Flowjo session! I am also grateful to **Prof Martha Clokie** for allowing me to access her NanoSight equipment.

I would like to thank **Dr Dylan Burger** for his invaluable suggestions for MP analysis. I am also thankful to **Dr Philippe Poncelet** for his helpful instructions in flow cytometry analysis.

My humble thanks to the **Ministry of Higher Education and Scientific Research in Iraq** for sponsoring and financially supporting me throughout my PhD study. Thanks to all the people I have met in the Medical Science Building at the University of Leicester for their kindness and support.

My final and most sincere thanks go to my husband Dr Jamal for his patience, immense love and support. I greatly appreciate how much he has helped me and made completing this project possible. Nevertheless, I cannot forget my lovely sons, Ammar, Layth and Yasir for making everything worthwhile.

Dedication

This thesis is dedicated to my late father, whose passion for both science and medicine served as a great inspiration.

<i>Title Page</i>	
<i>Abstract</i>	<i>(ii)</i>
<i>Acknowledgements</i>	<i>(iii)</i>
<i>Dedication</i>	<i>(iv)</i>
<i>Table of Contents</i>	<i>(v)</i>
<i>List of Tables</i>	<i>(xii)</i>
<i>List of Figures</i>	<i>(xiii)</i>
<i>List of Abbreviations</i>	<i>(xvi)</i>

Table of Contents

Chapter 1. General introduction	1
1.1 Diabetes mellitus	1
1.1.1 History and epidemiology	1
1.1.2 Diagnosis of DM.....	2
1.1.3 Classification of DM	3
1.1.3.1 Type 1 DM.....	5
1.1.3.2 Type 2 DM.....	5
1.1.4 Diabetic complications	6
1.2 The vascular system	9
1.2.1 Normal endothelium	11
1.2.2 Regulatory functions of the vascular endothelium.....	13
1.2.3 Endothelial cell activation versus dysfunction	16
1.2.4 Hyperglycaemia and vascular dysfunction	17
1.2.4.1 Bioavailability of nitric oxide.....	19
1.2.4.2 Adhesion molecule expression	19
1.2.4.3 Aberrant angiogenesis.....	19
1.2.4.4 Non-enzymatic glycation	20
1.2.4.5 Matrix protein production.....	21
1.2.5 Hyperphosphataemia and endothelial dysfunction.....	21
1.2.5.1 Phosphate	21
1.2.5.2 Hyperphosphataemia and cardiovascular risk	22
1.2.5.3 Diabetic kidney disease	23

1.2.5.4 Mechanism of phosphate-induced endothelial dysfunction.....	24
1.2.6 Assessment of endothelial function.....	25
1.2.7 Treatment of endothelial dysfunction in DM.....	28
1.3 Role of MPs in the vasculature.....	28
1.3.1 Extracellular vesicles: definition.....	28
1.3.2 Microparticles: formation and fate.....	31
1.3.3 Role of MPs in cell-cell communication.....	33
1.3.4 Clinical significance of MPs.....	34
1.3.5 Role of MPs in diabetes and its complications.....	35
1.3.6 Methods of MP analysis.....	36
1.3.6.1 Isolation of MPs.....	37
1.3.6.2 Quantification and characterisation of MPs.....	37
1.4 C-peptide.....	41
1.4.1 Background.....	41
1.4.2 Structure and body pharmacokinetics.....	42
1.4.3 Evidence for C-peptide interaction with the cell membrane.....	45
1.4.4 Intracellular signalling by C-peptide.....	46
1.4.4.1 Effects on Na ⁺ , K ⁺ -ATPase.....	46
1.4.4.2 Effect of C-peptide on intracellular calcium [Ca ⁺²] _i	47
1.4.4.3 Effect of C-peptide on ERK1/2 MAP Kinases.....	48
1.4.4.4 Effect of C-peptide on PI3K signalling pathway.....	48
1.4.4.5 Effect of C-peptide on eNOS.....	49
1.4.5 Biological effects of C-peptide.....	51
1.4.5.1 Effects of c-peptide on microvascular blood flow and haemorheology.....	51
1.4.5.2 Anti-inflammatory effects of C-peptide.....	52
1.4.5.3 Effects of C-peptide on cell growth and survival.....	53
1.4.6 C-peptide replacement in clinical studies of T1DM.....	54
1.4.7 C-peptide effects in T1DM versus T2DM.....	56
1.5 Experimental models of vascular endothelium in DM.....	57
1.5.1 In vitro modelling of vascular endothelium employing EC lines.....	57
1.5.2 Experimental animal models of T1DM.....	58
1.6 Thesis hypothesis and aims.....	59
Chapter 2. Materials and methods.....	60
2.1 Materials.....	60

2.1.1 General materials	60
2.1.2 Cell lines.....	60
2.1.3 Experimental animals	60
2.1.4 Antibodies.....	60
2.2 Methods	62
2.2.1 Culturing of EC lines.....	62
2.2.1.1 EA.hy926 endothelial cells.....	62
2.2.1.2 HMEC-1 endothelial cells.....	63
2.2.2 Cell treatments	63
2.2.3 Isolation of microparticles (MPs)	64
2.2.4 Stimulation of EA.hy926 cells with endothelial MPs (EMPs)	65
2.2.5 Protein measurement assays	65
2.2.5.1 Lowry protein assay	65
2.2.5.1.1 Sample preparation	65
2.2.5.1.2 Assay methodology.....	66
2.2.5.2 Bio-Rad RC DC protein assay.....	66
2.2.6 Cell viability assay (MTT Assay)	67
2.2.7 SDS-polyacrylamide gel electrophoresis (SDS-PAGE).....	67
2.2.8 Western blot analysis (immunoblotting)	68
2.2.9 ELISA for detection of IL-8	69
2.2.10 Nanoparticle tracking analysis	70
2.2.11 Flow cytometry analysis of MPs	71
2.2.11.1 Setting up the flow cytometer for MP analysis	71
2.2.11.2 Optimising the antibodies and MP concentrations	72
2.2.11.3 Labelling of MP samples for FCM	73
2.2.11.4 Data acquisition and analysis.....	74
2.2.12 Immuno-gold labelling of EMPs	75
2.2.13 Proteomic analysis of MPs	76
2.2.14 Diabetic rat study	78
2.2.14.1 Induction of DM and animal groups.....	78
2.2.14.2 Histological analysis of aorta sections	79
2.2.14.2.1 Haematoxylin and eosin staining.....	79
2.2.14.2.2 Masson's trichrome staining.....	79
2.2.14.2.3 Elastic Van Gieson (EVG) Miller's stain	80

2.2.14.3 Immunohistochemistry (IHC).....	80
2.2.14.4 Semi-quantitative analysis of IHC and histology data	81
2.2.15 Statistical analysis.....	81
Chapter 3. Flow cytometry of nanoparticles: method refinement.....	82
3.1 Introduction.....	82
3.2 Results	83
3.2.1 Resolution level achieved with FACSCelesta®.....	83
3.2.2 MP population included in the analysis delimited by MP gate.....	87
3.2.3 Absence of “swarming artefact” during flow cytometric measurements. ...	88
3.2.4 Optimising MP labelling for FCM.....	90
3.2.4.1 Annexin V titration.....	90
3.2.4.2 Antibody titration	92
3.2.4.3 Specificity of MP labelling.....	94
3.2.4.4 Double labelling of MPs: positive controls	95
3.2.4.5 Double labelling of MPs: negative controls	96
3.2.4.6 Post-staining washing versus no washing protocols for MP labelling.....	98
3.2.4.6.1 Single stained MP samples.	98
3.2.4.6.2 Double stained MP samples.	102
3.3 Discussion.....	103
3.3.1 Resolution limit and the optimal threshold.	103
3.3.2 Calibration of the flow cytometer for size measurement.....	104
3.3.3 Effects of coincidence “swarming artefact” on MP quantification by FCM	104
3.3.4 Selecting the appropriate fluorochromes	106
3.3.5 Identifying the optimal antibody concentration.	106
3.3.6 Techniques for data analysis.	106
3.3.7 The impact of unbound fluorescent dye on MP detection by FCM.....	107
Chapter 4. Effect of C-peptide on the vascular endothelium	109
4.1 Introduction.....	109
4.1.1 Effect of C-peptide on endothelial NO production	109
4.1.2 Effect of C-peptide on EC proliferation and/or apoptosis	109
4.2 Result.....	111
4.2.1 C-peptide stimulates ERK1/2 phosphorylation in EA.hy926 cells.....	111
4.2.2 Effect of C-peptide on protein content of EA.hy926 cells.....	115
4.2.3 Effect of C-peptide on EA.hy926 proliferation and viability	116

4.2.4 Effect of C-peptide treatment on caspase-3 level in serum starved EA.hy926 cells	117
4.2.5 Effect of C-peptide on MP release from EA.hy926 endothelial cells.	119
4.2.5.1 Characterisation of C-peptide-derived MPs: Confirmation of vesicles' morphology.....	119
4.2.5.2 Effect of C-peptide on MP generation estimated by nanoparticle tracking analysis.....	121
4.2.5.3 Effect of C-peptide on the size distribution of EMPs.....	123
4.2.5.4 Effect of C-peptide on MP shedding quantified by Flow cytometry	125
4.2.6 Level of MP estimated by total protein determination	128
4.2.7 Endothelial functional activity of C-peptide.....	129
4.2.7.1 C-peptide enhances eNOS protein expression in EA.hy926 cells.....	129
4.2.7.2 C-peptide stimulates the protein expression of Thrombospondin-1	131
4.2.8 A possible modifier for C-peptide signalling in ECs: Pi	133
4.3 Discussion	135
4.3.1 Effect of C-peptide on ERK1/2 phosphorylation	135
4.3.2 Effect of C-peptide on EC proliferation and/or survival.....	136
4.3.3 Effect of C-peptide on MP release from EA.hy926 cells	136
4.3.4 Effect of C-peptide on eNOS protein expression	138
4.3.5 Effect of C-peptide on TSP-1 protein expression	139
Chapter 5. Endothelial dysfunction: effect of high glucose and/or high Pi on MP shedding from ECs	141
5.1 Introduction.....	141
5.1.1 Role of MPs in endothelial dysfunction.....	141
5.2 Results	143
5.2.1 Effect of high glucose on EA.hy926 endothelial cells.....	143
5.2.1.1 Effect of glucose load on MP shedding from EA.hy926 cells quantified by nanoparticle tracking analysis	143
5.2.1.2 Effect of high glucose treatment on particle release from EA.hy926 cells assessed by protein content.....	145
5.2.1.3 Effect of high glucose on MP release from EA.hy926 cells quantified by flow cytometry.....	147
5.2.1.4 Effect of high glucose on EA.hy926 cell protein content.....	148
5.2.2 Effect of high glucose on HMEC-1 endothelial cells.....	150
5.2.2.1 Effect of glucose load on MP shedding from HMEC-1 cells.....	150
5.2.2.2 Effect of glucose load on cell mass of HMEC-1 monolayers.....	151

5.2.3 Biological significance of high glucose and/or C-peptide derived EMPs	152
5.2.3.1 Effect of EMPs induced by high glucose and/or C-peptide on the inflammatory status of EA.hy926 cells	152
5.2.3.2 Effect of EMPs derived from high glucose and/or C-peptide treated EA.hy926 cells on apoptosis level of fresh EA.hy926 culture.....	156
5.2.3.3 High glucose and C-peptide alter the protein composition of EMPs.	158
5.2.4 Simultaneous stimulation of EA.hy926 endothelial cells with high glucose and Pi concentrations.....	160
5.2.4.1 Effect of high glucose and/or high Pi on particle release from EA.hy926 cells	160
5.2.4.2 Effect of high glucose and/or high Pi on EA.hy926 cell mass	162
5.2.5 Modulation of Pi-induced MP generation by C-peptide	164
5.2.5.1 Effect of C-peptide on Pi-induced MP shedding from EA.hy926 cells quantified by nanoparticle tracking analysis.....	164
5.2.5.2 Effect of C-peptide on protein content of Pi-loaded EA.hy926 cells.....	166
5.3 Discussion	168
5.3.1 Suitability of EA.hy926 endothelial cells as a glucose-responsive model ...	168
5.3.2 Effect of high glucose on MP release from EA.hy926 endothelial cells	169
5.3.3 High glucose increases EA.hy926 endothelial cell mass during serum deprivation.	170
5.3.4 High glucose EMPs alter EC properties	171
5.3.5 Effect of high Pi on MP release from EA.hy926 cells	172
5.3.6 Simultaneous in vitro stimulation of ECs with high glucose and Pi.	173
5.3.7 Effect of C-peptide on ECs challenged by hyperphosphataemic milieu	174
Chapter 6. Effect of C-peptide replacement on functional and structural alterations in aorta of STZ-diabetic rat.....	176
6.1 Introduction.....	176
6.1.1 Effect of C-peptide on diabetic macrovasculopathy	176
6.1.2 Assessment of vascular function	176
6.1.2.1 von Willbrand factor as a marker of endothelial cell activation/injury.....	176
6.1.2.2 Collagen deposition	177
6.1.2.3 Formation of AGEs.....	177
6.1.2.4 Oxidative stress level	177
6.2 Results	179
6.2.1 Effect of C-peptide on diabetic aorta morphology	179
6.2.2 Effect of C-peptide treatment on vWF expression in aorta of diabetic rat	179

6.2.3 Effect of C-peptide treatment on collagen content in the aorta of diabetic rat	182
6.2.4 Effect of C-peptide treatment on accumulation of advanced glycation end products in the aorta wall of diabetic rat.....	185
6.2.5 Effect of C-peptide treatment on the oxidative stress level in diabetic rat aortas.....	188
6.3 Discussion	191
6.3.1 Effect of C-peptide on aorta morphology of diabetic rat.....	191
6.3.2 C-peptide improves vascular EC health in diabetic rat by restoring intimal vWF content to normal	192
6.3.3 C-peptide ameliorates collagen accumulation in aortic wall of diabetic rats	193
6.3.4 Effect of C-peptide on AGE accumulation in diabetic aorta.....	196
6.3.5 Effect of C-peptide on oxidative stress level in diabetic aorta.....	198
Chapter 7. General discussion and future work.....	200
Appendix.....	207
References.....	220

List of Tables

Table	Page
Table 1.1 <i>The 2018 American Diabetes Association diagnostic criteria for DM</i>	2
Table 1.2 <i>Classification of DM</i>	4
Table 1.3 <i>Biologically functional molecules synthesised by the vascular endothelium.</i>	12
Table 1.4 <i>Circulating biomarkers of endothelial function.</i>	27
Table 1.5 <i>Classification of extracellular vesicles based on their biogenesis and size.</i>	30
Table 2.1 <i>Primary antibodies used for IHC and western blot analysis</i>	61
Table 2.2 <i>Secondary antibodies used for IHC and western blot analysis</i>	62
Table 2.3 <i>Settings applied to FACSCelesta for scatter (SSC, FSC) and fluorescent (FITC, BV421, APC) parameters during MP analysis.</i>	74
Table 2.4 <i>Compensation matrices applied for data analysis.</i>	75

List of Figures

Figure	Page
Figure 1.1 Diabetes triggers a spectrum of adverse vascular effects in the human body.	9
Figure 1.2 Basic structure of different blood vessel types.	10
Figure 1.3 Structure of eNOS in its active form (dimer), presenting binding sites for cofactors and substrates.	14
Figure 1.4 Regulatory functions of the vascular endothelium.	15
Figure 1.5 Hyperglycaemia disturbs normal metabolic pathways in ECs.	18
Figure 1.6 Schematic representation of the events involved in MP generation during cell activation or apoptosis.	32
Figure 1.7 Schematic view illustrates the main parts of a flow cytometer	39
Figure 1.8 Covalent structure of human proinsulin.	44
Figure 1.9 Proposed signaling pathways activated by C-peptide	50
Figure 1.10 C-peptide exerts multiple beneficial actions in diabetes.	55
Figure 2.1 Standard curve for IL-8 ELISA.	70
Figure 2.2 NanoSight LM10 System used for NTA analysis.	71
Figure 2.3 Gating applied to MP-Count beads.	75
Figure 3.1 FACSCelesta® flow cytometer demonstrated high SSC resolution among submicron beads.	83
Figure 3.2 FACSCelesta® flow cytometer showed clear separation between Megamix-Plus SSC bead subsets and the instrument noise based on fluorescent detection.	84
Figure 3.3 FACSCelesta® flow cytometer demonstrated good separation between Megamix-Plus SSC bead subsets and the instrument noise based on SSC detection.	85
Figure 3.4 Low FSC resolution between submicron beads in FACSCelesta® flow cytometer.	86
Figure 3.5 Dual scatter dot plot depicting the final MP analysis window defined by Megamix-Plus SSC beads.	87
Figure 3.6 Flow cytometric measurement was free from coincidence.	88
Figure 3.7 Absence of swarm detection during MP counting by flow cytometry.	89
Figure 3.8 Annexin V titration curve showing the number of Annexin V+ MPs detected at various concentrations of Annexin V.	90
Figure 3.9 Determination of the optimal Annexin V concentration for MP labelling.	91
Figure 3.10 CD31 antibody titration curve showing the number of CD31+ MPs detected at various concentrations of anti-CD31.	92
Figure 3.11 Determination of the optimal anti-CD31 concentration for MP labelling.	93
Figure 3.12 Efficiency of MP labelling with endothelial markers or Annexin V.	94
Figure 3.13 TNF α and Ca-ionophore augment MP generation from ECs.	95

Figure 3.14 Representative dual fluorescence dot plots (FITC-H/BV421-H) illustrating the negative controls used.	96
Figure 3.15 Representative dual fluorescence dot plots (FITC-H/APC-H) demonstrating the negative controls used in this study.	97
Figure 3.16 The influence of the unbound antibody on MP detection.	98
Figure 3.17 The difference between washing and no washing approaches for MP labelling for flow cytometry.	99
Figure 3.18 Comparison between washing and no washing methods for MP labelling with Annexin V.	100
Figure 3.19 The effect of removing the unbound Annexin V stain during MP labelling.	101
Figure 3.20 Comparison between washed versus unwashed labelling methods of MPs.	102
Figure 3.21 Schematic representation of the flow cytometer fluidics system.	105
Figure 4.1 C-peptide induces phosphorylation of ERK1/2 in EA.hy926 cells after 24h exposure.	112
Figure 4.2 Effect of short-term C-peptide treatment on ERK1/2 activation in EA.hy926 cells.	114
Figure 4.3 C-peptide stimulation does not influence the protein mass of EA.hy926.	115
Figure 4.4 Assessment of EA.hy926 proliferation after stimulation with C-peptide.	116
Figure 4.5 Assessment of apoptosis level in serum starved EA.hy926 cells after C-peptide stimulation.	118
Figure 4.6 Representative immuno-EM micrographs of EMPs.	120
Figure 4.7 Release of MPs from EA.hy926 endothelial cells in response to C-peptide.	122
Figure 4.8 Size distributions of EMPs as measured by NTA	123
Figure 4.9 Effect of C-peptide on size of MP generated from EA.hy926 cells.	124
Figure 4.10 Shedding of MPs from EA.hy926 endothelial cells treated with C-peptide.	126
Figure 4.11 Co-treatment of ECs with PTX mitigates MP release in response to C-peptide.	127
Figure 4.12 Effect of C-peptide on protein content of released particles in the conditioned medium.	128
Figure 4.13 C-peptide increases eNOS protein expression in EA.hy926 cells after 24h treatment.	130
Figure 4.14 C-peptide stimulates TSP-1 protein expression in EA.hy926 cells.	132
Figure 4.15 Effect of elevated Pi concentration on C-peptide ERK1/2 activation in EA.hy926 cells.	134
Figure 5.1 Effect of high glucose on MPs release from endothelial EA.hy926 cells estimated by NTA.	144
Figure 5.2 Effect of high glucose on the protein content of released particles sedimented from the test medium of EA.hy926 cells.	146
Figure 5.3 Effects of high glucose treatment on MP release from cultured EA.hy926 cells.	147

Figure 5.4 <i>Effect of high glucose on total protein content of EA.hy926 cells.</i>	149
Figure 5.5 <i>Effect of high glucose on MP shedding from HMEC-1.</i>	150
Figure 5.6 <i>Effect of high glucose on total cell monolayer protein of HMEC-1 cells.</i>	151
Figure 5.7 <i>Effect of high glucose and/or C-peptide derived EMPs on ICAM-1 expression in ECs.</i>	153
Figure 5.8 <i>Effect of EMPs generated from high glucose and/C-peptide on E-selectin expression in ECs.</i>	154
Figure 5.9 <i>Effect of EMPS derived from high glucose and/or C-peptide treatment on IL-8 secretion from ECs.</i>	155
Figure 5.10 <i>EMPs generated from high glucose treated ECs stimulate endothelial apoptosis.</i>	157
Figure 5.11 <i>High glucose and C-peptide alters the proteome of EMPs.</i>	159
Figure 5.12 <i>Estimation of particle protein released in EA.hy926 supernatant after stimulation with high glucose (25mM) or high Pi (2.5Mm).</i>	161
Figure 5.13 <i>Effect of high glucose/high Pi on EA.hy926 cells protein content.</i>	163
Figure 5.14 <i>Effect of C-peptide on MP shedding from high Pi-treated cells.</i>	165
Figure 5.15 <i>Effect of C-peptide on Pi-induced alteration in protein content of EA.hy926 cells.</i>	167
Figure 6.1 <i>Expression of vWF in the intima layer of healthy control and diabetic rat aorta.</i>	180
Figure 6.2 <i>Effect of C-peptide treatment on the intimal expression of vWF in diabetic rat aorta evaluated by immunohistochemical staining of vWF.</i>	181
Figure 6.3 <i>Masson trichrome staining of aortas demonstrating the amount of collagen deposition.</i>	183
Figure 6.4 <i>Effect of C-peptide treatment on collagen deposition in diabetic rat aorta evaluated by Masson trichrome staining.</i>	184
Figure 6.5 <i>Immunohistochemical staining for advanced glycation end products in sections of aorta.</i>	186
Figure 6.6 <i>Effect of C-peptide treatment on AGE content in diabetic rat aorta measured by immunohistochemical staining.</i>	187
Figure 6.7 <i>Immunohistochemical staining for 3-NT in sections of aorta.</i>	189
Figure 6.8 <i>Effect of C-peptide treatment on oxidative stress level in diabetic rat aorta assessed by immunohistochemical staining of 3-NT.</i>	190
Figure 7.1 <i>Schematic illustration of the mechanism by which C-peptide modulated biological activities in ECs.</i>	205

List of Abbreviations

3-NT	Nitrotyrosine
ADA	American Diabetes Association
ADMA	Asymmetric dimethylarginine
AGEs	Advanced glycation end products
Akt	Protein kinase B, PKB
APC	Allophycocyanin
ATP	Adenosine tri-phosphate
BH4	Tetrahydrobiopterin
BV421	Brilliant violet 421
[Ca ²⁺] _i	Intracellular calcium concentration
Ca-ionophore	Calcium ionophore
CaM	Calmodulin
CKD	Chronic kidney disease
C-peptide	Connecting peptide
CVD	Cardiovascular disease
DCCT	Diabetes Control and Complications Trial
DFBS	Dialysed foetal bovine serum
DKD	Diabetic kidney disease
DM	Diabetes mellitus
DMEM	Dulbecco's modified eagle medium
ECM	Extracellular matrix
ECs	Endothelial cells
EDIC	Epidemiology of Diabetes Interventions and Complications study
EM	Electron microscopy
EMPs	Endothelial microparticles
eNOS	Endothelial nitric oxide synthase
EPCs	Endothelial progenitor cells
ERK1/2	Extracellular signal-regulated kinase 1/2
ESRD	End-stage renal disease
EVs	Extracellular vesicles
FBS	Foetal bovine serum
FCM	Flow cytometry
FITC	Fluorescein isothiocyanate
FMD	Flow mediated dilatation
FPG	Fasting plasma glucose
FSC	Forward scatter
GAPDH	Glyceraldehyde 3-phosphate dehydrogenase
GDM	Gestational diabetes
GFR	Glomerular filtration rate
GPCR	G-protein-coupled receptor
H&E	Haematoxylin and eosin
HbA1C	Glycated haemoglobin

HBSS	Hanks' balanced salt solution
HEK-293	Human embryonic kidney cells
HMEC-1	Human microvascular endothelial cells
HRP	Horseradish peroxidase
ICAM-1	Intercellular adhesion molecules
IDF	International Diabetes Federation
IHC	Immunohistochemistry
IL-8	Interleukin-8
iNOS	Inducible nitric oxide synthase
ISAC	The International Society on Advancement of Cytometry
ISEV	International Society for Extracellular Vesicles
ISTH	International Society of Thrombosis and Haemostasis
LC-MS/MS	Liquid chromatography-tandem mass spectrometry
LPS	Lipopolysaccharide
MAPK	Mitogen-activated protein kinases
MCDB-131	Molecular and Cellular Developmental Biology-131 growth medium
MCP-1	Monocyte chemotactic protein-1
MEM	Minimum essential medium
MFI	Mean fluorescent intensity
MMPs	Matrix metalloproteinase
MPs	Microparticles
MTT	3-(4,5-dimethylthiazol-2-yl)-2,5-diphenyltetrazolium bromide
MVB	Multivesicular body
NADPH	Nicotinamide adenine dinucleotide phosphate
NF- κ B	Nuclear factor kappa light chain enhancer of activated B cells
nNOS	Neuronal nitric oxide synthase
NO	Nitric oxide
NTA	Nanoparticle tracking analysis
OGTT	Oral glucose tolerance test
4 TM ®PARP	Poly-ADP-ribose polymerase
PCA	Perchloric acid
Pi	Inorganic phosphate
PI3Ks	Phosphatidylinositol 3-kinases
PKC	Protein kinase C
PLC	Phospholipase C
PMPs	Platelet-derived microparticles
PMTs	Photomultipliers
PS	Phosphatidylserine
PTCs	Proximal tubular cells
PTX	Pertussis toxin
Q2 gate	Quadrant 2 gate
RAGE	Receptor for advanced glycation end-products
RAS	Renal renin-angiotensin system
RBCs	Red blood cells

Rho	Ras-homologous
ROCK	Rho-associated protein kinases
s.c.	Subcutaneously
SCC	Side scatter
SDS	Sodium dodecyl sulphate
SEM	Standard error measurement
SI	Separation index
siRNA	Small interfering ribonucleic acid
SMCs	Smooth muscle cells
STZ	Streptozotocin
SV-40T	Simian virus 40 (SV40) T antigen
T1DM	Type 1 diabetes
T2DM	Type 2 diabetes
TEM	Transmission electron microscopy
TF	Tissue factor
TFPI	Tissue factor pathway inhibitor
TGF- β	Transforming growth factor- β
TIMPs	Tissue inhibitors of metalloproteinase
TNF- α	Tumour necrosis factor alpha
tPA	Tissue-type plasminogen activator
TSP-1	Thrombospondin-1
UKPDS	United Kingdom Prospective Diabetes Study
VCAM-1	Vascular cell adhesion molecule 1
VEGF	Vascular endothelial growth factor
vWF	Von willebrand factor

Chapter 1. General introduction

1.1 Diabetes mellitus

1.1.1 History and epidemiology

Diabetes Mellitus (DM) is a heterogeneous metabolic disorder characterized by the presence of chronic hyperglycaemia with subsequent disturbances of carbohydrate, fat and protein metabolism, resulting from defects in insulin secretion, insulin action, or both (Warrell et al., 2010). The early diabetic manifestation of excessive drinking of water and increased urination frequency has been recognised since ancient times; however, understanding its pathology and treatment availability has developed only in the last century. The name of the disease has derived from the Greek word 'diabetes' which means siphon to pass through. Later the word mellitus was added (meaning sweet in Latin) to differentiate it from diabetes insipidus (tasteless). Thus, diabetes mellitus signifies 'sweet urine' passed by those patients (Patlak, 2002). Because polyuria was the earliest recognised symptom; it was thought for centuries that DM is a disease of the kidney, until in 1889 von Mering and Minkowski showed that removing the pancreas from a healthy dog caused symptoms similar to DM (Von Mering and Minkowski, 1889). Their study was the first evidence for the key role of the pancreas in regulation of blood glucose concentration. At that time, several researchers speculated that an internal secretion from the pancreas enables the body to utilise glucose. This pancreatic secretion was later called insulin (Polonsky, 2012). Since then, several approaches have been developed to manage DM; for instance, increasing insulin secretion from the pancreatic islets, increasing tissue sensitivity to insulin or replacement of insulin - depending on the disease class (Section 1.1.3). As the lifespan of diabetic people increased, it becomes obvious that insulin alone does not cure DM and that many organs are affected by the progressive diabetic complications, which has created a new challenge for scientists to tackle.

DM represents a global problem which involves a huge financial, social and health burden. According to the latest estimates from the International Diabetes Federation (IDF) for DM prevalence, there were 451 million people with DM across the world in

2017. Projection to 2045 expects this to soar to 693 million. It is, estimated however that nearly half of all people living with DM are undiagnosed. The global healthcare expenditure on people with DM was estimated to be \$850 billion in 2017; whereas, DM was responsible for approximately 5 million deaths worldwide in the same year (Cho et al., 2018). These estimates necessitate an effective intervention to battle the disease progression at early stages.

1.1.2 Diagnosis of DM

In view of the recently published ‘Standards of Medical Care in Diabetes’ by the American Diabetes Association (ADA) (2018), a diagnosis of DM may be made using FPG (fasting plasma glucose), 2-h plasma glucose after a 75g glucose load (OGTT), or HbA1C (glycated haemoglobin), as summarised in Table 1.1. However, test selection may depend on a number of factors such as convenience, availability, cost, presence of certain haemoglobinopathies or conditions associated with increased RBC turnover, such as sickle cell disease, pregnancy, haemodialysis, recent blood loss or transfusion or erythropoietin therapy (American Diabetes Association, 2018).

Table 1.1 The 2018 American Diabetes Association diagnostic criteria for DM

	FPG \geq 7.0 mmol/L. Fasting is defined as no caloric intake for at least 8 h.
OR	
	2-h plasma glucose \geq 11.1mmol/L during OGTT. Assay method described by the WHO, using a glucose load equivalent to 75-g anhydrous glucose in water.
OR	
	HbA1C \geq 6.5%. Using certified assay by the National Glycohaemoglobin Standardization Program.
OR	
	A random plasma glucose \geq 11.1 mmol/L in a patient with classic symptoms of hyperglycaemia.

1.1.3 Classification of DM

The aetiology of DM can vary widely but always involves defects in insulin secretion/response at some point in the disease course. Increasing knowledge has led to better understanding of DM pathophysiology and the existence of multiple new variants of the disease has become appreciated. Early categorisation of DM was based on the type of pharmacological treatment, i.e. insulin dependent and non-insulin dependent DM. However, this classification has been subject to revision and debate over years. Alternative criteria for DM classification were suggested by the ADA which classified the disease based on its aetiology (Gavin III et al., 1997). The most recent and widely accepted classification divides the disease into two broad categories: type 1 DM (T1DM) and type 2 DM (T2DM). In addition, there are other specific types of DM, as well as gestational DM (GDM) (Table 1.2).

Table 1.2 Classification of DM (American Diabetes Association, 2014)

Type of DM	Description
T1DM	β -cell destruction, usually leading to absolute insulin deficiency (immune-mediated or idiopathic).
T2DM	Progressive insulin secretory defect which is related to insulin resistance.
Specific types of DM due to other causes:	<ul style="list-style-type: none"> • Genetic defects of β-cell function (e.g. neonatal DM and maturity-onset diabetes of the young (MODY)). • Genetic defects in insulin action. • Diseases of the exocrine pancreas (e.g. cystic fibrosis, neoplasia and pancreatitis). • Endocrinopathies (e.g. Cushing's syndrome and acromegaly) • Drug- or chemical-induced (e.g. glucocorticoids & thiazides) • Infections (e.g. cytomegalovirus and congenital rubella) • Uncommon forms of immune-mediated DM (e.g. Anti-insulin receptor antibodies) • Other genetic syndromes associated sometimes with DM (e.g. Down's syndrome)
Gestational diabetes mellitus (GDM)	<ul style="list-style-type: none"> • DM diagnosed for the first time in the 2nd or 3rd trimester of pregnancy.

1.1.3.1 Type 1 DM

Type 1 DM (T1DM) is characterized by autoimmune destruction of insulin-producing β -cells in the islets of the pancreas gland, resulting in deficiency of insulin. Therefore, individuals with T1DM ultimately need daily insulin injections to survive (Warrell et al., 2010). Notably, from normal β -cells, insulin is released along with its cleaved connecting peptide (C-peptide) (Steiner et al., 1967); whereas, in people with T1DM, β -cells produce little if any insulin and C-peptide (Warrell et al., 2010). Insulin is provided to people having T1DM; however, they remain C-peptide-deficient (discussed further in Section 1.4).

The aetiology of T1DM is associated with an autoimmunity against β -cells. Accordingly, T1DM is typified by the presence of autoantibodies: anti-insulin, anti-GAD65 (65 kDa glutamic acid decarboxylase) or insulinoma-associated protein 2 (IA-2) and zinc transporter 8 (ZNT8) antibodies. Autoimmune damage to β -cells is mediated by CD4+ and CD8+ T cells and infiltrating macrophages. T1DM is classified as idiopathic in the absence of these autoantibodies. The initiation of this immune response is not fully understood, although a combination of genetic susceptibility and environmental triggers has been implicated (Katsarou et al., 2017).

According to IDF estimates, T1DM accounts only for a minority of total DM while the disease occurs most frequently during childhood or adolescence. Globally, there are over a million children and adolescents below 20 years having T1DM. The incidence of T1DM is increasing worldwide by around 3% annually, although there is a huge variation between different geographical areas in the world, suggesting an influence of genetic and environmental factors on disease incidence (International Diabetes Federation, 2017).

1.1.3.2 Type 2 DM

Type 2 DM (T2DM) is the most common type of DM, accounting for more than 90% of the total DM burden (International Diabetes Federation, 2017). It is characterised by impairment of carbohydrate, lipid and protein metabolism resulting from inadequate insulin production, insulin resistance (body unresponsiveness to insulin) or a combination of both (DeFronzo et al., 2015). Patients with T2DM may remain

undiagnosed for many years because the disease develops gradually, and the classic symptoms of hyperglycaemia might not be noticeable at early disease stages. Indeed, some patients with T2DM are first diagnosed when they present with one of the DM long-term complications (American Diabetes Association, 2014).

Two key components entail T2DM: β -cell dysfunction and insulin resistance, but which one precedes the other remains unknown. The proposed cellular mechanisms for β -cell dysfunction include: direct toxicity of β -cells induced by glucose or free fatty acid, ' β -cell exhaustion' and impaired proinsulin transcription (Leahy, 2005). Resistance to insulin action results from the phosphorylation of insulin receptor substrates (IRSs) at an inhibitory site, thereby inhibiting insulin signalling. Of note, insulin resistance is not confined to the major tissues responsible for glucose clearance, i.e. muscle and liver; it occurs as well in adipose tissue, kidney, gastrointestinal tract, vasculature, and brain, and pancreatic β -cells themselves (DeFronzo et al., 2015).

Despite the genetics of T2DM being poorly understood, the disease has a strong link to genetic and familial predisposition, even more than T1DM (Leahy, 2005). Some of the identified risk factors include: obesity, age, family history of T2DM, ethnicity, sedentary lifestyle, prior GDM, hypertension, dyslipidaemia and polycystic ovary syndrome (American Diabetes Association, 2018). T2DM is most common in older adults, although it is increasingly diagnosed in children, adolescents and younger adults as a result of the wide spread of obesity, lack of physical activity and poor diet (International Diabetes Federation, 2017). Unlike T1DM, T2DM patients may not need insulin throughout their lifetime to survive, whereas several classes of anti-hyperglycaemic drugs are available which aim to lower glucose levels in blood. Because the majority of T2DM patients (80%) are obese or overweight, and obesity is linked to insulin resistance, management of T2DM may start with non-pharmacological interventions including lowering the body mass index (BMI) and adapting a healthy lifestyle (Inzucchi et al., 2012).

1.1.4 Diabetic complications

Better understanding of DM pathophysiology and advances in disease management have improved the life expectancy of diabetic patients. However, the development of long-term diabetic complications remains very common. Diabetes is not simply a

disorder of glucose metabolism. Serious vascular sequelae are caused by DM, which are responsible for the high morbidity and mortality among diabetic people. Although T1DM and T2DM are distinctive in aetiologies, their complications are similar (White et al., 2000). Broadly, diabetes complications can be divided into acute and chronic complications (Figure 1.1). The acute complications comprise hypoglycaemia, diabetic ketoacidosis, hyperglycaemic hyperosmolar state, and coma. Chronic complications are subdivided into microvascular and macrovascular complications. Microvascular complications manifest as nephropathy, neuropathy and retinopathy, which are unique to DM. Macrovascular complications involve atherosclerosis related diseases, such as coronary artery disease, leading to angina or myocardial infarction, cerebrovascular disease and peripheral artery disease. These conditions are not specific to DM (Warrell et al., 2010).

According to the most recent IDF Atlas, DM increases the prevalence of end-stage renal failure in the population several fold; whereas, it is considered to be the leading cause for vision loss in adults (20-65 years). The rate of lower limb amputation in diabetic patients is one per 30 second worldwide. Most notably in terms of mortality, people with DM are 2 to 3-fold more susceptible to developing cardiovascular disease (CVD). The diabetic complications can be present at the moment of diagnosis in people with T2DM and early (around 5 years) after onset of T1DM (International Diabetes Federation, 2017).

Chronic hyperglycaemia has identified as the chief driving force for diabetic vascular complications. In accord with this, the two landmark studies, Diabetes Control and Complications Trial (DCCT) (1993) and the United Kingdom Prospective Diabetes Study (UKPDS) (1998) demonstrated that intensive control of hyperglycaemia effectively delays the onset and reduces the progression of diabetic microvascular complications. Multiple factors can affect atherosclerosis-related complications: the long-term follow-up study of DCCT, Epidemiology of Diabetes Interventions and Complications study (EDIC) (2005) showed that in patients subjected to tight regulation of blood glucose, the risk of cardiovascular diseases reduced. These clinical observations underscore the crucial role of hyperglycaemia in the pathogenesis of diabetic vascular complications. Patients with T1DM who enrolled in the DCCT study, after 10 years' follow-up continued

to have microvascular complications whilst maintaining similar glycaemic control. The findings in these studies demonstrate that restoring blood glucose within normal range, even for a long period, is insufficient to protect from the development of diabetic microvascular complications. C-peptide could be the missing link for successful treatment of diabetic complication (discussed further in Section 1.4).

As mentioned earlier, DM is associated with unique microvascular complications—nephropathy, retinopathy and neuropathy. Diabetic nephropathy is characterized by particular structural and functional alterations in the kidney. The components of early diabetic renal changes include: glomerular hyperfiltration, glomerular and renal hypertrophy, and increased urinary excretion of albumin, increased basement membrane thickness, and mesangial expansion with the accumulation of extracellular matrix (ECM) proteins (Schrijvers et al., 2004). On the other hand, diabetic neuropathy is associated with damage in somatosensory and autonomic nerves. As a result of tissue hyperglycaemia, nerve damage may happen due to glycation of vital proteins in nerves; in addition to impaired nerve conduction arising from inhibition of the activity of Na⁺, K⁺-ATPase (Warrell et al., 2010). Lastly, diabetic retinopathy escalates from the mild nonproliferative stage (marked by increased vascular leakage), to moderate and severe nonproliferative diabetic retinopathy (marked by vascular closure), to proliferative diabetic retinopathy (defined by the growth of new blood vessels on the retina and posterior surface of the vitreous body (Fong et al., 2004). The complications of nephropathy and retinopathy result mainly from abnormalities in blood flow in the microcirculation. Even the neuropathy is associated with damage in the microcirculation of nerves (vasa nervorum). The perturbation in blood flow through the microcirculation, apparently reducing the supply of nutrients and oxygen to target tissues. Resting blood flow is augmented in the retina, glomerulus and other tissues in response to hyperglycaemia. This may damage the endothelium, promote thrombogenesis and stimulate the release of vasoconstrictors, resulting in occlusion in the small blood vessels (Warrell et al., 2010).

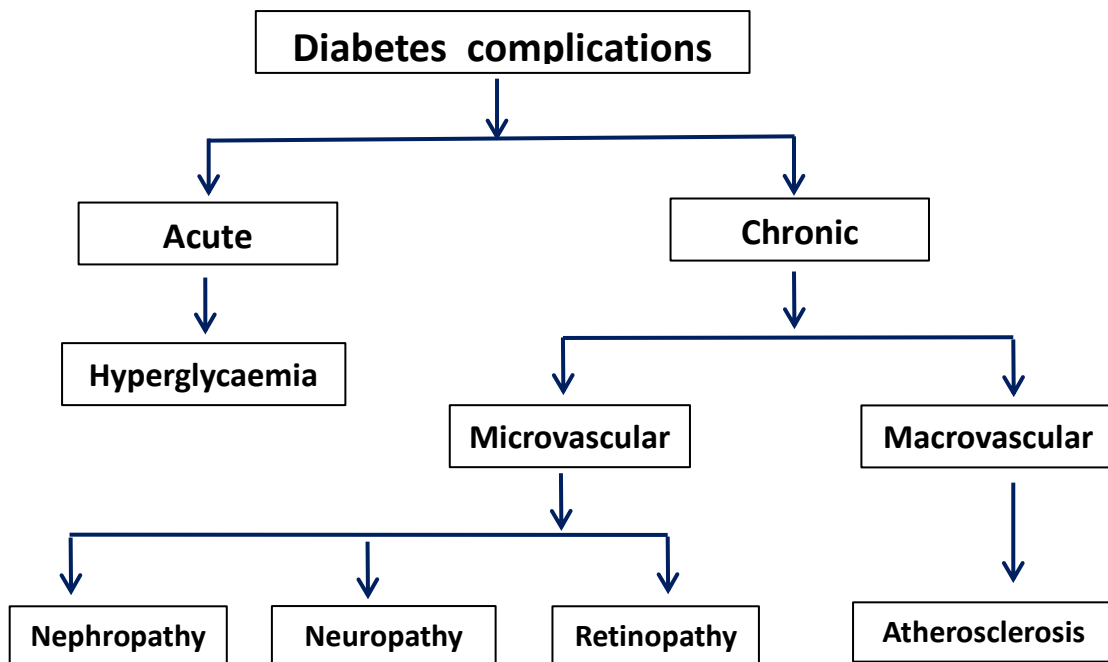


Figure 1.1 Diabetes triggers a spectrum of adverse vascular effects in the human body.

1.2 The vascular system

The vascular system of the human body consists of a large number of blood vessels which are responsible for maintaining tissue homeostasis. Circulation of blood through these vessels removes cellular and metabolic waste products whilst supplying tissues with oxygen and essential nutrients (Pugsley and Tabrizchi, 2000).

The blood vessel network consists of arteries, capillaries and veins, and broadly most blood vessels are composed of three histologically distinct layers. Starting from the internal surface of the blood vessel and moving outwards, these layers are tunica intima (or interna), tunica media and tunica adventitia (or externa). The tunica intima, typically the thinnest layer consisting of a single layer of endothelial cells (ECs), rests on a basement membrane. The tunica media mostly comprises smooth muscle cells (SMCs) and elastin fibres. The medial layer becomes more organized and is thicker in large arteries to withstand high blood pressure. The external cover of the blood vessel is tunica adventitia which mainly consists of connective tissue (Tortora and Derrickson, 2014 , p.730). Variation in the basic structure of the vessel wall results in distinct types of blood vessels (see Figure 1.2).

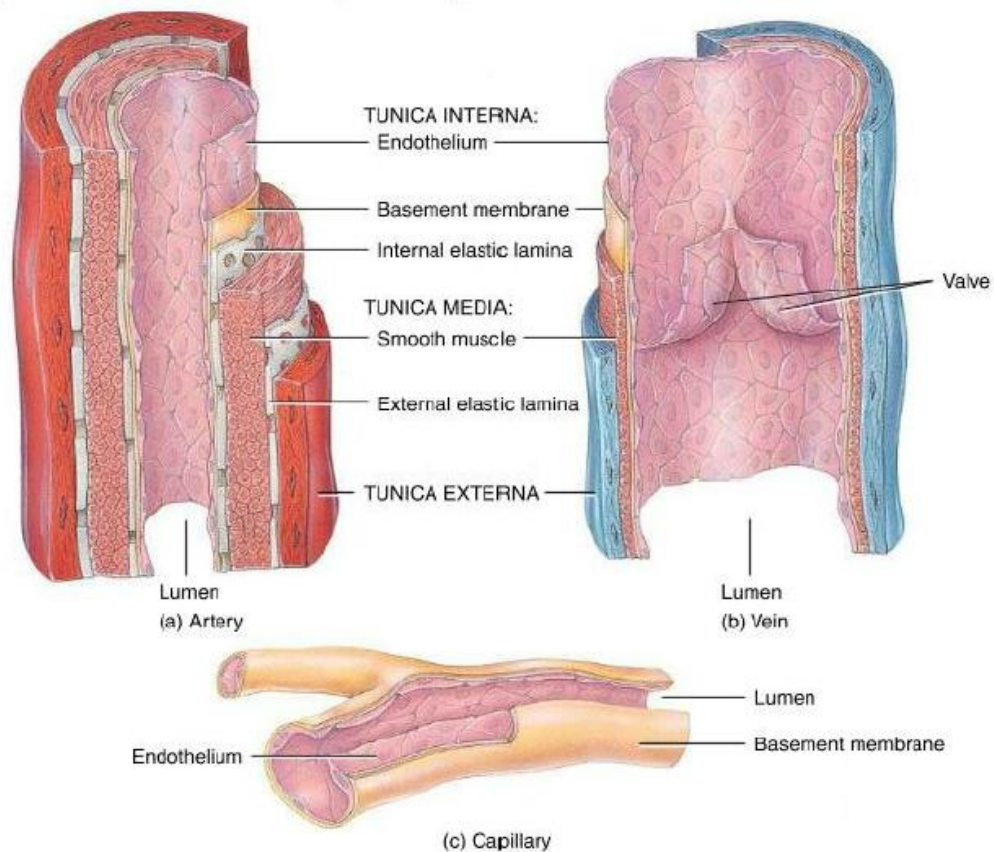


Figure 1.2 Basic structure of different blood vessel types. A) An artery which has a thick media layer. B) A thin-wall vein due to small SMCs and elastic components in the wall lining. C) The smallest blood vessel, i.e. capillary that lacks both tunica media and externa. (The capillary image is enlarged for illustration) (Tortora and Derrickson, 2014 , p.731). (Permission for using the image was granted by the publisher).

The EC layer has a strategic position at the interface between the blood and the underlying tissue, and these cells have a critical role in the normal physiology of the vasculature as well as the pathophysiology in disease states. This location of ECs permits sensing and responding to diverse blood-borne signals. Successive findings in the EC research field during the last few decades have confirmed this assumption, whereby a plethora of physiological functions has been ascribed to ECs (Pearson, 2000), including barrier function, regulation of vascular tone, modulation of inflammatory and immunological responses and the involvement in fibrinolysis and coagulation processes (discussed further in Section 1.2.2).

1.2.1 Normal endothelium

The cellular lining of blood vessels, the endothelium, is a dynamic environment owing to its crucial synthetic, secretory, metabolic, and immunologic activities (Verma and Anderson, 2002). ECs participate actively in maintaining the vascular homeostasis by synthesising and secreting several important biological mediators (see Table 1.3).

Due to their position, ECs act as an active barrier. Three types of intercellular junctions are present in ECs: tight, gap and adherens junctions, which play a key role in maintaining EC integrity and selective permeability (De Caterina et al., 2007a). These cells also have characteristic membrane-bound granules, Weibel–Palade bodies. These granules store and release von Willebrand factor (vWF) into the plasma, or within the subendothelial matrix. In addition to carrying factor VIII, vWF binds to vascular collagen exposed to the bloodstream (De Meyer et al., 1999, Pearson, 2000). Consequently, vWF plays a pivotal role in vascular thrombosis and inflammation by recruiting platelets and leukocytes to damaged vessel wall (Gragnano et al., 2017).

Despite having common structural elements, ECs display a certain degree of heterogeneity which allows them to accommodate the special physiological requirements of different organs. For instance, the endothelium is continuous in the retina and blood brain barrier, while a fenestrated endothelium is present in the kidney glomerulus (Cines et al., 1998). Interestingly, even adjacent ECs may be relatively different in function by having a specific pacemaker activity (Pries and Kuebler, 2006).

In addition to morphological diversity, ECs may differ in mediator release, antigen presentation and responses to stimuli. For instance, endothelial-dependent relaxation is generally more marked in arteries than in veins, whereas leucocyte-endothelial interactions mainly occur on the venous side in which the expression of adhesion molecules such as P-selectin, E-selectin and intercellular adhesion molecule (ICAM-1) is predominant in intima of veins (Pries and Kuebler, 2006). Importantly, EC phenotype depends not only on the embryonic stage; but also, on the surrounding microenvironment which can alter the primary phenotype. For example, aortic ECs, grown on extracellular matrix obtained from kidney-derived cells, develops fenestrae (Cines et al., 1998).

Mediator	Function
Nitric oxide (NO), prostacyclin (PGI ₂), endothelium-derived hyperpolarizing factor (EDHF), bradykinin, C-natriuretic peptide	Vasodilation
Endothelin-1 (ET-1), angiotensin-II (Ang II), thromboxane A ₂ (TXA ₂), prostaglandin H ₂ , oxidant radicals, angiotensin converting enzyme (ACE), leukotrienes.	Vasoconstriction
NO, PGI ₂ , transforming growth factor- β (TGF- β), heparin sulphate	Antiproliferative
ET-1, Ang II, oxidant radicals, platelet-derived growth factor (PDGF), basic fibroblast growth factor (FGF), insulin-like growth factor (IGF-1), interleukins	Proproliferative
NO, PGI ₂ , plasminogen activator, protein C, tissue factor inhibitor, thrombomodulin, antithrombin.	Antithrombotic
ET-1, plasminogen-activator inhibitor-1, TXA ₂ , fibrinogen, tissue factor (TF), platelet activating factor, thromboplastin, vWF	Prothrombotic
Interleukins 1, 6 and 8, P-selectin, E-selectin, ICAM-1, vascular cell adhesion molecule 1 (VCAM-1), monocyte chemotactic protein-1 (MCP-1), major histocompatibility complex class II (MHC II)	Inflammatory markers
Receptor for advanced glycosylation end-products (RAGE)	Permeability
Vascular endothelial growth factor (VEGF)	Angiogenesis

Table 1.3 Biologically functional molecules synthesised by the vascular endothelium. Endothelial cells express/secrete a wide range of key mediators that are involved in vascular homoeostasis (Verma and Anderson, 2002).

1.2.2 Regulatory functions of the vascular endothelium

Until recently, the vascular endothelium was viewed as a passive barrier in the vessel wall, but now it is evident that ECs are chief participants in vessel-related functions (Figure 1.4). In the physiologic state, the endothelium contributes to regulation of vascular hemodynamics by secreting a set of vasodilators, as well as vasoconstrictors (listed in Table 1.3). One key regulator of vascular tone, synthesised and released by the endothelium, is nitric oxide (NO). The multifunctional molecule NO plays an essential role in many aspects of vascular biology. Endothelium-derived NO is a very potent vasodilator (Laurindo et al., 2018). Resting endothelium displays an antiplatelet, anticoagulant and fibrinolytic surface to the blood. NO contributes in preservation of this tendency by inhibiting platelet aggregation, suppressing the activity and expression of certain leukocyte adhesion molecules, and inhibiting the proliferation of SMCs. Diminished endothelium-derived NO produces an atherogenic surface which is more prone to vascular accidents (Cines et al., 1998, De Caterina et al., 2007a).

Vascular endothelia release NO continuously at a basal level. NO is produced by converting L-arginine to L-citrulline in the presence of nicotinamide adenine dinucleotide phosphate (NADPH). Nitric oxide synthase (NOS) is the enzyme that catalyses this reaction; whilst several cofactors and substrates are required to assist the reaction such as calmodulin (CaM) and tetrahydrobiopterin (BH₄) (Figure 1.3) (Laurindo et al., 2018). There are three isoforms of NOS: endothelial NOS (eNOS), is a constitutive EC enzyme that consistently provides a basal level of NO surrounding the endothelium (Hunt and Jurd, 2002). The other enzyme types are the inducible NOS (iNOS) and the neuronal NOS (nNOS). In the resting state of ECs, eNOS binds to caveolin protein in cell membrane *caveolae*; this binding inhibits eNOS activity. During EC activation, increased cytosolic calcium promotes a reversible dissociation of eNOS from caveolin and induces CaM binding, which augments eNOS activity (De Caterina et al., 2007a). Although eNOS activation is calcium-dependent, more recent findings revealed eNOS activation in a calcium-independent manner via signal transduction machinery such as tyrosine phosphorylation (De Caterina et al., 2007a). Ultimately, NO diffusing to SMCs activates guanylate cyclase, resulting in vascular relaxation. Released NO is rapidly scavenged by oxyhaemoglobin in red blood cells (RBCs) (Radi, 2004); however, it maintains activity in

close vicinity to the EC surface in sufficient amount to perform other biological functions.

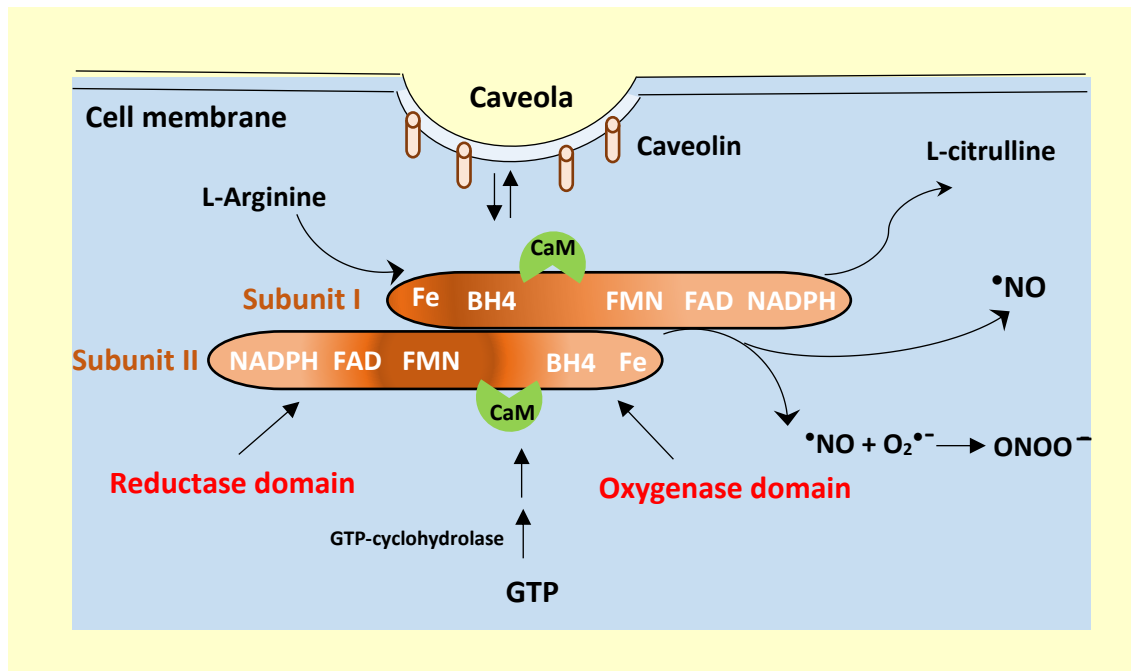


Figure 1.3 Structure of eNOS in its active form (dimer), presenting binding sites for cofactors and substrates. The reductase domain contains binding sites for FMN, FAD, and NADPH, while the oxidase domain contains binding sites for BH4 and haem iron. BH4, tetrahydrobiopterin; CaM, calmodulin; FMN, flavin mononucleotide; FAD, flavin adenine dinucleotide; GTP, guanosine triphosphate; $\bullet\text{NO}$, nitric oxide; $\text{O}_2^{\bullet-}$, superoxide; ONOO^- , peroxynitrite. Adapted from (Laurindo et al., 2018).

The vascular endothelium also plays a vital role in providing an anticoagulant interface for the blood vessel. ECs utilise three distinct anticoagulant pathways: heparin-antithrombin, tissue factor pathway inhibitor (TFPI) and thrombomodulin-protein C anticoagulant. Whereas, the fibrinolytic activity is maintained by modulating the activities of tissue-type plasminogen activator (tPA) and plasminogen activator inhibitor (PAI-1) (De Caterina et al., 2007a). In addition, ECs activated during inflammation contribute actively in the inflammatory status of the vascular tree by overexpressing multiple types of cell adhesion molecules and secreting cytokines and chemokines (Paulus et al., 2011) (Table 1.3). It is noteworthy that the vascular inflammatory

response is an important defence process which participates in tissue repair following infection or cell insult. Conversely, exacerbated or sustained inflammatory responses can cause tissue destruction. In addition, ECs regulate VSMC proliferation and differentiation by secreting several growth factors, such as IGF-1, PDGF, FGF, and TGF- β (Table 1.3).

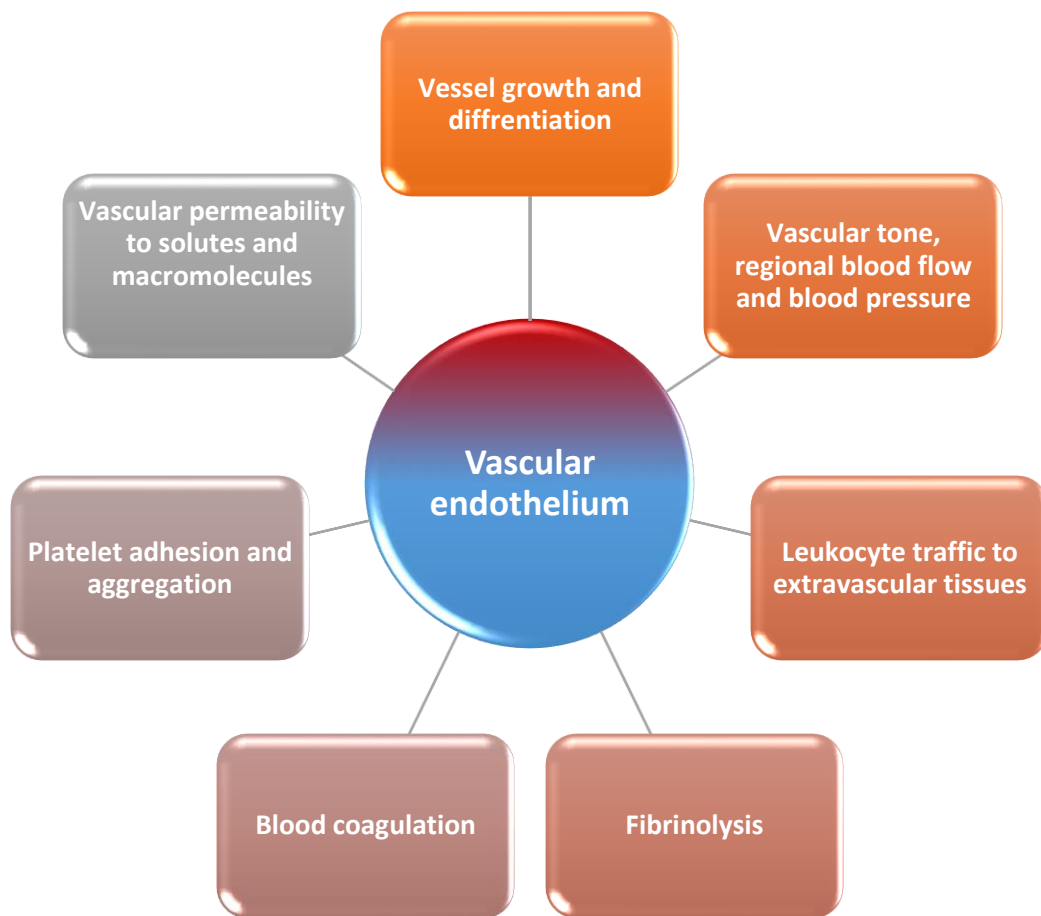


Figure 1.4 Regulatory functions of the vascular endothelium. ECs control key cellular processes involved in regulation of vascular relaxation/contraction, movement of solutes across the vascular wall, smooth muscle proliferation and processes related to coagulation (Pearson, 2000).

1.2.3 Endothelial cell activation versus dysfunction

Exposing ECs to a stimulus can trigger cell activation or injury. Injured ECs may become dysfunctional, although not all forms of injury lead to cell death. The two terms, “endothelial activation” and “dysfunction” in fact overlap. Activated ECs acquire a new synthetic phenotype capable of performing new functions (Pober and Min, 2006). Autacoids and cytokines are the most widely studied stimulators of endothelial activation such as IL-1, TNF- α (tumour necrosis factor) and histamine; in addition to bacterial endotoxin (lipopolysaccharide: LPS), viral infections, complement and immune complexes (Hunt and Jurd, 2002).

An example of overlap in endothelial reactivity following stimulation, is the response to the proinflammatory cytokine, TNF α . ECs activated with TNF α exhibit new surface adhesion molecules and secrete certain cytokines (Unger et al., 2002). Depending on the context, pathological excess of TNF α (for example in septic shock) may also cause injury, dysfunction or even trigger apoptosis (Mallat and Tedgui, 2000). In general, cell activation is thought to be more related to host defence which might be desirable in some situations, such as in wound healing or at an infection site (Pober and Min, 2006). On the other hand, endothelial dysfunction may occur during exposure of ECs to sub-lethal doses of certain harmful agents (Hunt and Jurd, 2002). For instance, chronic reduction of NO production in DM (Magenta et al., 2014). Collectively, endothelial dysfunction is considered as a wide term applied to disturbance in the homeostatic capacity of ECs.

Two types of endothelial activation have been recognised: type I which does not necessitate gene upregulation or protein synthesis, such as in release of pre-formed vWF and P-selectin expression; whereas, type II needs a period of time for the activation mediator to exert its effect as in TF expression in cultured ECs which takes 4–6 h to develop. Similarly, regulation at the gene transcription level is mandatory for activation that involves ICAM, VCAM-1, E-selectin, IL-1, IL-6, IL-8 and MCP-1. Overall, the consequences for endothelial activation of any types include: loss of vascular integrity, expression of leukocyte adhesion molecules, secretion of proinflammatory cytokines, prothrombotic behaviour and upregulation of HLA proteins. (Hunt and Jurd, 2002).

1.2.4 Hyperglycaemia and vascular dysfunction

Diabetes leads to deleterious chronic changes in the vascular system (Figure 1.1). Among these long-term complications, endothelial dysfunction appears to be a common feature. In fact, endothelial malfunction precedes the development of overt macro- or micro-vasculopathy in DM (Stehouwer et al., 1997). It has been observed that the level of HbA1c positively correlates with markers of endothelial injury (el Khawand et al., 1993).

As discussed in Section 1.1.4, hyperglycaemia is considered the primary trigger for diabetes-related vascular damage. The main tissues affected by hyperglycaemia are the kidney, eye and peripheral nerves and are especially vulnerable to diabetes-related problems because they are inefficient in autoregulating their glucose uptake when exposed to excess extracellular concentration of glucose (DeFronzo et al., 2015, Brownlee, 2005). From the metabolic point of view, glucose enters ECs via insulin-independent glucose transporter-1. Despite being in an oxygen-rich environment, ECs are highly glycolytic in nature, opting for aerobic glycolysis rather than oxidative phosphorylation for energy production (Eelen et al., 2015). During hyperglycaemia, metabolic stress ensues, as ECs are unable to tightly regulate their glucose transporter activity, leading to high glucose concentration in the cytosol. This is opposite to the situation in SMCs for example, where glucose load elicits an adaptive response through modulation of glucose transport activity (Kaiser et al., 1993).

At the molecular level, several mechanisms have been proposed to elucidate the aetiology of hyperglycaemia-induced vascular dysfunction (Figures 1.5). These include increased polyol pathway, increased hexosamine pathway, activation of the protein kinase C (PKC) pathway, increased oxidative stress, and formation of advanced glycation end products (AGEs) (Figure 1.5) (Saad, 2018). A 'unifying mechanism' has been proposed by Brownlee (2005) for the pathogenesis of diabetic complications; it relates all the cellular events induced by hyperglycaemia to the excessive free radical production from the mitochondrial electron transport chain. Hyperglycaemia-induced oxidative stress activates the DNA repair enzyme, poly-ADP-ribose polymerase (PARP); in turn, PARP inhibits the pivotal glycolytic enzyme GAPDH (glyceraldehyde 3-phosphate dehydrogenase). As a result, a stalling of the normal glycolytic flux happens, shifting the

upstream metabolic intermediates of glucose to other (normally minor) unfavourable pathways i.e. polyol and hexosamine biosynthesis pathways, as well as, formation of AGEs, increased ROS production and eNOS uncoupling (Eelen et al., 2015).

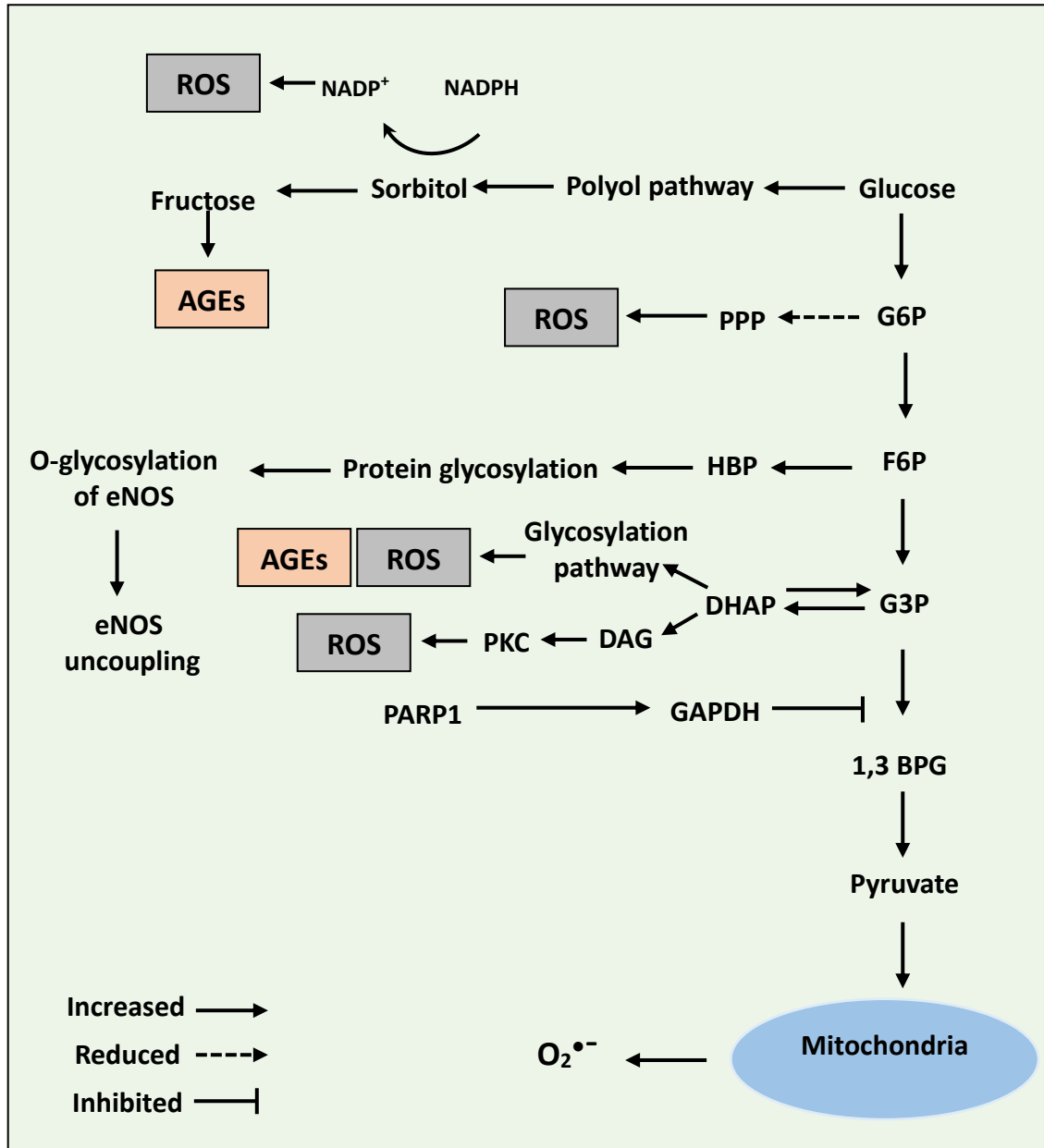


Figure 1.5 Hyperglycaemia disturbs normal metabolic pathways in ECs. During hyperglycaemia episodes, mitochondrial stress favours generation of excessive ROS and AGE formation. HBP, hexosamine biosynthetic pathway; PPP, pentose phosphate pathways; PARP1, poly-ADP-ribose polymerase; G6P, Glucose 6-phosphate; F6P, fructose-6-phosphate; G3P, glyceraldehyde 3-phosphate; GAPDH, glyceraldehyde 3-phosphate dehydrogenase; NADPH, reduced nicotinamide adenine dinucleotide phosphate; DHAP, dihydroxyacetone phosphate; DAG, diacylglycerol; PKC, protein kinase C; O₂^{•-} superoxide; AGEs, advanced glycation end products; ROS, reactive oxygen species. Adapted from (Saad, 2018).

1.2.4.1 Bioavailability of nitric oxide

A characteristic hallmark in DM is reduced endothelium-dependent relaxation in different vascular sites. This is thought to be largely related to increased oxidative stress. In such an oxidative environment, eNOS generates superoxide instead of NO due to eNOS uncoupling (Magenta et al., 2014). In addition, generated superoxide in the vasculature reacts with NO to form the toxic oxidant, peroxynitrite (Radi, 2004). Several factors are involved in diminished NO level in DM such as: decreased eNOS expression, oxidation of eNOS cofactors, and suppression of eNOS phosphorylation at an activating phosphorylation site, while promoting phosphorylation at an inhibitory site. In addition, eNOS inhibition occurs by the endogenous ADMA, an L-arginine analogue that competes with arginine at the catalytic centre of eNOS (Shi and Vanhoutte, 2017, Eelen et al., 2015) (Figure 1.3).

1.2.4.2 Adhesion molecule expression

A considerable body of evidence has shown that the level of soluble adhesion molecules expressed by the endothelium is elevated in plasma of diabetic patients (Tooke et al., 2002). Regardless of the DM type, the concentration of plasma E-selectin elevates in diabetic people; whereas, an increment in ICAM-1 level occurs mostly in patients with T2DM. Moreover, the levels of plasma E-selectin and HbA1c positively correlates, suggesting a specific role for E-selectin in DM (Cominacini et al., 1995). The elevation in the expression level of adhesion molecules in ECs results from activation of the transcription factor, NF- κ B. In hyperglycaemia settings, PKC activates NF- κ B; in turn, NF- κ B stimulates target proinflammatory genes that promote the expression of adhesion molecules (Brownlee, 2005).

1.2.4.3 Aberrant angiogenesis

The growth of new blood vessels is controlled by the balance between pro-angiogenic and anti-angiogenic factors (Table 1.3). Vascular endothelial growth factor (VEGF) is a potent angiogenic and vascular permeability agent. Disturbance in VEGF protein and mRNA levels has been observed in both micro- and macro-vascular beds of diabetic people. In some tissues like eye and kidney, VEGF exerts a pathologic angiogenic effect, while low levels of VEGF in other tissues exacerbates disease progression as in diabetic

cardiomyopathy, impaired wound healing and peripheral neuropathy (Wirostko et al., 2008). In hyperglycaemic settings VEGF expression is increased in ECs (Lansdown et al., 2014) and high serum VEGF levels have been observed in diabetic patients (Shi and Vanhoutte, 2017). Changes in VEGF levels in hyperglycaemia have been attributed to PKC activation (Geraldès and King, 2010). Alternatively, diabetes-induced tissue ischaemia also has been suggested as a stimulator for VEGF release (Hoeben et al., 2004).

Conversely to VEGF action, vascular thrombospondin-1 (TSP-1) acts as an endogenous inhibitor of angiogenesis, promoting a quiescent and differentiated endothelial phenotype (Sheibani and Frazier, 1999). Previous human and experimental studies have demonstrated reduction in TSP-1 level in diabetic eye (Shin et al., 2014). Moreover, exposing human dermal microvascular ECs to excess glucose downregulates TSP-1 expression (Sheibani et al., 2000). Diminished TSP-1 levels might permit uncontrolled proliferation of ECs in some diabetic tissues.

Overall, aberrant angiogenesis in the microvasculature of diabetic people contributes to the adverse complications of DM. Thus, therapies that antagonise the action of VEGF are under evaluation in clinical trials to treat diabetic retinopathy (Wirostko et al., 2008).

1.2.4.4 Non-enzymatic glycation

Abundance of glucose in the diabetic vasculature elicits non-enzymatic glycation of proteins and lipids, leading to AGE formation (Figure 1.5). Several pathological sequelae result from AGE accumulation, which occur either by direct alteration of protein structure and function or by cross-linking action: in the endothelium, AGEs quench NO activity, amplify ROS generation, upregulate the expression of adhesion molecules, and promote synthesis/secretion of pro-inflammatory cytokines by upregulating NFκB while shifting the endothelial balance toward a procoagulant state as reviewed in (Nowotny et al., 2015 346). Binding of AGE to their receptors, RAGE, augments vascular leakage, while stimulating SMC proliferation and migration (Yamagishi et al., 2009). AGEs also damage the blood vessel wall by increasing the cross linking of collagen, disrupting the binding sites for matrix metalloproteinase (MMPs) in the extracellular matrix (ECM),

thus limiting the turnover of ECM proteins. In addition, they impair binding sites for receptors that mediate cell-matrix interaction i.e. integrins (Voziyan et al., 2014). Currently, there is a growing interest in developing agents that halt AGE formation or bind to their receptors to tackle diabetes-induced complication (Martin et al., 2003).

1.2.4.5 Matrix protein production

Excessive generation of ECM proteins, such as collagen, in the endothelium may result from abnormal cellular metabolic activity or shear pressure (Tooke et al., 2002). The primary function of ECM is providing a structural support for cells; in addition to its pivotal roles in mediating the communication between cells. The environment of ECM is dynamic with continuous synthesis/degradation of its components. In the pathological condition of DM, hyperglycaemia causes overproduction of DAG which activates PKC (Figure 1.5). Consequently, one of the adverse effects of PKC activation is amplified ECM protein production (Geraldes and King, 2010). The proteins of ECM also represent a potential site for glycoxidative modifications because of their slow turnover rate compared to proteins in the circulation; combined with low level of antioxidant defence in ECM (Voziyan et al., 2014).

Deposition of AGEs in ECM causes stiffness of the vascular wall, thereby increasing the risk of developing cardiovascular accidents (Intengan and Schiffrin, 2001). ECM turnover is tightly controlled through a set of MMPs and their inhibitors, the tissue inhibitors of metalloproteinase (TIMPs). Multiple lines of evidence have shown that the MMPs/TIMPs equilibrium is disturbed in DM (Kadoglou et al., 2005). One important growth factor that governs ECM protein synthesis and degradation is TGF- β . Increased AGE level in DM upregulates TGF- β expression (Rumble et al., 1997). Consequently, ECM expansion that accompanies diabetic vasculopathy can result from increased formation of matrix proteins and/or their diminished break down.

1.2.5 Hyperphosphataemia and endothelial dysfunction

1.2.5.1 Phosphate

Phosphate is present in the human body either in organic (e.g. ATP) or inorganic (Pi) forms. The inorganic form in circulation is almost exclusively orthophosphate ($\text{HPO}_4^{2-}/\text{H}_2\text{PO}_4^-$) and the terms “inorganic phosphate”, Pi and orthophosphate are therefore

used interchangeably. Phosphate is an essential dietary constituent and is involved in many fundamental physiological functions, such as buffering action, preserving the skeleton and regulating many vital cellular functions. Examples of the cellular processes controlled by phosphate are: DNA synthesis, contributing to cell membrane structure, energy metabolism and transducing cellular signals that are mediated either via phosphorylation or dephosphorylation of proteins (Bevington et al., 1992, Hong et al., 2015).

The physiological concentration of Pi in blood plasma in humans is 0.8-1.5mM which is mainly regulated by the fibroblast growth factor 23 (FGF23)-Klotho axis, parathyroid hormone (PTH) and calcitriol (the active form of vitamin D); while, the main organs involved in Pi homeostasis are the kidneys, bone, intestine and parathyroid gland (Bevington et al., 1990, Gross et al., 2014).

1.2.5.2 Hyperphosphataemia and cardiovascular risk

Hyperphosphataemia is a common biochemical abnormality in serum of chronic kidney disease (CKD) patients especially at end-stage CKD. The progressive loss of kidney nephrons in CKD causes a variable degree of Pi retention, thereby elevating Pi levels in plasma and causing hyperphosphataemia (Bevington et al., 1990). Other conditions that might lead to hyperphosphataemia are those associated with large scale tissue destruction (Bevington et al., 1990). It is noteworthy that an unhealthy lifestyle and high consumption of a Western diet rich in Pi exposes the human body chronically to high postprandial Pi levels (although it might be subclinical or transient, and hence undetectable by conventional serum testing). Nevertheless this may cause cumulative long-term pathological consequences in the community (Ellam and Chico, 2012).

Significant perturbation to Pi homeostasis has been suggested as a risk for CVD. In fact, observational studies have shown that high Pi levels (even without exceeding the normal range) correlate with cardiovascular morbidity and mortality in CKD patients as well as in the general population. For instance, in the Framingham Offspring cohort study participants with normal estimated renal function and without history of clinical CVD disease, were followed up for 20 years. Higher serum levels of Pi were associated with an increased CVD risk in a continuous manner: for each 1 mg/dl increase in serum

Pi within the normal range, there was 31% increment in the adjusted incidence of CVD (Dhingra et al., 2007). Similarly, in a large-scale study of patients with previous coronary artery disease and serum Pi levels within the normal range, it was found that baseline serum Pi level was associated with adjusted risk of all-cause death (Tonelli et al., 2005). Moreover, in apparently healthy volunteers, high quantities of dietary Pi that increase serum Pi close to the high-normal limit were associated with temporary reduction in FMD of the brachial artery as a measure of endothelial function (Shuto et al., 2009). Collectively, a considerable body of evidence is emerging that supports a relationship between increased serum Pi and adverse cardiovascular outcomes.

1.2.5.3 Diabetic kidney disease

Diabetic kidney disease (DKD) is one of the serious microvascular complications of DM, affecting 25% to 40% of diabetic patients. DKD has been recognised as the leading cause of end-stage renal disease (ESRD), and cardiovascular morbidity and mortality worldwide (MacIsaac et al., 2014). Classically, the term diabetic nephropathy has been used to describe DM-induced renal injury. The disease initially displays glomerular hyperfiltration, then progressive albuminuria and declining glomerular filtration rate (GFR), and eventually culminating in ESRD (MacIsaac et al., 2014). Alternatively, the term DKD refers to all CKD found in patients with DM, including that which does not conform to the classical appearance diabetic nephropathy (Park, 2014).

Hyperglycaemia, hyperlipidaemia and insulin resistance initiate changes at multiple axes in the kidney, e.g. hemodynamic, metabolic, epigenetic, inflammatory and fibrotic alterations. These changes activate several intracellular signalling and transcription pathways leading ultimately to distinct structural changes in the kidney (Alicic et al., 2017, Badal and Danesh, 2014).

Disturbances in electrolyte and acid–base balance are also manifest in DM. Hyperphosphataemia is one of the changes that becomes evident at an advanced stage of DKD due to impaired dietary Pi clearance by the kidney (Bevington et al., 1990). In addition to vascular calcification, high Pi levels impose a significant burden on the human body including systemic inflammation and enhanced activation of renal renin-angiotensin system (RAS). In a study cohort of patients with T2DM having normal or

near-normal kidney function, it was found that elevated baseline or averaged (4.8 years) fasting serum Pi was associated with cardiovascular death independent of other potential confounders (Chonchol et al., 2009).

At the molecular level, increased mitochondrial oxidative stress has been recognised as an important initiating factor for DKD (Badal and Danesh, 2014). Features of metabolic disturbance resulting from hyperglycaemia or hyperphosphataemia are associated with enhanced oxidative stress and impaired mitochondrial function, promoting cellular disorders (Bevington et al., 1990, Brownlee, 2005). More specifically, animal studies of DKD have shown that endothelial dysfunction and loss of fenestrations represent an early event in DKD development (Qi et al., 2017).

1.2.5.4 Mechanism of phosphate-induced endothelial dysfunction

Hyperphosphataemia is a feature of CKD which leads to vascular toxicity either by direct or indirect mechanisms. Vascular calcification and endothelial dysfunction are the main direct negative effects of hyperphosphataemia on the vasculature, while the indirect effect is mediated via abnormalities in the phosphate-regulating hormones (Ellam and Chico, 2012). Collectively, multiple lines of evidence have shown that high extracellular Pi generally stimulates protein phosphorylation in various cell types. There is no convincing evidence that Pi directly activates protein kinases, but protein dephosphorylation is inhibited by direct action of Pi on phosphoprotein phosphatases (Abbasian et al., 2015) and this may lead to secondary activation of some kinases. Consequently, high Pi modulates intracellular signal transduction systems, decreases NO production, increases ROS generation and stimulates the apoptotic pathway (discussed below).

High levels of Pi stimulate mitochondrial oxidative phosphorylation, causing an increase in ROS formation. In addition, Pi enhances mitochondrial permeability transition, leading to necrosis or apoptosis. Longer duration of oxidative stress causes DNA damage, cell cycle arrest and cellular senescence (Hong et al., 2015). Stimulation of NADPH oxidase has also been suggested as a mediator for Pi-derived oxidative stress (Gross et al., 2014). *In vitro* culturing studies have shown that raising the Pi concentration of regular cell culture medium (1mM Pi) by 1-2mM, especially in absence

of serum, results in formation of insoluble crystals of Pi and calcium (Sage et al., 2011), suggesting that insoluble calcium-phosphate crystals may also contribute to the toxic effect of Pi. Calcium–phosphate crystals are endocytosed and trafficked to the acidic lysosomes, where they dissolve and release free calcium into the cytosol promoting cell apoptosis (Ewence et al., 2008).

Compared to the extensively-studied Pi effect on vascular calcification, evidence of Pi-induced endothelial dysfunction has only recently emerged. Pi loading resulted in impaired endothelium-dependent vasodilation of rat aortic rings. Exposing bovine aortic ECs to Pi load increased production of ROS through Pi influx across Na/Pi transporters, and decreased NO production via inhibitory phosphorylation of eNOS (Shuto et al., 2009). High Pi-induced activation of PKC contributes to phosphorylation of eNOS at an inhibitory site; in addition to promoting eNOS uncoupling (Gross et al., 2014). Furthermore, recent findings have shown that high Pi stimulates MP shedding from the EC surface (Di Marco et al., 2013, Abbasian et al., 2015). These MPs play an important role in endothelial cell activation and apoptosis (VanWijk et al., 2003) thus suggesting a direct interaction between Pi and the vascular cells.

Altogether, elevated Pi concentration impairs endothelial function at multiple levels. Estimation of serum Pi is not necessarily sensitive or frequent enough to predict early signs of vascular injury induced by fluctuating serum Pi level as seen with Western dietary habits. Thus, markers of endothelial function e.g. soluble adhesion molecules or NO production, in addition to novel biomarkers such as microRNAs or EMPs may provide a greater insight into vascular health at earlier points (discussed in Section 1.3).

1.2.6 Assessment of endothelial function

The most widely used non-invasive method for assessment of endothelial function is flow mediated dilatation (FMD). This method employs shear-stress to induce NO release from ECs (Celermajer et al., 1992). An alternative approach to evaluate endothelial function is by measuring the circulating markers of endothelial activity. Although estimation of certain markers in the circulation may not necessarily reflect the actual local situation in a tissue, measuring systemic marker provides important information about pathological perturbations. Accordingly, an array of adhesion molecules,

inflammatory cytokines, thrombogenic factors, indicators of NO level, and oxidative stress markers, serve as predictors of endothelial health and injury which can be monitored to highlight the endothelium status (Table 1.4).

Accurate direct measurement of NO levels in the circulation is not possible owing to its short half-life. However, NO can be estimated indirectly from the circulating amount of nitrite and nitrate which are more stable NO metabolites. The endogenous competitive inhibitor of eNOS, asymmetric dimethylarginine (ADMA), has been suggested as a marker of endothelial dysfunction. Higher levels of ADMA have been observed in diseases that associate with adverse cardiovascular outcomes, such as DM and dyslipidaemia (Lansdown et al., 2014). Endothelial activation elicits secretion of inflammatory cytokines and soluble adhesion molecules; therefore, their levels correlate with the magnitude of endothelial stimulus. Numerous studies have shown that the levels of these inflammatory molecules rise in cases associated with noxious cardiovascular events (Paulus et al., 2011). One common endothelial marker is the hemostatic cofactor vWF. The level of vWF associates with inflammatory activation of ECs, as well as reflecting endothelial damage (Paulus et al., 2011). For assessment of oxidative stress level in the vascular cells, 3-NT has been widely used as an independent biomarker for prediction of cardiovascular risk (Thomson, 2015). Elevated plasma 3-NT has been observed in various diseases: In diabetic patients, the level of 3-NT is positively correlated with plasma glucose concentration compared to undetectable level in healthy individuals (Ceriello et al., 2001)

Recently emerging markers, such as microRNAs may provide a powerful tool for assessment of endothelial function. microRNAs are a class of noncoding small RNAs which regulate gene expression by posttranscriptional repression. Multiple lines of evidence have demonstrated alterations in levels of certain microRNAs in vascular complications related to DM; whilst both increased and decreased expression of specific microRNAs has been recorded (Shi and Vanhoutte, 2017). Circulating endothelial progenitor cells (EPCs) are another useful measure which reflect an ongoing repair process in the endothelium. Estimation of their level in peripheral blood can be used to quantify the recovery competency of the vascular endothelium (Sabatier et al., 2009). Finally, plasma membrane microparticles (MPs) shed from the EC surface during cell

activation or apoptosis, represent an exciting new predictor of endothelial function (Hogas et al., 2010) (Discussed further in Section 1.3).

Table 1.4 Circulating biomarkers of endothelial function. Adapted from (Cines et al., 1998, Lansdown et al., 2014).
NO metabolites, i.e. nitrites
ADMA
Endothelin-1
Interleukins
Amyloid A
vWF
Adhesion molecules (VCAM-1, ICAM-1)
Selectins (E-selectin, P-selectin)
Plasminogen activator inhibitor- 1
Tissue plasminogen activator
Chemokines (IL-8, MCP-1)
C-reactive protein (CRP)
Nitro-oxidative stress markers such as nitrotyrosine, lipid radicals
Endothelial microparticles microRNAs
Circulating endothelial cells
Endothelial progenitor cells (EPCs)
Endothelial microparticles (EMPs)

1.2.7 Treatment of endothelial dysfunction in DM

Several pharmacologic interventions have shown improvement in endothelial dysfunction following their usage. Statins, insulin sensitizers, and ACE inhibitors are the main suggested therapies for restoring endothelial health (Lansdown et al., 2014). In addition, experimental data has reported beneficial outcome for supplementation with L-arginine, anti-oxidant vitamins, polyphenols or the AGE inhibitor: aminoguanidine (Magenta et al., 2014, Martin et al., 2003). Another promising agent for treatment of diabetic vascular complication, which is still under investigation, is C-peptide (discussed later in Section 1.4)

1.3 Role of MPs in the vasculature

1.3.1 Extracellular vesicles: definition

The generic term extracellular vesicles (EVs) includes various subtypes of cell-secreted, sub-micron, lipid bilayer structures that cannot replicate (Théry et al., 2018). During EV release many biologically active molecules such as enzymes, cytokines, bioactive lipids, proteins, mRNAs and noncoding RNAs are packaged into these vesicles (Jansen et al., 2016, Zu et al., 2015, Burger et al., 2017). Fusion of EVs with host cells permits transfer of genetic information that modulates the cellular activities of recipient cells (Jansen et al., 2017). Consequently, EVs are increasingly recognised as a means of intercellular communication.

The first description of EVs was by Chargaff and West (1946) who observed a sedimentable factor in platelet-free plasma that could enhance thrombin generation. By using electron microscopy, Wolf (1967) noted particles less than 1µm in diameter, termed “platelet dust,” shed from activated platelets and having procoagulant potential. Later, it was found that cells release membrane vesicles ubiquitously, and that this biological process is conserved amongst various species (Kulp and Kuehn, 2010).

Membrane-vesicles express antigenic molecules that reflect their precursor cell origin (Burger et al., 2011). Earlier views described EVs as passive debris that reflects cellular stress or as a disposal mechanism for redundant molecules (Abid Hussein et al., 2007).

However, newer ideas have identified EVs as active cell-cell messengers (Jansen et al., 2016). Compelling lines of evidence have shown that EVs selectively shuttle biomolecules from parent cells to other cells depending on the stimulus for their generation (Jimenez et al., 2003).

Three main forms of EVs are currently recognised (Table 1.5). Apoptotic bodies are membrane-surrounded fragments of cells undergoing apoptosis. The content of apoptotic bodies reflects their biogenesis process whereby nuclear material, proteins, RNA and cell organelles are packaged within these vesicles resulting in higher buoyant density compared to other EV subtypes. The size range of apoptotic bodies is 0.5-2 μ m and their membranes externalise phosphatidylserine (PS) and are permeable to propidium iodide as reviewed in (György et al., 2011).

Another subset of EVs are MPs with a size ranging between 100-1000nm. They form via direct outward budding of the plasma membrane. MPs enclose cytosolic proteins and RNA and expose PS on their surface as reviewed in (VanWijk et al., 2003). (See the next section).

Exosomes are smaller vesicles (30-150nm), produced by inward membrane invagination and envelopment by the multivesicular body (MVB). Thereafter, MVBs either fuse with lysosomes or migrate to the cell membrane to release the vesicle contents into the extracellular milieu by exocytosis. Exosomes are discriminated from MPs or apoptotic bodies by their expression of endosomal sorting proteins such as tumour susceptibility gene 101 (TSG101) and Alix, and tetraspanin proteins involved in endosomal vesicle trafficking (CD9, CD63 and CD81) as reviewed in (Shao et al., 2018).

Overall, the field of EV nomenclature is continuously evolving. Currently there is no consensus on EV terminology based on their biogenesis process i.e. endosome-derived (exosomes) or plasma membrane-derived (microparticles/microvesicles) due to absence of specific markers for each subset and the significant overlapping in their size (Théry et al., 2018). The last position statement from the International Society for Extracellular Vesicles (ISEV, <http://www.isev.org>) recommended using operational terms to describe EV subtypes that indicate biophysical properties such as size, density or biochemical composition rather than using conventional terms such as exosomes or

microparticles. Alternatively, if using these terms is unavoidable, a clear definition of the term used should be stated (Théry et al., 2018).

However, the classification of EVs into three broad classes, namely, exosomes, microvesicles and apoptotic bodies is still widely accepted within the scientific community (Shao et al., 2018). Of note, the terms microparticle/microvesicle refer to the same EV subset, and the term microvesicle has been suggested to replace microparticle to make it more distinguishable from other forms of microparticles such as biopolymer particles (György et al., 2011).

For the purposes of this thesis, the term microparticle (MP) is applied to EVs that have a size range between 100nm-1000nm. This EV subset represents vesicles shed directly from the plasma membrane and it is the main focus of the current work (Table 1.5).

Class	Size (nm)	Subcellular origin	Markers
Exosomes	30 – 150 nm	Multivesicular bodies	tetraspanins, Alix, TSG101
Microparticles/ microvesicles	100 – 1000 nm	Plasma membrane	PS, integrins, selectins, CD40
Apoptotic bodies	500-2000 nm	Plasma membrane, endoplasmic reticulum	PS, genomic DNA

Table 1.5 Classification of extracellular vesicles based on their biogenesis and size. Adapted from (Ling et al., 2011).

1.3.2 Microparticles: formation and fate

Generation of MPs from the cell surface can be instigated by a number of factors, such as cytokines, thrombin, LPS, calcium ionophore, and high shear stress as reviewed in (VanWijk et al., 2003).

In vitro studies have revealed that the process of MP formation is associated with elevation in cytosolic Ca^{2+} , following cellular activation or apoptosis (Figure 1.6). Elevated Ca^{2+} interferes with enzymes and other proteins that are responsible for maintaining the plasma membrane integrity and phospholipid asymmetry. Under normal conditions, the outer leaflet of the membrane bilayer is enriched with phosphatidylcholine and sphingomyelin, while PS and phosphatidylethanolamine are specifically sequestered in the inner leaflet. The bidirectional movement of lipid across the plasma membrane is regulated by ATP-dependent pumps: inward pump (flippase) and outward pump (floppase); in addition to lipid scramblase that controls the random distribution of lipid across the membrane. Upon cell activation, elevated intracellular Ca^{2+} stimulates scramblase resulting in redistribution of membrane lipids and PS externalization. Moreover, cytosolic Ca^{2+} activates Ca^{2+} -dependent protease, calpain, which degrades components in the cytoskeleton, thereby facilitating outward vesicle blebbing as reviewed in (Morel et al., 2011).

Calpain-independent mechanisms of MP generation have also been suggested (Figure 1.6). In ECs, activation of Rho-associated protein kinases (ROCKs) appears to be pivotal in MP formation (Burger et al., 2011). The Rho family of small GTPases are key regulators for cytoskeletal rearrangement as in cell migration, contraction and growth (Ridley, 2001). Activation of certain components of the Rho family is cell stress or cell lineage-dependent. In human microvascular ECs (HMEC-1), thrombin induces MP generation in absence of cell death. Caspase-2 mediated activation of ROCK II, a Rho kinase isoform, has been implicated in MP formation (Sapet et al., 2006). In coronary artery ECs, blocking the Rho/Rho kinase pathway suppresses MP release by impairing actin cytoskeleton organisation (Tramontano et al., 2004). Caspase-3 mediates cleavage of ROCK I and induces cell membrane contraction by myosin light chain phosphorylation in the Jurkat T-lymphocyte cell line (Sebbagh et al., 2001).

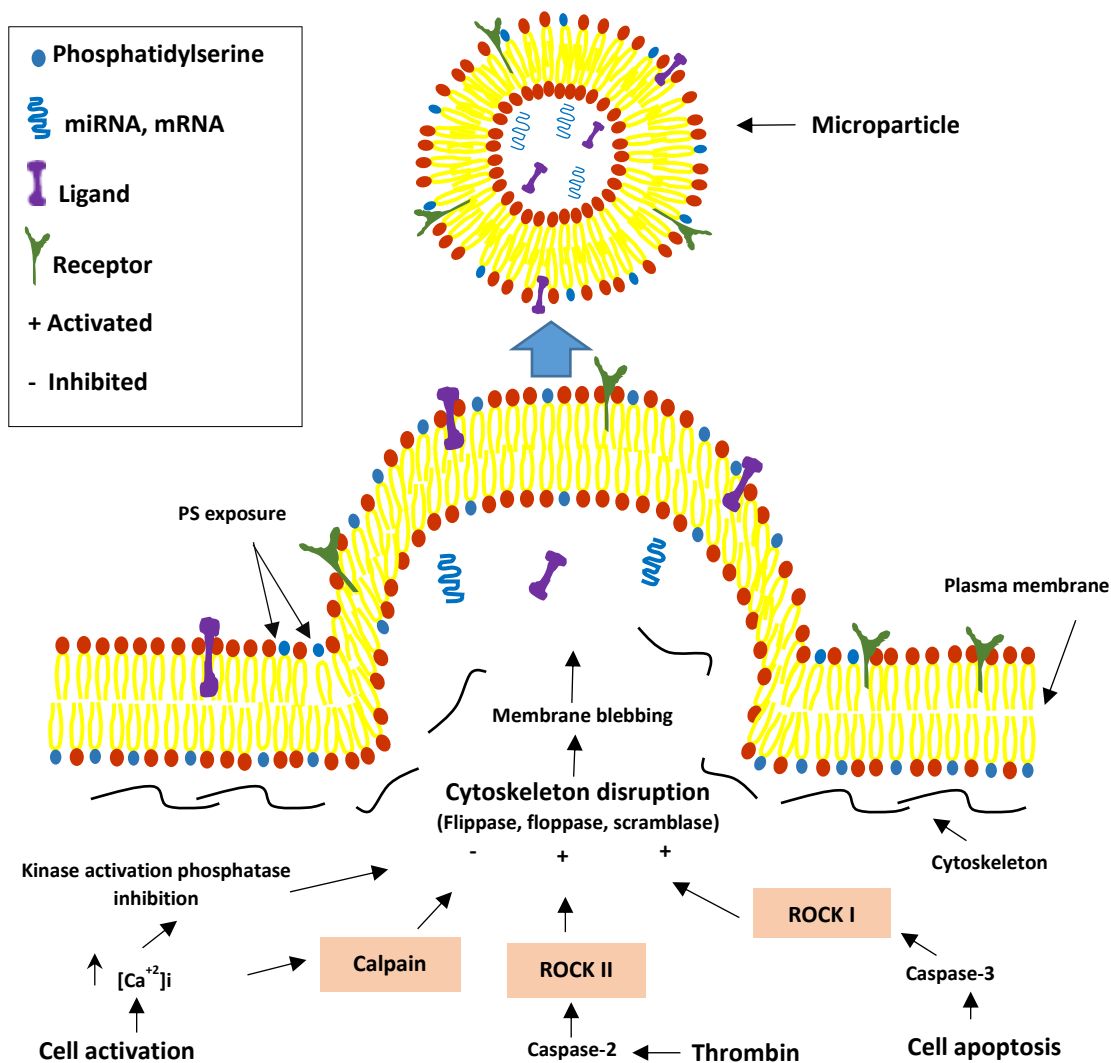


Figure 1.6 Schematic representation of the events involved in MP generation during cell activation or apoptosis. Under cell activation, elevated cytosolic Ca^{2+} activates scramblase leading to loss of membrane phospholipid assembly. Concomitantly, Ca^{2+} -dependent calpain triggers the breakdown of anchoring proteins which facilitates MP budding. During apoptosis, cleaved caspases induce ROCK activation, leading to cytoskeleton disruption and MP shedding. ROCK, Rho kinase. Adapted from (Shao et al., 2018).

The fate of MPs and the means of their clearance from body fluids are largely unknown. Nonetheless, several potential mechanisms have been proposed including engulfment by phagocytes due to altered-self recognition, whereby PS exposure tags MPs for elimination by the immune system (Schlegel and Williamson, 2001). Complement opsonisation by C3b has also been suggested (Flaumenhaft, 2006). Alternatively, degradation by circulating phospholipases, such as phospholipase A2 may also be involved (Fourcade et al., 1995).

1.3.3 Role of MPs in cell-cell communication

Compelling evidence have shown that a wide array of bioactive molecules is loaded within MPs, which reflects the cellular activity of the parent cells (Holnthoner et al., 2017). Compared to exosomes, the mechanism involved in trafficking of selective molecules into a MP, is less defined. However, the Vesicle Associated Membrane Protein 3 (VAMP3) (Clancy et al., 2015) and ADP Ribosylation Factor 6 (ARF6) (Muralidharan-Chari et al., 2009) have been implicated in sorting biomolecules into MPs. Encapsulation of proteins, nucleic acid and lipid inside the membranous structure of MPs protects these substances from degradation by extracellular enzymes (Hunter et al., 2008). Upregulation/downregulation of genes occurs subsequent to MP interaction with the plasma membrane of acceptor cells (Jansen et al., 2015). Over recent years, a host of studies has been published concerning MP content, culminating in the development of online field-specific databases for MP proteome and transcriptome, such as Vesiclepedia (<http://www.microvesicles.org/>). In addition, these proteomic studies have revealed that the diversity in EV size is reflected in their protein content (Kowal et al., 2016). Supportively, different levels of functional activities have been detected in MP subsets isolated according to their size (Holnthoner et al., 2017).

Various cell types can take up EVs including MPs. The mode of EV entry to target cell is influenced by the membrane composition and size of EVs (Caponnetto et al., 2017) as well as the type of the recipient cell (Lee et al., 2016). Although the means by which EVs cross the membrane of target cell is ill-defined, several mechanisms have been proposed. For instance, direct fusion of EVs with the plasma membrane of the invaded

cell followed by releasing of EV content (Parolini et al., 2009). Other reports have demonstrated the existence of EVs inside the acceptor cell (Burger et al., 2011). It has been suggested that EVs are internalised then trafficked either to endosomes to release their content or to lysosomes for degradation (Tian et al., 2010). Collectively, the capacity of MPs to work as a delivery vehicle may in principle open avenues for new therapeutic intervention.

1.3.4 Clinical significance of MPs

Lately, MPs have generated intense interest in multiple disciplines because of their promising clinical applications. The notion that their steady level in healthy people can be modulated in a variety of diseases (Burton et al., 2013) has opened new avenues for exploration of their use as surrogate diagnostic or prognostic biomarkers in diseases, as well as therapeutic tools or drug delivery vectors.

Membrane vesicles of heterogeneous cellular origin (e.g., platelets, monocytes, ECs, erythrocytes and granulocytes) have been shown to circulate in all bodily fluids of healthy individuals at certain levels (Yu et al., 2018). The most abundant type of MPs in the circulation are platelet-derived MPs (PMPs), representing 80% of the total number of circulating MPs (Connor et al., 2010). However, MP numbers are up or downregulated in pathophysiologic conditions such as during cell activation, or in other physiological processes like cell apoptosis, proliferation or differentiation as reviewed in (VanWijk et al., 2003). In the vascular system, diseases that change the rheology of the blood, such as atherosclerosis, have been associated with MP generation (Feng et al., 2010). Reduction in circulating MP numbers has also been observed in other pathological conditions (Castaman et al., 1997).

Over the past few years an accumulating body of evidence has demonstrated that MPs are involved in regulation of vascular inflammation, coagulation, angiogenesis and endothelial dysfunction (Burton et al., 2013, Holnthoner et al., 2017, Jing et al., 2017). Sustained increases in MP levels can be deleterious favouring adverse clinical outcomes (Jansen et al., 2016). Increased MP levels, especially PMPs, have been described in thrombotic and auto-inflammatory disorders, and in various cardiovascular diseases (Feng et al., 2010).

Despite the various detrimental effects of MPs in cardiovascular pathologies, a growing body of evidence highlights the beneficial effects of certain subtypes of MPs on vascular haemostasis and tissue repair. For instance, it has been found that endothelial MPs (EMPs) can promote anti-inflammatory (Jansen et al., 2015) and cytoprotective effects (Abid Hussein et al., 2007), or induce endothelial regeneration (Jansen et al., 2017). Generally, the procoagulant activity of MPs arises from PS exposure on their surface in addition to harbouring TF (Holnthoner et al., 2017). Several studies have demonstrated that EMPs counter vascular coagulation and promote fibrinolysis by exposing endothelial protein C receptor (Pérez-Casal et al., 2009) and urokinase-type plasminogen activator and its receptor (Lacroix et al., 2007). Altogether, it appears that MPs have a multifaceted nature, while their paracrine actions depend on the stimulus for their generation.

1.3.5 Role of MPs in diabetes and its complications

Concerning DM, a correlation between MP level and the pathogenesis of macro- and micro-vascular complications has been proposed, reinforced by the notion that MPs, including the EMPs, have pro-coagulant and inflammatory effects (Yu et al., 2018, Burger et al., 2017). Diabetes clinical studies showed that in patients with T1DM and T2DM, the level of circulatory EMPs is elevated (Jing et al., 2017, Sabatier et al., 2002). In addition, different MP profiles have been found according to the type of DM, while they correlate with the degree of glycaemic control (Sabatier et al., 2002). It is noteworthy that many of the reported observational clinical studies have addressed the effect of MPs in T2DM rather than T1DM (reviewed in (Deng et al., 2016)). Consequently, separating the direct effect of DM from insulin resistance might be perplexing since insulin resistance increases plasma MP level (Freeman et al., 2018). Supportively, the level of circulatory MPs in obese non-diabetic people, who are free from CVD, is significantly higher than in lean controls (Stepanian et al., 2013, Murakami et al., 2007).

On the other hand, previous studies have shown that the plasma level of EMPs positively correlates with the presence of macroangiopathy in diabetic people and it is the most significant compared to other traditional risk factors (Koga et al., 2005). While

exposing ECs to MPs isolated from diabetic people exerts proinflammatory effects and impairs EC angiogenesis (Jing et al., 2017), STZ-diabetic animals have shown significantly higher number of plasma MPs identified by PS exposure; whereas, infusing diabetic MPs into a normal blood vessel enhances leukocyte adhesion (Feng et al., 2019).

In DM complicated with microangiopathy, various MP patterns have been reported. For instance, it has been shown that patients with DKD have higher plasma level of MPs identified by PS exposure than healthy subjects; in addition, macroalbuminuric patients have significantly more circulatory MPs than normoalbuminuric patients (Yu et al., 2018). Interestingly, a positive correlation has been found as well between MP level, and uric acid and proteinuria; while, a negative correlation was seen with GFR (Yu et al., 2018).

The contribution of MPs in cell-cell communication is evident in numerous studies. For instance, Jansen et al (2016) have reported different miRNA expression patterns in circulatory EMPs isolated from diabetic patients compared to that of healthy individuals. Proteomic studies of high glucose-derived MPs have shown enrichment in proteins linked to distinct biological processes involved in oxidative stress, blood coagulation, cell signalling and immune cell activation (Burger et al., 2017); whereas, others have reported selective incorporation of the neurotoxin amyloid beta A4 protein in MPs generated under hyperglycaemic settings (Zu et al., 2015). In summary, elevated level of MPs in DM appears to have a pathogenic role; alternatively, it might be useful as a diagnostic or prognostic marker in diseases or aid in directing management plans.

1.3.6 Methods of MP analysis

Although substantial progress has been made in the MP field, the accompanying complexity and challenges remain noticeable. The heterogeneity of MP populations including variations in size and composition is reflected in the initial analytical steps (Ayers et al., 2011). Isolation and purification of MPs from biological samples holds difficulties due to overlapping with other biological and non-biological contaminants (Gyorgy et al., 2011). In addition, although wide varieties of equipment are available, each analytic method has limitations. For instance, methods that utilise light scattering properties suffer from the minute amount of scattered light by all nano-scale particles.

Fluorescence-based detection methods are limited by the number of copies of target antigen expressed on the MP surface as well as the optical background originating from the fluorescent antibody (Nolan and Duggan, 2018). Overall, selection of the analysis platform may be determined by the scientific question in conjunction with instrument availability.

1.3.6.1 Isolation of MPs

There is no consensus in the field of EV research on a gold standard protocol for the isolation and concentration of each EV subtype due to the significant overlap between these subpopulations (Théry et al., 2018). However, in the last position statement, ISEV has encouraged scientists to submit their methodological protocols to the online knowledgebase EV-TRACK (<http://evtrack.org>) to improve the transparency and reproducibility of experiments (Théry et al., 2018).

The importance of obtaining highly purified EV subpopulations has become more appreciated in recent years due to the notion that vesicle sizes influence the functional activities (Holnthoner et al., 2017). Various techniques are currently used such as ultracentrifugation, sucrose-gradient centrifugation, dialysis, co-precipitation, filtration, field flow fractionation, size-exclusion chromatography, immunoaffinity separation, magnetic bead and capture on beads or chips (reviewed in (Shao et al., 2018)). The choice of a certain isolation technique is determined by the sample volume and complexity; in addition to the down-stream applications, such as the requirement for high purity of the resulting preparation for proteomic analysis or enrichment of certain EV subtypes (reviewed in (Xu et al., 2016). Although each method has drawbacks and limitations, differential centrifugation appears as the most commonly used technique (Gardiner et al., 2016).

1.3.6.2 Quantification and characterisation of MPs

Standardisation of MP analysis is an area of controversy in this research field. As mentioned earlier, the variability between the published studies in the levels of MPs arises from their nanosize, diversity and lack of specific molecular markers (Chandler et al., 2011). This discrepancy has led to international efforts to standardise purification, quantification and characterisation of MPs to permit inter-laboratory comparisons

(Théry et al., 2018). Consensus statements and guidelines have been published by ISEV for the best practice and minimal experimental requirements for EV definition (Théry et al., 2018). Despite the current limitations in the methodology of MP detection and characterisation, different technologies have been implemented which rely either on the physical characters or on the biochemical composition of MPs, including electron microscopy, super-resolution microscopy, fluorescence correlation spectroscopy, atomic force microscopy, flow cytometry, Nanoparticle tracking analysis, dynamic light scatter, Raman spectroscopy, nuclear magnetic resonance, mass spectrometry and resistive pulse sensing. Numerous novel techniques are currently under development (reviewed in (Shao et al., 2018)).

Nanoparticle tracking analysis (NTA) is increasingly being used for quantification of MPs due its ability to detect particles as small as ~ 70 nm (van der Pol et al., 2014). Vesicular and non-vesicular particles are detected based on their Brownian movement and refractive index; while the concentration and size distribution is determined using a proprietary software (Gardiner et al., 2013). The variation in size estimated by NTA reaches $\sim 10\%$ while it becomes $\sim 70\%$ for estimating the concentration (van der Pol et al., 2014). Notably, the introduction of fluorescent NTA holds promises to improve the detectable range of the MP population although photobleaching remains an obstacle due to long analysis time (Gardiner et al., 2013).

On the other hand, flow cytometry (FCM) appears at the forefront in terms of phenotyping, versatility, availability, tolerance to polydispersity and for sizing purposes, especially for dedicated FCM (Welsh et al., 2017 27). In a recent survey, 90% of the respondents indicated using FCM for EV research (Valkonen et al., 2017). Generally, any flow cytometer platform integrates three systems, fluidics, optics and electronics (Figure 1.7). Particles in suspension pass in single file through a hydrodynamically-focused fluid stream. Upon illumination with a laser, the light scattered from each particle is collected at two angles: in line with the incident laser beam (forward scatter detector) and perpendicular to the laser beam (side scatter detector). Each detector produces electronic pulses proportional to the incident optical signals. In case of fluorescently labelled particles, the emitted fluorescent light is collected as well by different detectors (Shapiro, 2005).

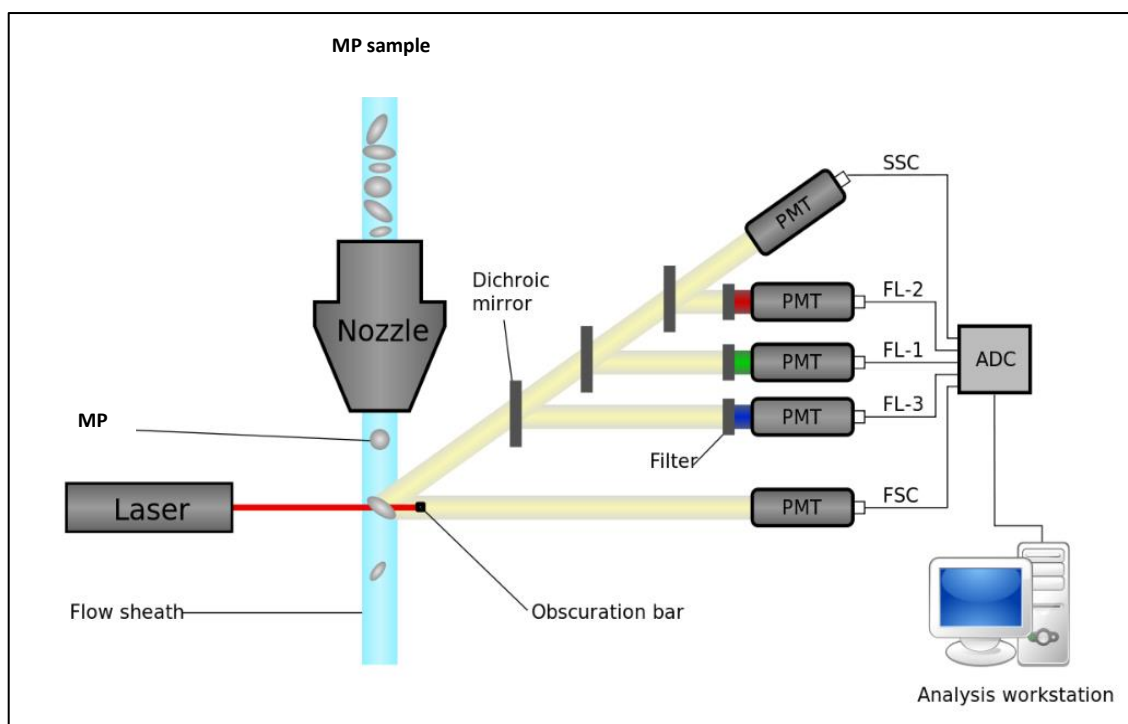


Figure 1.7 Schematic view illustrates the main parts of a flow cytometer. Samples pass through a hydrodynamically-focused sheath fluid. Upon illumination with a laser, the light scattered from each particle is collected at the forward (FSC) and side scatter (SSC) detectors. Emitted fluorescence is collected at the fluorescent channels (FL1, FL2, FL3) through a photomultipliers (PMTs). The dichronic mirror, optical filters and the obscuration bar are parts of the optical system. The scattered and emitted light signals are converted to electronic pulses via analogue-to-digital converter (ADC) for further analysis (Shapiro, 2005). The image is taken from https://en.wikipedia.org/wiki/Flow_cytometry.

The first obstacle in flow cytometric identification of MPs is the limited detection window (Robert et al., 2012). MPs scatter a minute amount of light due to their nanosize and low refractive indices; whilst, the flow cytometer performance is dependent on the amount of scattered and emitted light from any object (Welsh et al., 2017). Consequently, for nanoparticle applications, high sensitivity or dedicated small-particle flow cytometers are preferable (Tang et al., 2017).

Secondly, the scatter and fluorescent parameters collected by any flow cytometer are arbitrary units and instrument-dependent (Welsh et al., 2017); therefore, inferring the size of an object analysed by FCM is performed using materials of known size, such as synthetic beads (Erdrugger et al., 2014). However, the absence of accurate reference particles for size estimation of MPs hampers accurate size determination (Valkonen et al., 2017). The two commonly available bead types are polystyrene and silica beads; however, their refractive indices are higher than that of MPs (van der Pol et al., 2012). Beads of 400 nm have been shown to scatter the same amount of light to that of 1 μ m MPs and this is variable according to the flow cytometer design (Chandler et al., 2011). Recently, alternative approaches have been examined by using biological reference materials which potentially better reflect the chemical and physical properties of MPs (Valkonen et al., 2017). Thus, calibrating the flow cytometer for size measurement using synthetic beads should be considered as relative rather than absolute. In fact, the inherent problem in size determination by FCM has become more appreciated in recent years, which culminated in organizing of the most recent workshop by the Scientific Standardization Committee on Vascular Biology of the International Society of Thrombosis and Haemostasis (ISTH). In this workshop, the inter-laboratory reproducibility in measuring EV concentration was evaluated in 46 flow cytometers. Gating strategy depending on beads has been shown as a significant source of inconsistency between different FCM platforms, while suggestions have been made to convert the arbitrary scatter signal into a diameter unit to calibrate the flow cytometer for size measurement (van der Pol et al., 2018).

The other challenge in MP analysis by FCM is the variation in optical design between different FCM instruments i.e. collection angle and obscuration bar (Figure 1.7) (Shapiro, 2005), which impairs the inter-laboratory reproducibility (Poncelet et al.,

2016). Consequently, standardisation workshops have been held by ISTH to improve the reproducibility and reliability of the published results. Setting the analysis window using beads has been suggested to minimise the variability in measurement (Lacroix et al., 2010). Whereas, the difference in the optical configuration between SSC-oriented and FSC-oriented flow cytometers has been addressed more recently (Cointe et al., 2017, Poncelet et al., 2016). Moreover, a Flow Cytometry Work Group was initiated (www.evflowcytometry.org), in which members of the well-known scientific societies ISEV, ISTH and ISAC (the International Society on Advancement of Cytometry) have joined together aiming to standardize the detection of MPs by FCM.

Finally, in addition to the differences in flow cytometer performance discussed above, other variables in FCM analysis of nanovesicles, are sample preparation and labelling (Crompton et al., 2015). A common artefact specific to nanoparticles is “swarm detection” which happens more frequently in concentrated samples (van der Pol et al., 2012). The size of the fluidic system of any conventional flow cytometer is designed for analysing cells which allows many particles to cross the laser line simultaneously. Consequently, multiple vesicles are considered as a single entry (Welsh et al., 2017, Poncelet et al., 2015) (discussed further in Chapter 3).

In summary, emerging trends and promising strategies in calibration and standardisation of MP analysis by FCM may potentially permit their use for routine clinical laboratory investigation in the near future.

1.4 C-peptide

1.4.1 Background

Subjects with DM are at high risk of developing long-term complications, including CVD. Previous studies have shown that even strict glycaemic control does not fully halt the progression of diabetes-induced vascular complications (Section 1.1.4). The findings in these studies suggest the involvement of other contributing factors to disease development apart from insulin deficiency.

Insulin is synthesised in the pancreatic β -cells from its precursor, proinsulin. Subsequently, proinsulin is cleaved into insulin and its connecting peptide (C-peptide). When β -cells are stimulated, C-peptide is released in conjunction with insulin (Steiner

et al., 1967). Defective or destroyed pancreatic β -cells in patients with diabetes release little if any, insulin and C-peptide. Insulin is supplemented as part of treatment regimes in all patients with T1DM and many with T2DM, but C-peptide levels in diabetic patients with T1DM and in the later stages of T2DM remains deficient (Bell and Ovalle, 2006, Wahren et al., 2016).

Initially after its discovery by Steiner et al (1967), C-peptide was considered as an inert by-product of insulin metabolism (discussed below). However, the possibility that C-peptide may be a biologically active molecule was re-visited in the early 1990s. When patients with T1DM were treated with physiological concentration of C-peptide, a significant improvement in nerve conduction, peripheral circulation and kidney function was observed (Wahren, 2017). These earlier findings have provoked great interest in exploring the potential therapeutic implications of this peptide. Further consolidation of evidence for the beneficial effect of C-peptide has been generated throughout the last two decades, in which numerous molecular studies have recorded activation of multiple signalling pathways in different tissues by C-peptide (Hills and Brunskill, 2009). Collectively, C-peptide is now considered as an active biomolecule and a promising tool to combat the progression of vascular (and other) complications in diabetic subjects.

1.4.2 Structure and body pharmacokinetics

C-peptide is a 31-amino acid protein that links and stabilises A and B chains of proinsulin (Figure 1.8). During insulin biosynthesis in the pancreatic β -cells, proinsulin is cleaved into C-peptide and insulin (Steiner et al., 1967). Although secreted simultaneously and in equimolar concentrations, C-peptide and insulin differ in their pharmacokinetic properties. C-peptide maintains higher and more stable levels in the peripheral blood compared to insulin. In healthy individuals, the plasma C-peptide level ranges between 0.3-0.6 nmol/L under fasting conditions, whereas it rises to 1-3 nmol/L postprandially (Leighton et al., 2017). On the other hand, the basal plasma level of insulin (fasting) is less than 100 pmol/L, while the postprandial level peaks at 500-650 pmol/L (Warrell et al., 2010).

The half-life of C-peptide in the peripheral circulation is about 30 minutes compared to 3-5 minutes for insulin because insulin undergoes extensive hepatic first pass

metabolism with approximately 50% extracted by the liver. In addition, insulin is degraded and cleared also by the kidney, resulting in 0.1% excreted in the urine. In contrast, C-peptide escapes hepatic degradation and it is mainly metabolised and eliminated by the kidney. About 5-10% of secreted pancreatic C-peptide is excreted intact in the urine, thereby giving an alternative non-invasive method for measurement of its level (Leighton et al., 2017). As a result of the above features, measurement of C-peptide level has become a robust tool to estimate the residual β -cell function in clinical practice.

In regard to C-peptide structure, the mid-region of proinsulin comprises C-peptide (Figure 1.8). C-peptide consists of 31 amino acid residues, five of them are acidic in human C-peptide, while there are up to seven acidic residues in other species. In addition, basic and aromatic amino acids are absent in the C-peptide molecule except in a few species that have a single basic residue. This acidic property of C-peptide creates a negatively charged peptide having a hydrophilic nature. Moreover, the current available evidence does not reveal an ordered tertiary structure for this peptide under physiological circumstances; although the first 11 residues at the N-terminus of the C-peptide molecule can display an α -helical conformation under non-physiological condition (Johansson et al., 2002, Janabi, 2017).

C-peptide exhibits a wide structural variability among species. This feature resulted in neglect of C-peptide as a bioactive molecule because efficient biological mediators usually display interspecies conservation (Lu and Xu, 2006). However, this structural character of C-peptide does not exclude the possibility of having functional roles in the human body. In fact, other well-recognised bioactive mediators display similar structural diversity among different species, such as the peptide hormone relaxin, from the insulin superfamily. Nevertheless, C-peptide structure displays partial conservation in mammals, in which eight residues in the amino acid sequence are conserved to some extent in human C-peptide (Wahren et al., 2004).

Several trials addressed the functional element(s) in C-peptide structure. In a rat study, it was found that the C-terminal pentapeptide of rat C-peptide induces Na^+ , K^+ -ATPase activity in renal tubular segments to the same level as full-length C-peptide. However,

another study showed that effective stimulation of the extracellular signal-regulated kinase 1/2 (ERK1/2) signalling pathway requires the existence of conserved glutamic acid residues at positions 3, 11, and 27 of C-peptide, and the presence of α -helix forming residues in the N-terminal section. Collectively, the data presented in these studies suggest that the terminal portions of C-peptide molecules may hold the biological activity (Hills and Brunskill, 2008).

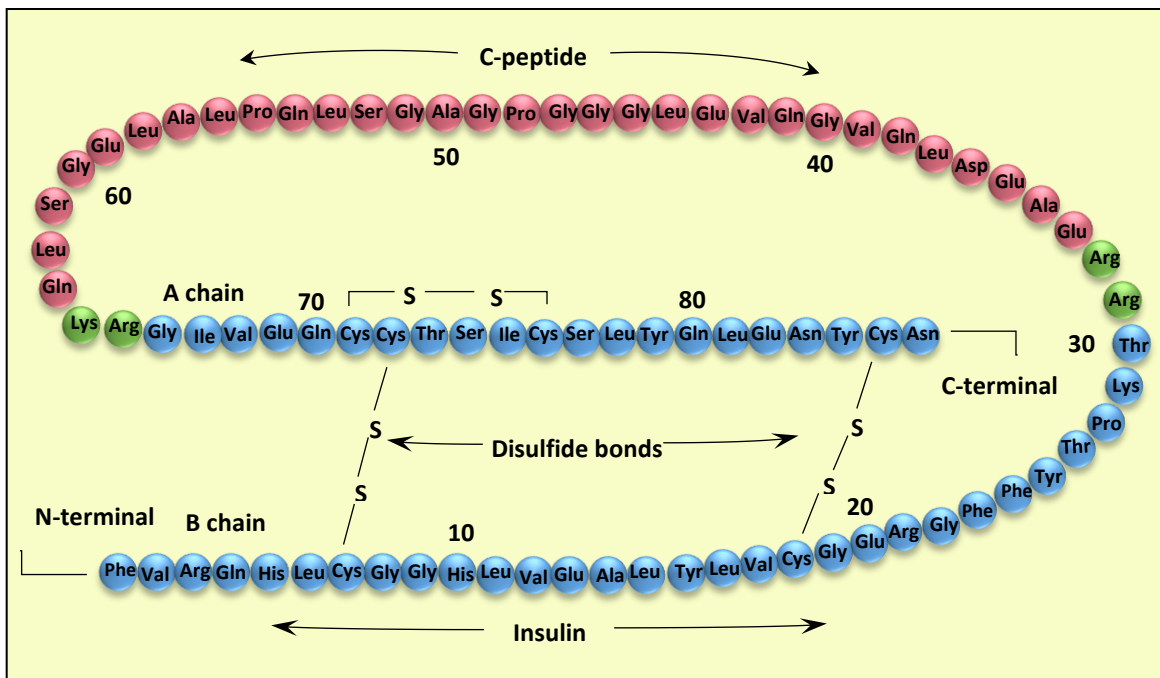


Figure 1.8 Covalent structure of human proinsulin. Post-translational cleavage of proinsulin by the proteolytic enzymes yields the mature insulin (blue circles) after excising the connecting peptide (C-peptide) (pink circles) and the basic amino acid pairs (green circles), i.e. lysine-arginine (Lys-Arg) and arginine-arginine (Arg-Arg). Insulin consists of A and B chains connected by disulphide bonds (Polonsky, 2012).

1.4.3 Evidence for C-peptide interaction with the cell membrane

C-peptide has the capacity to activate multiple signaling pathways in various tissues (discussed further in Section 1.4.4), however the exact mechanism for C-peptide binding/interaction with the cell membrane is poorly defined. Various efforts have been made to identify a receptor for C-peptide using several approaches. The earliest investigation was by Flatt et al (1986) utilised a radio-ligand binding technique (^{125}I -C-peptide) which revealed that C-peptide binds specifically and in a displaceable manner to the cell membrane of cultured pancreatic adenoma β -cells. Others have proposed a direct non-chiral interaction of C-peptide with cell membranes, which depends on a specific sequence of amino acids, although this hypothesis does not fit with the hydrophilic nature of the C-peptide molecule.

More recent experiments were performed using fluorescence correlation spectroscopy and showed stereospecific binding of rhodamine-labelled human C-peptide or (Rh-C-peptide) to the surface of various human cell types, such as renal tubular cells, dermal fibroblasts and ECs of saphenous vein. In these studies, displacement of fluorescent-labelled C-peptide happened when an excess of unlabeled full-length C-peptide or its C-terminal pentapeptide segment was added. Scrambled C-peptide, insulin, IGF-I and IGF-II were all unable to displace labelled C-peptide from cell membranes, suggesting specificity of the C-peptide interaction. In addition, this binding was significantly inhibited by pre-incubating the cells with pertussis toxin (PTX) (Rigler et al., 1999), indicating that C-peptide receptor might be a G α i-linked G-protein-coupled receptor (GPCR) or at least a G α i/o-coupled receptor. Numerous investigators have now confirmed that C-peptide binding and some downstream intracellular signaling are PTX-sensitive (Al-Rasheed et al., 2006, Maezawa et al., 2006).

Internalisation of C-peptide across the plasma membrane has also been reported. In aortic ECs and umbilical artery SMCs, internalization of AlexaFluor-labelled C-peptide results in initial localisation to early endosomes before termination at the lysosomes (Cifarelli et al., 2011b). Using confocal microscopy and Rh-C-peptide, internalization and localisation of C-peptide to the cytoplasm and to the nucleoli of Swiss 3T3 fibroblasts and human embryonic kidney cells (HEK-293) were reported (Lindahl et al., 2007). The

findings in these studies have shown that C-peptide modulates gene transcription and stimulates the expression of ribosomal RNA, suggesting an important role for C-peptide in regulation of cellular activities, such as cell growth and survival.

Most recently, Yosten et al (2013) have revealed a possible C-peptide receptor or a partner for the C-peptide receptor complex. These authors employed deductive ligand-receptor matching to identify a potential receptor. The orphan GPCR, GPR146, was found to mediate cFos mRNA expression elicited by 1 nmol/L C-peptide in HEK-293 cells, human gastric tumour cells (KATOIII) and human erythroleukemia cells (TF-1) cells. Co-localization of C-peptide and GPR146 was observed on the plasma membrane, whilst C-peptide stimulation mediated GPR146 internalisation, which is in agreement with general GPCR behavior upon ligand binding (Serge et al., 2011). In the same study, it was also found that siRNA-mediated knockdown of GPR146 blocks cFos transcription induced by C-peptide in KATOIII cells, an effect which was not reproduced when other orphan GPCRs were tested. However, the involvement of GPR146 in C-peptide mediated ERK1/2 signaling was not confirmed in a more recent study (Janabi, 2017). Altogether, encouraging data has emerged recently which might uncover the identity of the C-peptide receptor in the near future.

1.4.4 Intracellular signalling by C-peptide

Accumulating evidence has shown that C-peptide is a bioactive mediator (Brunskill, 2017). C-peptide exerts its effect by stimulating multiple signalling pathways in a variety of cell types. Intracellular pathways activated by C-peptide are summarised below:

1.4.4.1 Effects on Na⁺, K⁺-ATPase

Na⁺, K⁺-ATPase is an integral membrane protein that mediates ATP-dependent transport of sodium and potassium across the plasma membrane, thereby maintaining the electrochemical gradients inside versus outside cells (Hundal et al., 1993). Impaired Na⁺, K⁺-ATPase activity is a well-documented sequel in many tissues injured by DM, and it is linked to the pathogenesis of diabetic vascular complications. For instance, altered Na⁺, K⁺-ATPase function was observed in several tissues of diabetic rats; in addition, human studies have revealed that the activity of the Na⁺, K⁺-ATPase pump is reduced in RBCs of type 1 diabetic patients (Vague et al., 2004). On the other hand, previous

studies have demonstrated favourable effects for C-peptide replacement on Na⁺, K⁺-ATPase function. A significant increase in Na⁺, K⁺-ATPase activity of RBCs from patients with T1DM was observed following short-term C-peptide infusion, and the magnitude of Na⁺, K⁺-ATPase activation was significantly correlated with plasma C-peptide level (Forst et al., 2009). Similarly, *in vitro* incubation of diabetic RBCs with 6 nmol/L C-peptide restored normal Na⁺, K⁺-ATPase function (Djemli-Shipkolye et al., 2000).

Dysfunctional Na⁺, K⁺-ATPase pump was also reported in renal and nervous systems of patients with type 1 diabetes. *In vivo* and *in vitro* experiments have shown that attenuated Na⁺, K⁺-ATPase in hyperglycaemic conditions is amendable by C-peptide treatment. In diabetic animals, C-peptide restored Na⁺, K⁺-ATPase activity in renal tubule segments in a dose-dependent manner (Ohtomo et al., 1996). This effect was abolished by PTX pre-treatment and associated with an elevation in intracellular Ca²⁺ concentration [Ca]_i. Moreover, increased Na⁺, K⁺-ATPase protein expression was reported when human proximal tubular cells (PTCs) were treated with 1nmol/L C-peptide in presence of high glucose as well as in normal glucose concentrations (Galuska et al., 2011). Activation of PKC and ERK1/2 has been implicated in mediating this effect (Figure 1.9). In addition, restoration of attenuated neural Na⁺, K⁺-ATPase activity was observed in diabetic rats after C-peptide administration (Ekberg et al., 2007).

1.4.4.2 Effect of C-peptide on intracellular calcium [Ca²⁺]_i

Involvement of [Ca²⁺]_i in C-peptide intracellular signalling has been observed in multiple studies. Physiological levels of C-peptide caused a prompt and consistent increase in [Ca²⁺]_i in rat, opossum and human PTCs (Ohtomo et al., 1996, Shafqat et al., 2002, Al-Rasheed et al., 2004a). This effect was abolished when cells were pre-treated with PTX, indicating the dependency on a PTX sensitive G-protein-coupled receptor (Ohtomo et al., 1996).

The elevation in [Ca²⁺]_i following C-peptide stimulation is thought to be a consequence of calcium influx across the cell membrane rather than a release from the intracellular stores. C-peptide's effect on NO release from ECs was blocked by adding EDTA to the culture medium to bind extracellular calcium (Wallerath et al., 2003); however, EDTA may potentially chelate other metal ions required for C-peptide activity. By inhibiting

components in the intracellular signalling pathway of calcium, it was shown that C-peptide's effect on renal Na⁺, K⁺-ATPase activity is blunted (Ohtomo et al., 1996). Altogether, there is considerable evidence that modulation of [Ca⁺²] plays an important role in transducing signals generated by C-peptide.

1.4.4.3 Effect of C-peptide on ERK1/2 MAP Kinases

ERK1/2 is an essential subfamily of mitogen-activated protein kinases (MAPK) that regulates a wide range of cellular processes by phosphorylating specific serines and threonines of target protein substrates. Examples of physiological activities that are controlled by MAPK are: cell growth and differentiation, gene expression, metabolism, cell motility, cell survival and apoptosis (Lu and Xu, 2006).

At physiological concentrations, C-peptide activates ERK1/2 phosphorylation in a concentration-dependent manner in the Swiss 3T3 fibroblast cell line (Kitamura et al., 2001). This effect was blunted by pre-treatment with PTX or a MAPK inhibitor. Moreover, C-peptide activates ERK1/2 in capillary ECs of mouse lung (Kitamura et al., 2002). Similarly, in rat aortic ECs, C-peptide induces ERK1/2 phosphorylation, resulting in increased eNOS protein expression (Kitamura et al., 2003). In another study, C-peptide improved wound healing in diabetic mice and enhanced HUVEC migration via ERK1/2-mediated action (Lim et al., 2015). In opossum PTCs, C-peptide robustly stimulates ERK1/2 in a concentration-dependent manner (Al-Rasheed et al., 2004a). Notably, PKC-dependent translocation of the small GTPase, Ras gene homolog family member A (RhoA) to the cell membrane has been implicated in activation of one or several downstream components of the MAPK system (Wahren and Larsson, 2015) (Figure 1.9).

1.4.4.4 Effect of C-peptide on PI3K signalling pathway

The phosphatidylinositol 3-kinases (PI3Ks) are members of a distinct and conserved family of intracellular lipid kinases that phosphorylate the 3'-hydroxyl group of phosphatidylinositol and phosphoinositides. Activation of these kinases evokes a host of intracellular signalling pathways that control functions, such as cell metabolism, survival and polarity, and vesicle trafficking (Engelman et al., 2006).

Application of C-peptide stimulates PI3K signalling pathways in various cell types. Examples of these cells are: L6 myoblasts (Grunberger et al., 2001), opossum kidney cells (Al-Rasheed et al., 2004b), SHSY5Y neuroblastoma cells (Li et al., 2003b), swiss 3T3 fibroblasts (Kitamura et al., 2001), and CD4⁺ T-cells (Walcher et al., 2006). C-peptide-induced activation of PI3K is linked with several physiological functions including: enhanced T-cell migration (Walcher et al., 2006), increased neuronal growth (Li et al., 2003b), increased glycogen synthesis in skeletal muscle (Grunberger et al., 2001), and increased renal tubular cell proliferation and renal PPAR- γ activity (Al-Rasheed et al., 2004b),

1.4.4.5 Effect of C-peptide on eNOS

The vascular effects of C-peptide are mediated at least partly by the endothelial NO system. Several reports have shown enhanced NO release from ECs upon C-peptide treatment. In accord with this, human C-peptide increased NO liberation from bovine aortic ECs in a concentration- and time-dependent manner, which was associated with elevation in $[Ca^{2+}]_i$. At the same time, blockade of NOS activity in these cells abolished C-peptide action (Wallerath et al., 2003). However, in the aforementioned study, no effect for C-peptide on eNOS expression or phosphorylation was detected. Conversely, Giebink et al (2013) observed neither NO release nor Ca^{2+} influx in bovine pulmonary artery ECs upon treatment with up to 100nM human C-peptide. Interestingly, near doubling of NO production was observed when C-peptide-stimulated RBCs were pumped underneath the cultured ECs in a microfluidic device. RBC-derived ATP was suggested as an alternative indirect mechanism for NO liberation. Of note, ATP stimulates NO release from ECs by acting on its purinergic receptors (Burnstock, 2014). In contrast, C-peptide stimulates NO release from HUVECs in absence of RBCs in other studies (Lim et al., 2015, Bhatt et al., 2013). Furthermore, in a study reported by Kitamura et al (2003), rat aortic ECs treated with human C-peptide showed increased mRNA and protein levels of eNOS via ERK-dependent up-regulation of eNOS gene transcription.

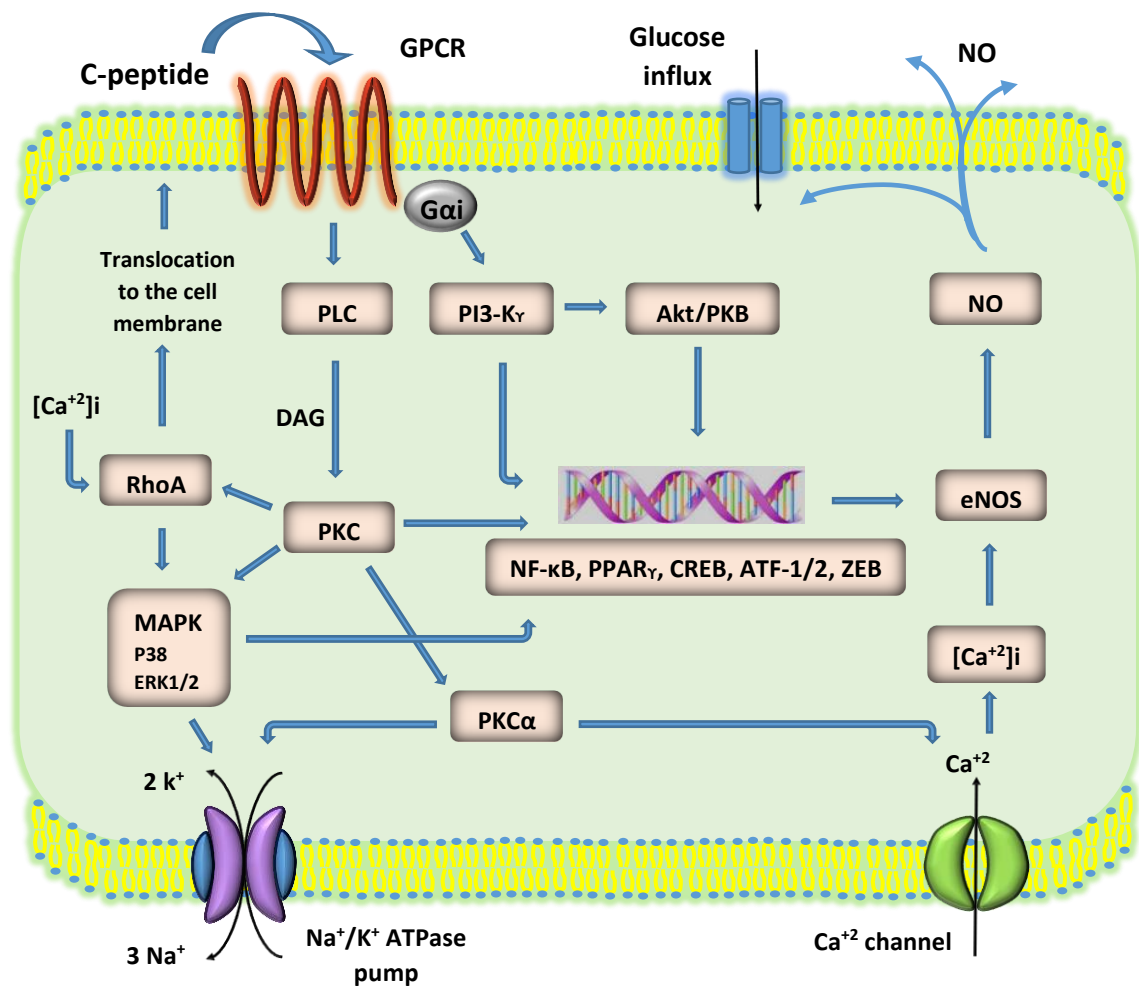


Figure 1.9 Proposed signaling pathways activated by C-peptide. C-peptide interacts with cell membranes in a G-protein-dependent manner. Stimulation of multiple cellular pathways ensues, such as PI3K and PLC (phospholipase C). Activation of PLC, in turn, activates PKC which stimulates MAPK pathway, RhoA and Ca²⁺ influx. Activation of MAPK and PI3K pathways also induces the transcription of several nuclear factors and promotes multiple cellular effects, such as reduced apoptosis and increased eNOS expression. CREB, cAMP-response-element-binding protein; ATF, activating transcription factor; ZEB, zinc finger E-box binding homeobox protein (Hills and Brunskill, 2009).

1.4.5 Biological effects of C-peptide

1.4.5.1 Effects of c-peptide on microvascular blood flow and haemorrhage

There is increasing evidence that the protective effects of C-peptide on diabetic microvascular complications are, at least in part, mediated through the modulation of microvascular blood flow. In this context, Lindstrom et al (1996), showed that infusion of C-peptide in isolated skeletal muscles of normal rats enhanced capillary recruitment by causing an active vasodilatation of the normothermic microvasculature. In another study, C-peptide evoked dilatation in skeletal muscle arterioles isolated from non-diabetic rat cremaster muscles. This effect was independent of C-peptide concentration and mediated via NO-related mechanism, and was observed only when C-peptide was administered along with insulin (Jensen and Messina, 1999). Physiological concentrations of C-peptide increased sciatic endoneurial blood flow in diabetic rats. Following enhanced endoneurial microvascular blood flow, the conduction velocity of both motor and sensory nerve fibres was improved, whereas, co-administration of a NOS inhibitor blunted all the observed changes (Cotter and Cameron, 2001).

Human studies have shown that during exercise, C-peptide restores defective forearm blood flow, capillary diffusion capacity, and glucose uptake in type 1 diabetic patients, without causing any additional effect to healthy subjects (Johansson et al., 1992). In further investigations, the author showed that C-peptide vasodilatory effect on skeletal muscle microcirculation is invoked by an NO-mediated mechanism (Johansson et al., 2003). In the skin microcirculation, short term infusion of C-peptide in type 1 diabetic patients improved microvascular skin blood flow by redistribution of blood flow from the subpapillary thermoregulatory to the nutritive capillary beds. Thirty minutes after discontinuation of C-peptide infusion, capillary skin blood flow returned to the previous level observed before the start of C-peptide treatment. Interestingly, no changes were observed when C-peptide was given to non-diabetic individuals (Forst et al., 2000).

Generation of free radicals altered Na^+ , K^+ -ATPase activity, and non-enzymatic glycation of key proteins and lipids in RBCs impair RBC function in DM. These changes are manifest partly by decreased RBC deformability and ATP release. Several reports have described correction of both defects by C-peptide substitution. Compared to healthy

volunteers, the RBCs of C-peptide deficient type 1 diabetic people are significantly less elastic under shear stress. In turn, incubation with 6.6 nmol/L human C-peptide or its C-terminal fragments restored the deformability of RBCs obtained from diabetic people, while it did not affect that from healthy individuals. This effect was calcium-dependent and abolished when the activity of Na⁺, K⁺-ATPase was blocked (Hach et al., 2008).

C-peptide normalises impaired ATP release from RBCs obtained from type 2 diabetic patients. In a study performed by Richards et al (2015), RBCs collected from type 2 diabetics exposed to low oxygen tension showed defective ATP release. This effect was reversible when these RBCs were pre-treated with C-peptide plus insulin. The author suggested cross-talk between C-peptide and insulin signalling pathways, in which C-peptide might be involved in fine-tuning of insulin action. It is noteworthy that another group of researchers showed that C-peptide also stimulates ATP release from non-diabetic RBCs and under normal oxygen environment; albeit in the presence of Zn²⁺ and albumin which were found to be essential for C-peptide-mediated ATP release from RBCs (Liu et al., 2015).

1.4.5.2 Anti-inflammatory effects of C-peptide

Experimental studies in animals have shown that C-peptide exerts anti-inflammatory effects on various tissues in response to multiple stimuli. For instance, C-peptide reduces the abundance of inflammatory cells in renal tissue during non-diabetic kidney injury (Chima et al., 2011b). Moreover, C-peptide protects the heart against ischaemia-reperfusion damage (Young et al., 2000). In lung tissue and plasma, C-peptide blunts the inflammatory response triggered by haemorrhagic shock (Chima et al., 2011a). Similarly, in LPS-induced endotoxic shock C-peptide protects lung tissue (Vish et al., 2007). In addition, human C-peptide blunts the vascular inflammatory response in rat mesentery exposed to thrombin. Inhibition of P-selectin and ICAM-1 surface expression on the mesenteric venules was observed following C-peptide administration, while this effect was associated with increased eNOS mRNA level (Scalia et al., 2000). In diabetic rat, C-peptide downregulates the inflammatory status in brain tissue (Sima et al., 2009). On the other hand, C-peptide attenuates the inflammatory response resulting from exposure to high glucose in vascular cells. For instance, C-peptide exerts anti-

inflammatory effects on human aortic ECs injured by hyperglycaemia. The expression of VCAM-1, and IL-8 and MCP-1 secretion, was blunted upon co-treatment with C-peptide (Luppi et al., 2008). Additionally, in human SMCs exposed to hyperglycaemic milieu, C-peptide suppresses the pro-inflammatory nuclear transcription factor, NF- κ B (Cifarelli et al., 2008).

1.4.5.3 Effects of C-peptide on cell growth and survival

Several studies have reported a growth factor-like activity for C-peptide in some cell types, in addition to the anti-apoptotic effect observed during cell exposure to apoptotic stimuli. Mughal et al (2010) demonstrated that ECs cultured from saphenous vein of non-diabetic patients and exposed to 0.1-10 nM C-peptide in 10% serum for 5 days proliferate at higher rate (40% increase) compared to cells grown without C-peptide. The authors suggested an important role for C-peptide in promoting re-endothelialisation of damaged vessels which in turn limits neointima formation. In another study, C-peptide induced HUVEC proliferation and migration in a dose-dependent manner; in addition, it increased their viability to a comparable level to that observed on treating with VEGF. These actions were mediated via activation of ERK1/2 and Akt (Lim et al., 2015). C-peptide exerted a mitogenic effect in rat and human aortic SMCs (Walcher et al., 2006). Lastly, at physiologically-relevant concentration, C-peptide significantly enhances the proliferation of opossum PTCs (Al-Rasheed et al., 2004a).

A protective anti-apoptotic effect for C-peptide has also been described. For instance Ha and colleagues (2016) demonstrated that C-peptide ameliorates endothelial dysfunction induced by high glucose treatment of HUVEC cultures. It was concluded that C-peptide abrogates ROS-mediated endothelial apoptosis at both mitochondrial and transcriptional levels (Bhatt et al., 2016, Bhatt et al., 2013, Bhatt et al., 2012). Moreover, Cifarelli et al (2011a) described C-peptide as the 'endogenous antioxidant' because it rescues aortic ECs from ROS and apoptosis. *In vivo* studies have also confirmed the anti-apoptotic effect of C-peptide: in a spontaneously type 1 diabetic rat, C-peptide decreased hippocampal cell apoptosis as assessed by caspase-3 activation (Sima et al., 2009). In fact, the beneficial cytoprotective effect of C-peptide is not restricted to DM-induced insults. For instance, C-peptide protects PTCs from apoptotic death induced by TNF- α (Al-Rasheed et al., 2006), antagonises TNF- α -induced apoptosis

of ECs (Cifarelli et al., 2011a), significantly decreases H₂O₂-induced ROS and prevents apoptosis of INS1 beta cells (Luppi and Drain, 2014).

1.4.6 C-peptide replacement in clinical studies of T1DM

Clinical studies have shown that C-peptide administration in type 1 diabetic patients, who lack this peptide, results in partial correction of long-term complications (Figure 1.10). Early clinical trials in subjects with type 1 diabetes have investigated the potential renoprotective effects of C-peptide. Treatment of type 1 diabetic patients with C-peptide in replacement doses ameliorates early signs of diabetic nephropathy, in which significant reduction of both glomerular hyperfiltration and urinary albumin excretion was observed (Johansson et al., 2002). Others have assessed the effect of C-peptide on development of diabetic neuropathy. C-peptide was given to type 1 diabetes patients without overt symptoms of neuropathy to achieve physiological levels. After three months of treatment with C-peptide, a significant improvement of sensory nerve conduction velocity and vibration thresholds was observed (Johansson et al., 2002). These results were further confirmed in a later study. A randomized double-blind placebo-controlled study performed by Ekberg et al (2007) showed that administration of C-peptide for six months significantly ameliorates the impaired sensory neuronal function in patients with established early-stage diabetic neuropathy. However a more recent 52 week trial of a long-acting C-peptide preparation in type 1 diabetic patients having neuropathic complication failed to improve sural nerve conduction velocity relative to placebo, although other aspects of nerve function were improved by this treatment (Wahren et al., 2016).

The effect of C-peptide on retinal vascular function has been evaluated in T1DM. Subcutaneous infusions of insulin and C-peptide were given for four weeks to diabetic patients without previous history of structural retinal damage. Evaluation of retinal vascular permeability was performed by using fluorescein leakage across the blood-retinal barrier as an indicator. The data showed that there was approximately 30% decrease in retinal vascular damage in patients receiving C-peptide infusion, but not in those receiving insulin alone (Wahren and Larsson, 2015). Although not conclusive, these clinical investigations suggest that C-peptide replacement therapy in type 1 diabetic patients may be beneficial in alleviating or retarding diabetes-induced vascular

dysfunction. However, further longer clinical studies are mandatory to confirm these preliminary observations.

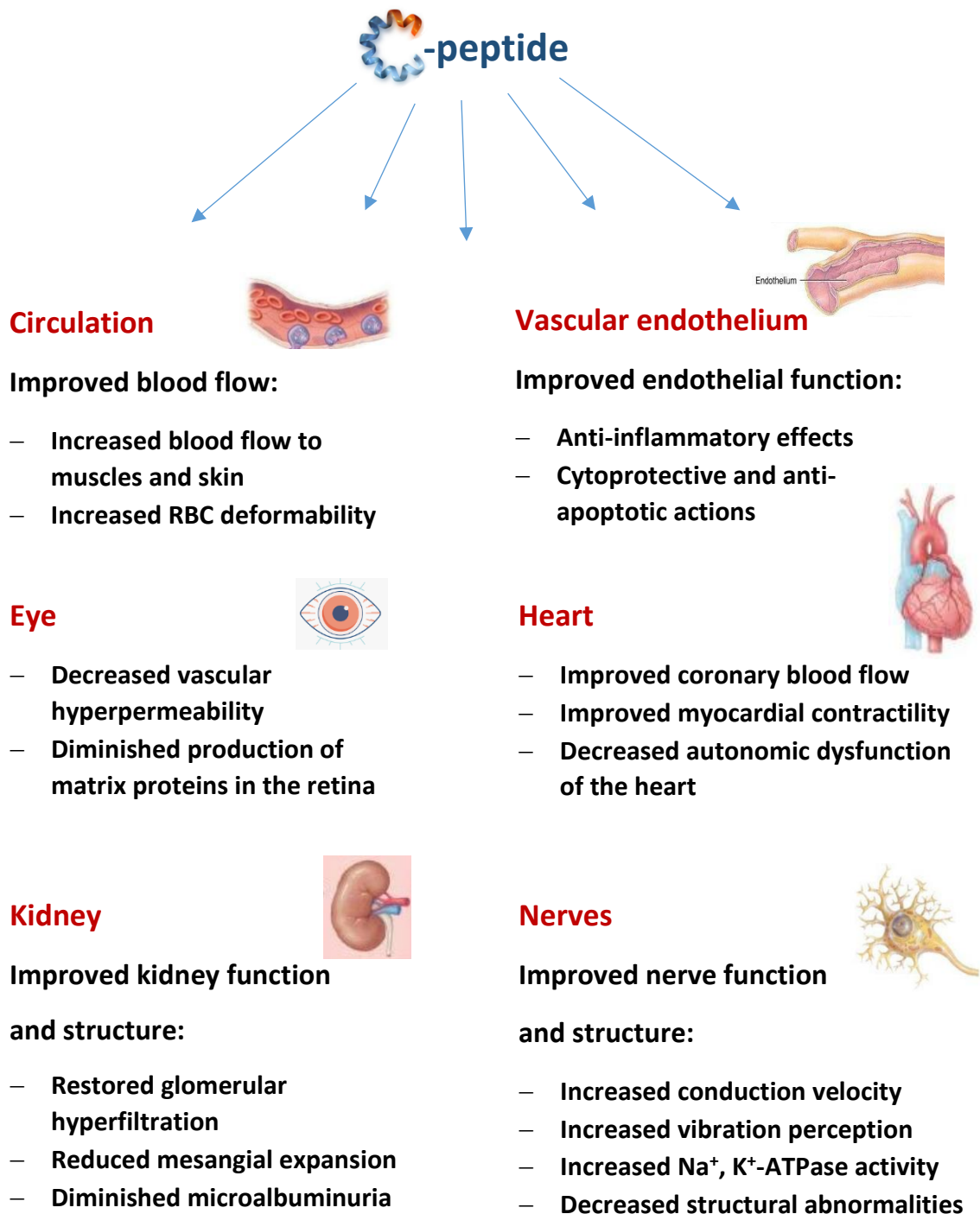


Figure 1.10 C-peptide exerts multiple beneficial actions in diabetes. *In vivo* experimental and clinical studies have shown that C-peptide replacement improves numerous functional and structural changes induced by DM. Adapted from (Wahren et al., 2007, Wahren, 2017, Bhatt et al., 2014). See text for further details.

1.4.7 C-peptide effects in T1DM versus T2DM

C-peptide may exert its effect in different fashion according to the type of DM. This can be explained by the fact that each type has its own aetiology (Section 1.1.3). In contrast to T1DM, insulin resistance represents an important component in T2DM. In addition, as the majority of type 2 diabetic patients are obese, excess fatty acids in blood may further complicate the picture (Section 1.1.3.2). Different plasma levels of C-peptide and insulin are present in each type of DM. For instance in T2DM, elevated C-peptide level may associate with undesirable effects (Vasic and Walcher, 2012). In contrary, in T1DM, almost always there is C-peptide deficiency.

Numerous studies have shown improvement in vascular dysfunction in T1DM after C-peptide replacement. However, understanding the role of C-peptide in T2DM is more perplexing because elevated C-peptide level may potentially lead to saturation of C-peptide receptors with subsequent downregulation or de-sensitisation (Hills and Brunskill, 2009). C-peptide data is inconsistent in T2DM. In a retrospective cohort study, Bo et al (Bo et al., 2012) found that high baseline C-peptide level in patients with T2DM is associated with lower incidence of microvascular complications with no effect on the macrovascular complications. In contrast Sari et al (2005) observed a positive correlation with the macrovascular complications but none with the microvascular. Other researchers have suggested pro-inflammatory and pro-atherogenic effects for high C-peptide level in T2DM (Walcher and Marx, 2009). Consistently, recent studies have shown a significant correlation between C-peptide level and increased risk of cardiovascular complication (Marx et al., 2013). This association has led to the suggestion of using endogenous C-peptide level as a predictor for development of macrovascular complication in T2DM (Kim et al., 2011). It seems that the magnitude of C-peptide concentration in plasma reflects the degree of insulin resistance in T2DM, which might explain its association with adverse cardiovascular outcome in some reported studies. In contrast, there is strong evidence that C-peptide substitution in T1DM, to achieve physiological plasma levels, retards the development of diabetic complications especially microvascular-related outcomes.

1.5 Experimental models of vascular endothelium in DM

1.5.1 In vitro modelling of vascular endothelium employing EC lines

Typically, to simulate the hyperglycemic conditions seen in diabetic people, an *in vitro* culturing of ECs is performed under high glucose concentration in the cell medium. Primary ECs as well as cell lines are available for these purposes; however, each has its drawbacks. Despite their foetal phenotype, the most widely adopted ECs to assess endothelial function in normal and disease conditions, are primary HUVECs (Hauser et al., 2017). However, they lose their responsiveness to stimuli and enter senescence after a few passages. In addition, the isolation process is laborious and fluctuation in results is seen between different donors, which might compromise data reproducibility (Hauser et al., 2017). Alternatively, using a stable permanent cell line is considered advantageous in general (Baranska et al., 2005); although, cell lines also display variation compared to their parallel primary cells. Strictly, ECs growing in a culture system are not in a real quiescent resting state as *in vivo*; in fact, these conditions elicit endothelial activation (Cines et al., 1998). In aggregate, *in vitro* culturing of ECs either primary or cell line is a well-accepted method despite having some limitations. In fact, EA.hy926 cells is considered the best characterized human vascular endothelial cell line (Baranska et al., 2005). These cells were originally derived by fusing HUVECs with the continuous human lung carcinoma cell line A549. EA.hy926 cells retain endothelial phenotype and grow rapidly with no need for special growth medium (Edgell et al., 1983). In addition, EA.hy926 cells have been widely used to study physiological and pathological alterations in human vascular endothelium (Koziel et al., 2015). Alternatively, a well-characterised microvascular endothelial cell line is the human dermal microvascular endothelial cells (HMEC-1) immortalised by SV-40T. These cells are derived from the skin and frequently used in modelling the microvascular endothelium (Edwin et al., 1992).

1.5.2 Experimental animal models of T1DM

Several animal models are available to perform a diabetic study; however, each model has been created to address a certain aspect of DM. Therefore, selecting the appropriate model depends on the experimental question; whether studying the pathogenesis of DM or testing a new therapeutic modality. Animals that develop DM spontaneously or transgenic animals are commonly used to study the auto-immunological basis of DM (King and Bowe, 2016). However, to find a cure for DM, modelling of DM is performed by using diabetogenic agents that destroy β -cells by non-immunological mechanisms, such as alloxan and streptozotocin (STZ) (King and Bowe, 2016). When Alloxan enters β -cells through glucose transporter-2 (GLUT-2), cell death ensues as a result of ROS generation. The use of alloxan becomes limited due to its low efficacy compared to STZ; in addition to causing direct adverse effects on the liver and kidney (Islam and Wilson, 2012). On the other hand, STZ is considered the agent of choice for producing a reproducible induction of DM in animals. It produces a stable long-term hyperglycaemia (Lenzen, 2008). Injection of a single moderate dose of STZ in rats, after an overnight fast, damages the pancreatic β -cells. STZ is transported across β -cells via GLUT-2 competing with glucose. Upon successful entry, STZ irreversibly damages cellular DNA by alkylation while its selectivity in destroying β -cells arises from their high expression of GLUT-2 (Lenzen, 2008).

In the above-mentioned models of T1DM, insulin resistance does not develop; however, introducing a high-fat diet to STZ-treated animal can produce insulin resistance (Wu and Yan, 2015). Alternatively, obese animals are commonly used to model insulin resistance in T2DM (King and Bowe, 2016).

1.6 Thesis hypothesis and aims

C-peptide is biologically active in the vasculature and protects the vascular endothelium under diabetic conditions including high glucose/high Pi.

To achieve the goal of this project, the findings of this study were presented in four results chapters, each with its own specific aims and objectives (- particular objectives of individual chapter are introduced in each results chapter).

The overall study aims can be summarised by the following:

- Utilising a novel method for assessment of endothelial function by measuring the level of microparticle shedding.
- Developing an optimised method for measurement of microparticles by flow cytometry (Chapter 3).
- Confirming the direct bioactivity of C-peptide in the vascular endothelium using EA.hy926 endothelial cells (Chapter 4).
- Developing an *in vitro* model of endothelial dysfunction induced by high glucose/high Pi (Chapter 5).
- Further exploration for the protective effect of C-peptide on vascular dysfunction via an *in vivo* study of diabetic animals treated with C-peptide (Chapter 6).

Chapter 2. Materials and methods

2.1 Materials

2.1.1 General materials

Plastic consumables were purchased from VWR International (Lutterworth, UK), Sarstedt (Beaumont Leys, UK) and Fisher Scientific (Loughborough, UK). All chemicals used were of analytical grade and purchased from Fisher Scientific or Sigma-Aldrich (Poole, UK). Tissue culture plastics including culture plates and flasks were from Thermo Scientific Nunc™ while growth culture media and supplements were from Gibco™ Life Technologies (Paisley, UK).

2.1.2 Cell lines

A permanent human endothelial cell line (EA.hy926) was provided by Dr Alan Bevington's laboratory (Department of Infection, Immunity and Inflammation, University of Leicester, UK). Immortalised human dermal microvascular endothelial cell line (HMEC-1) was kindly provided by Prof Eustace Johnson (Department of Biological Sciences, University of Chester).

2.1.3 Experimental animals

Male Wistar rats weighing 280-300g were used for the diabetic animal study. This animal study had already been performed in this laboratory and I was given access to aorta from these animals for further analysis courtesy of my supervisor Prof Nigel Brunskill. All of the animal experiments were performed in the University of Leicester Preclinical Research Facility (PRF) under a project licence from the Home Office held by Prof Nigel Brunskill.

2.1.4 Antibodies

The primary antibodies used throughout this project for the immunohistochemistry (IHC) and western blot analyses are listed in Table 2.1. Primary antibodies were purchased from Abcam (Cambridge, UK), Cell Signaling Technology (London, UK), Sigma-Aldrich (Darmstadt, Germany), Santa Cruz Biotechnology (Dallas, TX) and Invitrogen (Paisley, UK). Secondary antibodies were bought from Dako (Glostrup, Denmark) and

Sigma-Aldrich (Table 2.2). Antibodies used in flow cytometry (FCM) and immunogold EM are indicated in the relevant sections.

Table 2.1 Primary antibodies used for IHC and western blot analysis

Primary antibody	Host	Species specificity	Dilution	Ref. number	Manufacturer
Phospho-p44/42 MAPK (ERK1/2) (Thr202/Tyr204)	Rabbit (monoclonal)	Human & other species	1:1000	9101	Cell Signaling Technology
β-actin	Mouse (monoclonal)	Human & other species	1:4000	A-5441	Sigma-Aldrich
Caspase-3	Mouse (monoclonal)	Human, mouse & rat	1:500	sc-373730	Santa Cruz Biotechnology
GAPDH	Mouse (monoclonal)	Human & other species	1:5000	ab9482	Abcam
vWF	Rabbit (polyclonal)	Human & other species	1:200	ab6994	Abcam
AGE	Rabbit (polyclonal)	Pan specific	1:200	ab23722	Abcam
Nitrotyrosine	Rabbit (polyclonal)	Pan specific	1:200	A21285	Invitrogen
ICAM-1 (15.2)	Mouse (monoclonal)	Human, mouse & rat	1:1000	sc-8439	Santa Cruz Biotechnology
E-selectin (D-7)	Mouse (monoclonal)	Human, mouse & rat	1:1000	sc-137054	Santa Cruz Biotechnology

eNOS (A-9)	Mouse (monoclonal)	Human, mouse & rat	1:1000	sc- 376751	Santa Cruz Biotechnology
TSP-1 (A6.1)	Mouse (monoclonal)	Human, mouse & rat	1:1000	sc-59887	Santa Cruz Biotechnology

Table 2.2 Secondary antibodies used for IHC and western blot analysis

<i>Secondary antibody</i>	<i>Dilution</i>	<i>Reference Number</i>	<i>Manufacturer</i>
Polyclonal Swine Anti-Rabbit Immunoglobulins/Biotinylated Swine F(ab')₂	1:200	E0431	Dako
Goat Anti-Rabbit Immunoglobulin (Peroxidase Conjugated)	1:4000	A-6154	Sigma-Aldrich
Goat Anti-Mouse Immunoglobulin (Peroxidase Conjugated)	1:5000	A-4416	Sigma-Aldrich

2.2 Methods

2.2.1 Culturing of EC lines

2.2.1.1 EA.hy926 endothelial cells

EAhy926 cells were grown in Dulbecco's Modified Eagle Medium (DMEM) (Ref 24020-091, Life Technologies) containing 10% heat inactivated Foetal Bovine Serum (FBS) (Ref 10270, Life Technologies), 2 mM L-glutamine (Ref 25030081, Life Technologies), penicillin (100 IU/ml), streptomycin (100 µg/ml) (Ref 15140122, Life Technologies) and phenol red, at 37°C in an atmosphere of 5% CO₂. Cells were used between passages 8 and 25. Cells were routinely sub-cultured on 75cm² culture flasks weekly before

reaching ~80% confluence. For cell passaging, growth medium was aspirated and cells were rinsed thrice with Hanks' Balanced Salt Solution (HBSS) (Ref 24020-091, Life Technologies). Detachment of cells was performed by adding trypsin-EDTA (Ref 25300054, Life Technologies) for 2 min at 37°C. After centrifugation at 200g for 5 min at room temperature, cells were re-seeded in 75cm² culture flasks at a density of 60x10⁴ cells per flask and fed with 15ml of growth medium twice weekly. When cells reached passage number 25, another batch of frozen cells was revived and used.

2.2.1.2 HMEC-1 endothelial cells

HMEC-1 cells were grown in Molecular and Cellular Developmental Biology (MCDB) 131 growth medium (MCDB-131) (Ref 10372019, Life Technologies) supplemented with 10ng/mL human Epidermal Growth Factor (hEGF) (Ref E9644, Sigma-Aldrich), hydrocortisone (1 µg/ml) (Sigma-Aldrich), 10% FBS, 2 mM L-glutamine, penicillin (100 IU/ml) and streptomycin (100 µg/ml) at 37°C in an atmosphere of 5% CO₂. Cells were used between passages 15 and 20. A method similar to that used for EA.hy926 cell passaging was also used for HMEC-1 passaging, except that cells were fed with 15ml of their specialised medium, MCDB-131, after re-seeding.

2.2.2 Cell treatments

Experimental incubations were performed in Minimum Essential Medium (MEM) (Ref 21090, Life Technologies) with 2mM L-glutamine, penicillin (100 IU/ml) and streptomycin (100µg/ml). For experiments that involved Pi treatment, to restore the medium pH to 7.4, supplementation with an additional 4.6ml of 7.5% w/v NaHCO₃ per 500ml of culture medium was performed to all the tested conditions. ECs were grown to 80% confluence in 6-well plates, then the test agent(s) of interest dissolved in MEM was added to the cultures after discarding the previous medium (either the growth media that were described in Sections 2.2.1.1 and 2.2.1.2, serum-free DMEM or an overnight serum-free MEM incubation according to the experiment).

In studies that involved C-peptide stimulation, synthetic human C-peptide (TAG Copenhagen A/S, Denmark) was used. C-peptide stock was prepared by dissolving C-peptide powder in sterile 0.9% w/v NaCl at 500µM. C-peptide concentration was brought to the required concentration by adding sterile water (C-peptide vehicle). Cells

were treated with various concentrations of C-peptide at several time points. (Detailed cell treatments are presented at the beginning of the relevant results sections of Chapter 3 and Chapter 4).

In the case of high Pi stimulation, Pi stock solution was prepared from $\text{NaH}_2\text{PO}_4 \cdot 2\text{H}_2\text{O}$ (Ref 71505, Sigma) and added to MEM in an amount sufficient to raise the Pi concentration of the medium from 1mM Pi (already present in MEM) to 2.5mM, representing a high Pi condition as described elsewhere (Hsu et al., 2015, Di Marco et al., 2013, Abbasian et al., 2015).

To mimic the elevated plasma glucose level seen in diabetic patients, D-glucose was added to the test medium (MEM) to raise its D-glucose (referred to hereafter simply as glucose) concentration from 5.5mM up to 45mM. Different time points and glucose concentrations were examined because stimulation of EA.hy926 cells by high glucose has been observed after 24h (Natarelli et al., 2015) or up to 72h (Liu et al., 2012, Xu et al., 2018, Jing et al., 2017). In addition, various high glucose concentrations were tested; for instance, 25mM as reported by Natarelli et al (2015), 35mM as described by Karbach et al (2012) and 40mM (Gerö and Szabo, 2016).

At the end of experimental incubations, cell supernatants were aspirated for MP isolation (Section 2.2.3), while cell monolayers were either lysed for western blotting (Section 2.2.8) or precipitated with perchloric acid (PCA) for protein determination with the Lowry protein assay (Section 2.2.5).

2.2.3 Isolation of microparticles (MPs)

For flow cytometry (FCM) (Section 2.2.11), EM (Section 2.2.12) and for assessment of MP biological activity (Section 2.2.4); MPs were isolated from stored culture media via differential centrifugation as described elsewhere (Jansen et al., 2015). A low speed spin at 1800xg for 20min at room temperature was followed by one at 20,000xg for 30min at 4°C. The resultant MP pellets were washed with 0.2µm filtered MP buffer (14.5mM NaCl, 0.27mM KCl, 1mM HEPES, pH 7.4) and centrifuged again at 20,000xg for 30min at 4°C. Collected MPs were then resuspended in 25µl of MP buffer. If storage was required, this was done at -80°C for later analysis. For proteomic analysis (Section 2.2.13), a similar isolation procedure was followed, except that the first low speed spin was at

2500xg to further eliminate possible contaminants to the MP population (Burger et al., 2017). For NTA analysis (Section 2.2.10), conditioned medium was centrifuged at 1800xg for 20min at room temperature only and the resultant supernatant was used for MP measurement.

2.2.4 Stimulation of EA.hy926 cells with endothelial MPs (EMPs)

Media containing MPs harvested from either normal glucose-, high glucose-, C-peptide- or C-peptide plus high glucose-treated EA.hy926 cells were used to isolate MPs as described in Section 2.2.3. The pelleted MPs suspended in MP buffer were used immediately to treat new healthy cultures of EA.hy926 cells for 24h (as no significant degradation of MPs has been reported up to this time point (Jimenez et al., 2003). Cultures were treated with MPs, generated under various conditions, at 1×10^5 Annexin V+ MPs/ml as quantified by FCM (Section 2.2.11) (Jing et al., 2017, Burger et al., 2011).

2.2.5 Protein measurement assays

2.2.5.1 Lowry protein assay

2.2.5.1.1 Sample preparation

At the end of cell treatment (Section 2.2.2), cell monolayers were processed to determine total protein concentration. After aspirating the conditioned medium, cells grown in 35mm six-well plates were rinsed thrice with ice-cold 0.9% w/v NaCl and scraped on ice with 150 μ l of 0.3M Perchloric Acid (PCA), followed by centrifugation at 3000xg at 4°C for 10min to collect the precipitated protein. The resultant protein pellet was used to determine total cell layer protein.

A slightly modified procedure was used to determine the total protein content of particles released into the test medium. At the end of each incubation, test medium was aspirated and ultracentrifuged at 20,000g for 30min at 20°C. The upper 90% of the supernatant was discarded and to the remaining pellet and residual supernatant, 0.5ml of 0.3 M PCA was added to precipitate protein. Then, samples were pelleted again at 20,000g for 30min at 20°C then 100ul of 0.5M NaOH was added to the collected sediment. Protein measurement was performed on the resulting pellets (Abbasian, 2015).

2.2.5.1.2 Assay methodology

Lowry protein assay (Lowry et al., 1951) was performed to determine the total cell monolayer protein or the protein content of released particles in the test medium that had been sedimented at 20,000xg. Briefly, PCA-treated cell monolayer or sedimentable protein particles from the medium (see above) was dissolved in 200µl or 100µl respectively of 0.5M NaOH then incubated in a water bath at 70°C for 30min to dissolve the proteins.

Solubilized proteins were further diluted in 0.5M NaOH where appropriate to bring sample concentration within the standard curve range. Eight standards were prepared from BSA from zero to 500µg/ml to build the standard curve. Lowry assay Reagent A (2% Na₂CO₃, 0.02% L(+)-potassium sodium tartrate tetrahydrate in 0.1N NaOH) and Reagent B (0.5% CuSO₄) were mixed in a ratio of 50:1 to prepare Reagent C. Afterwards, 50µl of each sample and standard was pipetted into a 3-ml test tube and mixed with 600µl of Reagent C, then vortexed immediately. Subsequently 60µl of 3-fold diluted Folin-Ciocalteu's phenol reagent (Ref F-9252, Sigma) was added to each tube, briefly vortexed then incubated for 40 min at room temperature. In a 96-well microtitre plate, 300µl of the resulting blue reaction product from each sample and standard was transferred to the wells, and then absorbance was read at 650nm in a microplate reader (Labtech LT-4500).

2.2.5.2 Bio-Rad RC DC protein assay

To ensure equal loading of protein in SDS-PAGE (Section 2.2.7), the RC DC™ protein assay (Reducing agent and Detergent Compatible) (Ref 500120, Bio-Rad) was chosen to determine protein concentration in cells lysed (Section 2.2.2) in Lysis Buffer (50mM Tris-HCl (pH 7.5), 10mM glycerophosphate, 1mM EDTA, 1mM EGTA, leupeptin (1µg/ml), pepstatin (1µg/ml), 1mM benzamidine, 50mM NaF, 0.2mM phenylmethanesulphonyl fluoride (PMSF), 1mM sodium orthovanadate, 1% Triton X-100 and 0.1% 2-mercaptoethanol).

Eight protein standards were prepared from BSA in 1% IGEPAL® detergent (Ref CA-630, Sigma) from zero to 2mg/ml to build the standard curve. From each standard or cell lysate, 25µl was pipetted into 1.5ml Eppendorf tubes then mixed with 125µl of RC

Reagent I. After vortexing and incubation for 1 min at room temperature, 125µl of RC Reagent II was added to each tube, vortexed then centrifuged at 14,000xg for 5min. Thereafter, tubes were inverted to drain the supernatant followed by addition of 127µl Reagent A (1:50 DC Reagent S to DC Reagent A) to each tube. Tubes were vortexed and incubated at room temperature for 5min or until the protein precipitate was completely dissolved. The tube was then vortexed during addition of 1ml of DC Reagent B. The tubes were then incubated for 15min at room temperature followed by measurement of absorbance at 750nm.

2.2.6 Cell viability assay (MTT Assay)

Cells were allowed to grow in 24-well plates to 80% confluence then stimulated with a series of concentrations of C-peptide (0.5, 1, 3, 5, 10 nM) for different time points. In the last hour of incubation, 60µl of the prepared MTT stock solution (2mg/ml in HBSS) (Ref M5655, Sigma) was added to each well and incubated for 1 h at 37°C under 5% CO₂ (Abbasian, 2015). After aspirating the medium, cells were rinsed with 0.9% w/v NaCl then the insoluble formazan crystals formed in the cell layer were dissolved with dimethylsulphoxide (DMSO). Aliquots of 50µl were transferred to wells of a 96-well plate and the absorbance was measured at 540nm using a microplate reader (Labtech LT-4500).

2.2.7 SDS-polyacrylamide gel electrophoresis (SDS-PAGE)

To separate proteins in cell lysates (Section 2.2.2) gel electrophoresis was performed. Resolving gels of 12% (for most of the experiments) or 15% (for caspase-3) were prepared and casted in the gel apparatus (Mini-PROTEAN[®], Bio-Rad Laboratories, Hemel Hempstead, Uk)) then overlaid with Isopropanol to obtain a uniform gel edge. After solidifying, the 4% stacking gel was poured over the resolving gels and a comb was placed in the stacking gel to form sample wells. When polymerization had completed, gels were mounted in the electrophoresis chamber then the tank was filled with running buffer (25 mM Tris base, 1.92 M glycine and 0.1% w/v SDS, pH 8.3). Laemmli sample loading buffer (Ref 1610747, Bio-Rad) premixed with 2-mercaptoethanol (ratio 10:1) was added to cell lysates then samples were placed in a heating block preset at 95°C for 5 min to denature proteins.

Markers of known molecular weight (Precision Plus, Bio-Rad Laboratories, ref 1610374) were loaded onto the gel as well as the cell lysates. Electrophoresis was performed at 50v until the dye front (bromophenol) had migrated to the top of the resolving gel then the voltage was increased to 100v for the rest of the run. Electrophoresis was stopped when the dye front had just passed the bottom of the resolving gel. Gels were detached from the glass plates to be readied for immunoblotting.

2.2.8 Western blot analysis (immunoblotting)

Proteins separated by SDS-PAGE were blotted onto PVDF membranes (Immobilon™-P, Merck™, ref IPVH00010) using a Bio-Rad Mini Trans-Blot apparatus. Briefly, a 'sandwich' was prepared from three filter papers, the gel and the PVDF membrane then immersed in the tank that contained transfer buffer (25 mM Tris base, 1.92 M glycine, 20% (v/v) methanol). The transfer was run at 100v constant voltage for 1h. Nonspecific binding was blocked by incubating the membranes with 5% w/v BSA in TTBS buffer (0.05% Tween-20, 50 mM Tris base, 0.9% w/v NaCl, pH 7.6) for pERK1/2 or 5% in TTBS skimmed milk powder for other experiments for 1h at room temperature. Membranes were washed with TTBS then the primary antibodies (Table 2.1) were applied in TTBS overnight at 4°C. Immunoblots were probed with secondary antibodies in TTBS (Table 2.2) conjugated to horseradish peroxidase (HRP) for 1h at room temperature then developed with SuperSignal™ West Pico PLUS substrate (Ref 34580, Thermo Scientific) for 5 min. The chemiluminescence signal was imaged by a ChemiDoc imaging system (Bio-Rad) and bands were quantified using Image Lab™ software (version 5.2.1, Bio-Rad). Analysis of data was performed by dividing the band intensity of the target protein by the band intensity of the housekeeping protein (β -actin or GAPDH).

In some experiments, after initial probing of a PVDF membrane with primary and secondary antibodies, it was necessary to detach the primary and secondary antibodies then reprobe the membrane with another antibody. Briefly, after developing the membrane, it was washed three times with TTBS for 5 min each. The membrane was then incubated in 15ml Stripping buffer (Restore™ Western Blot Stripping Buffer, ref 21059) for 15 min at room temperature. The membrane was washed three times for 5 min in TTBS, blocked in 5% skimmed milk for 1hr then probed with the new primary antibody.

2.2.9 ELISA for detection of IL-8

The concentration of IL-8 in the culture supernatants of EA.hy926 cell treated as described in Section 2.2.2 was determined by using an IL-8 ELISA kit (Ref 900-TM18, Peprotech Ltd., London, UK). Following the manufacturer's instructions, the wells of a 96-well plate (Nunc MaxiSorp) were coated with 100µl of capture antibody (rabbit anti-human IL-8) diluted in PBS to a concentration of 0.125µg/ml, then sealed and incubated overnight at room temperature.

After aspirating the liquid from the wells, the plate was washed with wash buffer (0.05% Tween-20 in PBS, pH 7.4) three times. To remove residual wash buffer from the wells, the plate was inverted and blotted onto a paper towel several times. The wells were then blocked with 300µl block buffer (1% BSA in PBS) for 1h at room temperature. Afterwards, the liquid was discarded, and the plate was washed three times then blotted on a paper towel. Cell supernatants were thawed and centrifuged at 1000xg for 10min to remove debris then 100µl from each condition was loaded onto the plate in duplicate. Seven standards were prepared from recombinant human IL-8 from zero to 300pg/ml (Figure 2.1) and added to the plate in duplicate, then the plate was sealed and incubated at room temperature for 2h. Next, similar washing steps were performed and 100µl of detection antibody (biotinylated rabbit anti-human IL-8) was added then the plate was incubated for 2h at room temperature.

After applying similar washing steps, the plate was probed with streptavidin-HRP at 100µl per well. The plate was then incubated in the dark for 30 min at room temperature. After washing the plate, the bound antibodies were visualized by adding 100µl of substrate solution tetramethylbenzidine (TMB Peroxidase EIA Substrate Kit, Biorad, Ref 1721066) to each well then, the plate was incubated in the dark for 20 min at room temperature. The reaction was stopped with 100µl of 1 N H₂SO₄ then colour development was monitored with a microplate reader (Labtech LT-4500) at 450nm, with subtraction of the background correction obtained at a wavelength of 620nm. IL-8 concentrations were calculated from the standard curve using GraphPad Prism (version 7.04) then the data was normalised to total cell layer protein.

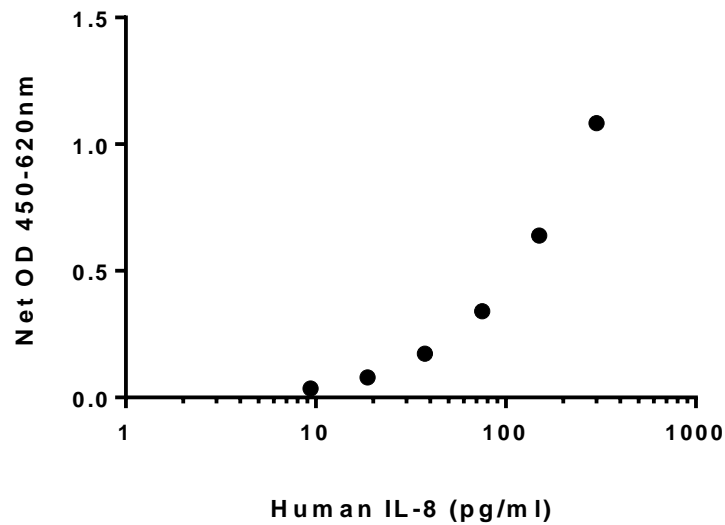


Figure 2.1 Standard curve for IL-8 ELISA.

2.2.10 Nanoparticle tracking analysis

Sizing and enumeration of MPs were achieved by Nanoparticle Tracking Analysis (NTA) using a NanoSight® LM10 system (NanoSight Ltd, Amesbury, UK) in which detection of nanoparticles is based on their random movement in a liquid (Brownian motion). Each MP sample was illuminated by a laser beam and the light scattered by each MP was tracked by a CCD camera (Figure 2.2). MP samples were prepared from ECs stimulated with C-peptide, glucose or Pi for different time points and according to the required experimental protocol (Section 2.2.2 and 2.2.3). At the end of the experimental incubations, the cell conditioned media were collected and subjected to centrifugation at 1500xg then stored at -80°C. For NTA analysis, MP samples were thawed at room temperature then diluted with MP buffer to an optimal concentration for NTA (10^8 - 10^9 particles/ml) (Gardiner et al., 2013). The settings applied for NTA software (version 2.2 build 0377) were: two videos of 90 seconds at 20 frame/second, camera level at 13, detection threshold 4, background extraction, automatic settings for blur and minimum track length, viscosity setting linked to water, automatic temperature monitoring, and the minimum expected particle size at 30nm. For data analysis, sample measurements that achieved at least 500 completed tracks were retained for further analysis, while detected particles of size range between 100nm and 1000nm were utilised for calculating MP concentration in samples.

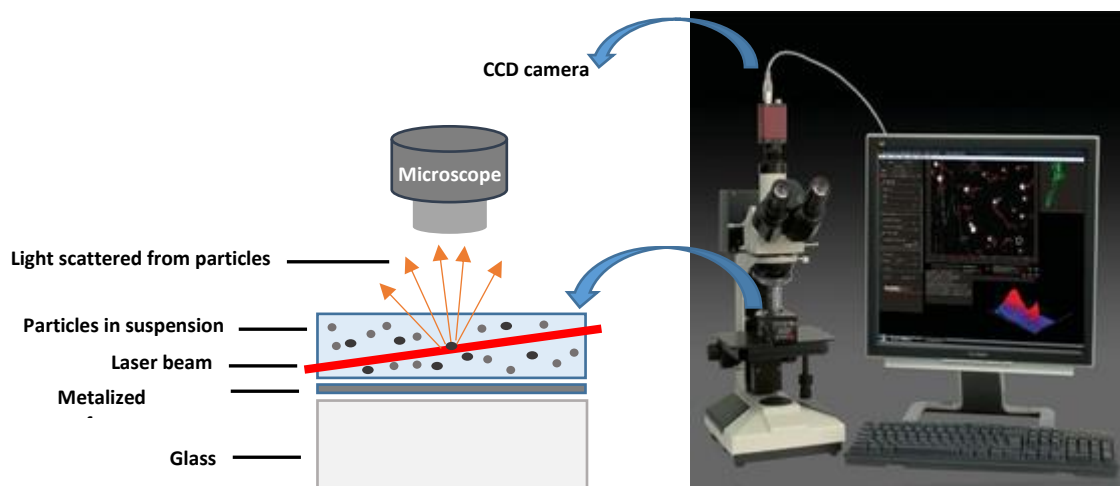


Figure 2.2 NanoSight LM10 System used for NTA analysis. The workstation and the dark-field dedicated microscope are shown on the right side, while the left side shows a schematic representation of the sample viewing unit. The image is taken from <https://en.wikipedia.org/wiki/NanoSight>.

2.2.11 Flow cytometry analysis of MPs

2.2.11.1 Setting up the flow cytometer for MP analysis

The flow cytometer used in this study, a FACSCelesta™ (BD Biosciences), is equipped with three lasers, blue (488nm), red (640nm) and violet (405nm) and has BD FACSDiva™ software v8.0.1.1 on the system workstation. The fluidics system operated at a pressure of 5.5 psi, where low sample pressure (12µl/min) was chosen for the entire study. Calibration beads, BD™ Cytometer Setup and Tracking beads (CST) (Ref 655051) were used before each set of measurements to monitor the instrument performance over time and to correct any deviation automatically.

Detailed flowcytometric optimisation of MP analysis is described in Chapter 3.

The MP analysis window was defined by synthetic green fluorescent beads, Megamix-Plus SSC® (Ref 1078, BioCytex, Marseille, France) which were used to standardise MP analysis settings as described in (Poncelet et al., 2016). Megamix-Plus SSC is a mix of 160, 200, 240 and 500nm polystyrene beads which allows setting of the MP analysis window between 170nm-500nm bead positions corresponding to a 0.3 - 1µm MP size

range (i.e. the MP gate) on SSC-oriented flow cytometers (i.e. with PMT applied on the SSC detector) (Cointe et al., 2017, Poncelet et al., 2016). Beads were run before each experiment to delineate the MP gate boundaries and to achieve reproducibility. SSC and FSC voltages were adjusted according to Megamix-Plus SSC instructions, while fluorescent detector voltages were adjusted according to the CST bead report generated by the flow cytometer (Table 2.3).

SSC resolution was monitored according to the Megamix-plus SSC beads data sheet and as suggested in (Poncelet et al., 2016). The separation index between the smallest two bead sets i.e. 160nm and 200nm was calculated according to the provided formula:

Separation index $(200\text{nm} - 160\text{nm}) = (d_{200\text{nm}} - Md_{160\text{nm}}) / (SD_{200\text{nm}} + SD_{160\text{nm}})$ where $Md_{200\text{nm}}$ is the median SSC of 200nm beads and $SD_{200\text{nm}}$ is the standard deviation of their SSC histogram, the same abbreviations applies to 160nm beads.

For defining the threshold value, the discriminator was applied on the SSC parameter and the threshold value was calculated according to the provided formula in the Megamix-plus SSC® bead instruction:

Lowest boundary in SSC scale = $Md_{160\text{nm}} + (0.3 \times (Md_{200\text{nm}} - Md_{160\text{nm}}))$

The instrument background was checked before each experiment with 0.2µm-filtered njano-pure water to determine the noise level and, in the case of a high background, standard sample line cleaning and priming procedures were adopted. Also, the sample line was cleaned frequently with filtered Nano-pure water at a fast flow rate between measurements to prevent sample carryover.

2.2.11.2 Optimising the antibodies and MP concentrations

To determine the assay linearity and the operational sample concentration which minimises the risk of swarm detection (i.e. simultaneous excitation of multiple MPs which are then detected as one MP) (van der Pol et al., 2012), concentrated MP samples were prepared then stained with Annexin V only. Next, the labelled samples were serially diluted in buffer. The number of Annexin V positive events and MFI (mean fluorescent intensity) were recorded for each dilution as described in (Nolan and Duggan, 2018).

In order to identifying the antibody saturating concentration and decrease the non-specific binding, the concentration of each antibody was titrated. Determination of the saturating antibody concentration was achieved by staining the sedimented MP pellets with serially diluted antibody stock (Arraud et al., 2016). The concentration which gave the highest number of positively stained MPs without causing a significant increase in the background fluorescence (MFI of the negative population) (Hulspas, 2010) was chosen.

2.2.11.3 Labelling of MP samples for FCM

For EMP identification, Annexin V was used as a marker for phosphatidylserine exposure; whereas, the endothelial markers CD31 (PECAM-1) or CD105 (Endoglin) were used to delineate the endothelial origin of MP samples. Frozen MP pellets prepared as described in Section 2.2.3 were thawed and mixed with 175 μ l of 1x Annexin V-Binding Buffer with calcium (Ref 556454, BD Pharmingen), and 1 μ l of Mouse Anti-Human CD31-BV421 (BD Horizon™ Brilliant Violet 421, Ref 564089); and 2 μ l of Annexin V-FITC (Ref 556419, BD Pharmingen) was added and samples were stored at room temperature in the dark for 25 min followed by centrifugation at 20,000xg for 30min. After discarding the supernatant, labelled MP pellets were resuspended in 200 μ l MP buffer before analysis on the FACSCelesta. Samples incubated with Mouse IgG₁-BV421 (Ref 562438, BD Biosciences) were used as isotype control. Samples incubated with Annexin V-FITC in Binding Buffer free of calcium were used as a negative control for Annexin V binding. In some experiments Mouse Anti-Human CD105-APC (Ref 323208, BioLegends) with its isotype control (Ref 400121, BioLegends) were used instead of CD31 labelling for comparison. As another negative control, labelled MPs were lysed with 0.05% Triton X100 (Robert et al., 2012); whereas, MPs from cells stimulated with 10ng/ml TNF α (Ref 210-TA-005, R&D Systems, Abingdon, UK) or 3 μ M Calcium ionophore (Ca-ionophore) (A23187 Sigma) were used as positive controls (Ayers et al., 2011).

To demonstrate the effect of the residual unbound fluorescent antibody in MP preparations on flow cytometric analysis, some samples were left unwashed after labelling (the centrifugation step after labelling was omitted) to compare them with washed samples (see Chapter 3).

2.2.11.4 Data acquisition and analysis

Events acquired in the MP gate (MP population) were further characterised based on their fluorescence. Matched antibody isotype control and Annexin V negative control were used to determine the gate boundaries between positive and negative populations. Signal height was chosen to present the data (Tang et al., 2017) on Log or biexponential scales to display the wide size distribution of the MP population (Table 2.3). Launching of data acquisition was performed after a delay of a few seconds to allow for flow stabilization, and data was recorded from each sample for 2 min.

Table 2.3 Settings applied to FACSCelesta for scatter (SSC, FSC) and fluorescent (FITC, BV421, APC) parameters during MP analysis. H denotes height of the signal. A denotes the signal area.

Parameter	Detector Voltage	Signal type	Threshold	Data display
FSC	546	H, A	_____	Log, Biexponential
SSC	515	H, A	2023	Log, Biexponential
FITC	615	H	_____	Biexponential
BV421	405	H	_____	Biexponential
APC	630	H	_____	Biexponential

The absolute MP number in samples was estimated based on the number of count beads. MP-Count[®] beads (Ref 1169, BioCytex), which are 3µm PE-labelled beads, were used as described in (Cointe et al., 2017). Count beads were added to each sample tube, and the concentration of MP/µl was calculated according to the manufacturer's instructions. Gating on these count beads was performed on PE-H histogram (as shown in Figure 2.3).

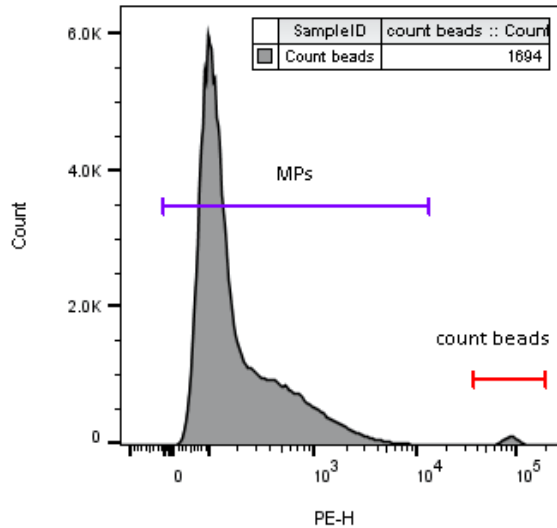


Figure 2.3 Gating applied to MP-Count beads. The red interval gate represents the 3µm count beads.

Data analysis and compensation for spectral overlap (result shown in Table 2.4) were performed using FlowJo® software version 10 (TreeStar, Ashland, OR).

A)

B)

Matrix 1	BV421-H	FITC-H
BV421-H	/	0.0
FITC-H	0.0	/

Matrix 2	APC-H	FITC-H
APC-H	/	0.0
FITC-H	0.0	/

Table 2.4 Compensation matrices applied for data analysis. **A)** Matrix 1 showed that the spillover value between FITC and BV421 channels is equal to zero on the FACSCelesta. **B)** Matrix 2 showed also that there is no spillover between FITC and APC channels. The compensation calculation was performed using FlowJo software.

2.2.12 Immuno-gold labelling of EMPs

Phosphatidylserine and surface antigen expression were examined using an immunogold labelling method with Annexin V and endoglin (CD105). Briefly, MPs were isolated from the medium of cultured EA.hy926 cells as in Section (2.2.3) after treating the cells with 5nM C-peptide for 24h in serum free medium. 10µl of MP pellets were

allowed to adsorb on gold-coated EM grids for 20min. Labelling of MPs was performed on fresh Parafilm sheets, in which grids were allowed to float face down on sequentially applied drops of labelling and washing solutions. Fixation with 2% paraformaldehyde for 15min was performed followed by quenching with 0.05M glycine then blocking with 2% BSA for 30min. The grids were washed with MP buffer twice for 5min between any labelling step and all steps were performed at room temperature. The primary antibody, mouse anti-human CD105 (1:20) (Ref sc-20072, Santa Cruz Biotechnology) was applied for an hour followed by the secondary antibody for another hour (15nm gold-conjugated goat anti-mouse, Sigma-Aldrich). Finally, grids were fixed with 2% glutaraldehyde and negatively stained with 2% uranyl acetate for 3min. For isotype control, the endothelial marker CD105 was replaced with an irrelevant marker CD235a (Ref sc-53905, Santa Cruz Biotechnology) that is exclusively expressed on RBCs (Latham et al., 2015).

Labelling with Annexin V-FITC (1:50) (Ref 556419, BD Pharmingen) in the presence of Binding Buffer (Ref 556454, BD Pharmingen) was performed for 30 min before fixing the MPs with paraformaldehyde then the same previously described labelling steps were applied. Annexin V-FITC was tagged with the secondary antibody, 10nm gold-conjugated mouse anti-FITC (Ref 25582, Electron Microscopy Sciences, Hatfield, PA). For the negative control, Annexin V labelling was performed in buffer free of calcium. Grids were visualised under Transmission Electron Microscopy (TEM) and images were collected with the JEOL 1400 (JEOL Ltd., Tokyo, Japan) at 80 kV at the Electron Microscopy Facility, University of Leicester.

2.2.13 Proteomic analysis of MPs

MPs were isolated from the medium of cultured EA.hy926 cells (as in Section 2.2.3) after treating the cells with 25mM glucose or 5nM C-peptide for 24h in serum free medium. EMP pellets were lysed with reducing lysis buffer (100mM Tris-HCl, 4% SDS, 0.1M dithiothreitol (DTT), pH 7.6) and heated for 3 min at 95°C. Protein extracts were separated on a 4-12% acrylamide gel, on which the electrophoresis was stopped once all the protein markers (ladders) migrated to the resolving gel. The stacking gel was then removed and the resolving gel was stained for 1 h with Coomassie brilliant blue (Bio-Rad Laboratories) followed by destaining in destain solution (H₂O:methanol:acetic acid

in a ratio of 50/40/10 (v/v/v)). The gels were then sent to The Protein Nucleic Acid Chemistry Laboratory (PNAAC, University of Leicester). Excision of each gel lane was performed in the PNAAC facility then gels were subjected to in-gel tryptic digestion and the resultant peptides were analyzed by label-free liquid chromatography coupled to tandem mass spectrometry (LC-MS/MS) using an LTQ-Orbitrap (ThermoFisher Scientific). Two search engines were employed to infer peptide and protein identities from the mass spectra: MASCOT (version 2.2.04, Matrix Science) and X! Tandem (version CYCLONE 2010.12.01.1, The Global Proteome Machine Organization). Acquired MS/MS data were queried against human entries in UniProt database (The Universal Protein Resource, updated 2016-11). Scaffold software (version 4.8.4, Proteome Software, Inc.) was used to calculate the normalized spectral counts, and to validate peptide and protein identifications. The filtering criteria used in Scaffold for screening proteins were: peptide probability at 95% or higher and protein probability at 99% or higher with at least 2 identified independent peptides, to ensure a false discovery rate (FDR) below 1% (de Jong et al., 2012).

Unique proteins (identified in C-peptide-treated or glucose-treated MPs) which have at least two spectral counts (Burger et al., 2017) were included in the ClueGo functional analysis (Bindea et al., 2009). After obtaining a license key from the author, ClueGo plugin (version 2.5.2) was installed in Cytoscape (3.6.1, java version: 1.8.0_162) which is an open source bioinformatics platform for biological network visualization and data integration (Shannon et al., 2003). UniPro accession numbers were imported into ClueGo and CluePedia (version 1.5.2) for functional enrichment of gene ontology (GO) biological processes (updated November 11 2018) and Reactome pathways (updated October 27, 2018). The p value was calculated using right-sided hypergeometric tests with Benjamini-Hochberg correction for multiple testing. An adjusted $p < 0.05$ was accepted for statistical significance of functional enrichment.

2.2.14 Diabetic rat study

2.2.14.1 Induction of DM and animal groups

Briefly, DM was induced in male Wister rats by a single intravenous injection of STZ solution prepared immediately in citrate buffer and injected at a dose of 65mg/kg after an overnight fast. After two days of STZ injection, confirmation of DM development was performed by measuring blood glucose. Only animals that achieved more than 14mmol/L blood glucose were included in the study. Animals were fed standard rat chow diet and water *ad libitum* throughout the study. Diabetic rats were randomly assigned to diabetic group and to C-peptide-treated diabetic group. Age- and sex-matched rats untreated with STZ served as healthy controls. For the C-peptide treatment group, diabetic rats were treated with synthetic long-acting pegylated human C-peptide (CBX129801, Cebix) 0.5mg/kg subcutaneously (s.c.) twice weekly for 29 weeks (Jolivalt et al., 2015, Wahren et al., 2016). While rats untreated with C-peptide were received C-peptide vehicle only (0.9%w/v NaCl). All diabetic animals were received s.c. respite insulin 2-3 units of long-acting insulin (Hypurin Bovine Protamine Zinc) twice weekly (Groß et al., 2004, Fukuda et al., 2005, Rumble et al., 1997, Lu et al., 2008) to prevent excessive weight loss and to improve long-term survival while achieving a blood glucose concentration between 25-33mM). Non-diabetic control animals were injected with normal saline instead of insulin. The parameters that were monitored during the study included body weight (twice weekly), blood glucose (daily), plasma C-peptide (monthly) and HbA1C (at the end of the study). After the animal sacrifice, the aorta was excised and placed in 10% formalin for the immunohistochemistry study.

Previous analysis of data from this diabetic rat study revealed that this model was established successfully, and the expected outcomes were achieved. For instance, injecting the diabetic rats with this C-peptide formulation maintained a physiological nanomolar range of plasma C-peptide in these animals throughout the seven-month study duration. Moreover, in addition to the daily monitoring of blood glucose, estimation of HbA1C level at the end of the study showed doubled values in the diabetic rats compared to the control rats (N. Brunskill, unpublished data 2017).

2.2.14.2 Histological analysis of aorta sections

Paraffin embedding and sectioning of aorta tissues were performed in the Histology Facility (Core Biotechnology Services, University of Leicester). Staining with haematoxylin and eosin (H&E) stain, Van Geison stain and Masson's trichrome stain was performed in the facility as well. For data analysis, imaging the slides was performed using digital slide scanner (NanoZoomer-XR, Hamamatsu Photonics, Japan) in the MRC Toxicology Unit (Hodgkin Building, Leicester). Images were acquired and viewed with NDP scan and NDP view software (NanoZoomer Digital Pathology, Hamamatsu). Slides were scanned at 40x resolution with semi-automatic batch scanning and fixed capturing settings for each type of staining.

2.2.14.2.1 Haematoxylin and eosin staining

Morphological alterations in rat aorta was evaluated by H&E staining. Briefly, paraffin embedded aorta sections were dewaxed in xylene (2 x 3 min) and rehydrated in a series of graded alcohols (99% (x2), 95% for 2 min each). After rinsing with tap water. Slides were stained with Mayer's haematoxylin for 5 min then washed in running tap water for 5 min. Eosin solution (1%) was prepared by dissolving eosin in water then adding 1% CaCl₂ prepared in 40% formaldehyde (1:1000). Sections were placed in eosin solution for 2 min then rinsed with running tap water. Slides were then dehydrated through 95% alcohol for 15 seconds and 99% ethanol (2 x 1 min) then cleared in xylene (2 X 5 min). After dehydration and clearing, slides were mounted with DPX resin and left to dry.

2.2.14.2.2 Masson's trichrome staining

To detect collagen fibres in aorta sections, Masson's trichrome staining was performed. Briefly, paraffin-embedded aorta sections were dewaxed in xylene (2 x 3 min) and rehydrated in a series of graded alcohols (99% (x2), 95% for 2 min each). After rinsing with tap water, sections were stained with Weigert's haematoxylin for 10 min and washed for 5 min in running tap water then rinsed with distilled water. Slides were then incubated for 10 min in Trichrome stain (solution A) (Trichrome Stain Kit-Masson, CellPath, ref RHS-773-LG) followed by rinsing with distilled water. A mixture of 1 part solution B (phosphotungstic Acid), 1 part of solution C (phosphomolybdic acid) and 2 parts of distilled water was prepared. Slides were treated with this mix for 5 min then

counterstained in Light Green (solution D) for 5 min. Afterwards, slides were immersed in 1% Acetic acid solution for 30 seconds, rinsed with water, dehydrated with graded alcohol then cleared in xylene and mounted in DPX.

2.2.14.2.3 Elastic Van Gieson (EVG) Miller's stain

To assess the organization and thickness of the elastic fibers in aorta tissue, the Miller method was used. Briefly, paraffin-embedded aorta sections were dewaxed in xylene (2 x 3 min) and rehydrated in a series of graded alcohols (99% (x2), 95% for 2 min each). After rinsing with tap water then distilled water, slides were treated with freshly prepared acidified potassium permanganate (0.25% potassium permanganate in 3% Sulphuric acid, 1:10) for 10 min. Afterwards, slides were rinsed with distilled water, bleached with 1% oxalic acid for 20 seconds, rinsed with distilled water then 99% alcohol. Miller's Elastin stain (Ref 35115, BDH) was applied for 1h then washed with 99% alcohol and distilled water. Slides were counterstained with Van Gieson stain (CellPath, ref RHS-780-100) for 2 min, rinsed with 99% alcohol then cleared in xylene and mounted in DPX.

2.2.14.3 Immunohistochemistry (IHC)

According to standard histological procedures, 4 µm thick sections from rat aorta were deparaffinised in absolute xylene (2 x 5 min), rehydrated in a series of graded alcohols (100%, 90% and 70%) and quenched with 0.6% hydrogen peroxide for 10 min to block endogenous peroxidase activity. Antigen unmasking was performed in sodium citrate buffer (0.01 M citrate buffer, pH 6.0) with microwaving for 10 min at 800w. Sections were allowed to cool down at room temperature for approximately 30 min. To prevent non-specific binding of primary antibody, samples were blocked with 0.5% BSA and 3% milk powder in 10% normal swine serum for 60 min at room temperature. Blocking of endogenous biotin was performed with an Avidin/Biotin Blocking Kit (Ref SP-2001, Vector Laboratories) for 15 min for avidin and for biotin, then slides were washed with phosphate-buffered saline (PBS, pH 7.4) before applying the primary antibody overnight at 4°C (Table 2.1). After washing off the excess primary antibody with PBS (3 x 5 min), slides were incubated with the secondary antibody (Table 2.2) for 25 min then washed (PBS, 3 x 5 min), then the tertiary detection was performed using horseradish

peroxidase (HRP) streptavidin (Ref SA-5704, Vector Laboratories) for 25 min at room temperature. Afterwards, slides were washed (PBS, 3 x 5 min) and the bound antibodies were visualized with Diaminobenzidine (DAB) Peroxidase Substrate kit (Ref SK-4100, Vector Laboratories). After development of the brown colour, slides were washed with tap water (3 x 5 min) then counterstained with haematoxylin (Ref GHS132, Sigma) for 10 seconds, and then washed in running tap water for 10 min. Dehydration of slides was performed in graded ethanol concentrations from 70%, to 90% then 100%, then slides were cleared in xylene (2 x 5 min). Finally, slides were mounted with DPX mounting medium and left to dry.

2.2.14.4 Semi-quantitative analysis of IHC and histology data

For image analysis, Macros were kindly created by Dr Kees Straatman (Advanced Imaging Facility, University of Leicester) using Fiji software (version 1.52d). Briefly, colour deconvolution was applied where appropriate to separate DAB staining from haematoxylin, then the channel of interest was further analysed. For vWF images, an analysis band was applied to enclose the intima layer only, while wider bands were used for nitrotyrosine (3-NT) and AGE staining to include the other aorta layers. For Masson trichrome, the total area of green staining was measured. These macros also allowed the ability to detach any remaining blood components in the vessel lumen before applying the analysis band. A fixed threshold value was applied for each type of staining and the fraction area stained (brown or green) was calculated. Because small aorta sections did not occupy all of the capturing field, correction for the empty space in the images was performed by calculating the total tissue area in the image then normalizing the fraction area stained to the total tissue area.

2.2.15 Statistical analysis

The data were statistically analysed using GraphPad prism, version 7.04 (GraphPad Software, San Diego, CA). All data are presented as mean \pm SEM. For comparison of two normally distributed groups, Student's t-test was used. Analysis of variance between multiple groups was carried out with one-way ANOVA followed by Tukey's *post hoc* test for multiple comparisons. The level of statistical significance was set at $P < 0.05$.

Chapter 3. Flow cytometry of nanoparticles: method refinement

3.1 Introduction

Flow cytometry (FCM) is a powerful technique which allows characterisation of antigenic markers expressed on cells or particles (Welsh et al., 2017). Although challenging, FCM is considered the gold standard technique for MP quantification and identification (Crompton et al., 2015). In FCM, various objects can be detected either based on their light scattering features or their fluorescence (Shapiro, 2005). Since the scattered light from nano-proteinaceous vesicles is little, the instrument noise might overwhelm the generated signal (Nolan and Duggan, 2018). In addition, fluorescent based detection is hampered by the small number of antigens per nanovesicle and by the presence of unbound fluorochromes floating between the vesicles (Inglis et al., 2015). Consequently, distinguishing true MPs from unrelated events represents a major technical challenge. Moreover, FCM of small particles requires working close to the sensitivity limit of the FCM. Consequently, choosing a wide analysis window leads to inclusion of background; conversely, a restricted one leads to loss of small MPs (Erdbrugger et al., 2014).

MPs represent a promising diagnostic tool for human diseases, however their current use in the clinical field is hampered by analytical problems. Despite efforts to standardise and optimise MP analysis by FCM, the reported data on MPs in the literature varies widely (Ayers et al., 2011).

The objectives of this chapter are:

- To adapt and validate the flow cytometric analysis of extracellular vesicles by establishing the assay specificity and linearity.
- To determine the optimal settings for analysis of MPs by flow cytometry.
- To examine the impact of some pre-analytical and analytical variables on the validity and reproducibility of flow cytometric measurements.

3.2 Results

3.2.1 Resolution level achieved with FACSCelesta®.

By setting the discriminator on fluorescence, the flow cytometer used in this study, FACSCelesta®, showed a superior resolution between nanobead populations (Megamix-Plus SSC beads) as demonstrated by its ability to discriminate between all bead populations without overlap based on their SSC and fluorescent detection (Figure 3.1). Using the MP analysis setting (Section 2.2.11.1), SSC sensitivity was evaluated by calculating the separation index between 160nm and 200nm beads which gave a value of 6 out of an accepted range from 3 to 8 in standard BD flow cytometers (Poncelet et al., 2015).

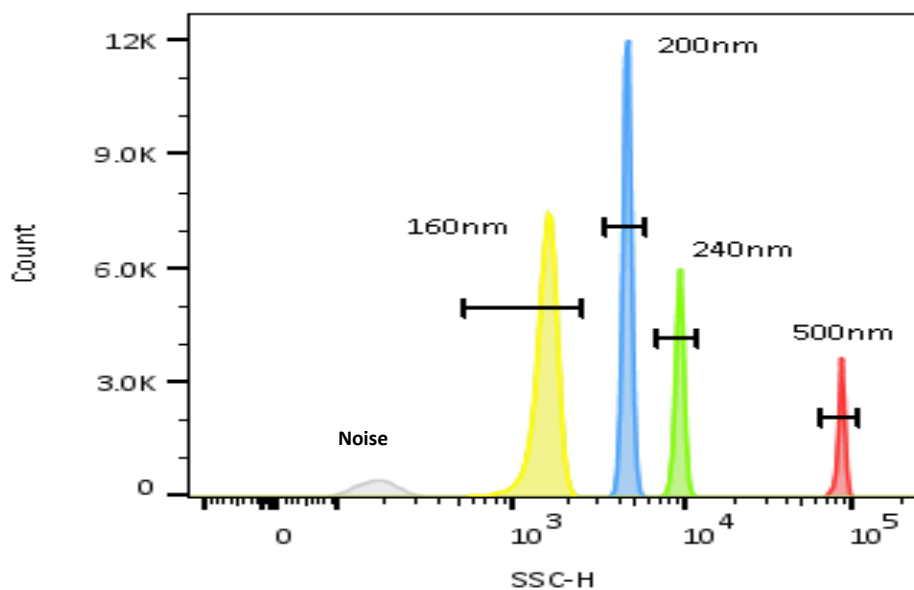


Figure 3.1 FACSCelesta® flow cytometer demonstrated high SSC resolution among submicron beads. Megamix-Plus SSC bead cocktail was run on the flow cytometer under optimized MP settings. All the four bead sets were nicely resolved without overlapping based on their SSC distribution. The plot shows SSC histogram for all events (ungated) using fluorescent as a trigger (FITC triggering).

Moreover, fluorescence and SSC sensitivity clearly showed the ability to differentiate between the smallest 160nm fluorescent beads and the instrument noise (Figure 3.2).

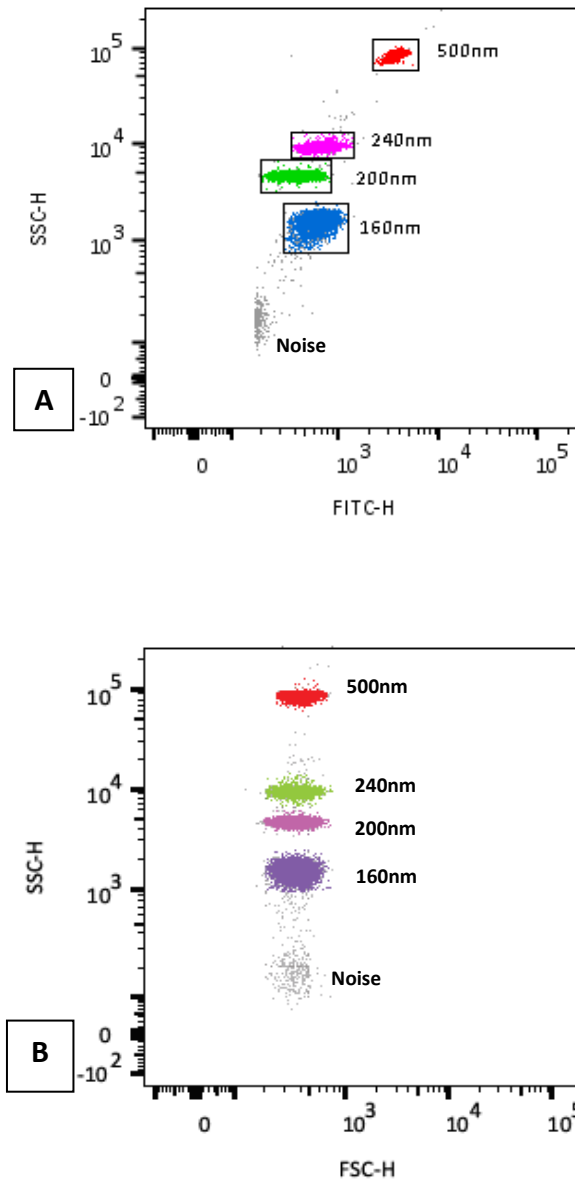


Figure 3.2 FACSCelesta® flow cytometer showed clear separation between all Megamix-Plus SSC bead subsets and the instrument noise based on fluorescent detection. A) The plot illustrates the location of all bead subsets in a SSC-H/FITC-H dot plot showing all events and triggered on FITC. **B)** The ungated plot depicts Megamix-Plus SSC bead clouds in a dual scatter dot plot with FITC discriminator using the standardised MP settings.

By switching to SSC discriminator, SSC parameter retained its capability to resolve all bead clouds with little contribution from the instrument noise (Figure 3.3).

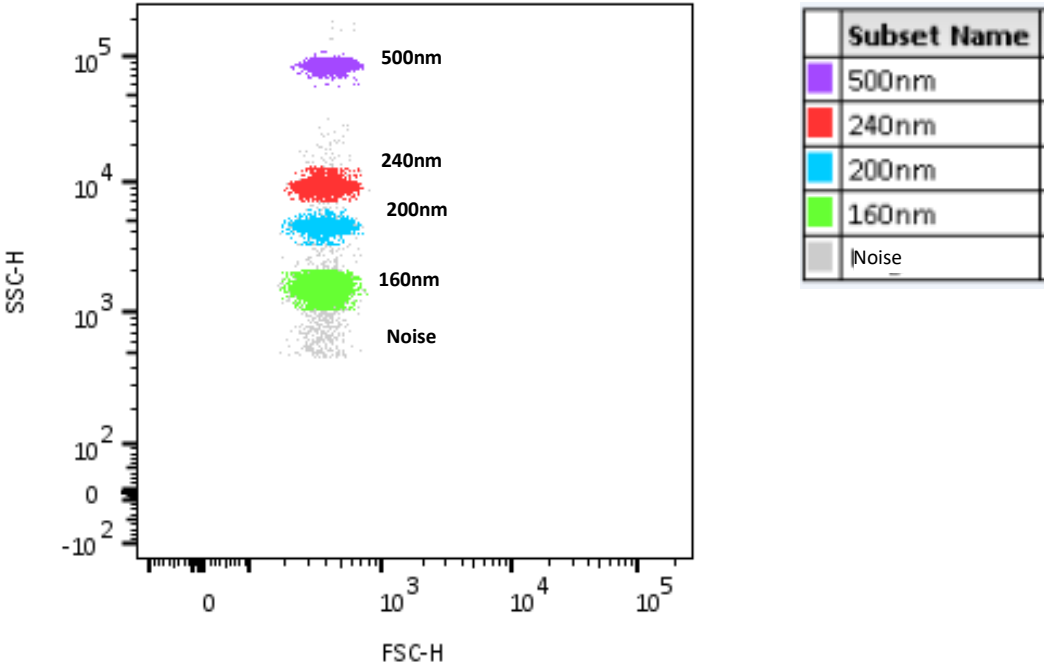


Figure 3.3 FACSCelesta® flow cytometer demonstrated good separation between Megamix-Plus SSC bead subsets and the instrument noise based on SSC detection. Ungated dual scatter dot-plot showing all the distinct Megamix-Plus SSC bead population with the discriminator set on the SSC detector.

FSC parameter was able to resolve only the biggest, 500nm beads, from the background noise. All three remaining beads were superimposed with each other into a one large cloud (Figure 3.4).

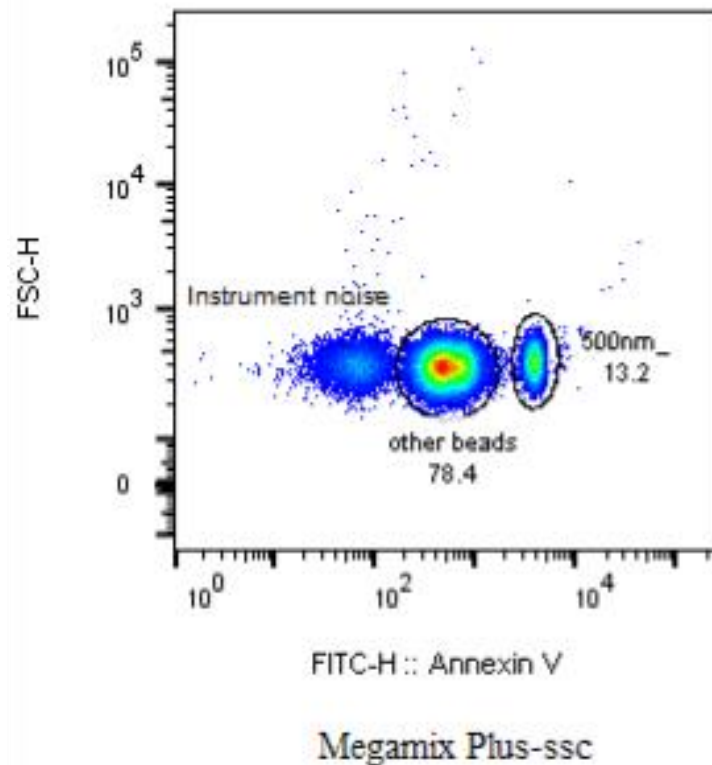


Figure 3.4 Low FSC resolution between submicron beads in FACSCelesta® flow cytometer. Megamix-Plus SSC beads were run on the FC under MP optimized settings. From the bead cocktail, only the biggest 500nm bead subset was distinguishable from the other smaller beads. Whereas, the remaining three beads (240nm, 200nm and 166nm) were not resolved from each other and appeared as one cloud. The density plot shows the distribution of Megamix-Plus SSC beads on FSC-H/FITC-H ungated with discriminator set on SSC detector.

3.2.2 MP population included in the analysis delimited by MP gate

The population involved in the FCM analysis of MPs was chosen based on the position of Megamix-Plus SSC beads. After determining the appropriate voltages for FSC and SSC detectors, the threshold value was calculated (Section 2.2.11.1). Applying this cut-off resulted in a voluntary exclusion of 160nm beads from the final MP region (Figure 3.5 B). Therefore, the MP gate boundaries was established by the 500nm beads cloud (upper limit) while the lower limit was defined by the SSC discriminator value corresponding to 170nm beads level. The final MP gate is expected to mimic MP size range between 0.3-1 μ m (Section 2.2.11.1).

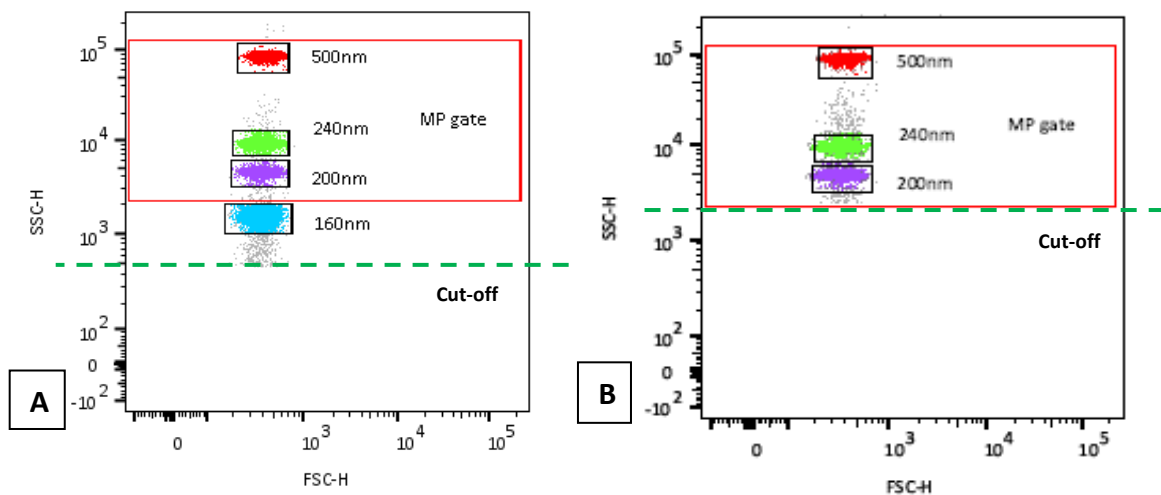


Figure 3.5 Dual scatter dot plot depicting the final MP analysis window defined by Megamix-Plus SSC beads. 500nm beads cloud is the upper margin while the lower margin is delimited by SSC discriminator value. This MP gate is expected to be comparable to MP size range between 0.3-1 μ m. The green dotted line specifies the cut-off level. **A)** Megamix-Plus SSC beads at low threshold showing all beads subsets. **B)** Megamix-Plus SSC beads at high threshold (at level of 170nm beads) showing only the remaining three beads subsets (500, 240 and 200nm beads).

3.2.3 Absence of “swarming artefact” during flow cytometric measurements.

To prove that coincidence of multiple MPs was not part of the cytometric measurement (swarm detection artefact) (Section 2.2.11.2) , concentrated MP samples were stained with Annexin V then serially double diluted with suspending buffer and analysed on the flow cytometer. The numbers of positively stained Annexin V MPs within the MP gate consistently diminished with the respective dilution factor while MFI value remained constant (Figure 3.6 and 3.7).

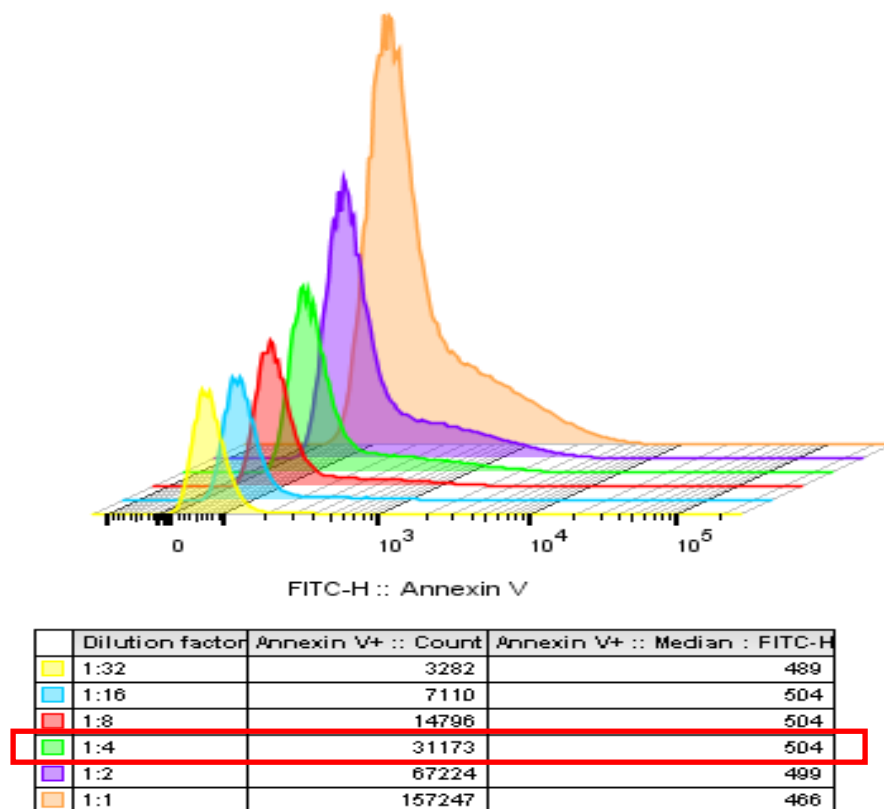


Figure 3.6 Flow cytometric measurement was free from coincidence. Stagger histograms of Annexin V-FITC showing an example of serially diluted MP sample stained with Annexin V. MFI of Annexin V for the positive MP population was stable with increasing the number of positive events, confirming the absence of swarm detection during measurements. The red rectangle highlights the MP sample concentration that was within the usual experimental range (the event count is shown without normalisation to the count beads).

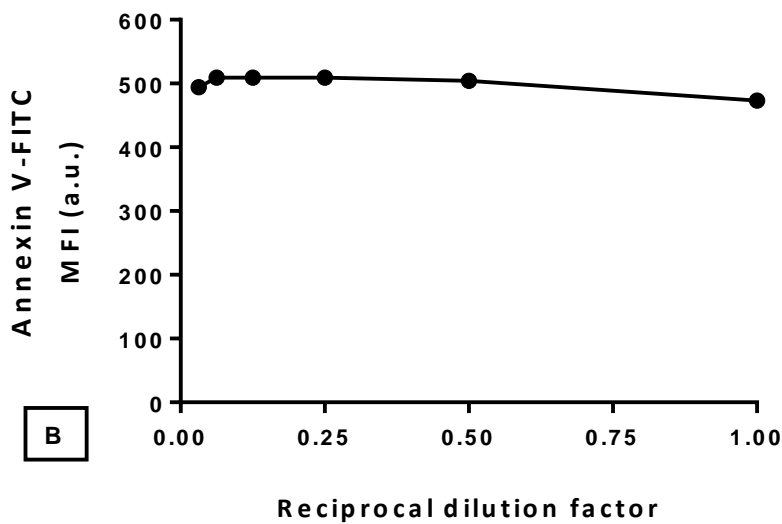
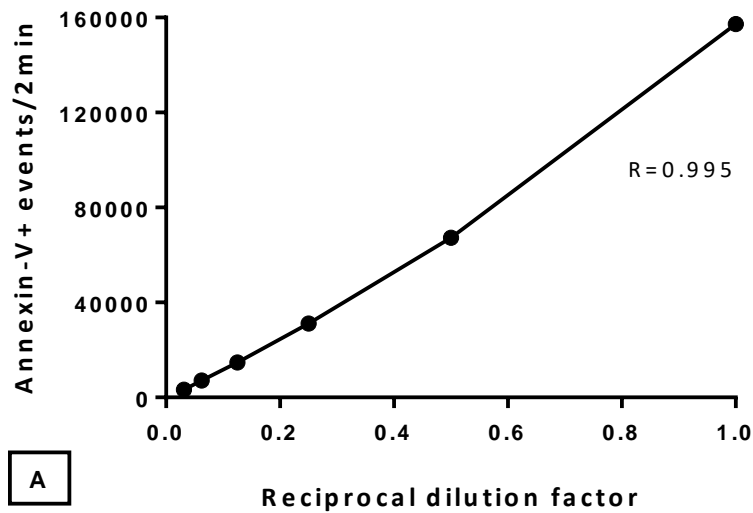


Figure 3.7 Absence of swarm detection during MP counting by flow cytometry. Concentrated MP sample was stained with Annexin V then serially double diluted. **A)** Dilution of sample decreased the number of positively stained MPs in a linear way. **B)** MFI of Annexin V-FITC remained stable with increasing the number of Annexin positive events which excludes a significant involvement of coincidence artefact during data acquiring. R refers to Pearson correlation.

3.2.4 Optimising MP labelling for FCM.

3.2.4.1 Annexin V titration

As shown in Figures 3.8, the number of Annexin V+ (Annexin V positive) events was increased with increasing the antibody concentration. However, at a dilution of 1:50 (high concentration), a shift in MFI of the Annexin V- (Annexin V negative) population was observed compared to that of unstained samples (Figure 3.9). Thus, a dilution of 1:100 corresponds to saturation without increasing the non-specific fluorescence was selected.

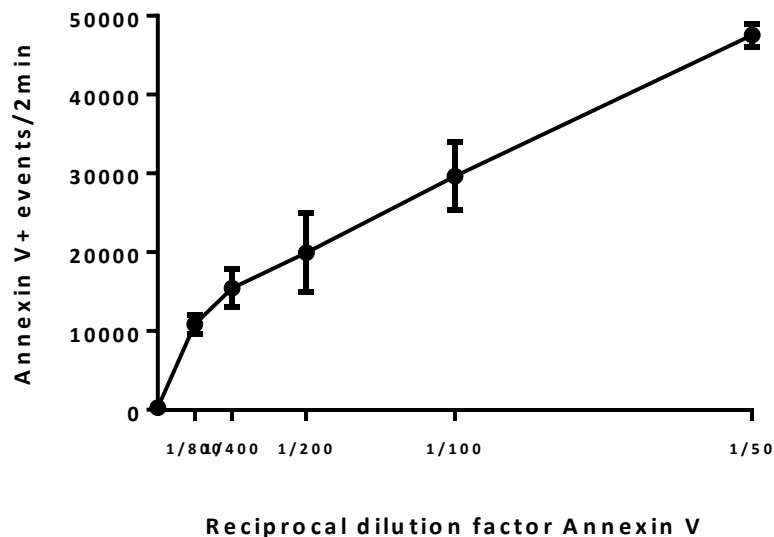


Figure 3.8 Annexin V titration curve showing the number of Annexin V+ MPs detected at various concentrations of Annexin V. The stain concentrations are expressed as reciprocal dilutions of stock solution. Each data point represents the mean \pm SEM of two independent experiments. Dilution of 1:100 corresponds to saturation without increasing the background fluorescence (refer to Figure 3.9) was used throughout the study.

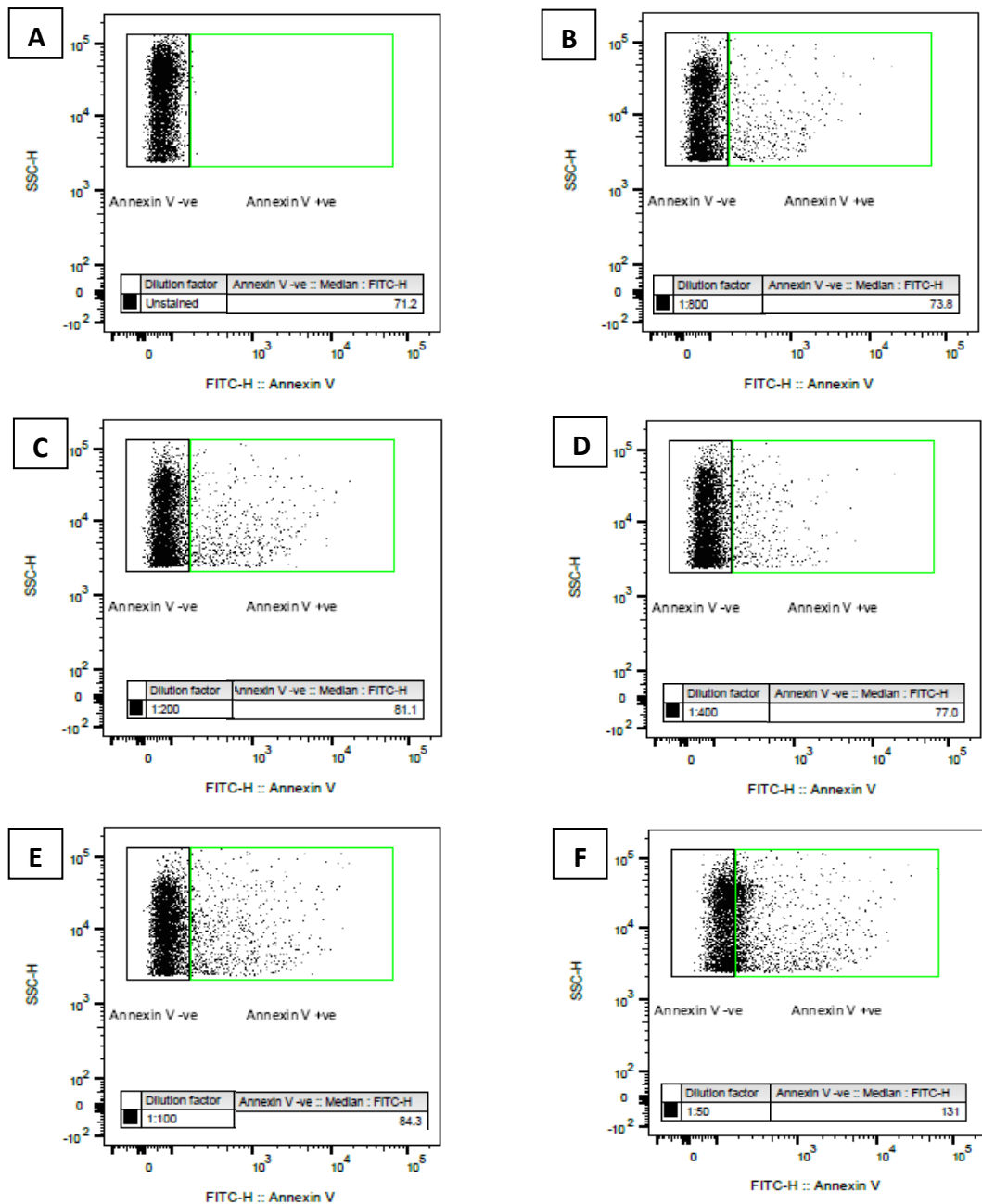


Figure 3.9 Determination of the optimal Annexin V concentration for MP labelling. SSC versus fluorescence intensity bivariate dot plots of MPs stained with Annexin V. MFI of Annexin V negative population for each antibody concentration was compared with that of the unstained MPs. (MFI value and dilution factor are presented in the tables). At dilution of 1:50, a major shift in MFI of the negative population was observed.

3.2.4.2 Antibody titration

Figure 3.10 shows CD31 titration, the number of CD31+ (CD31 positive) events was increased with increasing the antibody concentration reaching maximum at a dilution of 1:200. No further increase in the number of CD31+ MPs was observed by increasing the antibody concentration, whilst a dilution of 1:50 caused an increase in the background fluorescence of the CD31- population (CD31 negative) (Figure 3.11). Therefore, a dilution of 1:200 was chosen corresponding to saturation without increasing the non-specific fluorescence. A similar trend was obtained for CD105 titration (data not shown).

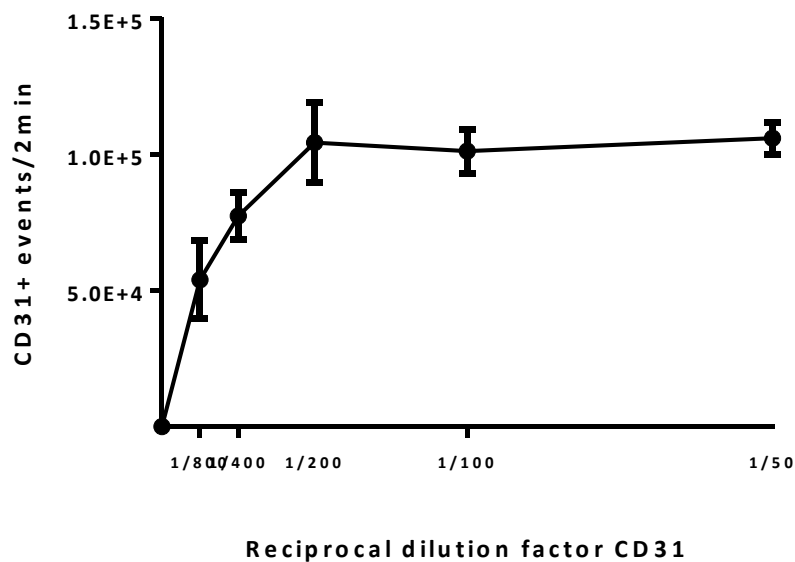


Figure 3.10 CD31 antibody titration curve showing the number of CD31+ MPs detected at various concentrations of anti-CD31. The antibody concentrations are expressed as reciprocal dilutions of stock solutions. Each point represents the mean \pm SEM of two independent experiments. Dilution of 200x corresponds to saturation was used throughout the study.

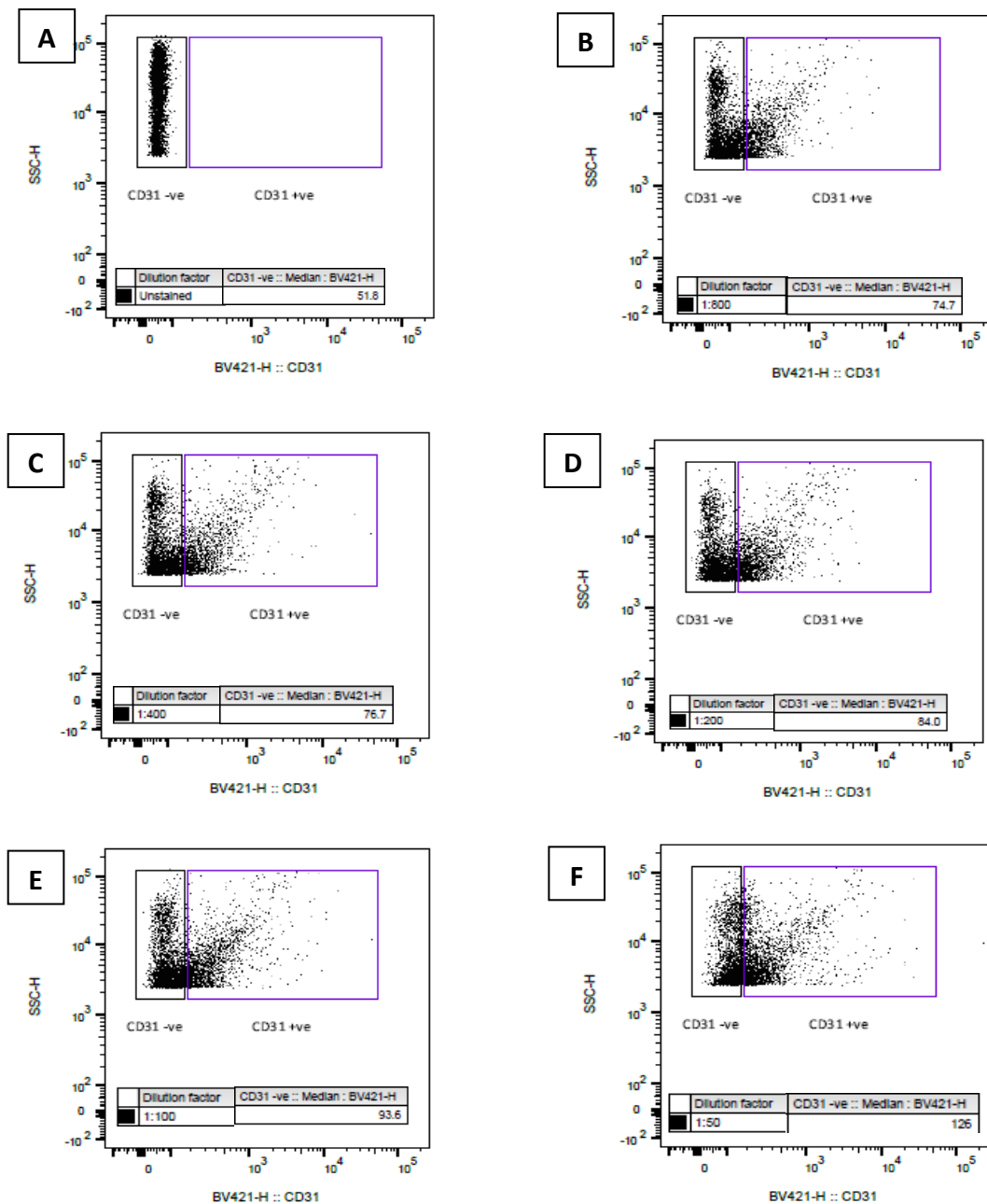


Figure 3.11 Determination of the optimal anti-CD31 concentration for MP labelling. SSC versus fluorescence intensity bivariate dot plots of MPs stained with anti-CD31. MFI of CD31 negative population for each antibody concentration was compared with that of the unstained MPs. (MFI value and dilution factor are presented in the tables). Dilution of 1:50 produced a considerable shift in MFI of the negative population.

3.2.4.3 Specificity of MP labelling.

The specificity of MP staining with the desired antibody was evaluated by comparing it with that of the matched isotype control. MPs samples were stained with the previously optimised concentration of endothelial marker (CD31 or CD105) or with the same concentration of their matched isotype controls. As shown in Figure 3.12 A and B, the number of positively stained MPs with the antibody of interest was several folds compared to that of the isotype which associated with higher MFI. Furthermore, depleting the suspending buffer from calcium during labelling with Annexin V showed a negligible number of Annexin V+ events (Figure 3.12 C).

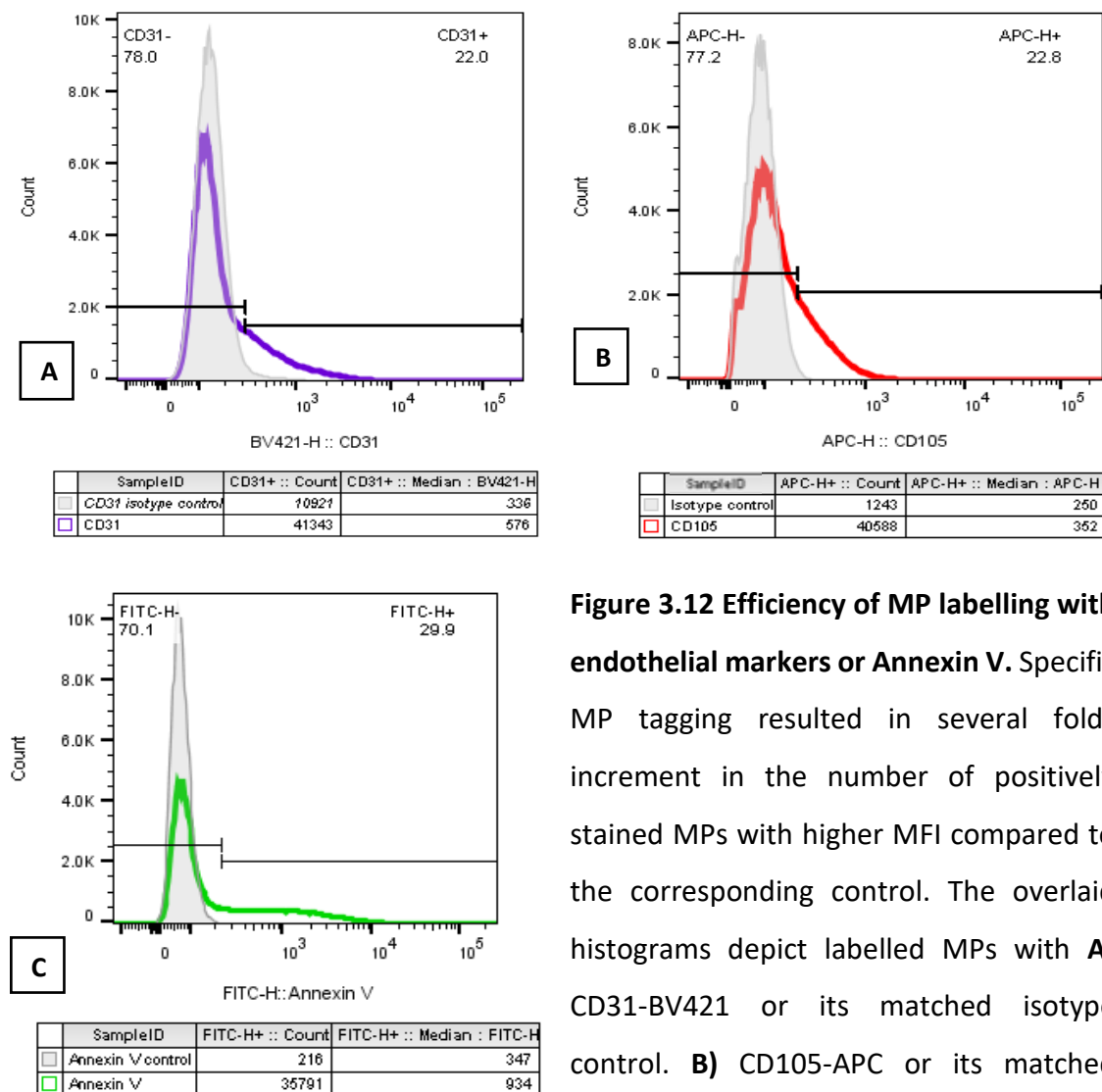


Figure 3.12 Efficiency of MP labelling with endothelial markers or Annexin V. Specific MP tagging resulted in several folds increment in the number of positively stained MPs with higher MFI compared to the corresponding control. The overlaid histograms depict labelled MPs with **A)** CD31-BV421 or its matched isotype control. **B)** CD105-APC or its matched isotype control. **C)** Annexin V or its negative control. Representative graphs were shown. The legends demonstrate the count and MFI for the positive events in MP samples stained with the antibody or its control.

3.2.4.4 Double labelling of MPs: positive controls

To further confirm that the MP analysis settings were appropriate, TNF α and Ca-ionophore were used as positive controls. The number of double labelled MPs in Q2 gate (quadrant 2) increased significantly with time (90min, 6h and 24h) for TNF α and Ca-ionophore compared to unstimulated cells (see Chapter 4 for quantitative data in).

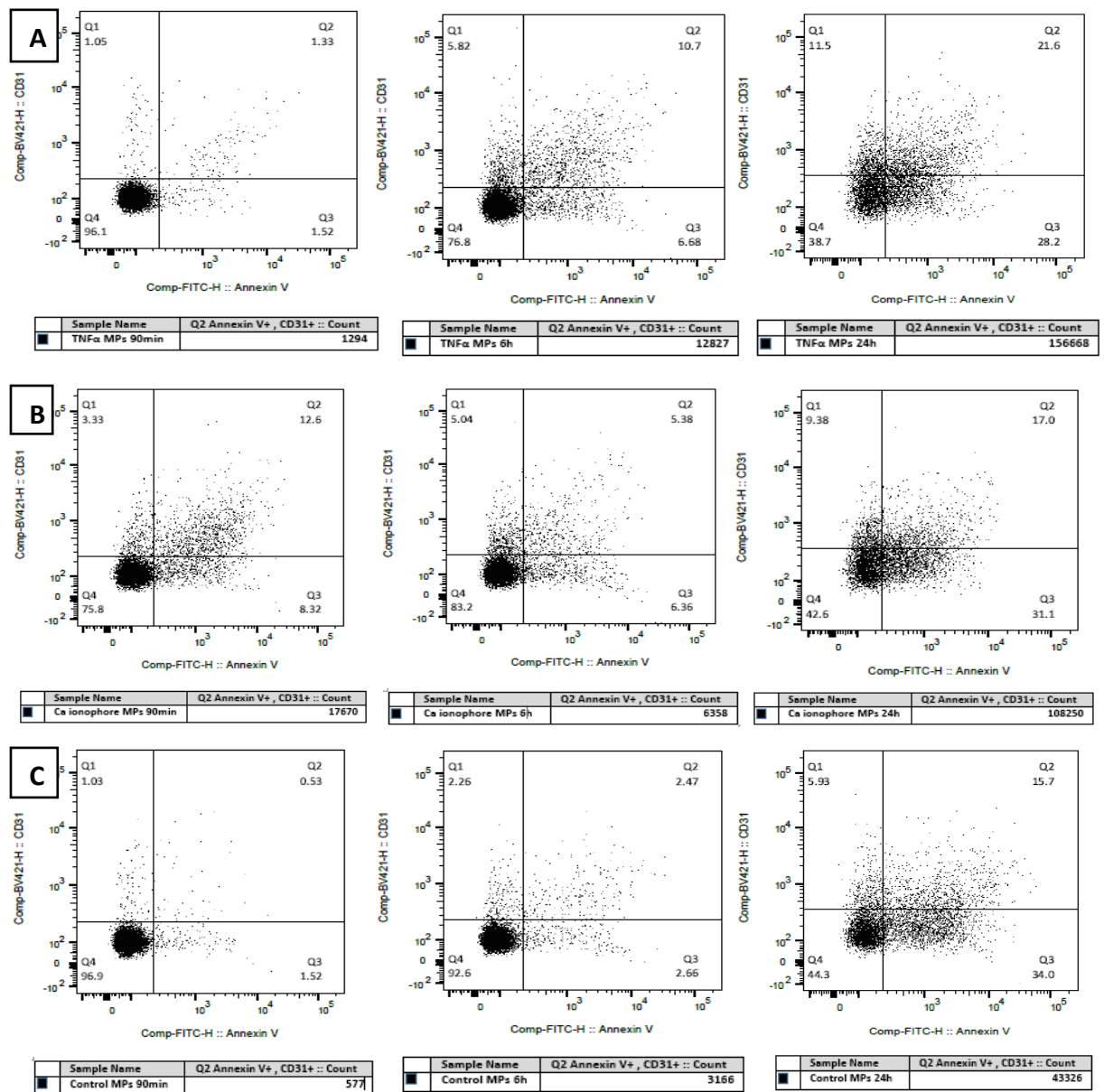


Figure 3.13 TNF α and Ca-ionophore augment MP generation from ECs. A) TNF α -induced MPs after 90min, 6h and 24h respectively. **B)** Ca-ionophore-induced MPs after 90min, 6h and 24h respectively. **C)** MPs from unstimulated cells (control MPs). MP pellets were double stained with anti-CD31 and Annexin V for FCM analysis. Representative dot plots are shown. The legends demonstrate the number of positively double labelled MPs in Q2 gate after 2min data acquiring.

3.2.4.5 Double labelling of MPs: negative controls

To further confirm the validity of the obtained data contaminant inclusion was evaluated. MPs samples were treated with detergent to dissolve the lipid content of MPs while leaving any potential protein aggregates intact. As shown in Figure 3.14 C Triton-X100 treatment resulted in the disappearance of dual labelled events in Q2 gate, confirming that the detected double labelled events were real MPs not protein or antibody aggregates. Furthermore, MP samples stained with CD31 or CD105 isotype control and Annexin V in absence of calcium (Double negative controls), resulted in a negligible number of events in Q2 (Figure 3.14 D).

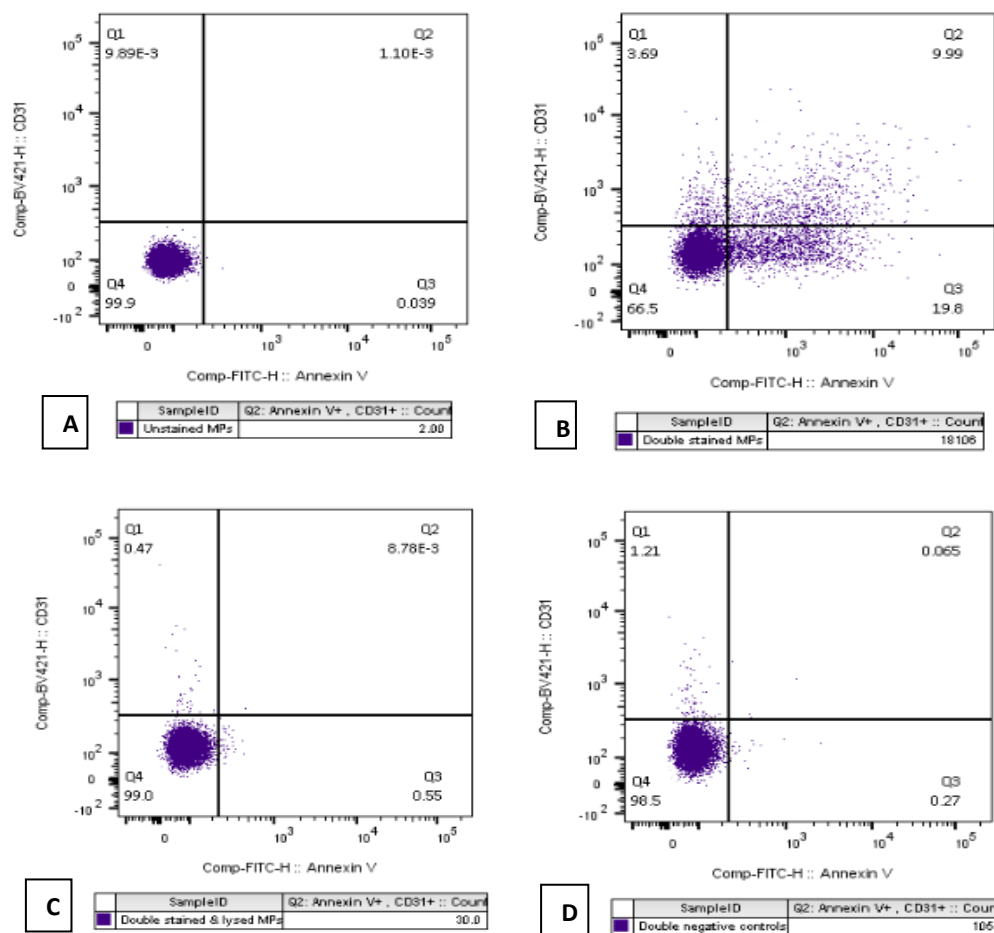


Figure 3.14 Representative dual fluorescence dot plots (FITC-H/BV421-H) illustrating the negative controls used. A) Unstained MPs B) Double labelled MPs with anti-CD31/Annexin V C) MPs stained with anti-CD31/Annexin V and then lysed by adding 0.05% Triton-X100 D) MPs stained with CD31 isotype control and Annexin V in absence of calcium. The legends demonstrate the number of CD31+/Annexin V+ MPs in Q2 gate per 2min acquisition.

The observed double labelling patterns with CD31 antibody were further verified by using another endothelial cells marker, CD105, where similar result was obtained.

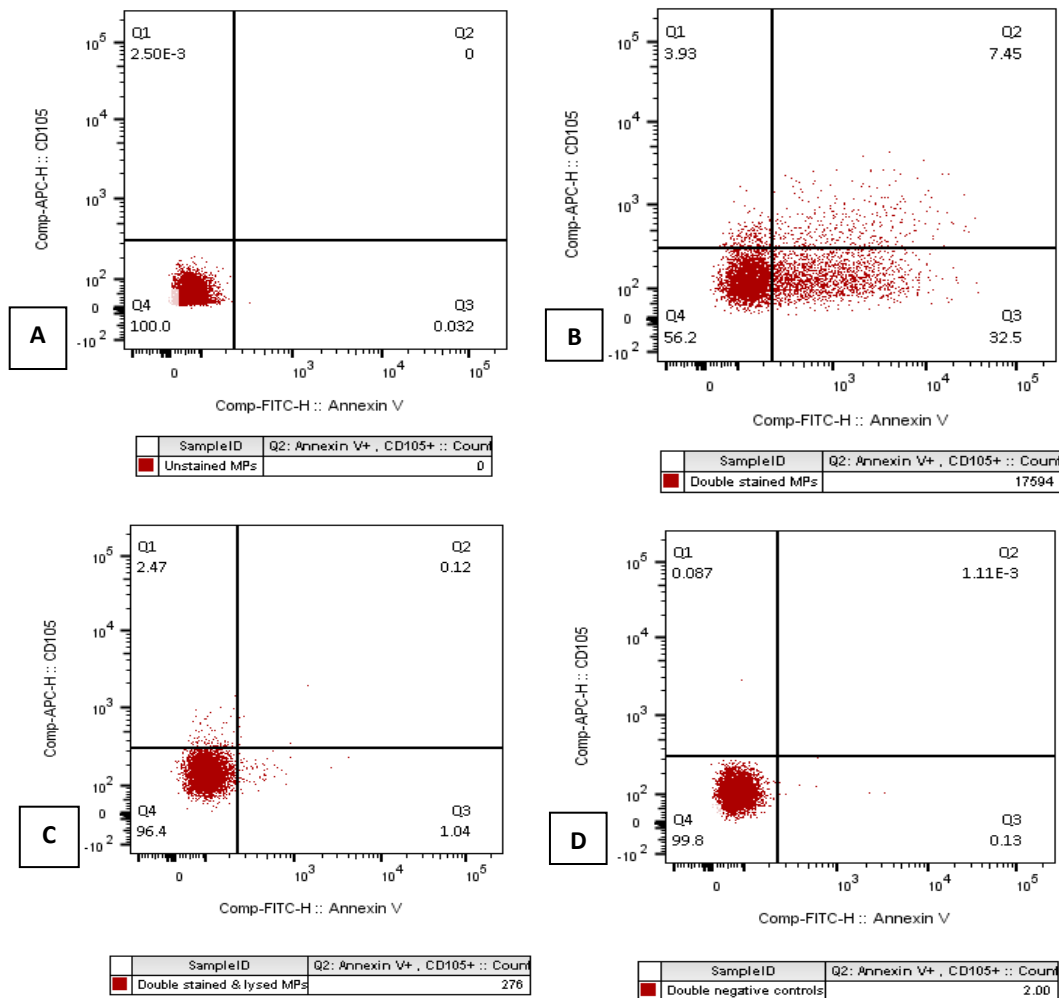


Figure 3.15 Representative dual fluorescence dot plots (FITC-H/APC-H) demonstrating the negative controls used in this study. A) Unstained MPs B) Double labelled MPs with anti-CD105/Annexin V C) MPs stained with anti-CD105/Annexin V and then lysed by adding 0.05% Triton-X 100 D) MPs stained with CD105 isotype control and Annexin V in the absence of calcium. The legends demonstrate the number of CD105+/Annexin V+ MPs in Q2 gate per 2min acquisition.

3.2.4.6 Post-staining washing versus no washing protocols for MP labelling

3.2.4.6.1 Single stained MP samples.

Most MP labelling for FCM does not involve removing the unbound fluorochrome after staining (herein named no washing protocol) to assist high throughput sample processing and to avoid further sample loss. However, washing methods are applicable for small-scale experiments (Jansen et al., 2012). To investigate the consequence of leaving the free dye while characterising samples by FCM, a comparison between the two labelling approaches was performed. MP pellets were single stained with CD31 antibody then either washed or left unwashed after staining. Leaving the free dye during measurement resulted in a marked increase in the number of CD31+ events in unwashed MP samples (Figure 3.16) compared to the washed samples where MFI values decreased (Figure 3.17). A high number of CD31+ events was detected when adding CD31 antibody to 0.2µm filtered buffer only without adding MPs (Figure 3.16 and 3.17). This interference from the unbound antibody was also observed when other antibodies such as CD105-APC, CD144-PE and CD54-APC, were tested (data not shown).

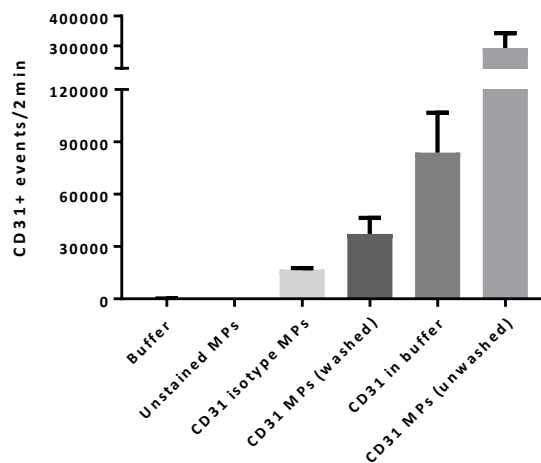
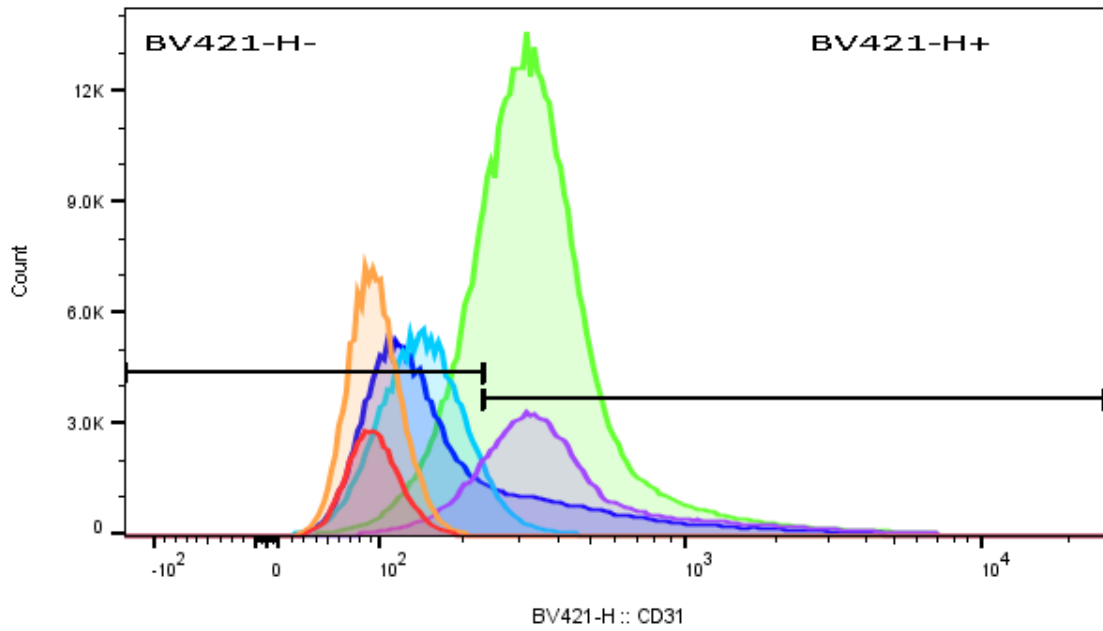


Figure 3.16 The influence of the unbound antibody on MP detection. MPs samples were either washed or left unwashed after staining with CD31 antibody. The numbers of CD31+ MPs were quantified by FCM. Positive events resulted from CD31 isotype control, unstained MPs and CD31 in buffer only were also overlaid for comparison. Data is expressed as mean \pm SEM (n=3).



	SampleID	BV421-H +ve :: Count	BV421-H +ve :: Median : BV421-H
■	Buffer	129	276
■	Unstained MPs	129	252
■	CD31 in buffer	115084	388
■	MPs stained with Isotype control (washed)	18585	261
■	MPs stained with CD31 (washed)	55573	439
■	MPs stained with CD31 (unwashed)	390152	357

Figure 3.17 The difference between washing and no washing approaches for MP labelling for flow cytometry. The overlaid histograms depict a representative comparison between the numbers of CD31+ events that resulted from the two methods. Positive events resulted from CD31 isotype control (washed), unstained MPs and CD31 in buffer only were also overlaid for comparison. The legend demonstrates MP count and MFI for CD31-BV421 positive events. The interval gate (black line) discriminates between CD31 positive and negative populations.

Nevertheless, when MP samples were stained with Annexin V only, a slight difference between the two labelling method was observed regarding the number of positively stained MPs (Figure 3.18) while MFI value was nearly doubles by removing the free flours in the washed samples (Figure 3.19).

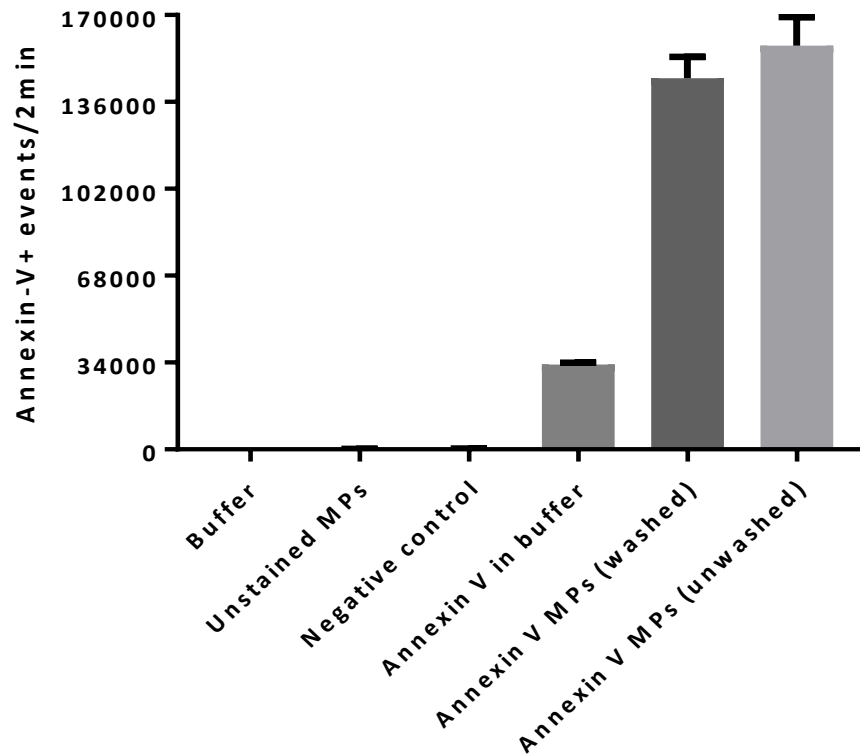
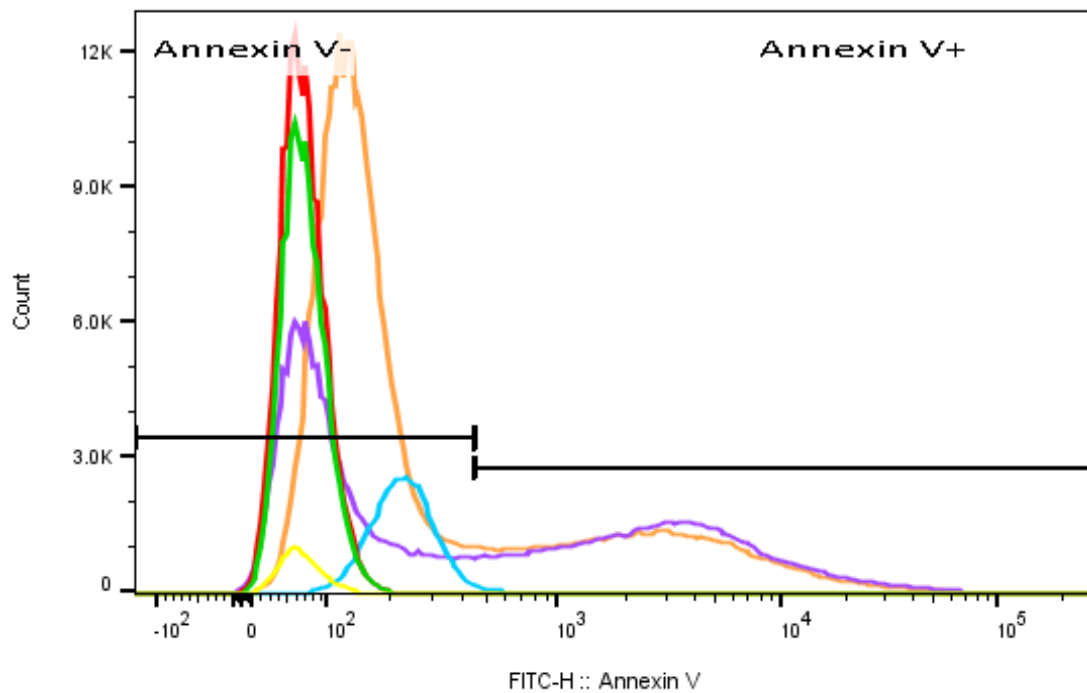


Figure 3.18 Comparison between washing and no washing methods for MP labelling with Annexin V. MPs samples were either washed or left unwashed after staining with Annexin V. The number of Annexin V+ MPs was quantified by flow cytometry. Positive events resulted from Annexin V negative control (washed), unstained MPs and Annexin V in buffer only were also presented for comparison. Data is expressed as mean \pm SEM (n=3).



	SampleID	Annexin V+ :: Count	Annexin V+ :: Median : FITC-H
■	Buffer	3.00	255
■	MPs stained with Annexin V control (washed)	250	293
■	Unstained MPs	113	231
■	Annexin V in buffer	33901	271
■	MPs stained with Annexin V (washed)	135157	2307
■	MPs stained with Annexin V (unwashed)	146814	1446

Figure 3.19 The effect of removing the unbound Annexin V stain during MP labelling. MPs were single stained with Annexin V and either washed or left unwashed after staining. The overlaid histograms depict a representative comparison between the numbers of Annexin V+ events that resulted from the two methods. Positive events resulted from Annexin V control (washed), unstained MPs and Annexin V in buffer only were also overlaid for comparison. The legend demonstrates MP count and MFI for Annexin V-FITC positive events. The interval gate (black line) discriminates between Annexin V positive and negative populations.

3.2.4.6.2 Double stained MP samples.

To investigate whether the background fluorescence from the unbound antibody also impacts on the double labelled samples, double staining of MPs with CD31 antibody and Annexin V was performed. Some of the samples were left unwashed (Figure 3.20 A) while the others were washed (Figure 3.20 B). Leaving the unbound antibody in samples during data acquisition resulted in a shift in the background fluorescence of the negative population (Q4) (Figure 3.20 A).

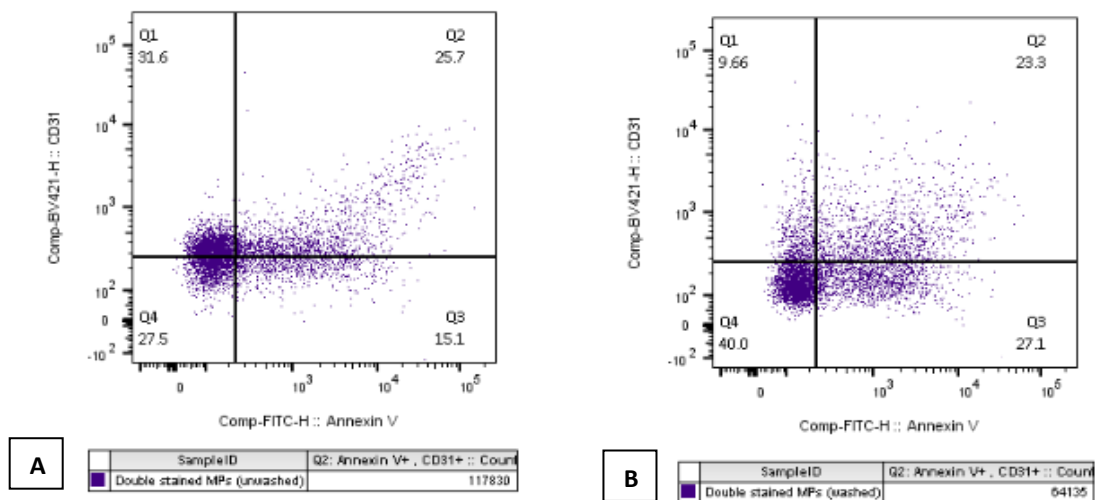


Figure 3.20 Comparison between washed versus unwashed labelling methods of MPs. The dual fluorescence plots illustrate the distribution pattern of MPs double labelled with anti-CD31 and Annexin V. **A)** When double labelled MP sample was analysed directly on the flow cytometer without removing the free flours. **B)** When double labelled MP sample was centrifuged to remove the unbound antibody before the flow cytometric analysis. The legends show event count in Q2 representing the double labelled MPs.

3.3 Discussion.

3.3.1 Resolution limit and the optimal threshold.

Assessment of the detection limit of flow cytometer can be achieved by using reference beads (Erdbrugger et al., 2014, van der Pol et al., 2018). Herein, Megamix-plus SSC fluorescent beads have been used to set up the analysis conditions. The suitability of FACSCelesta for high sensitivity MP analysis was confirmed through the separation index between 160nm and 200nm beads on SSC (Figure 3.1). FACSCelesta achieved a score of 6 while the current accepted value is ranging from 3 to 8; a value below 3 indicates that the flow cytometer is not suitable for high sensitivity measurement (Poncelet et al., 2015). However, as shown in Figure 3.4, FSC was not the best parameter for MP detection due to the absence of PMT on FSC detector. However it has been observed that even with flow cytometers that have PMT on FSC for small events detection, the SSC parameter remains superior and gives better resolution (Tang et al., 2017). This can be explained by the low noise-to-signal ratio in SSC zone (Zucker et al., 2016). In addition, when the particle size becomes below the diameter of laser wave length (here 488nm laser), the particle scatters light in all directions without preference toward the forward direction (Shapiro, 2005, p.106). Thus, SSC was chosen as a threshold parameter. In addition, it has been observed that applying very low threshold level aiming to detect the very small particles, impairs the flow cytometer performance (Robert et al., 2012). Thus, the threshold was set at a workable level just above 160nm beads to avoid a significant contribution from the electronic noise.

Another useful measure for fitness of any flow cytometer for high sensitivity analysis is by evaluating the instrument noise level. Because the performance of any flow cytometer can deteriorate with time, only well-maintained flow cytometer can be used for sensitive analysis. In this study, when the instrument background checked with 0.2 μ m filtered nano-pure water, it showed a noise level of 100-150 events/second. Given that the electronic system of FACS Celesta[®] can deal with 25,000 events/second, this background is considered acceptable (Poncelet et al., 2015).

3.3.2 Calibration of the flow cytometer for size measurement.

Sizing beads are often used to calibrate the flow cytometer for size measurement although this approach has been criticised (van der Pol et al., 2012). Because beads are composed of synthetic materials, their light scattering pattern is different from biological proteinaceous vesicles (Chandler et al., 2011). In this study, Megamix-Plus SSC beads were used to define MP population. It is recognised that this size estimation is relative rather than absolute, however it improves the reproducibility by keeping the analysis window constant between subsequent experiments (Cointe et al., 2017). Dependence on beads for size determination currently has unavoidable limitations (van der Pol et al., 2018). Moreover, as the amount of light scattered by particles is affected by the optical system of the flow cytometer (Bohren and Huffman, 2008), direct comparison of data from different flow cytometers is not feasible even when using the same sizing beads, which prevent laboratory collaborations. Recent trials have been performed to convert the arbitrary scatter units from beads to numerical diameter values but these trials still preliminary (van der Pol et al., 2018).

3.3.3 Effects of coincidence “swarming artefact” on MP quantification by FCM

A caveat associated with flow cytometric measurement is that several cells/particles can be excited by the laser beam at the same time, as a result, signals generated from multiple events erroneously interpreted as one voltage pulse (Figure 3.21) (van der Pol et al., 2012). In any flow cytometer, the hydrodynamic focusing directs cells/particles into one file to the laser interception point; however, because the size of sample core-stream in most standard flow cytometers allows multiple particles to be coincident at the interrogation site simultaneously, many particles can be illuminated at once (Poncelet et al., 2015). In FCM of cells, doublet or clump exclusion is easily performed by recording the signal width (Shapiro, 2005). However, this approach is not feasible for small particles because MP population is heterogenic in nature and obtaining an accurate measurement of signal width is unachievable (Nolan and Duggan, 2018).

The consequences of coincident detection of small events in FCM has drawn more attention recently. van der Pol et al (2012) termed this artefact in MP analysis by “Swarm phenomenon”. The authors urged that in addition to giving erroneous positive

signals, swarm detection results in an underestimation of sample concentration. Furthermore, in case of double labelling, false double positive signal might arise due to swarming of two single labelled particles. To minimise the contribution of swarm detection on MP measurement, a method has been proposed by Nolan and Stoner (2013). It involves acquiring serially diluted fluorescently labelled MP sample on the flow cytometer and recording the MFI for each dilution. Typically, in absence of coincidence, the intensity of fluorescent signal should remain stable with increasing sample concentration. In this study, coincidence was absent during data acquiring as shown in Figures 3.6 and 3.7. Moreover, by using a low flow rate, avoidance of coincidence was further guaranteed.

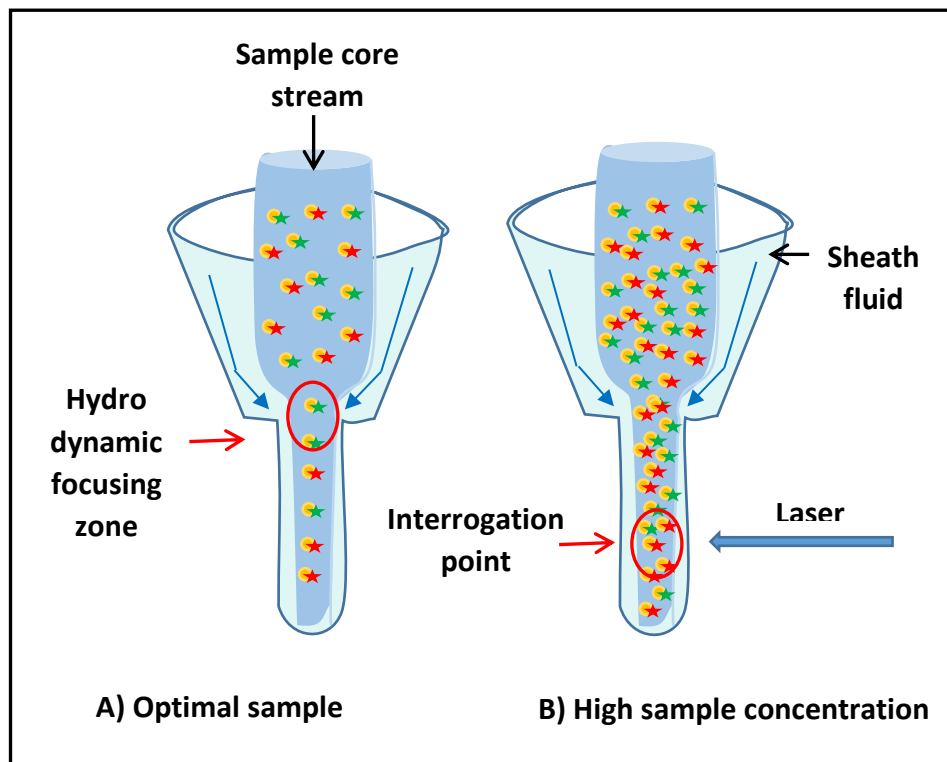


Figure 3.21 Schematic representation of the flow cytometer fluidics system. Sheath fluid hydrodynamically focuses the cell/particle suspension into a single file before passing through the laser intersection point. **A)** Sample concentration within the linear dynamic range of detection. **B)** Concentrated sample in which many particles arrived at the same time to the laser interrogation site resulting in “swarming phenomenon”. Adapted from (Poncelet et al., 2015).

3.3.4 Selecting the appropriate fluorochromes

In designing a FCM experiment, the proper choice of fluorochromes is essential. In the present study, to avoid the requirement for substantial compensation for spectral leakage, fluorochromes which are excited by independent lasers, were chosen (Table 2.2). FITC is excited by the blue laser, APC is excited by the red laser while BV421 is excited by the violet laser. It is well known that spectral bleeding from other channels causes data spread and contributes to higher background which decreases the resolution sensitivity in the primary channel (Maecker et al., 2004). On the other hand, the brightness of the chosen fluorochromes was also considered to provide better detection of the dim MPs. BD Horizon Brilliant™ Violet reagents, such as BV421 (brilliant violet 421) have gained popularity because of their brightness and photo-stability. BV421 used in this study is classified as a very bright fluorochrome, often as bright as or brighter than PE conjugates (BD Life Sciences, 2017).

3.3.5 Identifying the optimal antibody concentration.

Titration of antibodies is essential since non-specific binding occurs at high concentrations and the presence of free dye impairs the flow cytometer sensitivity (Arraud et al., 2016). In principle, the optimal antibody concentration is the one that gives the best discrimination between positive and negative populations calculated by the separation index (SI). However, when the positive and negative events are significantly overlapping, calculating SI is inapplicable (Hulspas et al., 2009). Thus, another technique was used in this study which relies on the saturating concentration of the antibody (Arraud et al., 2016) while the non-specific staining remains relatively stable (Hulspas, 2010) (Figure 3.10 and 3.11).

3.3.6 Techniques for data analysis.

For data presentation and analysis, pulse height was chosen over pulse area. This is in contrast to what is usually used for data analysis in FCM of cells. In general, the flow cytometer acquires height and width for each recorded voltage pulse. Signal area is calculated from the aforementioned parameters (Shapiro, 2005). In FCM of nanoparticles, it has been observed that signal width loses its accuracy, leaving the signal intensity (height) as the only dependable parameter for data analysis (Tang et al.,

2017). Moreover, comparison between data was achieved relying on the event count in a fixed time instead of percent of total population as the later was proved to be a less reliable measure in case of small particle (Inglis et al., 2015). This is because any increase in noise level will increase the total count, consequently, the percent of positive population will decrease.

3.3.7 The impact of unbound fluorescent dye on MP detection by FCM.

Despite of all the method adjustment performed in this study, adding the antibody to buffer only in absence of MPs resulted in high number of positive events in MP gate (Figure 3.16). In principle the antibody molecules should be very small and not detected in the MP gate defined by the sizing beads. However, similar findings have been reported by others (Aass et al., 2011, Inglis et al., 2015). Consequently, careful interpretation of data and application of appropriate controls are mandatory. It has been proposed that these false positive signals result from antibody aggregates (Gyorgy et al., 2011); therefore, the authors suggested adding a detergent to discriminate between MPs and the protein aggregates. Others have suggested spinning the antibody stock at high speed before use to eliminate the aggregates (Aass et al., 2011), although trying this procedure in the current study did not cause a noticeable change, highlighting that the optical background rather than antibody aggregates is the main source for the positive events detected from the antibody in buffer only samples.

Labelling of cells for FCM usually involves a washing step after staining to remove the unbound dye because the presence of free dyes produces an optical background which narrows the positive/negative cut-off (Stall, 2010, Hoffman and Wood, 2007). While cells can be pelleted at low g force, pelleting MPs requires ultracentrifugation. Apart from extra labour that is required for removing the unincorporated dye after MP tagging, this method might result in lower MP count because some might be lost during centrifugation. Clumping is also suggested to occur during ultracentrifugation, especially at speeds like 100,000xg (Ilse et al., 2010). Another disadvantage is the impracticality of this methodology for high-throughput clinical sample analysis, for instance using MP profiles to assess treatment progress or to diagnose diseases. Nevertheless, for the purpose of this study, a post-labelling washing step was applied

for two reasons: first, it was a comparative study therefore any decrease in MP numbers would be consistent throughout all the samples while getting an absolute MP count was not the primary goal. Second, improving the resolution degree by removing the unbound stain resulted in much better differentiation between true MPs and contaminants and decreased false positive signals (Erdburger et al., 2014, Saenz-Cuesta et al., 2015). In addition, the linear Annexin V dilution curve with stable MFI demonstrates that clumping was not an issue in the current study (Figure 3.7).

Quantification of MPs by FCM without applying a washing step appears valid, as displayed in Figure 3.20. However, more rigorous testing of controls should be adopted (Figure 3.14), such as the effect of antibodies alone in the suspension medium (Nolan and Duggan, 2018), MPs stained with matched isotype control, MPs stained and then lysed with a detergent (Gyorgy et al., 2011) and tagging of MPs with an irrelevant marker (Crompton et al., 2015). In this study, without applying a washing step, staining endothelial MPs with CD235a (unique RBC marker) resulted in more positive events than staining them with the specific endothelial marker CD144 (data not shown).

Although applying these controls is important, limitations have been identified for each control. For instance, it is not known if all nano-sized vesicles are lysed by detergent (Crompton et al., 2015); whereas, using the isotype control for gating is controversial and is recommended for qualitative studies but not quantitative ones (Hulspas et al., 2009).

To conclude, conventional flow cytometers obviously have the ability to detect nanovesicles but with varying detection limits. Although that the FCM data might reveal only the visible part of the “iceberg”, these data have proven to be clinically relevant (Amabile et al., 2012, Robert et al., 2012). Thus, depending on how fast the technology is developing, detecting the full-size range of MPs will be possible. While waiting for this to happen, standardisation of sample measurement and applying the appropriate controls are crucial to obtain a reliable data. Thus, performing a detailed optimisation for MP analysis with FCM in this chapter has allowed using this standardised method for studying the potential effect of C-peptide on endothelial function/dysfunction in the next two chapters.

Chapter 4. Effect of C-peptide on the vascular endothelium

4.1 Introduction

C-peptide is deficient in T1DM and in the late stages of T2DM (Bell and Ovalle, 2006, Wahren et al., 2016). Of note, several lines of evidence have demonstrated a regulatory effect for C-peptide on endothelial function (Section 1.4.4.5). Therefore, C-peptide insufficiency might contribute to vascular-related adverse effects.

4.1.1 Effect of C-peptide on endothelial NO production

Altered NO synthesis and/or bioavailability plays a paramount role in various vascular disorders, giving rise to endothelial dysfunction, decreased EC survival, vascular inflammation, plaque formation and instability, and invoking of a prothrombotic state (Magenta et al., 2014). Diabetes is associated with impaired endothelium-dependent vascular relaxation with diminished NO bioavailability (Magenta et al., 2014). Deficiency of C-peptide might contribute to the observed diminished NO production in diabetic patients (Brownlee, 2001). In this regard, multiple *in vivo* and *in vitro* studies have demonstrated a positive role for C-peptide on blood flow and NO production from ECs (discussed in Section 1.4.5.1).

4.1.2 Effect of C-peptide on EC proliferation and/or apoptosis

As the vascular endothelium is located at the interface between blood and the vessel wall, the integrity of this cell layer is essential for normal function. A wide variety of stimuli can trigger pathological EC apoptosis such as deprivation of growth factors or exposure to proapoptotic stimuli (Chavakis and Dimmeler, 2002). Apoptosis of ECs causes vascular leakage, inflammation and coagulation (Winn and Harlan, 2005). In turn, EC proliferation might also be detrimental as in intimal hyperplasia or diabetic retinopathy (Popov, 2010). In fact, in their normal physiological condition, ECs are quiescent with slow turnover rate (Popov, 2010). On the other hand, activated/apoptotic ECs are known to shed MP (Jimenez et al., 2003). Detection of MP release might be a useful tool to evaluate endothelial function. In this context, several studies have investigated the effect of C-peptide on endothelial cell health in general

where both antiapoptotic and proliferative effects were described (Lim et al., 2015, Cifarelli et al., 2011a).

The aim of the studies described in this chapter is to investigate the potential beneficial effect of C-peptide on endothelial function.

The chapter objectives are:

- To confirm EA.hy926 cell responses to C-peptide, as no previous C-peptide study has been conducted using this endothelial cell line. Former reports have described a possible positive role of 5nM C-peptide on eNOS and pERK1/2 protein phospho-activation/expression in ECs. Therefore, in this study the aforementioned observations will be further verified and confirmed in this cell line.
- To examine the possible effect of C-peptide on EC proliferation.
- To investigate the potential effect of C-peptide on MP release from serum-starved EA.hy926 cells.
- To further characterise endothelial MPs (EMPs) using TEM and NTA size measurement.

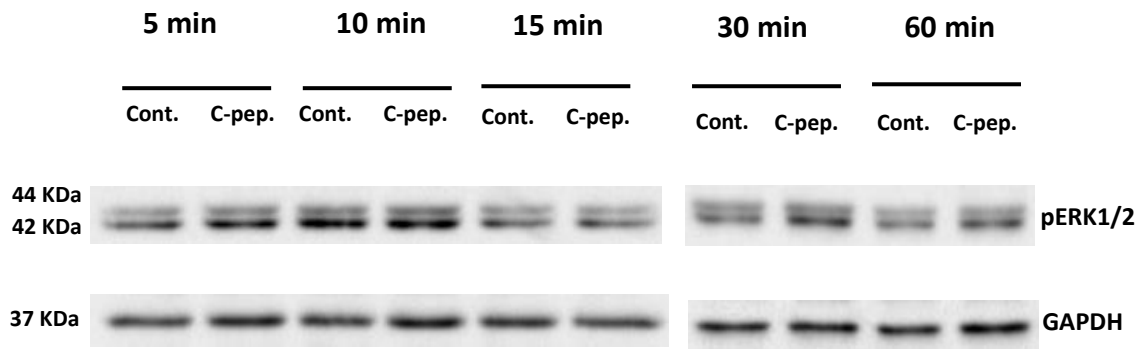
4.2 Result

4.2.1 C-peptide stimulates ERK1/2 phosphorylation in EA.hy926 cells

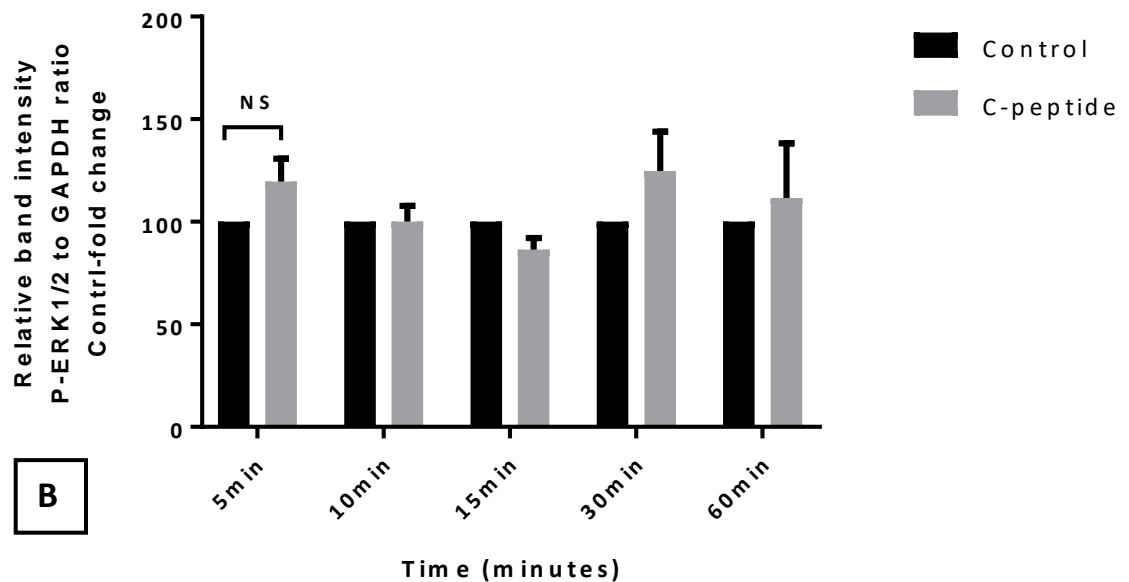
Although C-peptide has been shown to activate MAP kinase (ERK1/2) signalling in a multiple EC types (Hills and Brunskill, 2009) including HUVECs (Lim et al., 2015), its ability to stimulate ERK1/2 phosphorylation in EA.hy926 is unknown. Nevertheless, in a binding study, Rigler et al (1999) reported that C-peptide failed to bind to HUVECs. In the current study, the ability of human C-peptide to stimulate ERK1/2 phosphorylation in EA.hy926 cells was assessed. EA.hy926 cells were treated with human C-peptide accompanied with serum starvation (to avoid the contribution from serum C-peptide) in a dose-dependent manner for 24h (Figure 4.1 A and B). Control cells were treated with C-peptide vehicle under identical conditions. The expression of pERK protein was determined by western blotting.

Stimulation of EA.hy926 cells with increasing doses of C-peptide namely: 0.5, 1, 3, 5 and 10nM for 24h stimulates pERK protein expression significantly in comparison to control cells. Thus the result presented here demonstrated a clear dose-dependent ERK1/2 phosphorylation in EA.hy926 cells following C-peptide treatment for 24h (Figure 4.1 A and B).

For comparison, in another set of ERK1/2 experiments, a short-term incubation of EA.hy926 cells with C-peptide was performed. In these experiments, EA.hy926 cells were deprived of serum overnight then treated with 5nM C-peptide in a time-dependent manner for up to 60min (Figure 4.2 A and B). C-peptide dose was chosen based on previous studies of C-peptide-induced ERK1/2 activation (Al-Rasheed et al., 2004a, Kitamura et al., 2003) and according to the maximum ERK1/2 activation observed in the previous 24h experiment (Figure 4.1 A and B). For each time point, control cells were incubated with C-peptide vehicle for comparison at an identical condition. The expression of pERK protein was determined by western blotting. In these experiments, the effect of C-peptide on ERK1/2 activation which was observed after 24h exposure experiments (Figure 4.1 A and B), was more difficult to reproduce in short-term incubation conditions. Accordingly, an early exposure of EA.hy926 cells to 5nM C-peptide for up to 60min did not show an obvious ERK1/2 activation compared to control cells (Figure 4.2 A and B).



A



B

Figure 4.2 Effect of short-term C-peptide treatment on ERK1/2 activation in EA.hy926 cells. **A)** Expression of pERK1/2 in ECs treated with 5nM C-peptide for up to 60min analysed by western blotting. Control (cont) cells were treated with C-peptide (C-pep) vehicle for the same duration. A representative blot is depicted. **B)** Densitometric analysis for ERK1/2 is presented as the relative ratio to GAPDH. Data are expressed as fold change compared to respective control. The presented values are mean \pm SEM of 4 independent experiments. NS = non-significant difference compared to control condition.

4.2.2 Effect of C-peptide on protein content of EA.hy926 cells

Previous studies have reported a growth factor-like activity for C-peptide in several cell types (Vasic and Walcher, 2012).

In order to assess any growth factor-like ability of C-peptide, EA.hy926 cells were serum starved and treated with C-peptide in a concentration dependent manner for 24h (Figure 4.3). 2% DFBS was used as positive control. Cells treated with C-peptide showed no increase in cell protein content compared to untreated control cells. Conversely, 2% DFBS (Figure 4.3) was associated with a statistically significant ~22% increase in mean protein content after 24h. Thus, estimation of cell mass herein did not reveal a modulatory effect for C-peptide on EA.hy926 cell total protein content.

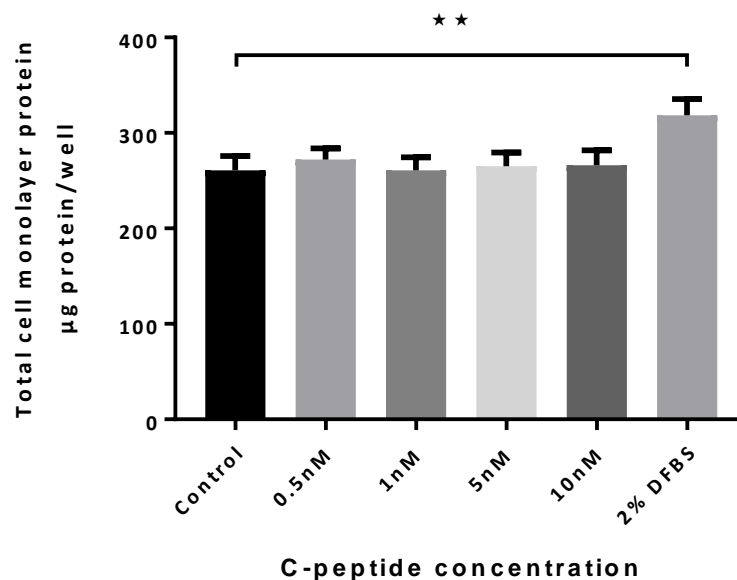


Figure 4.3 C-peptide stimulation does not influence the protein mass of EA.hy926. Cells were stimulated with C-peptide in increasing concentrations, namely, 0.5, 1, 5 and 10nM accompanied by serum starvation for 24h. Control cells were treated with C-peptide vehicle. 2%DFBS was used as a positive control. Total cell monolayer protein content was estimated by Lowry protein assay. Data is expressed as mean \pm SEM (n=6). ** P<0.01 compared to control cells.

4.2.3 Effect of C-peptide on EA.hy926 proliferation and viability

For further confirmation that C-peptide has no significant effect on cell number or protein content, a colorimetric MTT assay was performed as a measure of mitochondrial dehydrogenase activity which reflects the number of metabolically active cells in the cultures (Vistica et al., 1991). EA.hy926 cells were treated with 0.5, 1, 3, 5 and 10nM C-peptide for 24h and 48h to determine cell viability after the intervention (Figure 4.4 A and B). After treating EA.hy926 cells with C-peptide in a concentration- and time-dependent manner, cell viability did not significantly vary compared to untreated control cells (Figure 4.4 A and B)

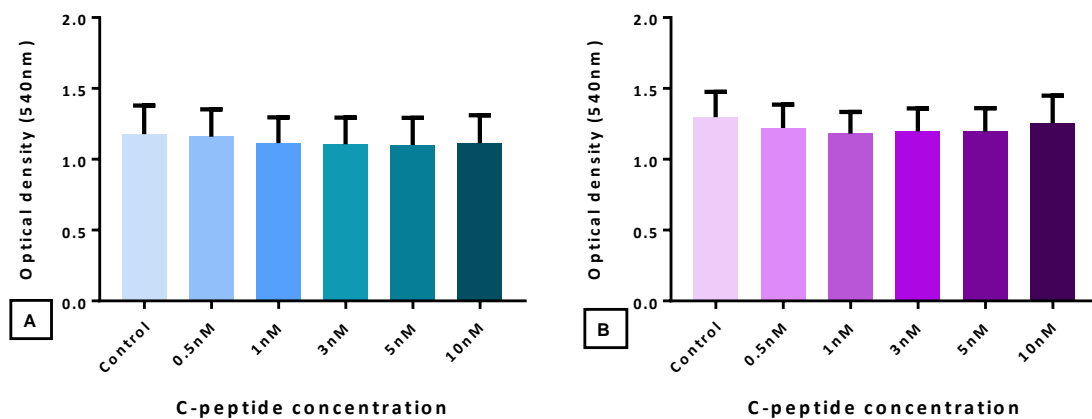


Figure 4.4 Assessment of EA.hy926 proliferation after stimulation with C-peptide. EA.hy926 cells were treated with 0.5, 1, 3, 5 and 10nM C-peptide or C-peptide vehicle for **A)** 24h and **B)** 48h. Cell mitochondrial activity was evaluated by MTT assay. Results are expressed as mean \pm SEM of 5 independent experiments.

4.2.4 Effect of C-peptide treatment on caspase-3 level in serum starved EA.hy926 cells

EC survival is preserved by growth factors and by contact to the extracellular matrix. Serum deprivation, and consequently growth factor deprivation, leads to programmed cell death (apoptosis) of ECs *in vitro* (Chavakis and Dimmeler, 2002). On the other hand, C-peptide has demonstrated anti-apoptotic activity in cells exposed to apoptotic stimuli. Thus, to investigate the possibility that C-peptide might affect apoptosis (estimated by caspase-3 cleavage) in serum starved ECs, caspase-3 activation was examined. EA.hy926 cells were exposed to serum starvation for 24h in with or without C-peptide treatment (Figure 4.5 A and B). The level of cleaved caspase-3 was determined by western blotting. As shown in Figure 4.5 A and B, C-peptide stimulation did not significantly affect the level of cleaved caspase-3 in cell monolayers compared to untreated control cells.

In another set of experiments, to confirm that EA.hy926 cells undergo apoptosis upon growth factor withdrawal (serum deprivation), a group of cells were treated with 2% DFBS for 24h while another group was serum starved. As shown in Figure 4.5 C and D, serum starvation significantly elevates the level of cleaved caspase-3 (17KDa band) compared to cells incubated with 2% serum.

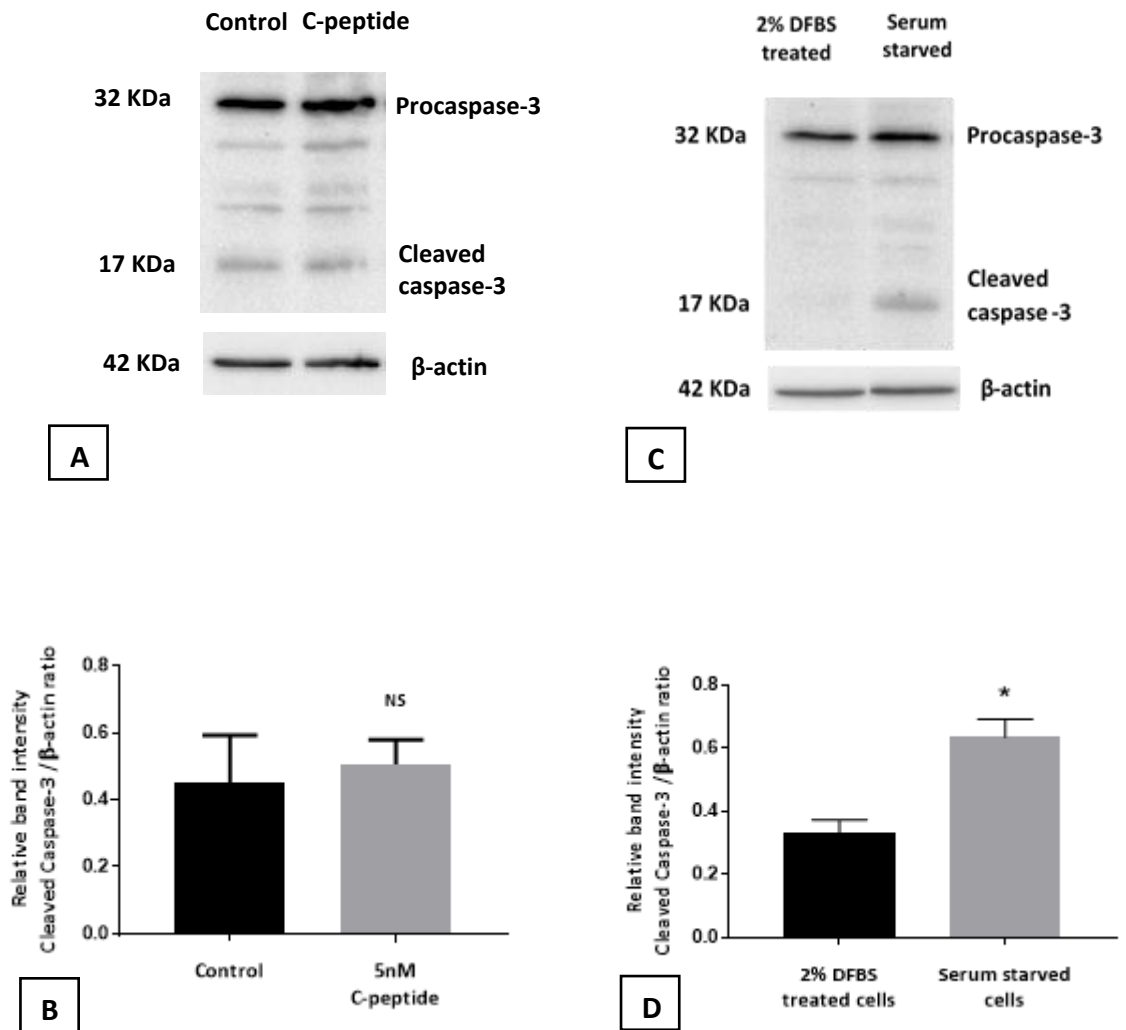


Figure 4.5 Assessment of apoptosis level in serum starved EA.hy926 cells after C-peptide stimulation. **A and B:** Cells were treated with 5nM C-peptide or C-peptide vehicle (control cells) accompanied by serum starvation for 24h. **C and D:** Cells were either treated with 2% DFBS or left serum starved for 24h. **A and C:** Cleavage of caspase-3 was determined by western blot using specific anti-caspase-3 antibody. **B and D:** Densitometric analysis for cleaved caspase-3 (17KDa band) is presented as the ratio relative to β-actin. Results are expressed as mean ± SEM (n=4 for B, n=3 for D). *P<0.05 compared to 2% DFBS treated cells. NS denotes insignificant difference compared to control cells.

4.2.5 Effect of C-peptide on MP release from EA.hy926 endothelial cells.

4.2.5.1 Characterisation of C-peptide-derived MPs: Confirmation of vesicles' morphology

To confirm the presence of EMPs in the prepared pellet, the morphology of the collected vesicles was observed under TEM. EA.hy926 cells were exposed to 5nM C-peptide and serum-starved for 24h. At the end of incubation period, EMP concentrate was prepared as described in Section 2.2.3. Subsequently, some vesicle samples were labelled with either anti-CD105 antibody or Annexin V in presence of binding buffer, to demonstrate their endothelial antigenic origin and phosphatidylserine externalisation (Figure 4.6 C and D). As a control for non-specific tagging, labelling with irrelevant antibody (CD235a) an RBC specific marker was employed (Figure 4.6 B); whereas, omitting the binding buffer was used to control for Annexin V non-specific tagging (Figure 4.6 E).

In general, TEM images depict a heterogeneous population of membranous vesicles with the majority about 200-400nm in diameter. The representative TEM micrograph in Figure 4.6 E demonstrates an extracellular vesicle of about 250nm labelled with CD105 (closed arrow); whereas, samples stained with isotype matched control or secondary antibody only did not show gold nanoparticle tagging (Figure 4.6 A and B). Additionally, phosphatidylserine exposure (open arrow) was demonstrated in Figure 4.6 D in presence of binding buffer while no labelling was observed in absence of binding buffer (Figure 4.6 C).

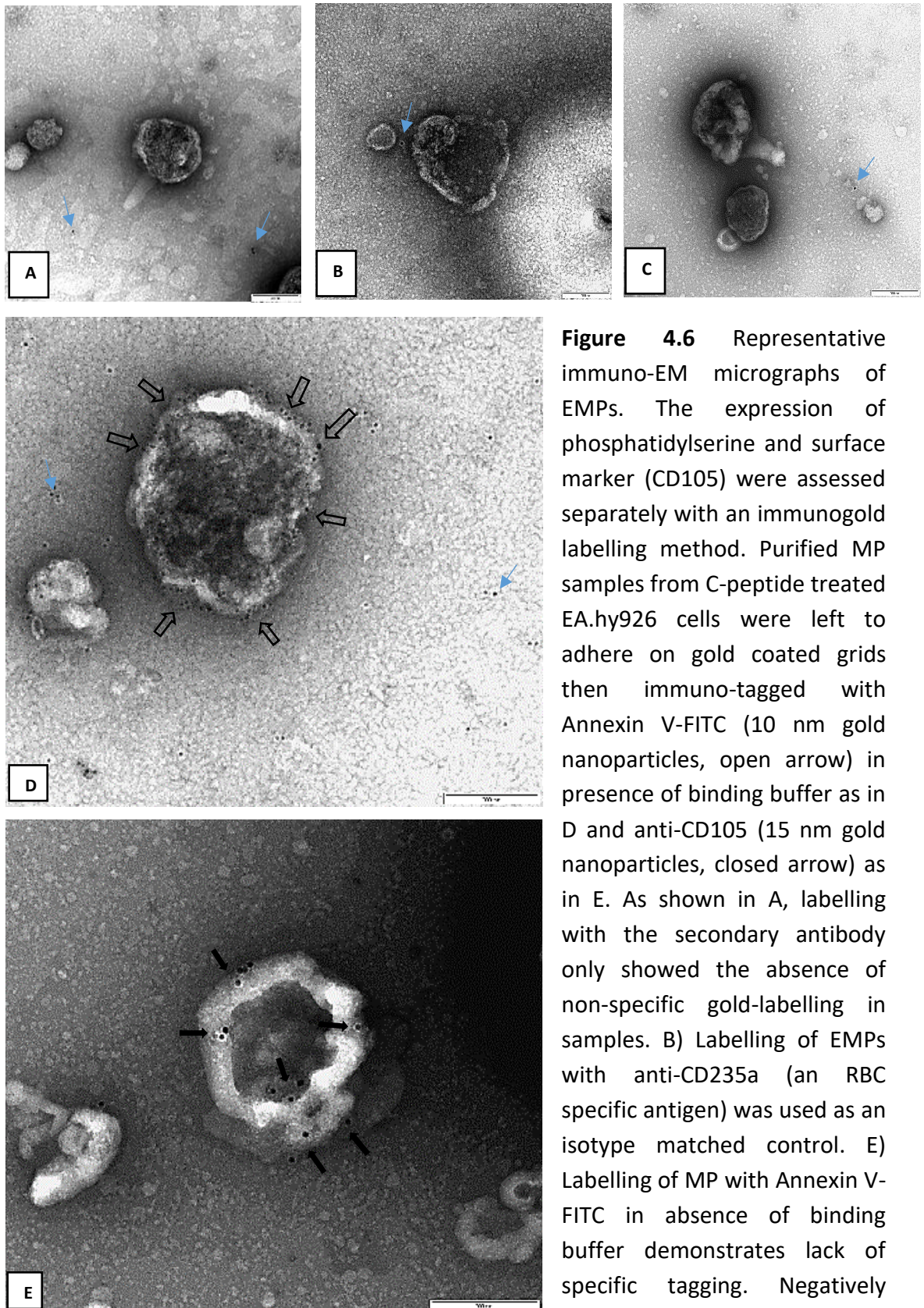


Figure 4.6 Representative immuno-EM micrographs of EMPs. The expression of phosphatidylserine and surface marker (CD105) were assessed separately with an immunogold labelling method. Purified MP samples from C-peptide treated EA.hy926 cells were left to adhere on gold coated grids then immuno-tagged with Annexin V-FITC (10 nm gold nanoparticles, open arrow) in presence of binding buffer as in D and anti-CD105 (15 nm gold nanoparticles, closed arrow) as in E. As shown in A, labelling with the secondary antibody only showed the absence of non-specific gold-labelling in samples. B) Labelling of EMPs with anti-CD235a (an RBC specific antigen) was used as an isotype matched control. E) Labelling of MP with Annexin V-FITC in absence of binding buffer demonstrates lack of specific tagging. Negatively stained Immuno-gold labelled

MP grids were imaged on the JEOL 1400 TEM. All images are to the same scale where scale bars equal 200nm. The blue arrow refers to background gold nanoparticles.

4.2.5.2 Effect of C-peptide on MP generation estimated by nanoparticle tracking analysis

It is well-established that serum-starved ECs shed MPs (Jansen et al., 2015). Apoptosis is considered the major trigger for MP release under these conditions (Jimenez et al., 2003). While C-peptide is reported to affect several aspects of endothelial health, its effect on EMP generation has not been addressed yet. Thus, in this study, the possible modulatory effect of C-peptide stimulation on EMP budding was examined. EA.hy926 cells were treated with increasing concentrations of C-peptide for 24 (Figure 4.7). The number of released MPs in the test medium was estimated by NTA after discarding cell debris.

C-peptide treatment did not significantly affect the number of generated MPs (100-1000nm) from EA.hy926 cells upon serum deprivation compared to untreated control cells (Figure 4.7), when particle count was estimated by NTA. Thus, after 24h cell exposure to C-peptide, there was no obvious change in the level of MP released to the cell medium under any of the tested concentrations.

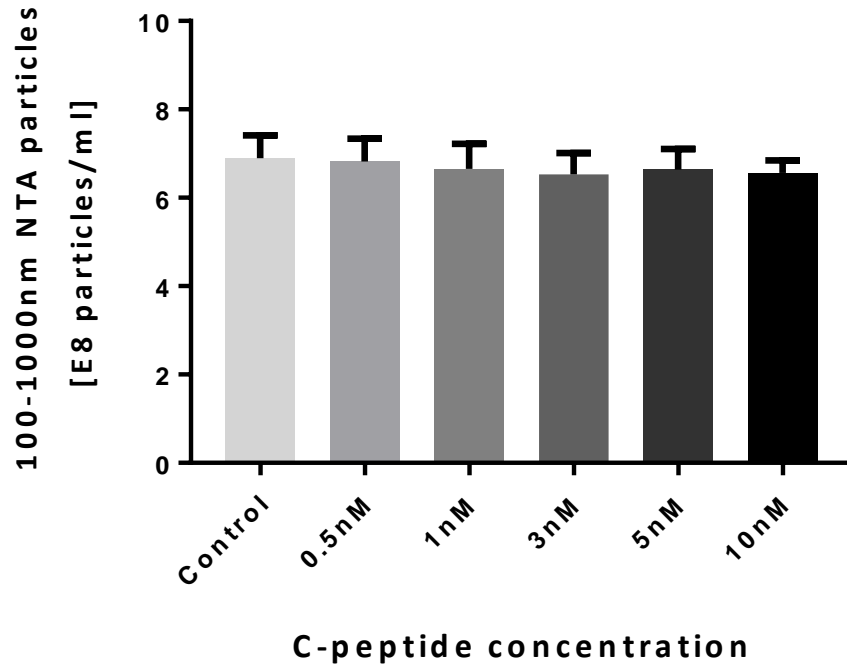


Figure 4.7 Release of MPs from EA.hy926 endothelial cells in response to C-peptide. Cells were treated with increasing C-peptide concentration for 24h. Control cells were treated with C-peptide vehicle. NTA was used for MP counting where only particles of 100-1000nm were included in NTA analysis. The final particle concentration is expressed as E8 (10^8) per ml of the test medium. Data is presented as mean \pm SEM (n=4).

4.2.5.3 Effect of C-peptide on the size distribution of EMPs

Further characterisation of EMPs was performed using NTA. The size range of extracellular vesicle population was determined. Herein, the size of the isolated vesicles was ranging between 30-1000nm (Figure 4.8), which is consistent with the size distribution of vesicle population reported elsewhere (Burger et al., 2017, Abbasian, 2015). In addition, NTA size measurement agrees with TEM data whereby the majority of the observed vesicles lie in a size range between 150-400nm.

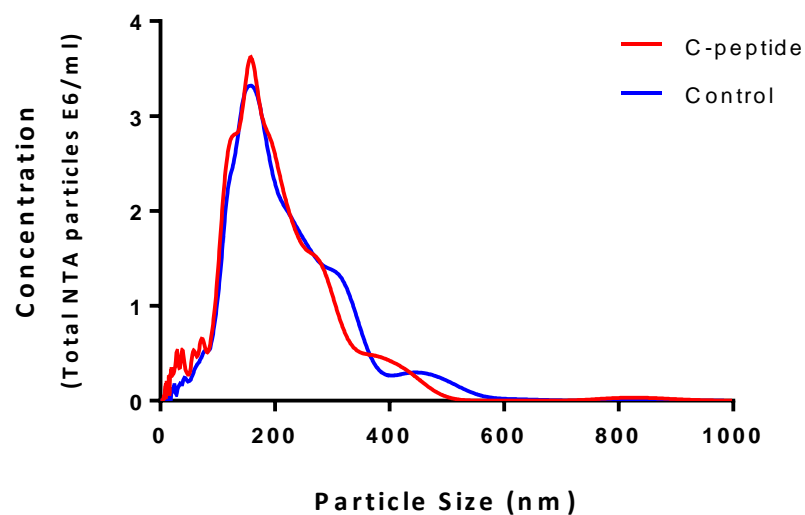


Figure 4.8 Size distributions of EMPs as measured by NTA. EMPs were prepared from EA.hy926 cells conditioned medium after 24h of cell treatment. Cells were treated with 5nM C-peptide or its vehicle for 24h, then the resulting cell supernatants were ultracentrifuged at 20,000xg after eliminating cell debris. NTA measurement using NanoSight LM10 were performed on MP pellet after resuspending in MP buffer. The graph depicts a representative size distribution of MP samples (particle size (x-axis) and concentration (y-axis)). E6 is equivalent to 10^6 .

The mean particle size of C-peptide-derived particles versus control-derived particles was also measured. As shown in Figure 4.9, C-peptide stimulation of EA.hy926 cells did not significantly influence the size of the generated particles ($195 \pm 4\text{nm}$ versus $205 \pm 3\text{nm}$).

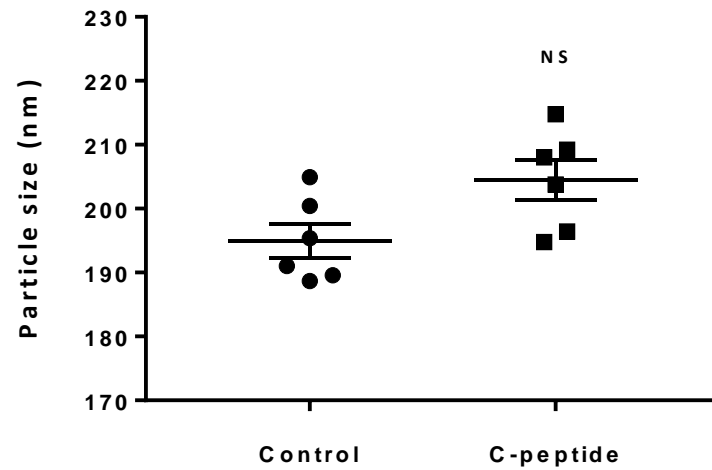


Figure 4.9 Effect of C-peptide on size of MP generated from EA.hy926 cells. Size range of EMPs formed from 5nM C-peptide treated cells or control cells (vehicle treated) after 24h treatment was assessed using NTA. Results are expressed as mean \pm SEM (n=6). NS insignificant difference compared to control cells.

4.2.5.4 Effect of C-peptide on MP shedding quantified by Flow cytometry

In light of the results obtained using NTA (Figure 4.7), a more sensitive and specific method was employed. The number of MPs was estimated by FCM based on MP antigenic determinants and externalisation of phosphatidylserine.

Initial experiments were performed to investigate the potential modulatory effect of C-peptide on MP release at early time points (Figure 4.10 A, B and C). EA.hy926 cells were treated with 5nM C-peptide for 1.5h, 3h and 6h accompanied by serum starvation. C-peptide concentration was selected based on the highest magnitude of activation observed in EA.hy926 upon exposure to C-peptide as assessed by pERK expression (Section 4.2.1). At the end of the incubation period, an MP pellet was isolated by differential centrifugation of the conditioned medium at 20,000xg as described in Section 2.2.3. The counts of double-labelled EMP, CD31⁺/Annexin V⁺ MPs were determined by FCM. For comparison, other groups of cells were treated with 10ng/ μ l TNF α or 3 μ M Ca-ionophore as positive controls. As a normal control, cells were treated with C-peptide vehicle in an identical way to C-peptide-treated cells (Figure 4.10).

FCM analysis demonstrates that the number of CD31⁺/Annexin V⁺ MPs after early exposure (up to 6h) of EA.hy926 cells to C-peptide was not statistically different from that of the normal control cells (Figure 4.10 A, B and C). However, Ca-ionophore stimulation elicits a significant early generation of MPs from ECs (Figure 4.10 A, B and C) at all the tested time points; whereas, the effect of TNF α (10ng/ μ l) stimulation on MP generation reached statistical significance only after 6h treatment duration (Figure 4.10 C). (The low TNF α dose employed in this study is expected to elicit EC activation without causing significant apoptosis (Jimenez et al., 2003).

Considering the data obtained in the previous set of experiments (see above), the duration of C-peptide stimulation was increased to 24h (Figure 4.10 D). Previous reports of MP release from activated or apoptotic ECs have demonstrated that this time point gives the highest number of particles without significant degradation (Jimenez et al., 2003). As demonstrated in Figure 4.10 D, C-peptide treatment elicits a significant MP generation from EA.hy926 cells after 24h.

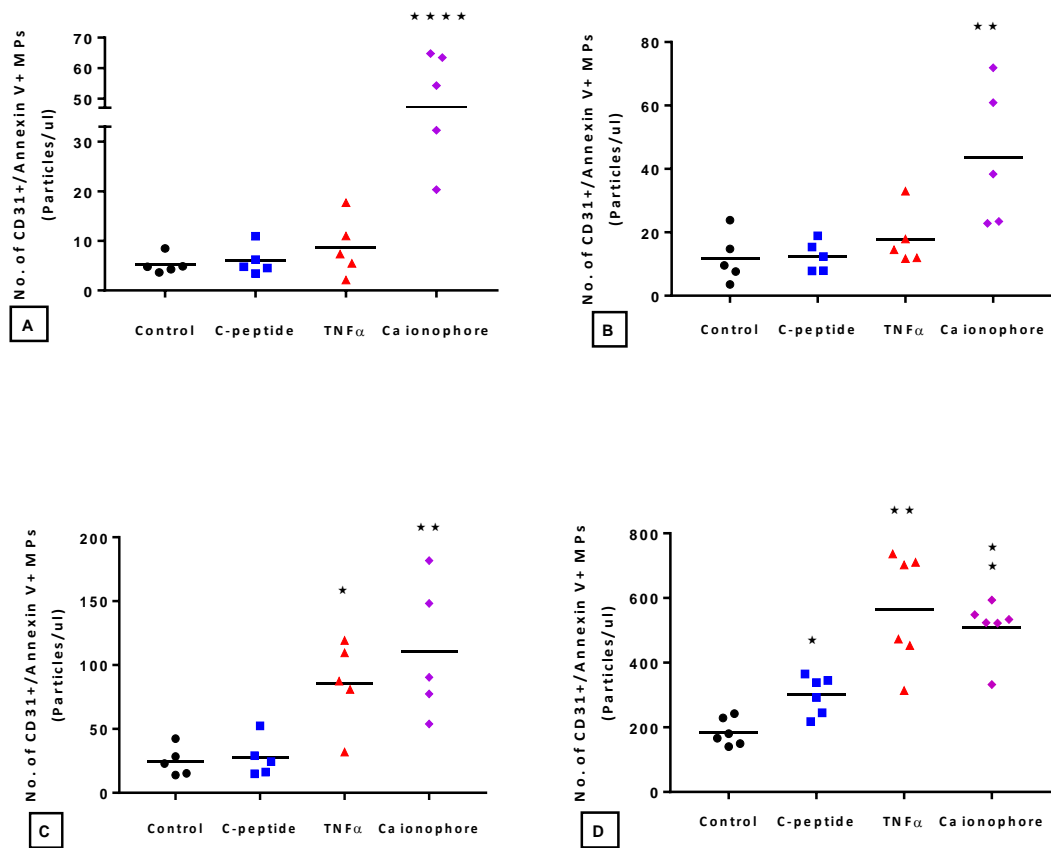


Figure 4.10 Shedding of MPs from EA.hy926 endothelial cells treated with C-peptide. MP levels were assessed by double labelling with CD31 and Annexin V and analysed by flow cytometry. EA.hy926 cells were stimulated with 5nM C-peptide for **A)** 1.5h **B)** 3h **C)** 6h **D)** 24h. 10ng/ml TNF α and 3 μ M Ca-ionophore treated cells were used as positive controls. Control cells were treated with C-peptide vehicle. Data is presented as mean \pm SEM (n=5 for A, B and C; n=6 for D). *P<0.05 compared to control ** P<0.01 compared to control. ****P<0.0001 compared to control.

To investigate whether the observed modulatory effect of C-peptide on MP generation was a specific GPCR-mediated effect, PTX was used. The results in Figure 4.11 show that co-treating cells with C-peptide and PTX diminish the stimulatory effect of C-peptide of MP output from EA.hy926 cells to an insignificant level compared to control cells.

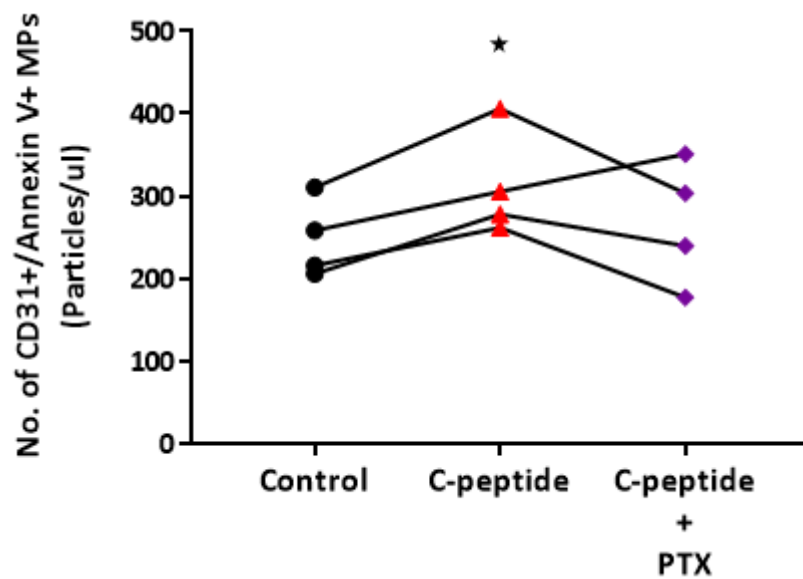


Figure 4.11 Co-treatment of ECs with PTX mitigates MP release in response to C-peptide. Released MPs in the culture medium were counted by double labelling with CD31 and Annexin V and analysed by flow cytometry. EA.hy926 cells were stimulated with 5nM C-peptide for 24h with or without PTX (100ng/ml). Control cells were treated with C-peptide vehicle. Data is presented as mean \pm SEM (n=4). *P<0.05 compared to control cell.

4.2.6 Level of MP estimated by total protein determination

As the stimulatory effect of C-peptide on MP release that was detected by FCM (Figure 4.10) had not been detected by NTA (Figure 4.7), the effect of 72h of incubation with C-peptide on MP release was also quantified by a third method i.e. measurement of the total protein content of particles in the medium using the Lowry assay (Figure 4.12). In agreement with the FCM data, a statistically significant increase in particle release was observed.

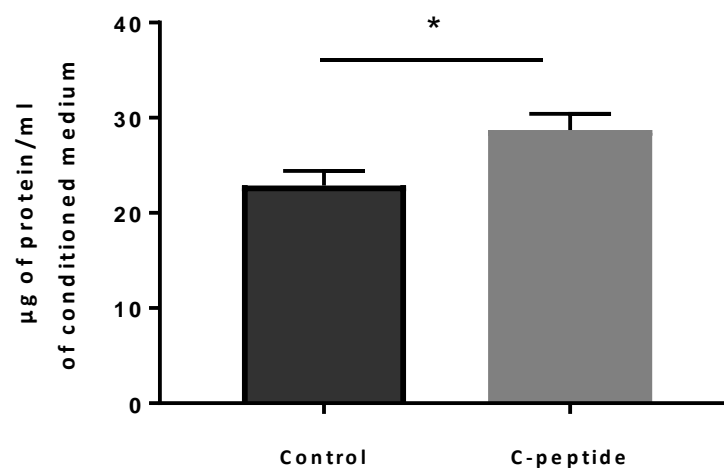


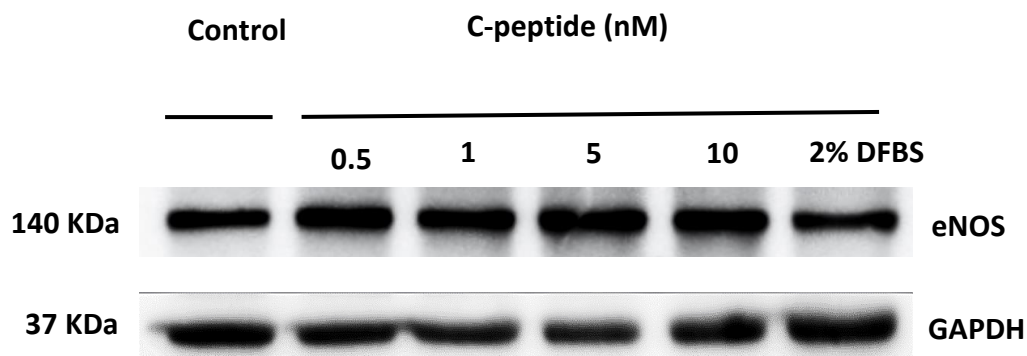
Figure 4.12 Effect of C-peptide on protein content of released particles in the conditioned medium. EA.hy926 cells were treated with 5nM C-peptide for 72h and total particle protein released in the test medium was estimated by Lowry protein assay. Control cells were treated with C-peptide vehicle. Results are represented as mean \pm SEM (n=5). *P<0.05 compared to control cells.

4.2.7 Endothelial functional activity of C-peptide

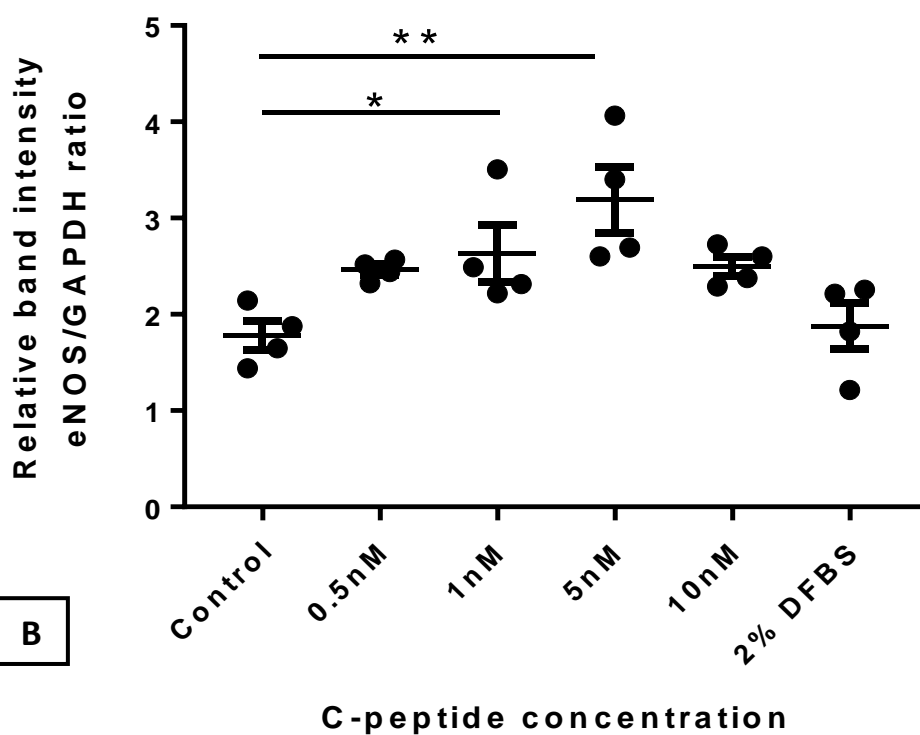
4.2.7.1 C-peptide enhances eNOS protein expression in EA.hy926 cells

To study further the potential modulatory effect of C-peptide on EC function, assessment of eNOS expression in EA.hy926 cells was performed. Previous observation has documented a stimulatory effect for C-peptide on eNOS protein expression in aortic ECs (Kitamura et al., 2003). Of note, Wallerath et al (2003) previously observed a variable response of HUVECs to C-peptide in terms of NO production, which is only detectable in freshly isolated cells (passage zero). Furthermore, multiple lines of evidence have demonstrated a reactivity of HUVECs to C-peptide stimulation with regards to NO release (Bhatt et al., 2012, Lim et al., 2015). However, the ability of C-peptide to stimulate eNOS protein expression in EA.hy926 cells is unknown.

EA.hy926 cells were treated with human C-peptide in a dose-dependent manner for 24h (Figure 4.13 A and B). The time point was chosen based on ERK1/2 activation as eNOS expression is downstream of ERK1/2 activation (Kitamura et al., 2003). Control cells were treated with C-peptide vehicle under identical conditions. The expression of eNOS protein was determined by western blotting. Accordingly, stimulation of EA.hy926 cells with increasing doses of C-peptide for 24h enhanced eNOS protein expression significantly in comparison with control cells. The dose-dependent experiment demonstrated that C-peptide elicits significant eNOS protein expression at a physiologically relevant concentration of 1nM with a peak effect at 5nM (Figure 4.13 A and B).



A

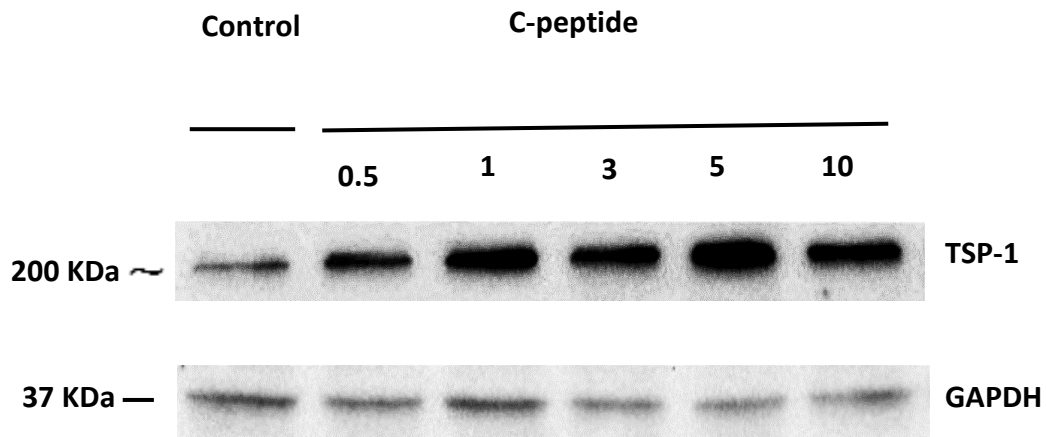


B

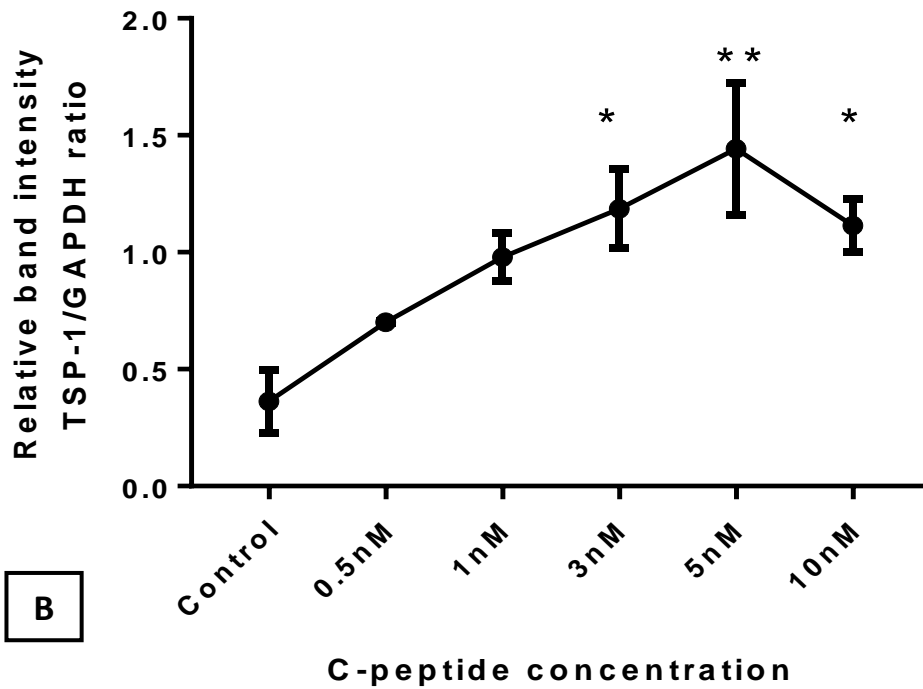
Figure 4.13 C-peptide increases eNOS protein expression in EA.hy926 cells after 24h treatment. **A)** Expression of eNOS in EA.hy926 cells treated with increasing concentration of C-peptide or C-peptide vehicle was evaluated by western blot analysis. A representative blot is depicted. **B)** Densitometric analysis for eNOS is presented as the relative ratio to GAPDH. 2% dialysed foetal bovine serum (DFBS) was used as a positive control. Results are expressed as mean \pm SEM of 4 independent experiments. * $P < 0.05$ compared to vehicle-treated cells. ** $P < 0.01$ compared to vehicle-treated cells.

4.2.7.2 C-peptide stimulates the protein expression of Thrombospondin-1

As shown above, C-peptide stimulates eNOS expression in unstimulated ECs (Figure 4.13). Previous studies also demonstrated an increment in the basal eNOS expression and the subsequent enhanced NO release from normal ECs upon exposure to C-peptide (Kitamura et al., 2003, Lim et al., 2015). NO is a multifunctional molecule: stimulation of angiogenesis is one of its biological functions (Martin et al., 2003). Thus, it was sought to investigate the effect of C-peptide on another vascular regulator of angiogenesis which might balance the observed effect of C-peptide on eNOS in terms of a possible angiogenic consequence. Herein, the effect of C-peptide on TSP-1 protein expression, an endogenous inhibitor of angiogenesis, was determined. EA.hy926 cells were stimulated with C-peptide for 24h in a dose dependent manner (Figure 4.14). The level of TSP-1 in cell monolayers was assessed by western blotting. As shown in Figure 4.14 A and B, the expression of TSP-1 protein was significantly augmented upon treating EA.hy926 cells with C-peptide reaching a maximal effect at 5nM C-peptide concentration which is in agreement with other C-peptide functional activities observed in EA.hy926 cells (Figure 4.1, Figure 4.10 and Figure 4.13).



A



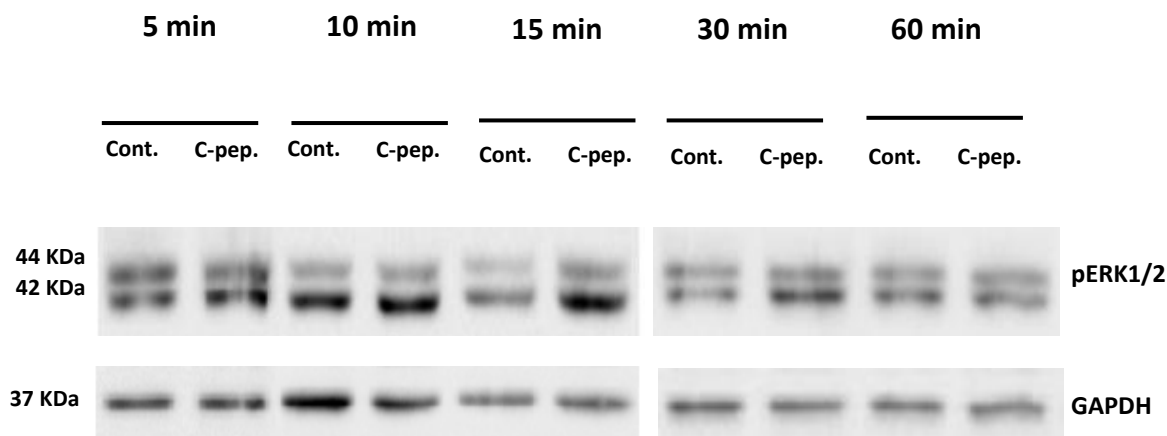
B

Figure 4.14 C-peptide stimulates TSP-1 protein expression in EA.hy926 cells. Treatment of cells with increasing concentrations of C-peptide for 24h was performed then the expression of TSP-1 protein evaluated by western blot. A representative blot is depicted. **B)** Densitometric analyses for TSP-1 is presented as the ratio relative to GAPDH. Results are expressed as mean \pm SEM of 3 independent experiments. * $P < 0.05$ compared with control cells (vehicle-treated cells). ** $P < 0.01$ compared to control cells.

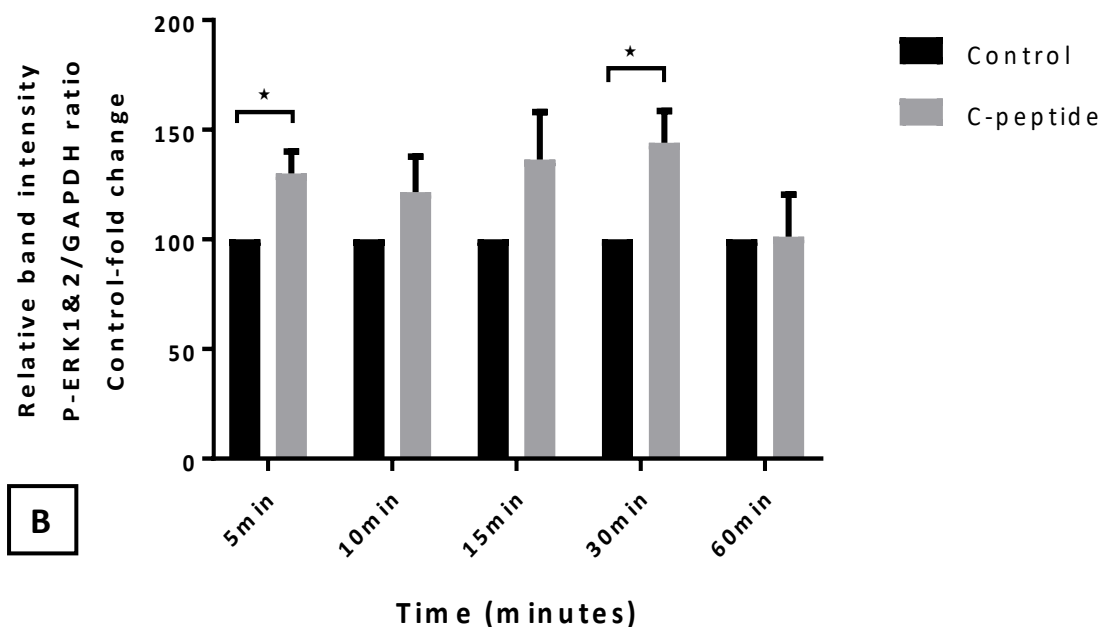
4.2.8 A possible modifier for C-peptide signalling in ECs: Pi

The response to 5nM C-peptide observed in this chapter seems consistently slow (24h for all parameters studied) i.e. slower than some effects (with a time scale of the order of minutes to a few hours) that have been reported in other cell systems (Al-Rasheed et al., 2004a, Kitamura et al., 2003). As some responses to C-peptide are more marked in rodent models than in humans, and a biochemical difference between rodents and humans is the large difference in the plasma Pi concentration (human ~ 1mM; rodent ~ 2 - 2.5mM) (Haut et al., 1980, Sage et al., 2011), an initial study was made here to investigate whether Pi load accelerates cell response to C-peptide. In these experiments, cells were pretreated overnight with 2.5mM Pi then treated with 5nM C-peptide in presence of 2.5mM Pi for 5, 10, 15, 30 and 60min (Figure 4.15 A and B). Control cells were run for each time point and treated with C-peptide vehicle with identical Pi incubation conditions to that of cells stimulated with C-peptide.

Compared to C-peptide time-course data presented earlier in Figure 4.2 when cells were incubated with normal Pi concentration, the result obtained here showed a more consistent ERK response (at 5 min – 60 min) in the Pi-loaded medium (Figure 4.15 A and B), especially for P42 p-ERK2.



A



B

Figure 4.15 Effect of elevated Pi concentration on C-peptide ERK1/2 activation in EA.hy926 cells. **A)** Expression of pERK1/2 in ECs treated with 5nM C-peptide for different time points in medium supplemented with high Pi concentration (2.5mM), was evaluated by western blot analysis. Control cells (cont.) were supplemented with medium contains high Pi concentration (2.5mM) without C-peptide (C-pep.) treatment. **B)** Densitometric analysis for ERK1/2 is presented as the relative ratio to GAPDH. Data is expressed as control-fold change. The presented values are mean \pm SEM (t-test) (n=4). *P<0.05 compared to control cells.

4.3 Discussion

4.3.1 Effect of C-peptide on ERK1/2 phosphorylation

Although widely believed to be inert, C-peptide is unequivocally biologically active. C-peptide activates ERK1/2 in several cell types (Hills and Brunskill, 2009). Accordingly, in the current study, C-peptide stimulates ERK1/2 in a dose-dependent manner in EA.hy926 cells after 24h exposure (Figure 4.1), although at earlier time points it did not elicit an effect on ERK1/2 phosphorylation (Figure 4.2). It is possible that the effect of C-peptide on ERK1/2 activation depends on the cell condition. For example, with longer duration of serum starvation, the cells might become more stressed which could in principle modulate any effect of C-peptide. However, evidence presented here suggests that such stress alone is unlikely to be the explanation for the slow C-peptide responsiveness because elevating the Pi concentration in the medium allowed a response to C-peptide to be detected within 5 min (Figure 4.15 versus Figure 4.2). The broader implications of this apparent Pi-sensitivity of C-peptide signalling are discussed in Chapter 7.

The activation of ERK1/2 in EA.hy926 cells demonstrates that these cells are responsive to C-peptide and suggests that C-peptide may be involved in vascular homeostasis. ERK1/2 are phosphorylated in response to a wide range of biological processes and generally, ERK1/2 activity is considered to be a pro-survival signal although it can also promote apoptosis under some circumstances (Lu and Xu, 2006). In addition, ERK has been suggested as an internal suppressor for NF- κ B activation and the subsequent inflammatory gene expression (Maeng et al., 2006). In accord with this, several *in vivo* and *in vitro* models of inflammation-mediated vascular injury have demonstrated an anti-inflammatory action for C-peptide, at least partially, via inhibition of NF- κ B activation (Haidet et al., 2009).

Furthermore, Kitamura et al (2003) observed that C-peptide induces ERK1/2 phosphorylation in rat aortic ECs, resulting in increased eNOS protein in absence of Akt activation. Blocking of ERK kinase activity however invoked an inhibitory action on ERK phosphorylation and reduced eNOS protein level. In another study, C-peptide improved

wound healing in diabetic mice and enhanced HUVEC migration via ERK1/2-mediated action (Lim et al., 2015).

Taken together, the ERK1/2 pathway has diverse physiological roles which can deliver cytoprotective effects and may, therefore, be of potential importance in the treatment of diabetic complications.

4.3.2 Effect of C-peptide on EC proliferation and/or survival

In the present work, treating serum-starved EA.hy926 cells with C-peptide did not influence the proliferation rate or apoptosis levels in cell monolayers. Both mitogenic and anti-apoptotic activities were unaffected following C-peptide addition to ECs.

Bhatt et al (2012) reported that C-peptide treatment did not influence HUVEC viability; however, a proliferative effect was described in another study where C-peptide induced HUVEC proliferation and migration in a dose-dependent manner. Furthermore, it increased their viability to a comparable level to that of VEGF. These actions were mediated via activation of ERK1/2 and Akt (Lim et al., 2015).

Collectively, despite previously reported growth factor-like activity for C-peptide in some cell types (Vasic and Walcher, 2012), it did not affect EA.hy926 cell proliferation in the present study. In addition, the vasoprotective effect of C-peptide has been described in multiple modalities of cell injury (Section 1.4.5.2); however, a significant reduction in the endothelial apoptosis triggered by growth factor deprivation was not observed in this study. It is possible that C-peptide is more sensitive to high glucose-induced endothelial apoptosis. In addition, the response to C-peptide might be stress- or cell-line dependent. Supportively, the putative C-peptide receptor is thought to be G-protein-coupled receptor(s); though, these receptors can couple with several G-proteins (Kitamura et al., 2003). Therefore, C-peptide action in a particular tissue might be governed by distinct downstream substrates coupled to its as yet unidentified receptor.

4.3.3 Effect of C-peptide on MP release from EA.hy926 cells

C-peptide modulates multiple signalling pathways in several cell types. Thus, it is possible that C-peptide mediates some of its biological activity by affecting the level or

the content of the extracellular vesicles released by cells. Notably, MPs can influence various physiological and pathological functions in the biological system by facilitating the intercellular communication. Accordingly in the current study, it was of interest that C-peptide stimulates MP generation from serum-starved ECs (Figure 4.10).

Initial investigation performed using NTA did not reveal a significant change in MP count upon C-peptide treatment for 24h; however, employing a more sensitive and specific method, FCM, has demonstrated a stimulatory effect for C-peptide on MP generation. The differences in the sets of MP populations analysed by each methodology (NTA versus FCM), might explain the variation in the obtained data from each method (as described in Section 2.2.10 and 2.2.11). Moreover, as shown in Figure 4.12, C-peptide treatment increased the particle level in the test medium estimated by total protein assay which may further support the flow cytometry data.

The biological significance of EMPs has been investigated in numerous studies and both beneficial and deleterious effects have been suggested (Pérez-Casal et al., 2009, Yu et al., 2018). Thus, contrary to the former view that MPs may be inert cellular debris, blebbing of MPs may represent a defence mechanism against harmful or redundant molecules, or as a way to escape phagocytosis. It has been proposed that silencing the mechanisms of MP generation may potentially injure cells and compromise survival (Abid Hussein et al., 2007). In addition, MP-encapsulated mRNAs have been shown to enhance cell survival and vascular repair under various stress conditions (Jansen et al., 2017), although MPs shed during pathological condition may contribute to the disease state (Section 1.3.3) by transporting deleterious messengers from one area of the vascular compartment to another.

The general underlying mechanisms of MP formation involve Ca^{+2} influx across the cell membrane, and C-peptide has been shown to activate Ca^{+2} influx in ECs (Wallerath et al., 2003). Alternatively, the Rho Kinase pathway is recognised for its involvement in EMP biogenesis (Sapet et al., 2006, Burger et al., 2011) and C-peptide is known to activate RhoA/Rho-kinase. Inhibition of Rho-kinase prevents some C-peptide actions on the vascular system (Nordquist et al., 2008, Wahren and Larsson, 2015).

Moreover, further characterisation of the EMP population was performed using TEM (Figure 4.6) and NTA size range measurement (Figures 4.8 and 4.9). The observed particle sizes were within the described extracellular vesicle size range, and C-peptide did not significantly change the size of the generated MPs (Figure 4.9). Indeed previous studies have demonstrated an insignificant effect for agonists such as TNF α on the size of the shed EMPs despite eliciting a significant increase in MP generation (Latham et al., 2015).

Taken together, MPs have multifaceted traits and can elicit diverse physiological and pathological activities; however, the nature of the stimulus and the cell condition might determine the final outcome. Thus, it is possible that the observed increase in number of MP formed from serum-starved ECs upon exposure to C-peptide assists the cells to get rid of noxious molecules by incorporating them within vesicles in a similar way to that which was observed with other EMPs released under non-pathological conditions (Jansen et al., 2015, Jansen et al., 2012, Abid Hussein et al., 2007). It should be noted however that the observed increase in number of MPs was modest, which might not exceed the capacity of the clearance mechanism for MP in *in vivo* conditions. Finally, the effect of PTX treatment on MP generation from C-peptide-treated ECs supports the observation that C-peptide receptor might be G-protein-coupled.

4.3.4 Effect of C-peptide on eNOS protein expression

In this study, treating EA.hy926 cells with C-peptide resulted in a dose-dependent increase in eNOS protein expression (Section 4.2.7.1). This finding is in agreement with a previous study performed by Kitamura et al (2003). It was found that C-peptide upregulated eNOS gene transcription and protein expression in rat aortic ECs, which subsequently enhanced NO liberation (Kitamura et al., 2003).

There is a mixture of data regarding the effect of C-peptide on NO production. C-peptide increased NO liberation from bovine aortic ECs in a calcium dependent manner without changing eNOS expression (Wallerath et al., 2003). Conversely, Giebink et al (2013) suggest that C-peptide has no direct effect on NO production from pulmonary artery ECs. Whereas, studies on HUVEC cultures have reported a direct stimulatory effect for C-peptide on NO release (Lim et al., 2015, Bhatt et al., 2013).

Collectively, there is no consensus on how C-peptide modulates NO production and/or activity in ECs. ECs from different levels of the vascular tree have been studied and thus comparing data might not be straightforward because C-peptide response is cell type-specific (Mughal et al., 2010). C-peptide abrogates eNOS overexpression in renal vasculature in diabetic rats (Kamikawa et al., 2008). Multiple clinical studies of T1DM have shown improvement in vascular blood flow upon C-peptide supplementation (Johansson et al., 1992, Johansson et al., 2003, Forst, 2000 #897).

To conclude, the present study supports a stimulatory role for C-peptide on NO production. Therefore, C-peptide might be a useful therapeutic approach to tackle diseases associated with NO deficiency.

4.3.5 Effect of C-peptide on TSP-1 protein expression

The data presented in this chapter (Figure 4.14) has also demonstrated a stimulatory effect for C-peptide on TSP-1 protein expression in EA.hy926 cells. TSP-1 is an endogenous inhibitor of angiogenesis, and its expression in the vascular endothelium favours a quiescent, differentiated phenotype (Sheibani et al., 2000). Since aberrant angiogenesis is a characteristic feature of DM (Martin et al., 2003), C-peptide might affect the endothelium function by modulating TSP-1 expression in ECs.

TSP-1 limits EC proliferation partly by binding to and inhibiting the activity of VEGF (Bornstein, 2009). C-peptide exerts a negative control action on VEGF hyperactivity in some diabetic tissues and ameliorates vascular leakage (Jeon et al., 2018, Lim et al., 2013).

In general, the upregulation of TSP-1 is associated with vascular pathology. ECs can synthesise and secrete TSP-1. Even though an *in vitro* proapoptotic action for TSP-1 has been described in ECs; this effect is thought to be confined to activated ECs that are forming a new vessel (Jiménez et al., 2000). Supportively, it has been shown that TSP-1 inhibits the proliferation of ECs in the absence of cell death by interfering with the cell cycle progression (Bornstein, 2009).

In aggregate, the structure of the vasculature can be altered by the actions of pro- and anti-angiogenic factors in the surrounding milieu. However, an equilibrium between

inhibitors and promoters of angiogenesis does exist, which is vital for maintaining the stabilisation of vascular structures. C-peptide may improve the aberrant angiogenesis in DM by affecting the expression of TSP-1 in ECs.

Finally, it is noteworthy to mention that the effects of C-peptide in this chapter were all investigated under basal conditions i.e. without the presence of pathological stimuli of relevance to DM such as hyperglycaemia. The possible interaction between C-peptide and such pathological stimuli is the subject of the next chapter.

Chapter 5. Endothelial dysfunction: effect of high glucose and/or high Pi on MP shedding from ECs

5.1 Introduction

The significance of the vascular endothelium in the regulation of cardiovascular homeostasis has become progressively clearer (Shi and Vanhoutte, 2017). In DM, hyperglycaemia contributes to the development of endothelial dysfunction (Stehouwer et al., 1997). Several potential biomarkers have been proposed to evaluate endothelial function, (Paulus et al., 2011), and endothelium-derived MPs (EMPs) have been suggested as a specific marker for endothelial dysfunction in patients with cardiovascular diseases (Hogas et al., 2010).

5.1.1 Role of MPs in endothelial dysfunction

In view of the fact that MP generation is a well-characterised and tightly controlled cellular process, a detailed exploration of the clinical application of MP measurements has emerged markedly (VanWijk et al., 2003). In addition, subsequent lines of evidence have revealed that the MP count may be upregulated or downregulated in various pathological conditions (Section 1.3.3) while quantifying MPs might be of diagnostic or prognostic value in diseases, or it may aid in directing management plans.

In vivo and *in vitro* studies have shown that in hyperglycemic conditions, the Moreover, recent *in vitro* studies showed that in cultured HUVECs treated with high glucose, the level of released MPs is significantly elevated compared to normal glucose cultures (Yu et al., 2018, Jing et al., 2017). Additionally, studying the functional activities of high glucose-derived MPs has revealed deleterious sequelae following exposure of healthy ECs to these particles (Bammert et al., 2017).

Hyperphosphataemia has been shown to promote endothelial injury and causes MP release (Di Marco et al., 2013), which might further complicate DM condition especially in later stages of diabetic nephropathy (Section 1.2.5.3) where serum phosphate levels become elevated. Notably, a recent study by the renal group in Leicester highlighted the role of elevated extracellular Pi as a causative factor for endothelial dysfunction,

manifest by enhanced release of pro-coagulant EMPs (Abbasian et al., 2015). Indeed, previous clinical studies have shown that high-normal Pi levels (near the upper normal limit) correlate with cardiovascular morbidity and mortality in the general population in absence of overt kidney disease (see Section 1.2.5.2).

Proinsulin C-peptide has been recognized for its pleiotropic cytoprotective effects including: anti-oxidant, anti-inflammatory and anti-apoptotic effects (Wahren and Larsson, 2015). Therefore, in the present study, it was hypothesised that DM (modelled by elevating the extracellular glucose concentration) would injure the vascular endothelium in terms of MP generation, and that C-peptide would potentially restore MP levels to normal values. Elevated Pi concentration was also included in the experiments as a positive control (Abbasian et al., 2015). However, as hyperphosphataemia may accompany hyperglycaemia in advanced diabetic nephropathy, it was also hypothesized that simultaneously elevating the concentration of D-glucose and Pi might yield an additive or even synergistic effect, which might also respond to C-peptide.

The chapter objectives are:

- To develop an *in vitro* model of endothelial dysfunction induced by high glucose/high Pi using EA.hy926 and HMEC-1 endothelial cells.
- To examine the effect of C-peptide on MP shedding from ECs treated with high glucose/high Pi.
- To determine the functional activities of high glucose- and C-peptide-derived EMPs.

5.2 Results

5.2.1 Effect of high glucose on EA.hy926 endothelial cells.

5.2.1.1 Effect of glucose load on MP shedding from EA.hy926 cells quantified by nanoparticle tracking analysis

EA.hy926 endothelial cells were treated with high glucose concentration, 25mM, for 24h in absence of serum to avoid the contamination from serum MPs. The released MPs in the test medium were counted using NTA (Section 2.2.3 and 2.2.10). Estimation of MP level in the conditioned medium of high glucose treated ECs did not reveal a significant change in number of liberated MPs (Figure 5.1A) when compared to control cells (5.5mM glucose).

As a previous study had shown that EA.hy926 cells require higher glucose concentration and longer treatment duration to demonstrate glucose-induced endothelial impairment (Karbach et al., 2012), time and dose dependent responses were performed. EA.hy926 cells were treated with increasing glucose concentrations (namely: 25, 35 and 45mM) for 24, 48 and 72h. The result shows no significant difference after glucose treatment for up to 48h (Figure 5.1 A and B); however, after 72h, the number of MPs released in response to high glucose exposure demonstrated significant elevation compared to control (Figure 5.1 C). These data suggest that exposure of EA.hy926 cells to high glucose concentration for up to 48h does not induce MP generation, whereas some effect may occur after 72h. However, the observed increase in number of generated MPs after 72h might reflect the increase in total cell mass (discussed later in Section 5.2.1.4).

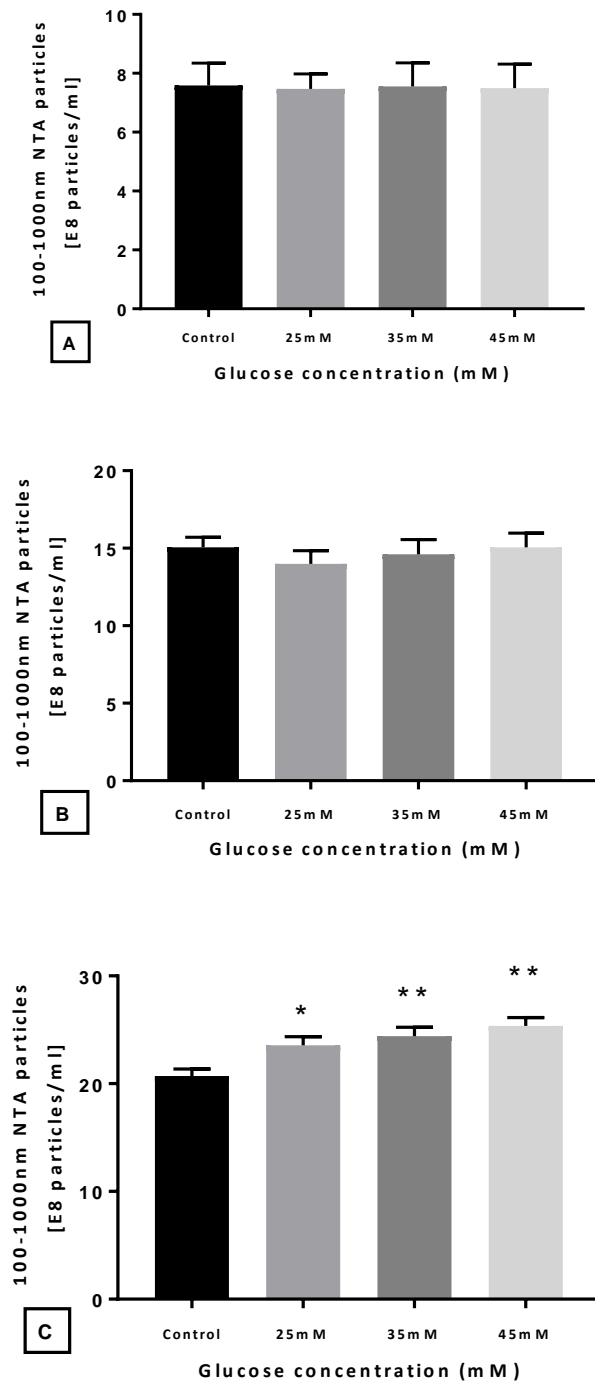


Figure 5.1 Effect of high glucose on MPs release from endothelial EA.hy926 cells estimated by NTA. Treatment of cells with increasing glucose concentrations i.e. 25mM, 35mM and 45mM glucose for **A)** 24h **B)** 48 h **C)** 72h was performed. The number of MPs released in the test medium was estimated by NTA. Data is expressed as mean \pm SEM (n=4 for A, B and C). *P<0.05 compared to control cells (5.5mM glucose). **P<0.01 compared to control cells. E8 is equivalent to 10^8 .

5.2.1.2 Effect of high glucose treatment on particle release from EA.hy926 cells assessed by protein content.

For comparison with the NTA data, the total protein content of the released particles was estimated by Lowry protein assay after ultracentrifugation of the conditioned medium (as described in Section 2.2.5.1.1). Serum-starved EA.hy926 cells were treated with high glucose concentration namely: 25, 35 and 45mM, for up to 72h (Figure 5.2 A, B and C). At none of the tested time points was an effect of high glucose observed on EA.hy926 cells compared to normal (5.5mM) glucose (Figure 5.2 A, B and C). The data presented here do not support an effect for glucose load on protein content of the total sedimentable particles liberated from EA.hy926 cells in the test medium.

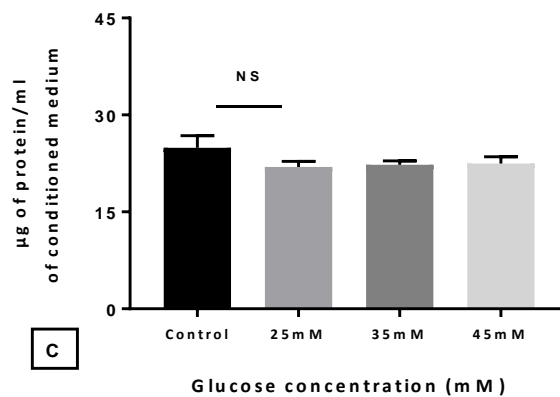
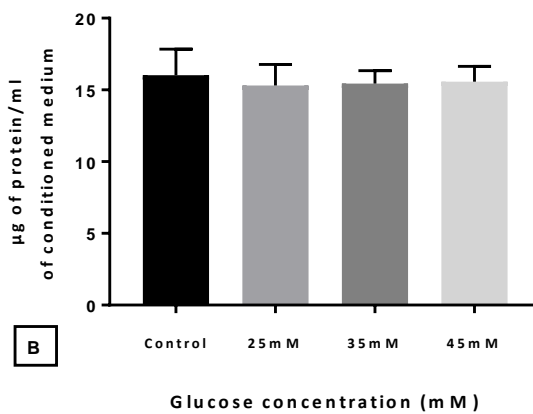
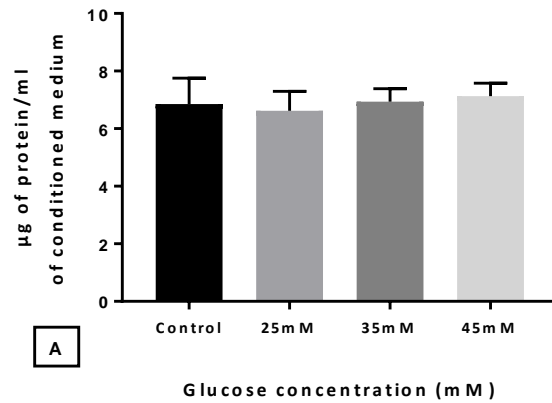


Figure 5.2 Effect of high glucose on the protein content of released particles sedimented from the test medium of EA.hy926 cells. Treatment of cells with increasing glucose concentrations i.e. 25mM, 35mM and 45mM glucose for **A)** 24h **B)** 48 h **C)** 72h was performed. The particle protein was quantified by Lowry protein assay. Results are expressed as mean \pm SEM (n=4 for A, B and C. NS is insignificant difference compared to control cells (5.5mM glucose)).

5.2.1.3 Effect of high glucose on MP release from EA.hy926 cells quantified by flow cytometry.

As a further independent measure of the number of released MPs in the test medium upon EA.hy926 cell exposure to high glucose, MPs were analysed by FCM (Section 2.2.11). Serum-starved EA.hy926 cells were treated with 25mM for 24h (Figure 5.3). MP pellets (section 2.2.3) were double-labelled with CD31 and Annexin V and analysed using a FACSCelesta® flow cytometer.

As in Figure 5.1, no statistically significant effect for high glucose load on the number of MPs generated from EA.hy926 cells was detected. The data presented herein are consistent with the NTA data where treating cells with high glucose for 24h did not enhance significantly MP shedding from EA.hy92 cells.

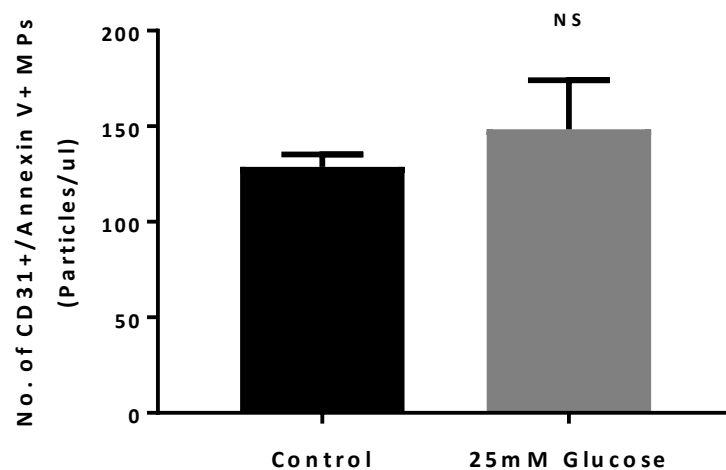


Figure 5.3 Effects of high glucose treatment on MP release from cultured EA.hy926 cells. To expose cells to high glucose environment, the extracellular level of D-glucose was elevated to 25mM. Cells incubated in a medium contains 5.5mM glucose was employed as a normal control. Vesicle levels were assessed by double labelling of MP pellet with CD31 and Annexin V followed by flowcytometric analysis. Results are presented as mean \pm SEM (n=3). NS denotes insignificant difference compared to control.

5.2.1.4 Effect of high glucose on EA.hy926 cell protein content.

To investigate the changes induced by high glucose at the cell level, EA.hy926 cell mass was estimated by measuring total protein content of the cell monolayer. Serum-starved EA.hy926 cells were treated with high glucose concentration 25, 35 and 45mM glucose for 24, 48 and 72h (Figure 5.4 A, B and C). Cell protein content was estimated by Lowry protein assay. The data in Figure 5.4 A, B and C revealed that EA.hy926 cell mass was significantly augmented upon exposure to supra-physiological glucose concentrations at all the examined glucose doses and time points. In addition, the marked increase in EA.hy926 cell monolayer protein which is demonstrated in Figure 5.4 A, B and C was not accompanied by a similar increasing trend in the amount of protein detected in the test medium (Figure 5.2 A, B and C).

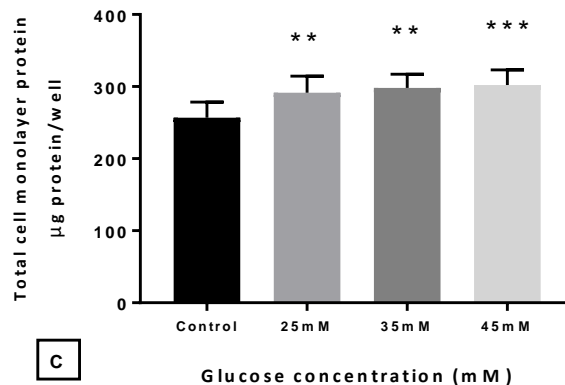
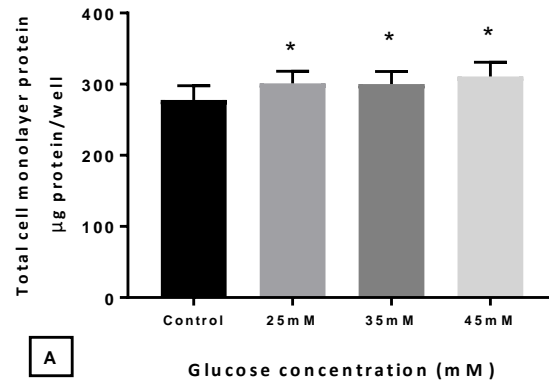


Figure 5.4 Effect of high glucose on total protein content of EA.hy926 cells. Treatment of cells with increasing glucose concentrations i.e. 25mM, 35mM and 45mM glucose for **A) 24h B) 48 h C) 72h** was performed. The protein level was estimated by Lowry protein assay. Results are expressed as mean \pm SEM (n=4 for A, B and C). *P<0.05 compared to control cells (5.5mM glucose). **P<0.01 compared to control cells. ***P<0.001 compared to control cells.

5.2.2 Effect of high glucose on HMEC-1 endothelial cells.

5.2.2.1 Effect of glucose load on MP shedding from HMEC-1 cells

As a modest but reproducible effect of high glucose concentration on MP output from EA.hy926 cells had been observed in Figure 5.1 at 72h, a similar effect was sought to verify in another human endothelial cell culture model. At the start of this study there was little data available regarding high glucose-induced MP shedding from ECs with only one published report showing insignificant MP release from human coronary artery ECs upon exposure to high glucose (Jansen et al., 2013). Therefore, HMEC-1 cells were chosen as an alternative model to investigate the effect of glucose load on MP shedding from ECs.

In the present study, exposing serum-starved HMEC-1 cells to 25mM glucose for only 24h resulted in a modest but statistically significant increase in level of released MPs in the test medium analysed by NTA (Figure 5.5A). In addition, estimation by total protein assay of released particles in the same medium again revealed a statistically significant induction of particle generation after glucose stimulation (Figure 5.5 B). These findings suggest that HMEC-1 cells (like EA.hy926 cells) give a measurable response to a glucose load and may respond more rapidly than EA.hy926 cells with regards to MP formation.

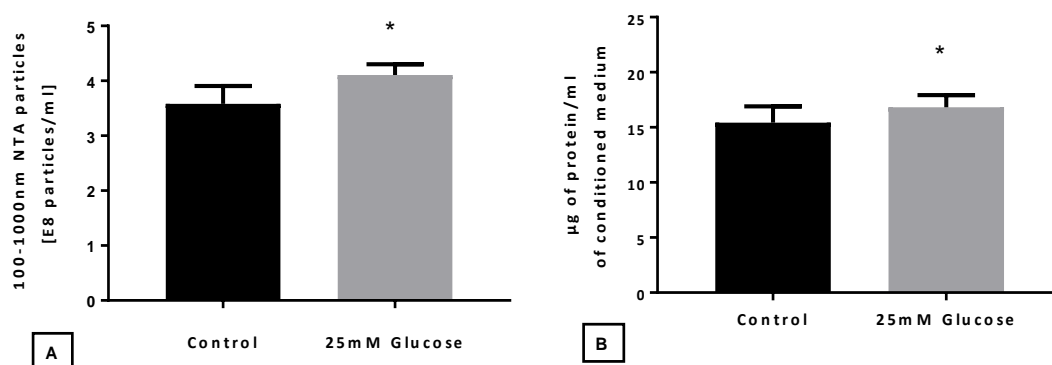


Figure 5.5 Effect of high glucose on MP shedding from HMEC-1. Cells were treated with 25mM glucose for 24h. Control cells were incubated in test medium with normal glucose concentration (5.5mM) and deprived from serum. **A)** Nanoparticle tracking by NanoSight was used for MP counting. **B)** Particle protein content was estimated by total protein assay following centrifugation of the particles. Data is expressed as mean \pm SEM (n=6 for A and B). *P<0.05 compared to control cells.

5.2.2.2 Effect of glucose load on cell mass of HMEC-1 monolayers.

To monitor changes triggered by high glucose at the cell level, HMEC-1 cell mass was assessed by measuring total protein content of the cell monolayer. Serum-deprived HMEC-1 cells were treated with 25mM glucose concentration representing high glucose concentration, whereas control cells incubated with normal (5.5mM) glucose in the test medium. After 24h, the test medium was aspirated, and the protein content of the adherent cells was determined.

Unlike EA.hy926 cells (Fig 5.4A), exposing HMEC-1 cells to an elevated glucose concentration resulted in no significant change in cell mass. In fact, HMEC-1 cells monolayer showed a slight but insignificant reduction in total protein content upon exposure to 25mM glucose (Figure 5.5), possibly arising from a shift of particles containing protein from the cell monolayer into the medium.

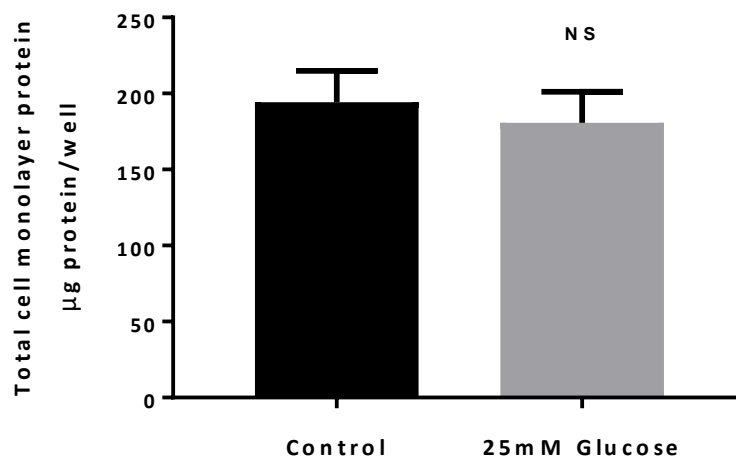


Figure 5.6 Effect of high glucose on total cell monolayer protein of HMEC-1 cells. Treatment of cells with 25mM glucose for 24h was performed. The protein level was estimated by Lowry protein assay. Results are expressed as mean \pm SEM (n=6 for A and B). **NS** denotes insignificant difference compared to control cells (5.5mM glucose).

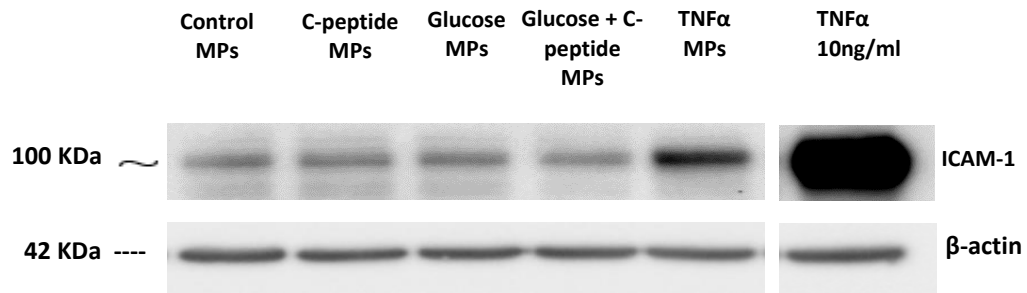
5.2.3 Biological significance of high glucose and/or C-peptide derived EMPs

5.2.3.1 Effect of EMPs induced by high glucose and/or C-peptide on the inflammatory status of EA.hy926 cells

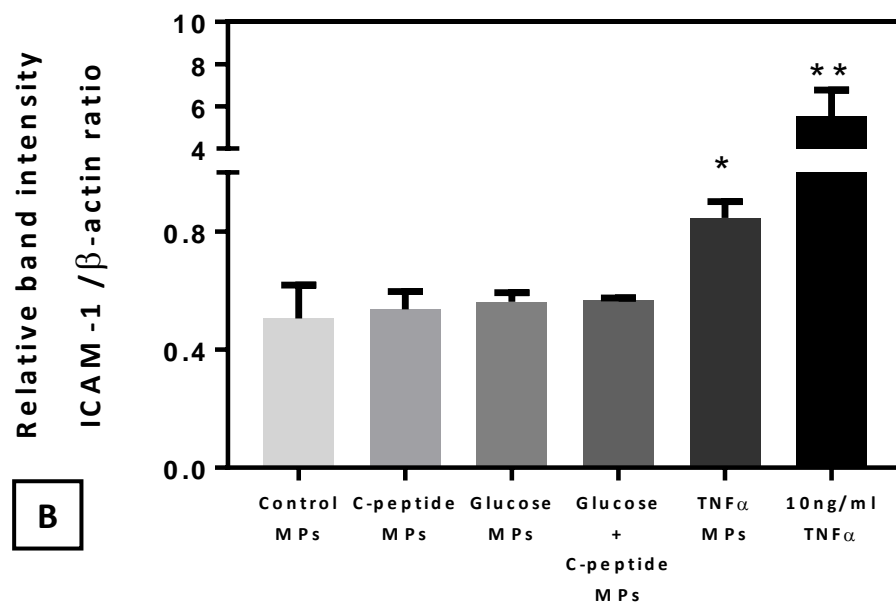
As demonstrated in Figure 5.1 (and possibly Figure 5.3), high glucose treatment did show a statistically significant stimulatory effect on MP generation from EA.hy926 cells, however this does not confirm any possible biological activity. MPs can influence cell function by delivering distinct biological molecules to the target cell. Likewise, previous studies have shown biological effects of high glucose derived MPs despite their number being similar to those generated under normal glucose conditions (Jansen et al., 2013).

To investigate whether EMPs derived from high glucose and/or C-peptide may provoke EC activation, the potential changes in the inflammatory status of EA.hy926 cells was investigated. Accordingly, the protein expression level of adhesion proteins, namely, ICAM-1 and E-selectin was determined. Moreover, the level of IL-8 secretion from EA.hy926 cells upon cell stimulation with EMPs was also measured by ELISA. EA.hy926 cells were treated with high glucose and/or C-peptide derived EMPs in an equal number (1×10^5 Annexin V+ MPs/ml) for 24h as described in Section 2.2.4. The expression level of ICAM-1 and E-selectin proteins was determined by western blot analysis. Cells treated with MPs derived from normal glucose were used as normal control (Figure 5.7). Other groups of cells treated with 10ng/ml TNF α or TNF α MPs for comparison.

As shown in Figure 5.7, TNF α treatment elicits a strong ICAM-1 expression in EA.hy926 cell monolayer. Similarly, TNF α induced MPs also caused a significant upregulation in ICAM-1 protein expression. However, there was no evidence of an increase in ICAM-1 protein level in cells treated MPs generated from high glucose treated cells with or without C-peptide (Figure 5.7). Similarly, neither E-selectin protein expression (Figure 5.8) nor IL-8 secretion (Figure 5.9) was different between the treatment groups. TNF α treatment significantly increased IL-8 secretion (Figure 5.9) from EA.hy926 cells without affecting the expression level of E-selectin in cell monolayer (Figure 5.8).

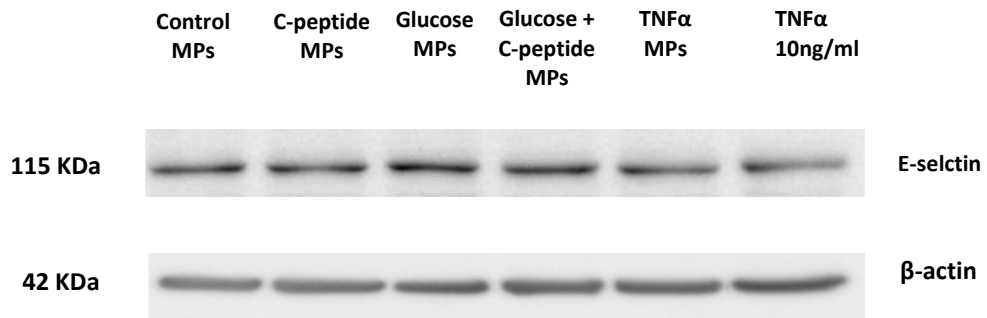


A

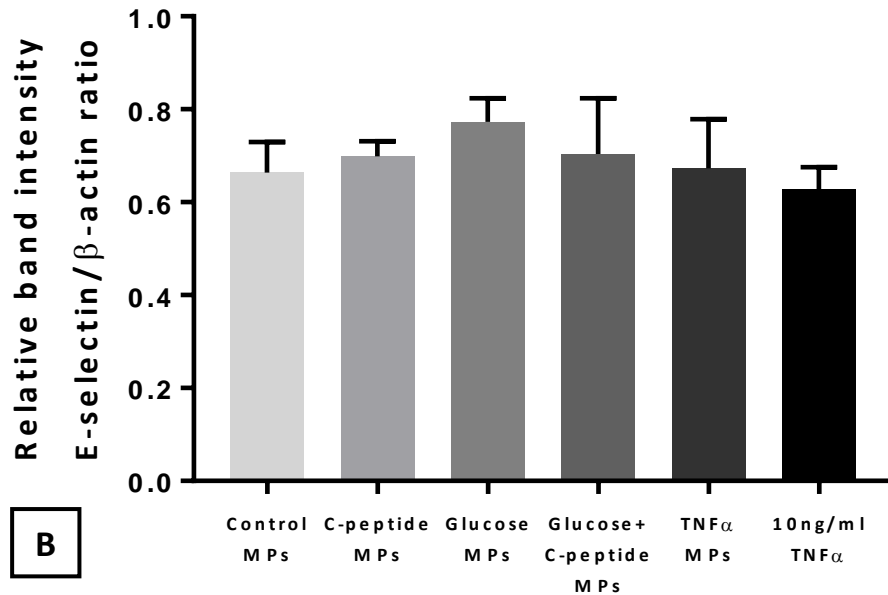


B

Figure 5.7 Effect of high glucose and/or C-peptide derived EMPs on ICAM-1 expression in ECs. EA.hy926 cells were treated with EMP-induced by 5nM C-peptide and/or 25mM glucose for 24h. MPs generated from C-peptide vehicle treated cells served as control MPs. TNF α was used as positive control. **A)** ICAM-1 expression determined by Western blot using specific anti-ICAM-1 antibody. **B)** Densitometric analysis for ICAM-1 are presented as the relative ratio to β -actin. Results are expressed as mean \pm SEM (n=4). *P<0.05 compared to control EMPs **P<0.01 compared to control EMPs.



A



B

Figure 5.8 Effect of EMPs generated from high glucose and/or C-peptide on E-selectin expression in endothelial cells. EA.hy926 cells were treated with EMP-induced by 5nM C-peptide and/or 25mM glucose for 24h. MPs generated from C-peptide vehicle treated cells served as control MPs. $\text{TNF}\alpha$ was used as positive control. **A)** E-selectin expression determined by Western blot using specific antibody against E-selectin. **B)** Densitometric analysis for E-selectin are presented as the relative ratio to β -actin. Results are expressed as mean \pm SEM (n=3).

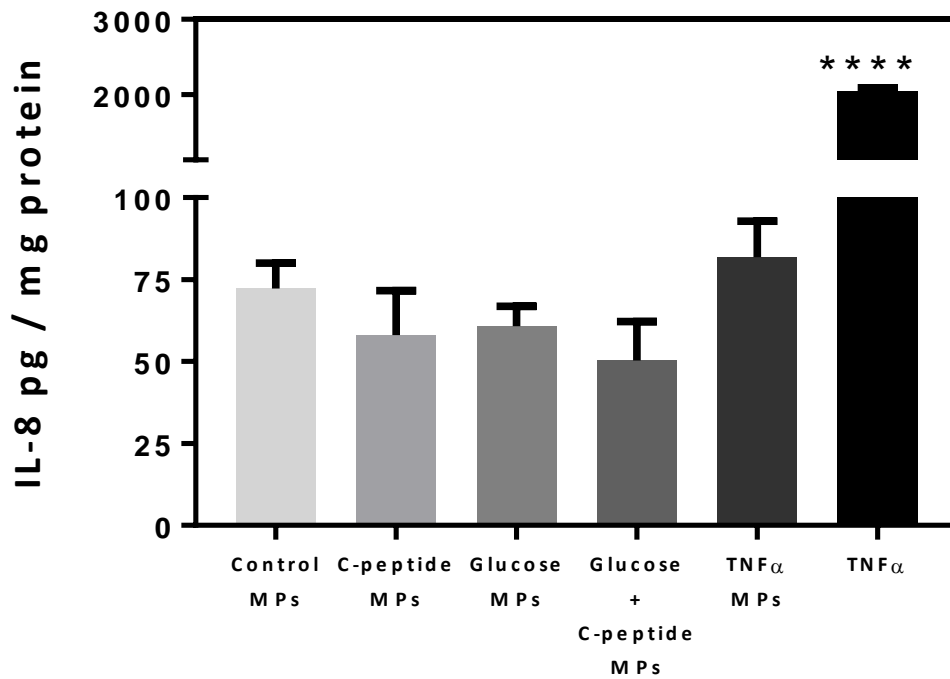


Figure 5.9 Effect of EMPS derived from high glucose and/or C-peptide treatment on IL-8 secretion from ECs. EA.hy926 cells were treated with EMP-induced by 5nM C-peptide and/or 25mM glucose for 24h. IL-8 level in cell supernatant was measured by ELISA. MPs generated from C-peptide vehicle treated cells served as control. TNF α (10ng/ml) was used as positive control. Results are expressed as mean \pm SEM (n=4). ****P<0.0001 compared to cells treated with control MPs.

5.2.3.2 Effect of EMPs derived from high glucose and/or C-peptide treated EA.hy926 cells on apoptosis level of fresh EA.hy926 culture.

While MPs derived from high glucose-treated HUVECs augment EC apoptosis (Bammert et al., 2017), the effect of MPs originated from EA.hy926 cells stimulated with high glucose on apoptosis level of fresh unstimulated culture of EA.hy926 cells still unknown. Thus, to investigate whether high glucose and/or C-peptide EMPs affect EC survival, apoptosis was determined in EAhy926 cells after treating cells with EMPs. Caspase-3 cleavage was used to assess the apoptosis level. Cells were treated with high glucose and/or C-peptide derived EMPs for 24h as described in Section 2.2.4. The expression of activated caspase-3 protein (17 KDa band) was determined by western blot analysis (Figure 5.10). Cells treated with MPs derived from normal glucose were used as normal control.

The data presented in Figure 5.10 demonstrates that high glucose MPs induced in presence or absence of C-peptide trigger significant caspase-3 activation in EA.hy926 cells compared to control cells.

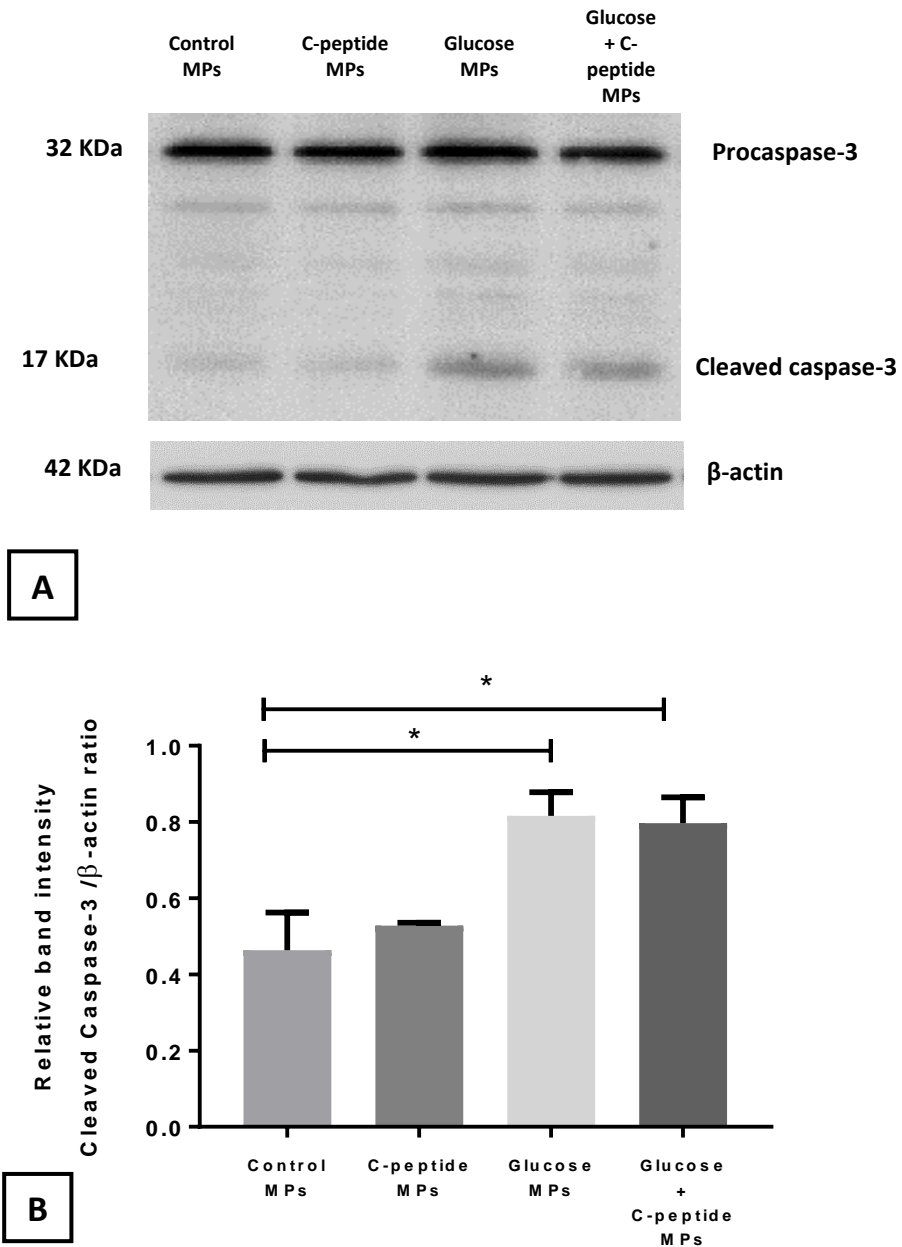


Figure 5.10 EMPs generated from high glucose treated ECs stimulate endothelial apoptosis. EA.hy926 cells were treated with EMPs induced by 25mM glucose with or without C-peptide for 24h. MPs generated from C-peptide vehicle treated cells served as control MPs. **A)** Active caspase-3 was determined by Western blot using specific anti-caspase-3 antibody. **B)** Densitometric analysis for active caspase-3 (17 KDa band) are presented as the relative ratio to β -actin. Results are expressed as mean \pm SEM (n=3). *P<0.05 compared with cells treated with control MPs.

5.2.3.3 High glucose and C-peptide alter the protein composition of EMPs.

While MPs can transfer various components to target cells, the effect of high glucose concentration or C-peptide on their distinct cargo is still unknown. Thus, to gain insight into the possible changes in protein composition of EMPs which might convey functional alteration, proteomic analysis was conducted on EMPs derived from EA.hy926 cells after 24h exposure to high glucose or 5nM C-peptide. MPs were prepared as described in Section 2.2.3. Label free LC-MS/MS was used to identify peptides from SDS gel digest of MP samples. Proteins with a minimum of two spectral counts per sample were accepted for further analysis (Section 2.2.13). Of the 709 proteins identified, 431 were common to all treatment groups while 23 were unique to the high glucose MPs and 18 were unique to C-peptide MP (Figure 5.11) (Appendix).

The MS data were analysed with MASCOT and Scaffold software demonstrating reproducible and exclusive presence of amyloid precursor-like protein 2 and renin receptor in high glucose derived MPs. Additionally, RhoA protein was consistently present in MP samples from all the treatment groups (Appendix).

To assess the possible implications of MP proteome change on the functional signature of high glucose or C-peptide MPs, functional analysis was conducted for the enriched biological processes and pathways. The Cytoscape open source plug-ins, ClueGO and CluePedia, were used for pathway identification (Section 2.2.13). The Gene ontology biological processes and Reactome pathways showed that C-peptide derived MPs are enriched with proteins involved in regulation of DNA replication and apoptosis; whereas, MP derived from high glucose are enriched in proteins associated with NFκB activation, regulation of tissue remodeling and apoptosis, regulation of blood pressure, PCP/CE pathway (planer cell polarity), human epidermal growth factor receptor 2 (HER2) signaling pathway and membrane disassembly

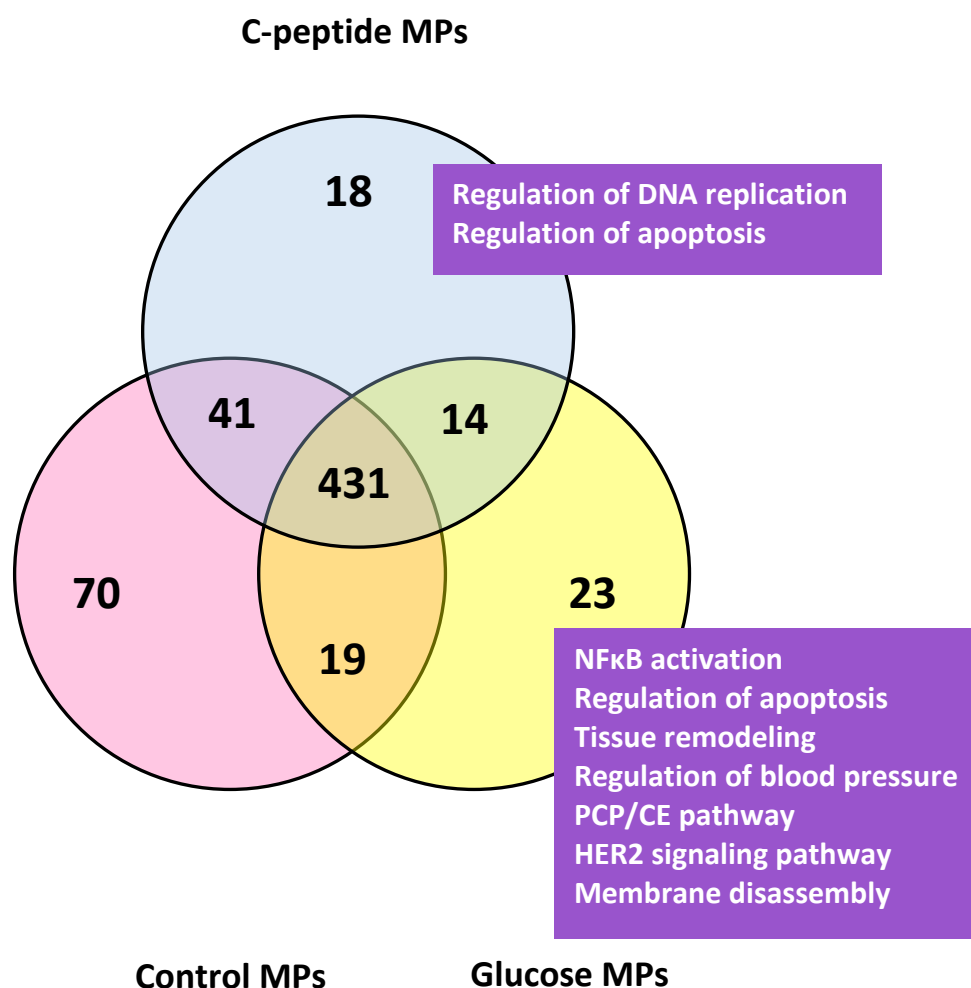


Figure 5.11 High glucose and C-peptide alters the proteome of EMPs. The Venn diagram illustrates variation in protein composition of stimulus dependent EMPs. Each circle demonstrates the number of identified proteins in the treatment group. Blue circle represents C-peptide MPs. Pink circle represents control MPs. Yellow circle represents high glucose MPs. The results of the functional enrichment (gene ontology biological processes and Reactome pathways) of the exclusive proteins (18 for C-peptide group and 23 for glucose group) using ClueGO plug-in for Cytoscape are depicted in the purple boxes on the corresponding group. (n=3 for control and C-peptide MPs, n=2 for glucose MPs). Functional enrichments with $p < 0.05$ are presented.

5.2.4 Simultaneous stimulation of EA.hy926 endothelial cells with high glucose and Pi concentrations

5.2.4.1 Effect of high glucose and/or high Pi on particle release from EA.hy926 cells

Even though in Fig 5.1 high glucose treatment did show a statistically significant stimulatory effect on MP generation from EA.hy926 cells detected by NTA, this increase was not detected when particle release into the medium was assessed by the alternative method of measuring the total protein content of the released particles: - indeed a measurable (but statistically insignificant) decrease may have occurred (Figure 5.2) To investigate further this limited protein particle response of EA.hy926 cells to high glucose, cells were co-stimulated with 2.5mM Pi in addition to 25mM glucose, representing the elevated levels of both agents previously shown to induce changes in endothelial function *in vitro* (Di Marco et al., 2008, Natarelli et al., 2015). Exposure to high Pi alone has been reported to induce endothelial MP release (Abbasian et al., 2015), possibly due to enhancement of apoptosis and ROS generation (Di Marco et al., 2013).

Cultured ECs were treated with 25mM glucose with or without 2.5mM Pi accompanied by serum deprivation for up to 72h. Control cells were incubated with medium containing 5.5mM glucose and 1mM Pi, representing normal values in human plasma. The protein content of released MPs was estimated by Lowry protein assay. Challenge of EA.hy926 cells with an elevated concentration of Pi alone for 24h did not reveal significant difference in released MPs compared to control cells (Figure 5.12 A). However, extending the treatment duration to 48 and 72h revealed a significant increase in amount of MP protein released in the test medium (Figure 5.12 B and C). In contrast, as previously demonstrated in Figure 5.2, high glucose exposure did not elicit changes in released particles in the medium at any time point (section 5.2.1.2), indeed again (as in Figure 5.2) some decrease in the output of particle protein may have occurred in this series of experiments, although it did not reach statistical significance (Fig 5.12 C).

Nonetheless, combining high glucose and Pi stimulation did result in a statistically significant reduction of the quantity of particles released in the test medium compared

to Pi-treated cells (Fig 5.12C). Thus, contrary to the original hypothesis (Section 5.1) high glucose did not enhance cellular stress induced by high Pi manifested by MP budding.

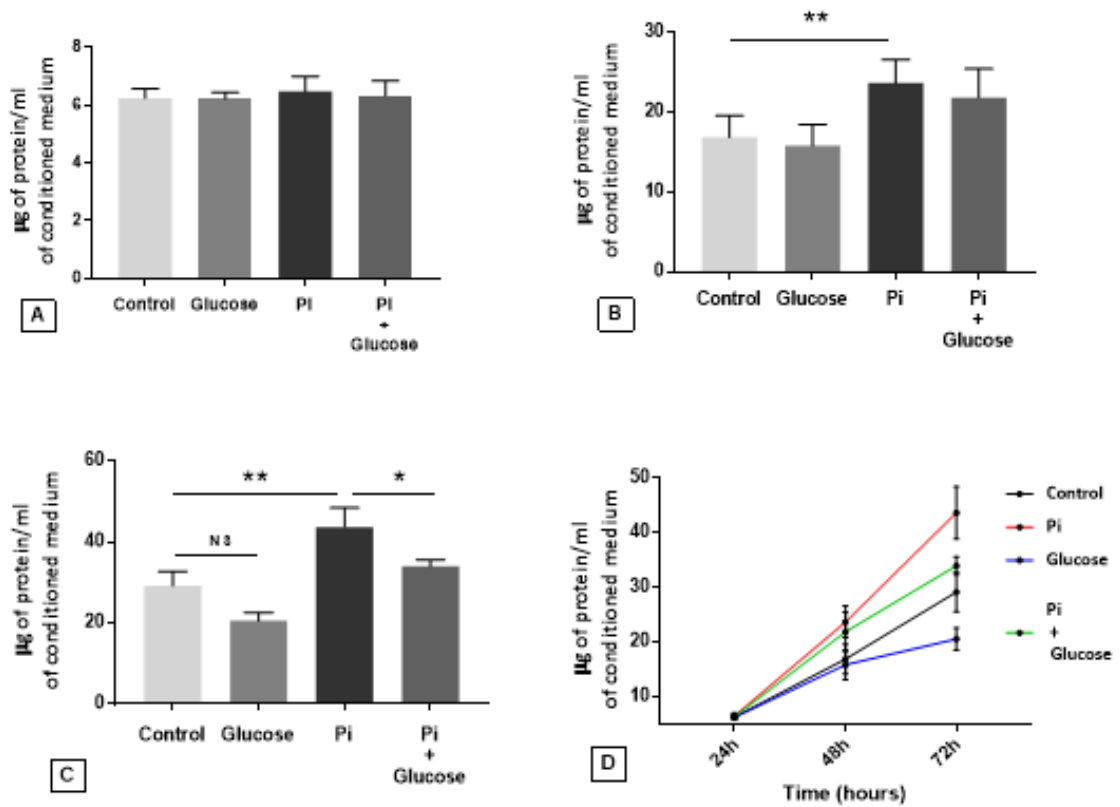


Figure 5.12 Estimation of particle protein released in EA.hy926 supernatant after stimulation with high glucose (25mM) or high Pi (2.5Mm). Cells were treated for **A)** 24h **B)** 48h **C)** 72h. **D)** The plot demonstrates changes in levels of liberated particles with time. Results are expressed as mean \pm SEM (A and B: n=4. C: n=5). **P<0.01 compared to control cells (5.5mM glucose and 1mM Pi). *P<0.05 compared to Pi-treated cells. **NS** denotes insignificant difference compared to control cells.

5.2.4.2 Effect of high glucose and/or high Pi on EA.hy926 cell mass

To examine the alterations induced by Pi addition to high glucose treated cells, cultured cell mass was evaluated by measuring total protein concentration of the cell monolayer. Serum-deprived EA.hy926 cells were stimulated by 2.5mM Pi in conjunction with 25mM glucose for up to 72h whereas, cells incubated with normal medium containing 5.5mM glucose and 1mM Pi served as normal control cells. Individual incubation of cells with either high Pi or glucose was performed for comparison.

As previously demonstrated, glucose exposure resulted in a significant increment in total cellular protein at all the tested time points (Figure 5.13 A, B and C). Conversely, Pi-treated cells showed a significant drop in cell monolayer protein after 48h and 72h exposure (Figure 5.13 B and C). Moreover, combined treatment with high Pi/high glucose resulted in no significant difference in cell mass compared to control cells at any time point. However, after 72h incubation, combined stimulation did demonstrate a significant increase in cell monolayer protein compared to Pi-treated cells (Figure 5.13 C), apparently consistent with the changes in the transfer of protein particles into the medium that were observed under these conditions in Figure 5.12 C.

These findings showed an obvious difference between the effect of glucose and Pi treatments on EA.hy926 protein content after 48h and 72h incubations, where Pi had a negative effect on cell mass by decreasing cell monolayer protein by more than 16% and 27% respectively. In clear contrast, glucose increased cell mass during serum starvation by increasing cell monolayer protein by more than 6% and 15% respectively (Figure 5.13 B and C). In addition, combined treatment demonstrated that glucose addition possibly retards Pi-induced adverse effect on cell health by partially restoring cell monolayer protein towards control values.

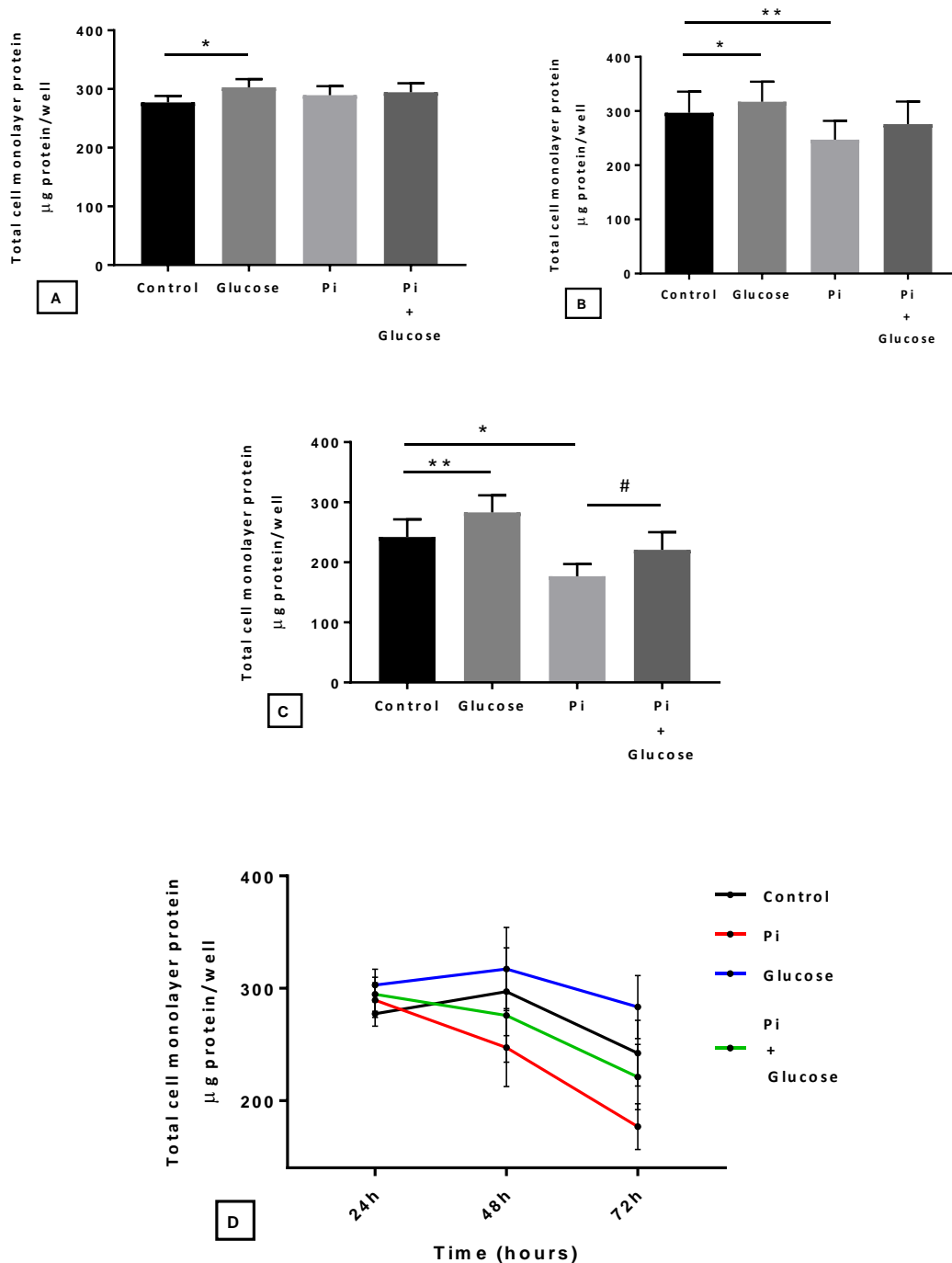


Figure 5.13 Effect of high glucose/high Pi on EA.hy926 cells protein content. Total protein mass of EA.hy926 monolayer was estimated after exposing cells to high glucose (25mM) and/or high Pi (2.5mM) concentration for **A)** 24h **B)** 48h **C)** 72h. **D)** The plot demonstrates changes in protein content of adherent cells with time. The protein level was estimated by Lowry protein assay. Data are expressed as mean \pm SEM (n=5 for A, B and C). *P<0.05 compared to control cells (5.5mM glucose and 1mM Pi). **P<0.01 compared to control cells # P<0.05 compared to Pi-treated cells.

5.2.5 Modulation of Pi-induced MP generation by C-peptide

5.2.5.1 Effect of C-peptide on Pi-induced MP shedding from EA.hy926 cells quantified by nanoparticle tracking analysis

As demonstrated in the previous section, in contrast to the relatively modest stimulatory effects seen with high glucose, Pi clearly stimulates particle release from EA.hy926 cells into the medium (consistent with earlier reports) (Abbasian, 2015). Cellular stress induced by ROS generation and apoptosis have been proposed as triggers for this MP generation (Di Marco et al., 2013). The proinsulin C-peptide has been recognised for its protective effect on endothelial dysfunction (Cifarelli, 2011 #569). Thus, in this study, the potential modulatory effect of C-peptide on Pi-induced MP formation was examined.

EA.hy926 cells were subjected to serum deprivation then stimulated with 2.5mM Pi with and without 5nM C-peptide. Cells incubated with medium containing 1mM Pi served as normal control cells. At the end of each incubation condition, cell supernatants were collected to quantify MP number by NTA.

Consistent with the protein particle output data above (in Figure 5.12 B and C), high Pi also induced significant MP release from EA.hy926 cells for up to 72h as detected by NTA. However, treating Pi-stimulated ECs with C-peptide did not reveal a significant difference in number of liberated MPs compared to the Pi-treated group at all the tested time points (Figure 5.14 A, B and C). However, at the early time point (24h) C-peptide addition to Pi-treated cells showed some tendency to give a modest decline in MP level in culture supernatant when compared with Pi-treatment alone (Figure 5.14 A).

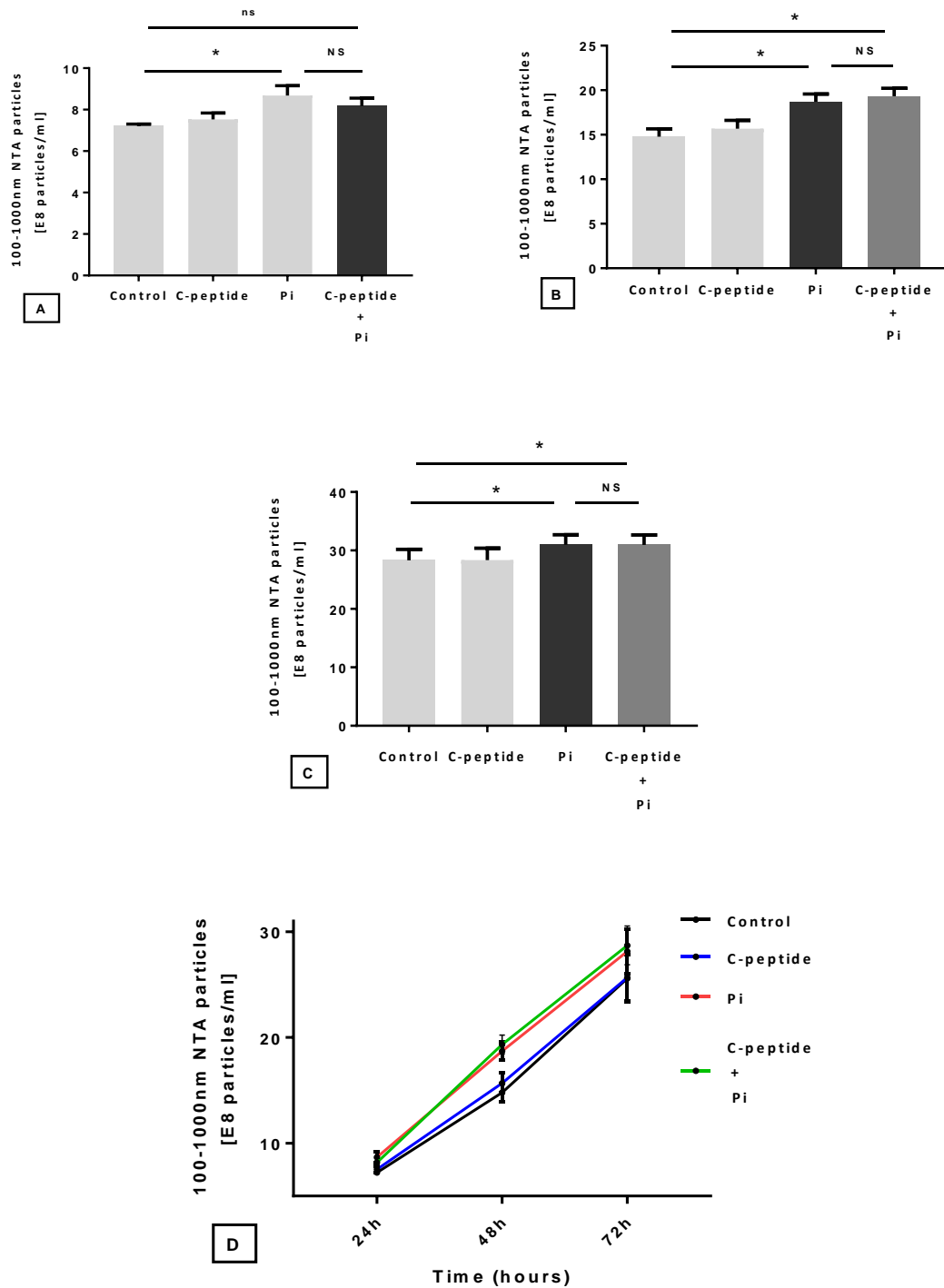


Figure 5.14 Effect of C-peptide on MP shedding from high Pi-treated cells. EA.hy926 cells were treated with 5nM C-peptide, 2.5mM Pi or both of them for **A)** 24h **B)** 48h **C)** 72h **D)** The plot illustrates the variation in MP level in the conditioned medium with time. NTA was used for MP counting. Results are represented as mean \pm SEM (n=5). *P<0.05 compared to control cells (1mM Pi). NS denotes insignificant compared to Pi-treated cells. ns denotes insignificant compared to control cells.

5.2.5.2 Effect of C-peptide on protein content of Pi-loaded EA.hy926 cells.

To investigate whether the alteration in the number of MPs generated from EA.hy926 cells in response to Pi and /or C-peptide treatment was associated with any alteration at the cell layer level, the total cell monolayer mass was estimated (Figure 5.15 A). The longer treatment duration, 72h, was chosen to assess the relationship between NTA data (Figure 5.14 C) and total cell mass. The data in Figure 5.15 A illustrates that the significant Pi-induced increase in MP quantity observed with NTA (Figure 5.14 C) was accompanied by a significant decrease in cell monolayer protein (Figure 5.15 A). High Pi treatment caused a significant decrease in cell mass after 72h of exposure to Pi load; whereas, combined treatment with 5nM C-peptide did not modify the effect of Pi remarkably (Figure 5.15 A).

For further confirmation, the level of particle protein in the conditioned medium was also measured. Similar to NTA data, no significant effect of C-peptide addition to high Pi-treated cells was observed when the protein content of particles released into the test medium was measured after 72h of treatment (Figure 5.15 B). In contrast, Pi treatment alone demonstrated a clear increment effect on the level of released protein particles at the indicated treatment time compared to control cells (Figure 5.15 B). As previously noted (Section 4.2.6.3) C-peptide alone also significantly increased the level of particle protein in the conditioned medium relative to control medium with 1mM Pi and no C-peptide (Figure 5.15 B).

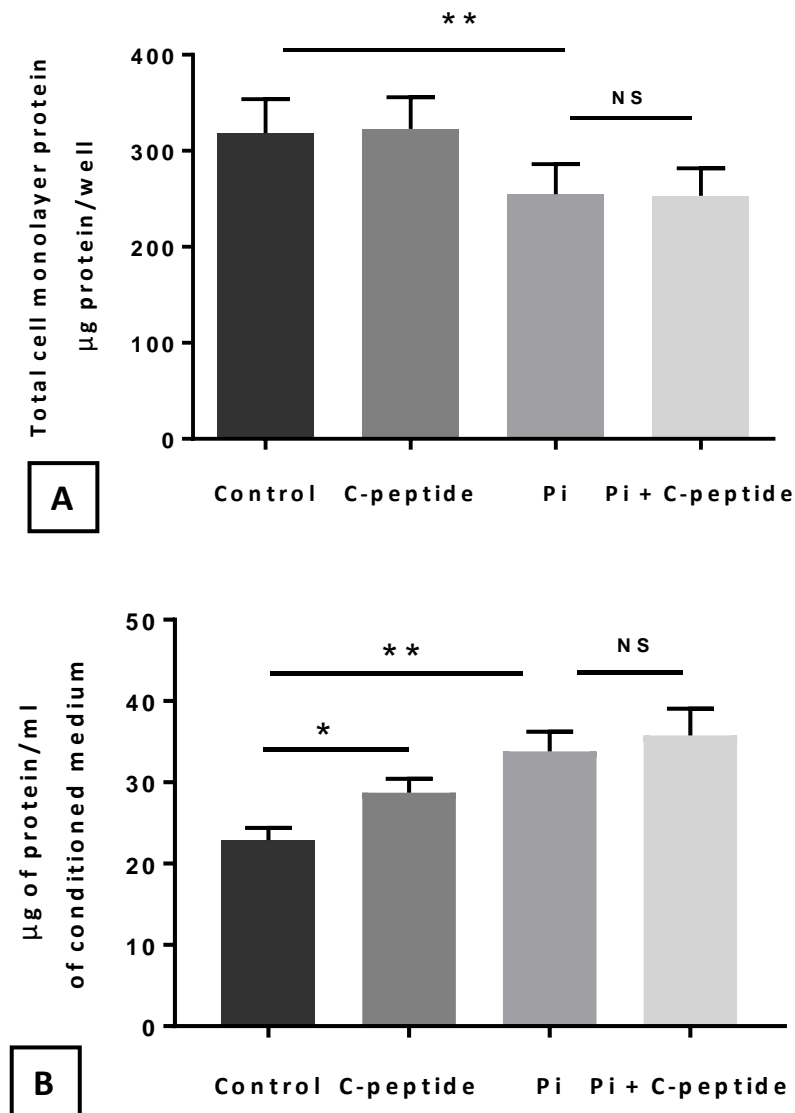


Figure 5.15 Effect of C-peptide on Pi-induced alteration in protein content of EA.hy926 cells. Treatment of cells with 5nM C-peptide, 2.5mM Pi or both of them for 72h was performed. **A)** Total protein mass of cell monolayer **B)** Protein content of released particles in the conditioned medium. Results are represented as mean \pm SEM (n=5). *P<0.05 compared to control cells (1mM Pi). **P<0.01 compared to control cells. NS denotes insignificant compared to Pi-treated cells.

5.3 Discussion

The effect of high glucose, in addition to high Pi, on the vascular endothelium has been investigated in the current study. An *in vitro* incubation of ECs with high glucose concentration was used to mimic the hyperglycemic conditions observed in diabetic patients.

There is a great body of evidence showing that exposing cultured ECs to an elevated extracellular glucose concentration triggers oxidative stress and apoptosis (Brownlee, 2001). In turn, apoptosis and oxidative stress are well-defined stimulators for MP budding (Szotowski et al., 2007, Distler et al., 2005). Consequently, studying MP might represent a valuable clinically relevant tool by providing information about cell activation, proliferation, apoptosis and cell death. Therefore, in the presented study, MP shedding as a measurable parameter for endothelial function was used to investigate the effect of high glucose/high Pi on cultured vascular endothelium.

5.3.1 Suitability of EA.hy926 endothelial cells as a glucose-responsive model

Numerous studies have shown that modelling of hyperglycaemia-triggered endothelial dysfunction using EA.y926 cells is successful in displaying many of the DM-derived features of endothelial dysfunction such as apoptosis, impaired NO/cGMP signalling, mitochondrial dysfunction and oxidative stress development (Gerö and Szabo, 2016, Karbach et al., 2012, Natarelli et al., 2015). Similarly, previous publications have demonstrated that EA.hy926 cells are responsive to high glucose and produce features of endothelial injury similar to primary HUVECs (Liu et al., 2012). On the other hand, variations in responsiveness of EA.hy926 cells (compared to primary cells) were especially observed during exposure to stimuli such as TNF α (Cao et al., 2017) which, in EA.hy926 cells, does not upregulate E-selectin or VCAM-1, a normal feature for ECs. However, it did induce ICAM-1 overexpression and IL-8 secretion as primary HUVECs do (Figure 5.7 and 5.9). Similar findings have been reported elsewhere (Gapizov et al., 2018, Unger et al., 2002).

Collectively, EA.hy926 cells are considered a suitable model for vascular hyperglycaemia; albeit they required higher glucose concentration and longer treatment duration compared to primary HUVECs to display signs of endothelial

dysfunction such as impaired NO/cGMP signalling and development of oxidative stress (Karbach et al., 2012).

5.3.2 Effect of high glucose on MP release from EA.hy926 endothelial cells

The relationship between high glucose and endothelial dysfunction in terms of MP shedding has not been studied previously in EA.hy926 cells; however, increased MP release in response to other injurious stimuli has been confirmed in this cell line (Abbasian et al., 2015, Zhang et al., 2017). In the present study, treating EA.hy926 cells with high glucose concentration resulted in only a modest increase in MP release into the test medium after 24h analysed by FCM; but it did reach statistical significance (Figure 5.3). In turn, NTA measurements (Figure 5.1 C) revealed significant increase in MP count only after 72h; however, this increase in MP output was associated with an increase in the total cell mass (see below).

As the effect of a glucose load on particle output from EA.hy926 cells was relatively small, further investigation of the potential modulatory effect of C-peptide on MP generation induced by high glucose was not performed in this study. In fact, the relative resistance of EA.hy926 cells to enhanced MP formation triggered by high glucose has also been observed by others (D. Burger, personal communication).

On the other hand, using another endothelial cell line in this study, HMEC-1, demonstrated a similar statistically significant enhancement of MP release in response to high glucose (Figure 5.5 A and B), and this occurred more rapidly than in EA.hy926 (i.e. after only 24h). Unfortunately, these cells grow extremely slowly which did not allow their use for further studies.

Several studies have reported a more marked increase in number of MP released from primary HUVECs in response to high glucose treatment (Burger et al., 2017, Jing et al., 2017, Bammert et al., 2017, Yu et al., 2018). However, FCM analysis of CD31/Annexin V MPs released from high glucose-treated primary cultures of coronary artery ECs did not reveal a remarkable change compared to normal glucose (Jansen et al., 2013). Primary HUVECs may therefore be a more suitable future model in which to investigate the effect of C-peptide on glucose-induced MP output. Unlike the present study detection of MPs by double labelling in FCM was not employed in the above mentioned HUVEC

studies; whereas only phosphatidylserine exposure was used to identify MPs in other studies (Burger et al., 2017, Yu et al., 2018). Phosphatidylserine is not a specific marker for MPs and it does not exclude contamination with apoptotic bodies. Therefore, differences in methodology might explain some variation in the reported data. Surprisingly, in the above-mentioned studies, the mechanism for the augmented MP formation under high glucose environment was not investigated; albeit, high glucose-induced apoptosis was suggested as a possible trigger (Bammert et al., 2017).

5.3.3 High glucose increases EA.hy926 endothelial cell mass during serum deprivation.

To further investigate the possible cause for the observed weak response of EA.hy926 cells to MP formation induced by high glucose concentration, estimation of cell protein content was performed. Treating EA.hy926 cell with 25, 35 and 45mM glucose for up to 72h resulted in an increase in total cell mass.

It is possible that the observed increase in EA.hy926 cell protein content is a growth effect. In fact, enhancement of EA.hy926 cell growth upon high glucose addition has been reported previously (Xu et al., 2018, Karbach et al., 2012). It has been observed that 35mM glucose treatment for 5 days increases EA.hy926 cell count in spite of the significant (potentially toxic) increment in ROS generation. This was in contrast with the 55% cell death noted in the third day of treatment in primary HUVECs (Karbach et al., 2012). Other studies have confirmed that there is no significant effect of high glucose feeding on EA.hy926 viability; in spite of a significant development of oxidative stress (Koziel et al., 2015).

Intriguingly, in a study by Xu et al (2018), the authors interpret the observed proliferation enhancement and reduction in apoptosis in the HUVEC-derived cell line EA.hy926 when treated with high glucose as an endothelial hyperactivity, which might happen during atherogenesis or in diabetic retinopathy. Even though ECs in their normal physiological state are quiescent with a turnover rate of months to years, stimuli can switch them to an active biosynthetic phenotype. ECs originated from different vascular beds demonstrate variation in reaction to high glucose in terms of viability/proliferation. Apoptosis is the main described event; however, proliferation is

detected in retinal ECs (Popov, 2010), and angiogenesis has been reported in both diabetic retinopathy and diabetic nephropathy (Tahergorabi and Khazaei, 2012).

In clear contrast, it has been demonstrated that EA.hy926 cells undergo significant reduction in number following 25mM glucose exposure for 24h. A stimulatory signal to the apoptotic pathway was postulated as a contributing factor (Natarelli et al., 2015). Nevertheless, high glucose-induced EC proliferation was also reported in another EC culture model: rat aortic ECs proliferate with increasing glucose concentration up to 35mM (Feng et al., 2017). The authors linked their finding to DM-related intimal hyperplasia.

To summarise, it was concluded that the possible growth effect of high glucose on EA.hy926 cells might retard MP shedding, the main interest of this study. However, this does not exclude the possibility that high glucose injures EA.hy926, as a wide-range of hyperglycaemia-triggered vascular injuries, apart from MP release, have been confirmed in this cell line. Therefore, further investigation of the potential biological activity of EMPs was performed as discussed in the next section.

5.3.4 High glucose EMPs alter EC properties

As MP carry biologically active molecules, they can alter the function of target cells. Despite the fact that exposing fresh and apparently healthy cultures of EA.hy926 cells to MPs originating from high glucose-treated cultures (named herein high glucose EMPs) did not show an obvious effect on endothelial inflammatory markers after 24h (Figures 5.7, 5.8 and 5.9) or even at 6h (data not shown), the level of apoptosis as demonstrated by caspase-3 cleavage was increased after 24h (Figure 5.10), which was not markedly different from the level of apoptosis in cells treated with EMPs derived from cultures treated simultaneously with high glucose and C-peptide.

In fact, damaging effects of high glucose-derived MPs have been described in the literature when fresh cultures of HUVECs are exposed to these particles. As a result, endothelial dysfunction develops which is manifested by reduction in NO production and increased inflammatory cytokine release (Jing et al., 2017). Moreover, *in vitro* and *in vivo* studies revealed that MPs produced by exposing ECs to high glucose are defective in microRNAs which regulate endothelial repair and inflammatory activity

(Pfeifer et al., 2015). Another study showed that high glucose MPs enhance ROS production in cultured ECs which upregulates ICAM-1 expression (Jansen et al., 2013). On the other hand, these high glucose vesicles stimulate endothelial apoptosis: diminished packing of anti-apoptotic microRNA in high glucose-derived MPs compared to normal glucose MPs was suggested as a possible mechanism (Bammert et al., 2017).

A limitation in this functional activity study is the potential effect of remnant soluble mediators, like TNF α , in MP preparation. However, isolation of MPs by differential centrifugation (Section 2.2.3) involved a washing step followed by complete elimination of the resultant supernatant.

Additional evidence for the possible detrimental effect of high glucose derived MPs on other cell function was suggested here by the proteomic study. Analysis of the high glucose MP proteome demonstrated enrichment in several pathways involved in vascular health and disease (Figure 5.11). In addition, amyloid precursor-like protein 2 and renin receptors were detected only in high glucose MPs suggesting a possible disposal or defense mechanism. In a study reported by Zu et al, enhanced packaging of amyloid beta A4 protein was observed in MPs generated from high glucose stimulated ECs (Zu et al., 2015); although in another study any amyloid-associated proteins was not detected in EMPs (Burger et al., 2017).

5.3.5 Effect of high Pi on MP release from EA.hy926 cells

After loading cells with Pi, an elevation in EMP number released into the test medium was observed. These findings are in line with previous studies that showed an increase in EMP budding in response to high Pi (Di Marco et al., 2013, Abbasian et al., 2015).

Different sequelae have been proposed for Pi-mediated EMP release. Proteomic analysis revealed that these MPs are enriched with Annexin II: as a consequence, cells become depleted of this functional protein which might lead to deterioration in EC health (Di Marco et al., 2013). Another scenario has been hypothesised in a more recent study: Pi-induced alterations in phosphorylation status of cellular proteins has been implicated in MP detachment from the cell membrane (Abbasian et al., 2015). Notably, Pi level exerts a feedback control on phosphatase activities, whilst proper protein phosphorylation is fundamental for maintaining cellular integrity (Dick et al., 2011). In

fact, it has been reported that suppression of phosphatases by the phosphate analogue vanadate enhances MP formation; whereas, inhibition of some kinases hinders MP generation (Morel et al., 2011).

Regarding cell monolayer protein, after 24h, Pi loading did not provoke significant change in total cell protein; however, extending the exposure duration to 48h or 72h decreased the protein content (Figure 5.8). A possible explanation for the observed decrease in cell mass is that Pi might stimulate the apoptotic pathway in ECs. In support of this, it has been reported that high Pi treatment induces oxidative stress, phosphatidylserine externalization and stimulates the apoptotic pathway in EA.hy926 cells (Di Marco et al., 2008). The pro-apoptotic effect of Pi has also been confirmed in other EC types, for instance, HUVECs, HMEC-1 and HCAECs (Zhou et al., 2016, Di Marco et al., 2008, Hsu et al., 2015). Conversely, in another study, a negligible effect for high Pi on EA.hy926 cells apoptosis and oxidative stress was demonstrated (Abbasian, 2015).

In general, cell integrity is affected by the level of ROS, and the mitochondrion represents an important generator for cellular ROS. Excess Pi is believed to interfere with mitochondrial energy metabolism (Oliveira and Kowaltowski, 2004). Disturbance in mitochondrial function due to Pi overload has been reported in a previous study in events that lead to programmed cell death. Treatment with antioxidant alleviates these disturbances suggesting enhancement of ROS formation as a causative factor (Kowaltowski et al., 2001).

5.3.6 Simultaneous in vitro stimulation of ECs with high glucose and Pi.

As previously mentioned, both high glucose and high Pi have been reported to induce intracellular oxidative stress and stimulate the apoptotic pathway. Therefore, a trial was performed to test if their combination represents an extra burden to ECs.

The result presented in Figure 5.13 B and C indicates that the addition of glucose to Pi-treated ECs resulted in relative restoration of cell monolayer protein. In addition, protein particle released in the test medium showed a moderate repression compared to treatment with Pi alone (Figure 5.7). As an excessive mitochondrial ROS generation is reported to play an important role in both hyperglycaemia and hyperphosphataemia, exposing ECs to elevated concentrations of high glucose and Pi was expected to apply

more load on the aerobic cell metabolism resulting in mitochondrial dysfunction and possibly cell collapse. The observation in this study does not support this suggestion.

On the other hand, Pi is an indispensable substrate for glucose metabolism and the subsequent ATP synthesis. It has been observed that exposing ECs to high glucose environment augments glucose uptake into the cells, arising from the inability of ECs to autoregulate their glucose transporter expression in the face of a glucose load (Huang et al., 2012). Furthermore, to a certain limit, glucose load enhances glucose utilization by increasing the glycolytic pathway flux and ATP production (Kitada et al., 2010). It is therefore likely that Pi will enter the cell and become metabolically trapped in the form of sugar phosphate glycolytic intermediates (Cox, 2002). Consequently, this will diminish the intracellular Pi pool and protect cells from the detrimental effect of high cytosolic Pi. A similar effect was observed by Abbasian et al (2015) when combining high Pi with the slowly metabolised sugar, fructose.

In summary, exposing ECs to diabetic concentrations of glucose in addition to high Pi did not give the additive stress effect that was originally predicted. On the contrary, a glucose load apparently ameliorated the effects of high Pi.

5.3.7 Effect of C-peptide on ECs challenged by hyperphosphataemic milieu

As demonstrated earlier, Pi injures ECs and augments MP formation. In turn, MPs are generated from apoptotic or activated cells. A beneficial effect of C-peptide has been observed in several vascular disorders. Therefore, the potential protective effect of C-peptide on Pi-induced changes in EA.hy926 cells was investigated.

In the present study, C-peptide treatment did not rescue EA.hy926 cell from Pi-induced cell stress and particle output (Figure 5.14 and Figure 5.15 B). In addition, C-peptide did not significantly improve cell mass compromised by high Pi (Figure 5.15 A). However, a possible mild effect was observed after 24h exposure to Pi which may merit further investigation (Figure 5.14 A). In spite of the fact that C-peptide is described as having anti-apoptotic and antioxidant effects (Bhatt et al., 2016, Cifarelli et al., 2011a), these actions were not proved in the setting of high Pi in the present culture model: indeed C-peptide alone seemed to enhance MP output from the cells (Fig 5.15 and Chapter 4). In view of these diverse effects of C-peptide in cultured EC models, it is important to

determine the net effect of C-peptide on vascular endothelium *in vivo*. Such an *in vivo* study is described in the next chapter.

Chapter 6. Effect of C-peptide replacement on functional and structural alterations in aorta of STZ-diabetic rat

6.1 Introduction

Cardiovascular disease in diabetic patients represents the leading cause of premature morbidity and mortality (Morrish et al., 2001). Since a treatment for diabetes-associated vasculopathy is lacking, the present chapter aimed to investigate the possible therapeutic use of C-peptide in a long-term diabetic animal model.

6.1.1 Effect of C-peptide on diabetic macrovasculopathy

The effect of C-peptide on diabetic macrovasculopathy is poorly studied compared to microvasculopathy (Wahren et al., 2016). However, previous *in vitro* studies have demonstrated improvement in endothelial dysfunction under hyperglycaemic settings upon C-peptide addition (Luppi et al., 2008, Bhatt et al., 2013). Moreover, C-peptide blocks the hyperproliferative activity of aortic SMCs triggered by high glucose; thus, retarding one of the primary events in atherosclerosis development (Cifarelli et al., 2008, Kobayashi et al., 2005). Whereas, few C-peptide studies have reported unfavourable mitogenic and proinflammatory effects in the vessel wall (Walcher and Marx, 2009, Vasic et al., 2012).

6.1.2 Assessment of vascular function

Multiple modalities can be used for examining the vascular health (Section 1.2.6). One of the important markers that reflect endothelial functions is vWF; while other measures such as collagen deposition, oxidative stress or AGE accumulation reflect the pathological changes in the entire blood vessel wall.

6.1.2.1 von Willbrand factor as a marker of endothelial cell activation/injury

The bioactive mediator, vWF, plays a key role in the thrombotic cascade and vascular inflammation. It is mainly synthesised by the ECs; therefore, it has been proposed as an indicator for endothelial cell activation or injury, and as a prognostic marker in cardiovascular, metabolic and inflammatory diseases, such as DM, stroke, MI and sepsis (reviewed in (Gragnano et al., 2017)).

6.1.2.2 Collagen deposition

The biochemical abnormalities induced by long exposure to hyperglycaemia eventually cause tissue injury. One of the pathophysiological responses of the human body to injury is by accumulating ECM proteins, such as collagen (Ban and Twigg, 2008). DM produces tissue insults both at the micro and macro vascular levels. Alteration in ECM constituents or amount in response to DM has been widely described in most of the end-organ targets for chronic diabetic complications (Tsilibary, 2003). Moreover, these abnormal changes in ECM composition in DM were found to be positively correlated with functional failure of particular cells or tissue (Ban and Twigg, 2008). Collagen is the most abundant protein in ECM; therefore, quantifying collagen is a well-established method for assessing modification of ECM in tissues (Rumble et al., 1997).

6.1.2.3 Formation of AGEs

Prolonged hyperglycaemia results in augmented formation of AGEs. AGEs damage the vascular wall via several pathways, notably collagen cross linking and modification of binding sites for MMPs in ECM; thereby, rendering ECM less susceptible to degradation (Voziyan et al., 2014). Another pathway which permits AGEs to exert their deleterious effect is through binding to their receptor, RAGE (Nowotny et al., 2015). Consequently, AGE-associated alterations in wall structure ultimately promote vascular stiffness and dysfunctional changes, which lead to the development and progression of diabetic long-term vascular complications (Intengan and Schiffrin, 2001). As AGE formation represents an important pathway for hyperglycaemia-induced cell injury, AGE deposition in the vascular wall was assessed in this study.

6.1.2.4 Oxidative stress level

It is generally accepted that elevated extracellular glucose activates several intracellular signals. Excessive generation of superoxide from the mitochondrial electron transport chain has been recognised as an important aetiological factor in hyperglycaemia (Brownlee, 2005). Overexpressing superoxide dismutase in transgenic animals blocks all the pathogenic downstream signals of hyperglycaemia (Brownlee, 2005). In the vasculature, liberated ROS, in particular, superoxide, react with NO to form the potent oxidant and nitrating agent, peroxynitrite. Consequently, proteins nitrated on their

tyrosine residues, yielding 3-nitrotyrosine (3-NT) residues, are formed (Radi, 2004). Overall, 3-NT represents a widely-accepted measure of oxidative/nitrosative stress (Radi, 2004); therefore, in the present study, 3-NT was selected as an indicator of oxidative stress level in aorta tissue.

Accordingly, this chapter aims to study the consequences of DM with and without C-peptide treatment on the following parameters:

- Morphological changes in aorta wall.
- The expression of vWF as measure of endothelial cell function.
- Collagen deposition as an indicator of vascular remodelling.
- Oxidative stress level assessed by 3-NT.
- Accumulation of AGEs in the aorta tissue.

6.2 Results

6.2.1 Effect of C-peptide on diabetic aorta morphology

Having established the diabetic animal model in our laboratory, we sought to explore the effect of C-peptide on the vascular tissue. Formalin-fixed sections were used to identify the morphological changes in rat aorta. In this study, staining aorta sections with H&E and Miller's elastic van Gieson stains did not reveal obvious histopathological changes in aortic wall architecture in any of the study groups (data not shown), after independent assessment by two histopathologists. Staining with EVG did not show abnormal disruption or fragmentation in elastin fibres in the medial layer. Furthermore, by examining the aorta sections with H&E staining, apparent loss of endothelial cell integrity or intimal thickening was not observed.

6.2.2 Effect of C-peptide treatment on vWF expression in aorta of diabetic rat

To determine the effect of DM on vWF expression in the intima layer of rat aorta and whether C-peptide administration modulates this, aorta tissues from all the study groups were analysed using IHC technique (Section 2.2.14.3). Figure 6.1 shows localisation and expression of vWF in the aorta vessel wall of vehicle-treated control, STZ-diabetic, and C-peptide treated rats. vWF immunoreactivity was detected in the intima layer of the aorta as demonstrated by the arrows in the diabetic aorta image. The brown staining which represents vWF expression was strong in diabetic tissue (Figure 6.1B) compared to weak staining in the vehicle-injected control group (Figure 6.1A); whereas, the staining in the C-peptide group was closely similar to that of the control group (Figure 6.1C). No positive brown staining was detected when the primary antibody was omitted as a negative control (Figure 6.1D). To quantify vWF expression, the area of brown staining was measured using Fiji software (Figure 6.2) and expressed as % of total intima layer (Section 2.2.14.4). Analysis of data showed that induction of DM in rats resulted in a significant increase (7.67 ± 0.71 % stained area) in vWF level in the vessel wall compared to healthy rats (4.26 ± 0.58 % stained area). In contrast, C-peptide replacement restored vWF level to close to normal values (4.57 ± 0.53 % stained area). These data suggest that C-peptide reduces vWF content in aorta tissue of diabetic rats.

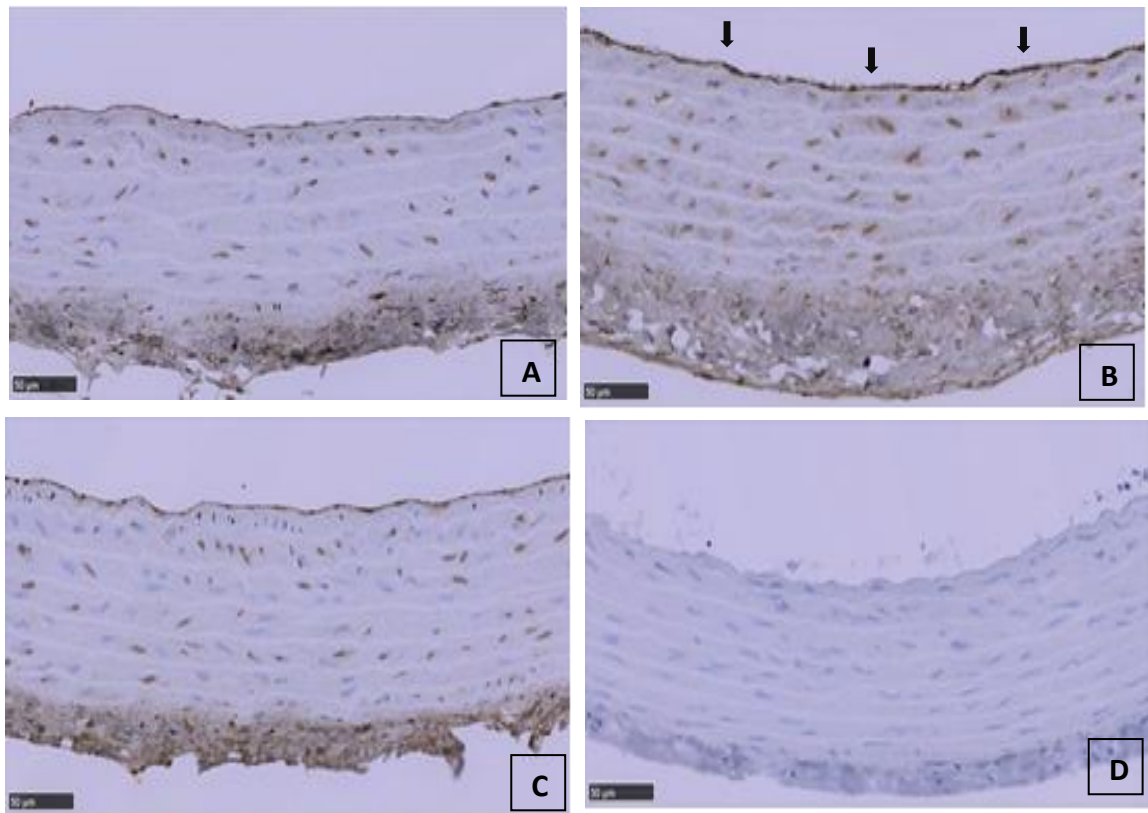


Figure 6.1 Expression of vWF in the intima layer of healthy control and diabetic rat aorta. Immunostaining of aortas A) control saline-treated rats B) diabetic rats C) diabetic rats treated with C-peptide D) example of the negative control from the diabetic group is shown (no primary antibody was added), also negative controls from the other groups showed similar results (data not shown). Localisation of vWF is illustrated by the black arrows in the diabetic aorta image. Haematoxylin and eosin were used for counterstaining. Scale bar = 50µm.

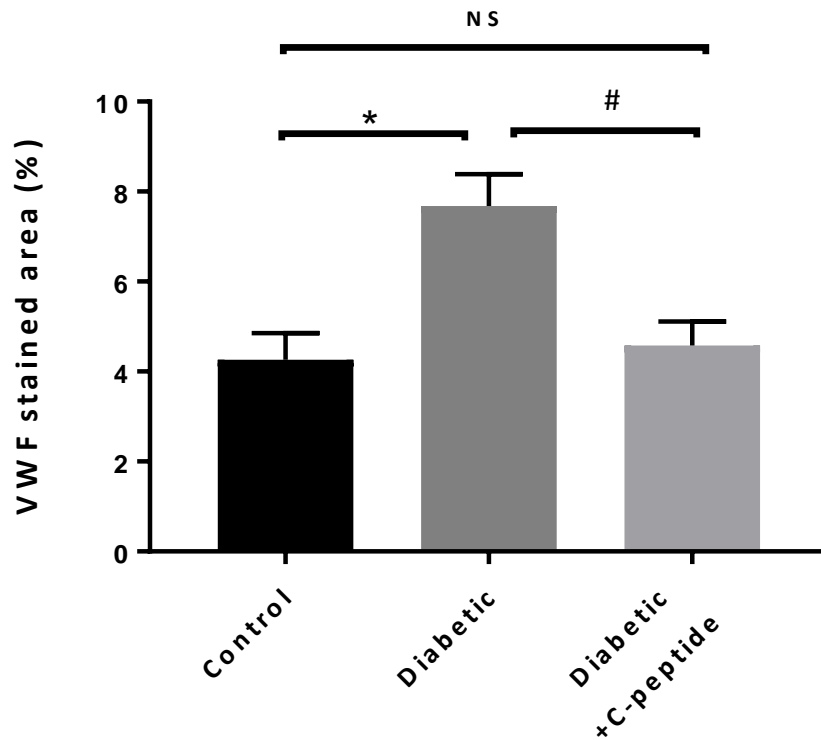


Figure 6.2 Effect of C-peptide treatment on the intimal expression of vWF in diabetic rat aorta evaluated by immunohistochemical staining of vWF. For C-peptide treatment group, diabetic rats were treated with long-acting C-peptide 0.5mg/kg subcutaneously twice weekly for 29 weeks. Positive areas of brown staining in the endothelium were quantified using Fiji software and expressed as (%) of total intima layer. Results were presented as mean \pm SEM of 6 rats from the diabetic and C-peptide groups and 2 rats from the control group. * $P < 0.05$ compared to saline-treated control group. # $P < 0.05$ compared to untreated diabetic group. NS insignificant difference compared to control group.

6.2.3 Effect of C-peptide treatment on collagen content in the aorta of diabetic rat

To assess the effect of DM on ECM protein accumulation, specifically, collagen in the aorta wall of STZ-diabetic rats and whether C-peptide treatment modifies this, aorta sections from vehicle-treated control, STZ-diabetic, and C-peptide treated rats were evaluated using Masson trichrome staining. Figure 6.3 shows the distribution and organisation of collagen bundles in the vascular wall of all the treatment groups. As illustrated, green-stained collagen fibres are arranged within all aorta layers from endothelial basement membrane, internal lamina, media, external lamina and the adventitia. The green staining which represents collagen was stronger in diabetic tissue (Figure 6.3B) compared to less staining in vehicle-injected control group (Figure 6.3A); whereas, the staining in the C-peptide group was similar to that of the control group (Figure 6.3C). To quantify collagen accumulation, the area of green staining was measured using Fiji software (Figure 6.4) and expressed as % of total tissue area (Section 2.2.14.4). According to software analysis, induction of DM in rats resulted in a significant increase ($52.15 \pm 2.19\%$ stained area) in collagen content in diabetic vessel wall compared to that of healthy rats ($33.57 \pm 10.98\%$ stained area). Conversely, C-peptide replacement restored collagen deposition close to normal values ($32.96 \pm 3.44\%$ stained area). These data suggest that C-peptide halts excessive collagen accumulation in the vascular wall of diabetic rats.

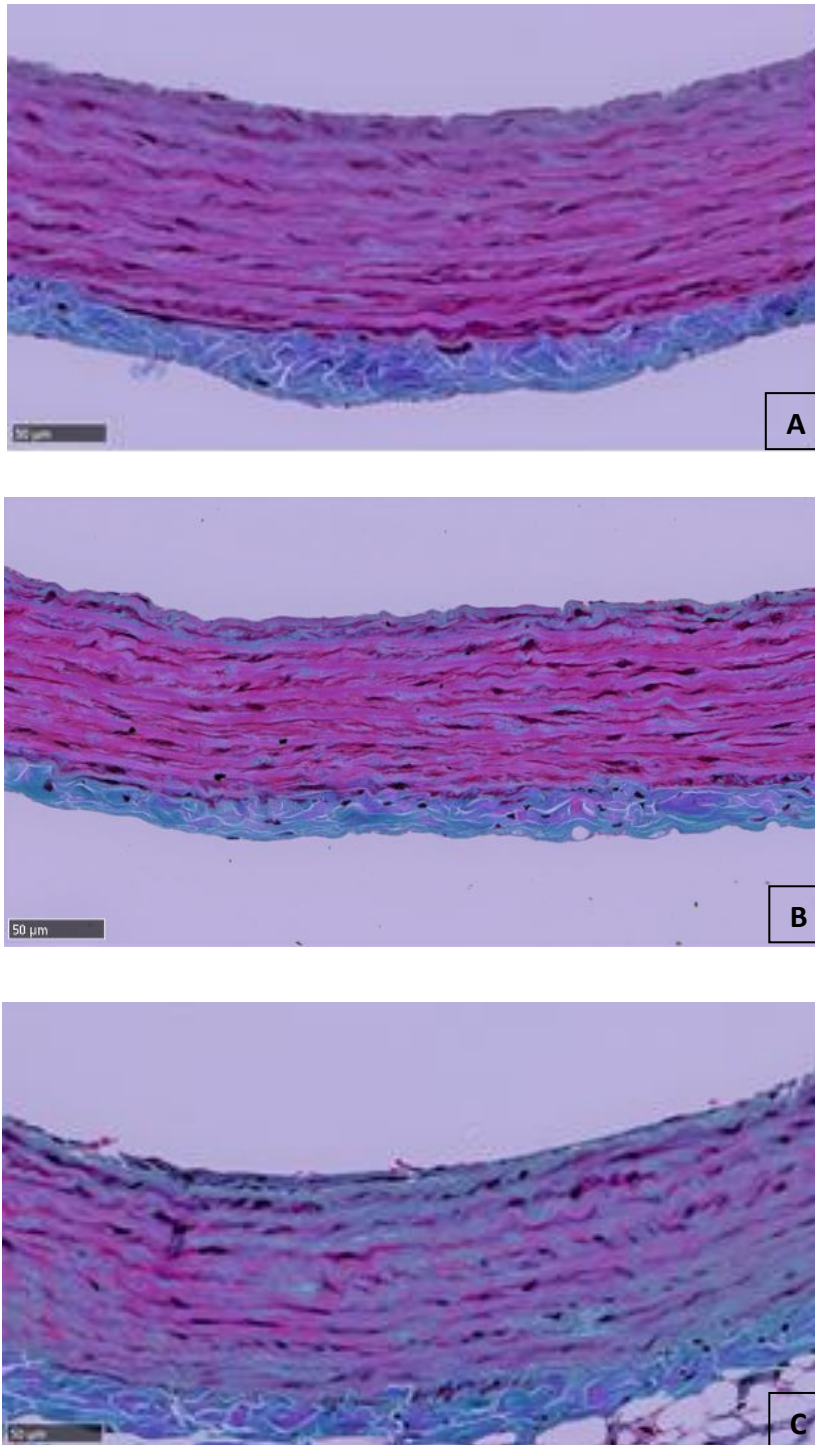


Figure 6.3 Masson trichrome staining of aortas demonstrating the amount of collagen deposition. Control saline-treated (A), diabetic (B) and diabetic treated with C-peptide (C) aortas. Collagen fibres were stained in green, muscles were stained in red and nuclei were stained in black. Scale bar = 50µm.

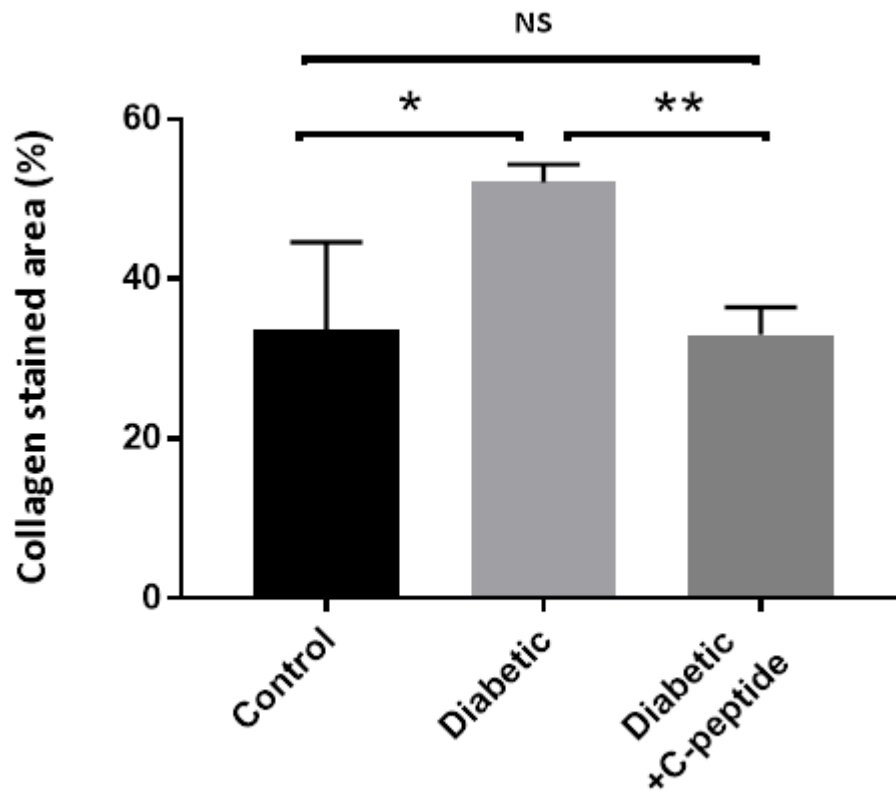


Figure 6.4 Effect of C-peptide treatment on collagen deposition in diabetic rat aorta evaluated by Masson trichrome staining. For C-peptide treatment group, diabetic rats were treated with long-acting C-peptide 0.5mg/kg subcutaneously twice weekly for 29 weeks. Area of positive green staining were quantified using computer-assisted analysis (Fiji software) and expressed as (%) of total tissue area. Results were expressed as mean \pm SEM of 6 rats from the diabetic and C-peptide groups and 2 rats from the control group. * P < 0.05 compared with saline-treated control group. ** P < 0.01 compared to the untreated diabetic group. NS insignificant difference compared to control group.

6.2.4 Effect of C-peptide treatment on accumulation of advanced glycation end products in the aorta wall of diabetic rat

In order to evaluate the effect of DM on AGE deposition on rat aorta wall and whether C-peptide administration modulates this, aorta tissues from all the study groups were analysed using IHC. Figure 6.5 shows aortic AGE deposit loci in vehicle-treated control, STZ-diabetic, and C-peptide treated rats. As demonstrated, AGE accumulation occurs in all aorta layers. The brown staining which represents AGE deposition was more intense in diabetic tissue though not significantly (Figure 6.5B) compared to the vehicle-treated control group (Figure 6.5A). AGE staining in C-peptide group was similar to that of the control group (Figure 6.5C). No positive brown staining was detected when the primary antibody was omitted as a negative control (Figure 6.5D) and expressed as % of total tissue area. To quantify AGE expression, the area of brown staining was measured using Fiji software (Figure 6.6). Analysis of data showed that induction of DM in rats did not show a marked increase (4.54 ± 0.80 % stained area) in AGE accumulation in the vessel wall compared to that of healthy rats (3.98 ± 0.33 % stained area). C-peptide treatment gave an apparent, but statistically insignificant, decrease in AGE level in aorta wall (2.85 ± 0.12 % stained area).

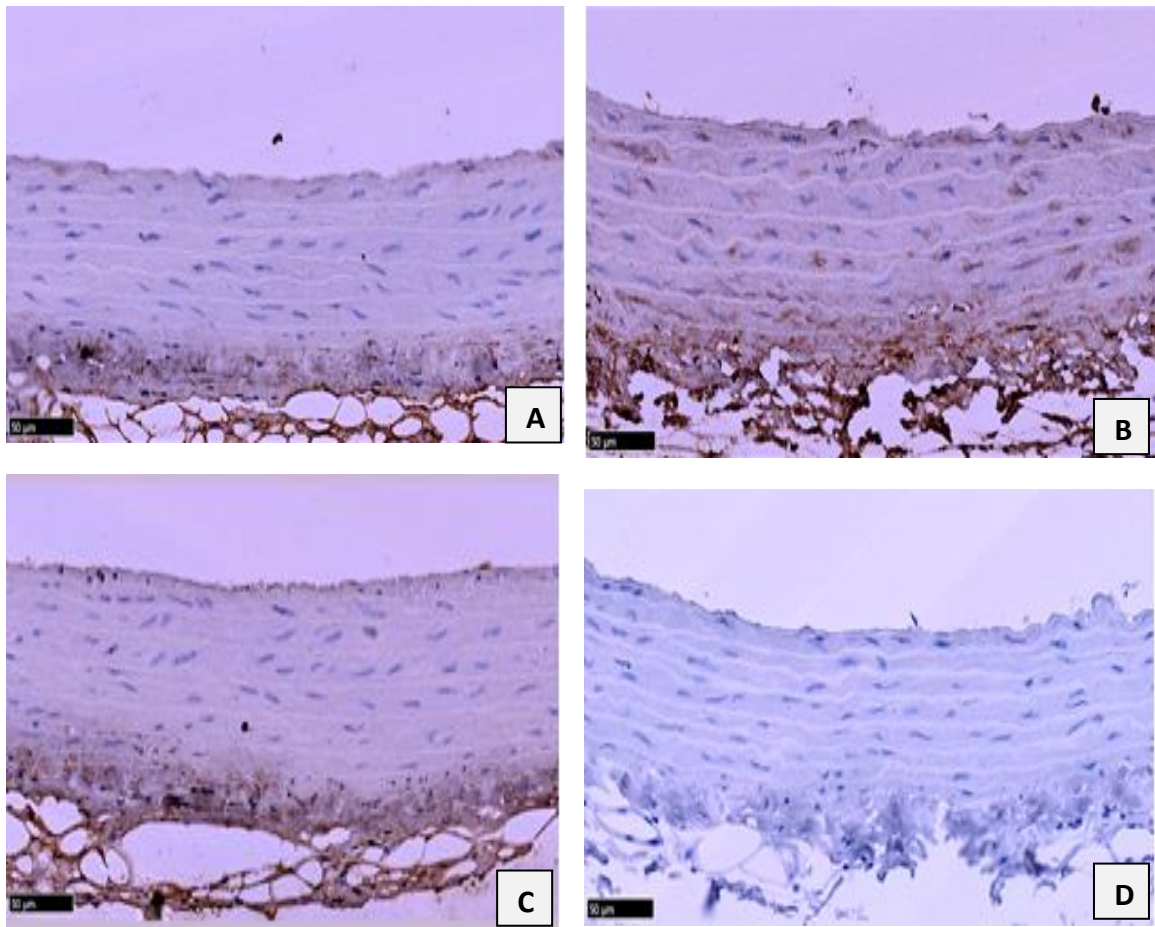


Figure 6.5 Immunohistochemical staining for advanced glycation end products in sections of aorta. Positive staining is shown in brown. A) Control saline-treated rats B) diabetic rats C) diabetic rats treated with C-peptide D) negative control (without primary antibody). Haematoxylin and eosin were used for counterstaining. Scale bar = 50 μ m.

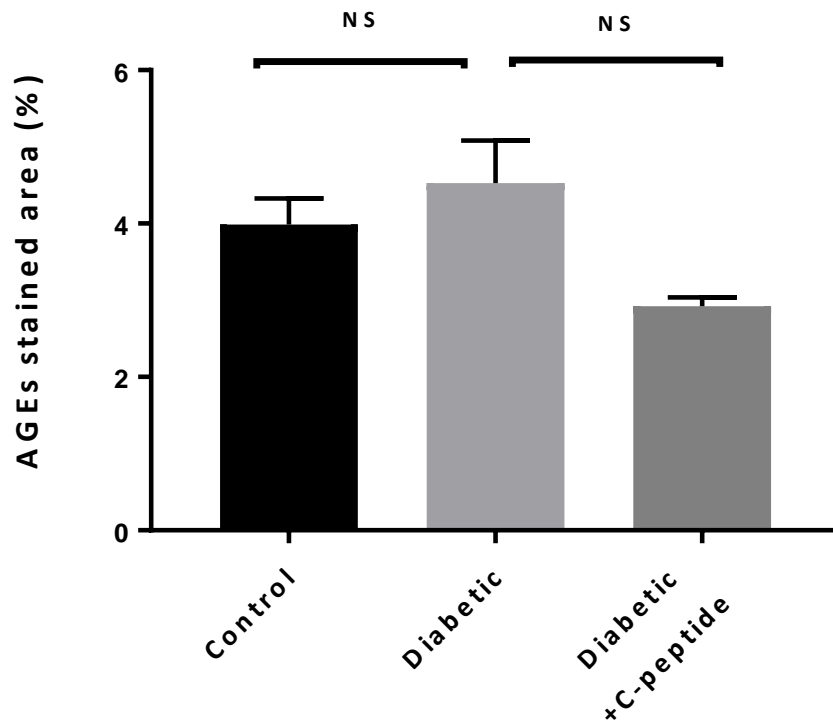


Figure 6.6 Effect of C-peptide treatment on AGE content in diabetic rat aorta measured by immunohistochemical staining. For the C-peptide treatment group, diabetic rats were treated with long-acting C-peptide 0.5mg/kg subcutaneously twice weekly for 29 weeks. Aorta sections were stained with anti-AGE antibody and positive areas of brown staining were quantified using Fiji software and expressed as (%) of total tissue area. Results were expressed as mean \pm SEM of 6 rats from the diabetic and C-peptide groups and 2 rats from the control group. NS insignificant difference compared to control group.

6.2.5 Effect of C-peptide treatment on the oxidative stress level in diabetic rat aortas

To examine the effect of DM with or without C-peptide treatment on oxidative stress status in vasculature, 3-NT level in the aorta wall was determined. Aorta sections from vehicle-treated healthy rats, STZ-diabetic rats and C-peptide treated rats were analysed by IHC. Figure 6.7 shows aortic 3-NT deposits in vehicle-treated control, STZ-diabetic, and C-peptide treated rats. As demonstrated, 3-NT formation occurs in all aorta layers. The brown staining which represents 3-NT deposition showed a slight (but insignificant) increase in the diabetic rats (Figure 6.7 B) when compared to the vehicle-treated healthy control group (Figure 6.7 A). Positive staining of 3-NT in the C-peptide group was similar to that of the control group (Figure 6.7 C). No positive brown staining was detected when the primary antibody was omitted as a negative control (Figure 6.7 D). To quantify 3-NT expression, the area of brown staining was measured using Fiji software (Figure 6.8) and expressed as % of total tissue area. According to software analysis, induction of DM in rats did not show noticeable difference (6.37 ± 0.57 % stained area) in 3-NT accumulation in the vessel wall compared to that of healthy control rats (4.84 ± 1.65 % stained area). C-peptide treatment also did not cause a statistically significant change in 3-NT level in aorta wall (4.08 ± 0.44 % stained area).

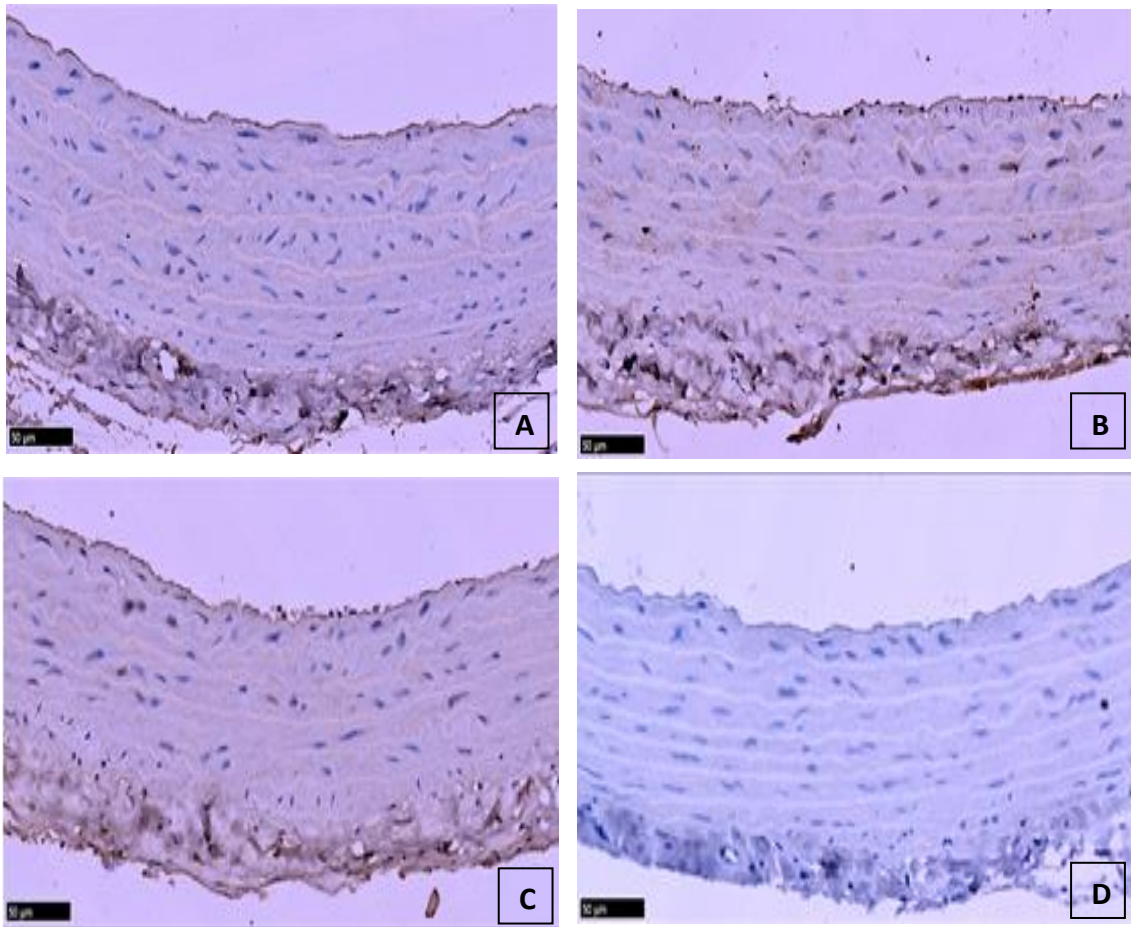


Figure 6.7 Immunohistochemical staining for 3-NT in sections of aorta. Positive staining is shown in brown. A) Control saline-treated rats B) diabetic rats C) diabetic rats treated with C-peptide D) negative control (without primary antibody). Haematoxylin and eosin were used for counterstaining. Scale bar = 50µm.

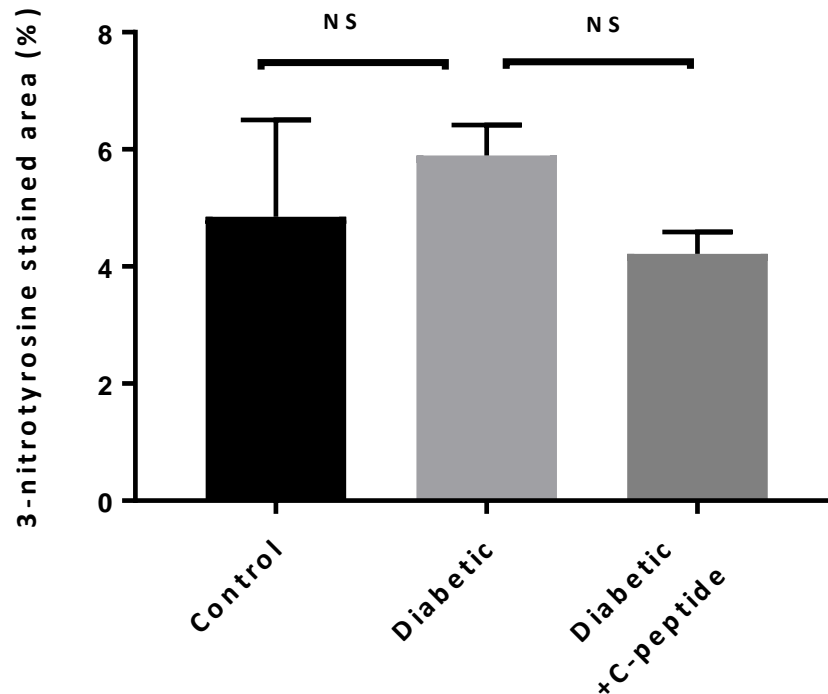


Figure 6.8 Effect of C-peptide treatment on oxidative stress level in diabetic rat aorta assessed by immunohistochemical staining of 3-NT. For the C-peptide treatment group, diabetic rats were treated with long-acting C-peptide 0.5mg/kg subcutaneously twice weekly for 29 weeks. Aorta sections were stained with anti- Nitrotyrosine antibody and positive areas of brown staining were quantified using Fiji software and expressed as (%) of the total tissue area. Results were expressed as mean \pm SEM of 6 rats from the diabetic and C-peptide groups and 2 rats from the control group. NS insignificant difference compared to control group.

6.3 Discussion

6.3.1 Effect of C-peptide on aorta morphology of diabetic rat

In the present study staining diabetic aorta sections with H&E and EVG stains did not reveal gross histopathological changes in the aortic wall in any of the study groups (Section 6.2.1).

Development of DM is associated with morphological changes in the arterial wall. Clinical investigations have shown that these structural alterations in the vessel wall and the associated stiffness occur at early stages of the disease (Christen et al., 2010); nevertheless, reproducing these changes in experimental animals is more challenging. At the ultrastructural level, Reinila et al (1981) showed that two months of untreated STZ-induced DM in rat did not produce any observable morphological changes in the aorta wall apart from a few vacuoles in the intima layer observed under EM, despite the fact that only 12 out of 35 diabetic rats survived at the end of the study. However, in a 5 months diabetic study, Searls et al (2012) observed structural and ultrastructural alterations mainly in the media layer of the aorta wall of diabetic rats consistent with increased vascular stiffness: a reduction in the aorta wall thickness was associated with loss of smooth muscle cells whilst there was an increase in elastin band width. However, in this study, from each group only 3 rats out of 12 survived to the end. Other studies have reported disruption and degradation of elastin fibres in diabetic aorta medial layer in conjugation with diminished media thickness (Fiordaliso et al., 2006, Salum et al., 2014). Differences in DM duration in these studies might explain some variations in reporting DM-induced changes in aorta layers.

On the other hand, intimal thickening is one of the primary structural changes in the arterial wall during the course of DM, which normally precedes atherosclerosis (De Caterina et al., 2007b). It has been observed that long-term induction of DM by STZ does not produce atherosclerosis in rats fed standard chow-diet, despite the high death rate (Wei et al., 2003). Notably, development of atherosclerosis in animals is usually associated with a state of hyperlipidaemia (Wu and Huan, 2007). In fact, changing the fat content in animal diet is considered as a model for T2DM; whereas, treating animals with STZ alone produces T1DM because insulin resistance does not normally develop in

this model (Wu and Yan, 2015). Studying the effect of C-peptide in T2DM is more complex (discussed in Section 1.4.7) and beyond the scope of the present study, which was designed to study the effect of C-peptide replacement in T1DM.

To conclude, significant structural modifications in the aorta wall was not observed in this study by light microscopy; however, it is not a prerequisite for functional or ultrastructural changes to happen. Thus, further investigation was conducted to evaluate the effect of C-peptide treatment in diabetic rats using different analytical techniques.

6.3.2 C-peptide improves vascular EC health in diabetic rat by restoring intimal vWF content to normal

The expression of vWF protein in the intimal layer of diabetic aortas was significantly increased compared to control aortas (Figure 6.1 and 6.2). These results are in line with other studies (Ribau et al., 2000). Whereas, treating diabetic rats with C-peptide restored vWF expression close to normal suggesting at least an improvement in the overall endothelial cell health status. This is apparently the first study to explore the effect of C-peptide treatment of endothelial cell dysfunction *in vivo* by measuring vWF as a marker of cell injury.

The observed increment in vWF content in the intima layer of diabetic aorta detected by immunohistochemical methods could be due to an augmented protein expression, a decrease in degradation of the vWF protein, or increased deposition of circulating vWF in the damaged endothelium. Ribau et al (2000) observed a significant increase in vWF quantity in the diabetic aorta despite the fact that vWF mRNA level was not different from that in control vessels. In general, vWF is released from the endothelial cells to the plasma and also toward the subendothelial layer. vWF presents in soluble form in the plasma, intracellularly and in the basement membrane; however, in the normal situation, there is minimal deposition in the basal lamina. Conversely, experimental studies have demonstrated enhanced vWF accumulation in the subendothelial layer during the process of intimal thickening, and it contributes to smooth muscle cell migration and endothelial cell adhesion (De Meyer et al., 1999). Moreover, it has been hypothesized that the secreted vWF might be entrapped by ECM proteins resulting in

enhanced immunohistochemical reactivity for vWF in vasculature (Boerma et al., 2004), supported by an *in vitro* study which showed binding sites for vWF on collagen (Ribau et al., 2000).

The underlying mechanism behind the upregulated vWF expression and secretion in DM is still largely unknown. Xiang et al (2015) observed that enhanced ROS formation under hyperglycaemic conditions modulates vWF protein expression. Moreover, by blocking ROS generation in HUVECs, the intracellular level of vWF and vWF release were both diminished. These data suggest that ROS play a role in vWF expression on endothelial cells. The antioxidant activity for C-peptide has been documented (see Section 1.4.5.3). Therefore, it is conceivable that C-peptide restores vWF expression to normal level in diabetic aorta by suppressing ROS generation.

Another possible modulatory effect for C-peptide on vWF might be through the feedback inhibitory effect of NO on vWF release (Gragano et al., 2017). In the current study and in previous studies, it has been observed that C-peptide increases eNOS expression in vascular endothelial cells. In addition, C-peptide augmented NO release from rat aorta tissue in response to inflammatory insult (Scalia et al., 2000). Thus, the potentiated NO formation associated with C-peptide might be responsible for altering vWF release and the subsequent deposition in the intima layer.

In summary, elevated vWF level may possibly predict cardiovascular events incidence in DM, therefore, normalizing its level implies better disease prognosis. C-peptide treatment was apparently successful in achieving this. Therefore, C-peptide might ameliorate the progression of diabetes associated vascular complications.

6.3.3 C-peptide ameliorates collagen accumulation in aortic wall of diabetic rats

The results of the current study indicate that following induction of T1DM in rats, a significant increase in collagen content in aorta wall was observed at the end of the study (Figure 6.3 and 6.4). These findings are in agreement with previous studies which showed development of aortic fibrosis in diabetic animals (Searls et al., 2012, Miao et al., 2012). Interestingly, in the aforementioned studies, a noticeable collagen accumulation in aorta wall was observed only after 5-6 months from DM induction.

The underlying mechanism behind the observed ECM expansion in diabetic aorta in the present study could be due to the effect of DM on MMPs and their tissue inhibitors. *In vitro* studies showed that exposing ECs to high glucose concentration increases the expression and activity of MMP-2 and MMP-9 (Tarallo et al., 2010). However, studies on STZ-diabetic animals revealed reduction in MMP-2 and MMP-9 activities in aorta tissue (Lu et al., 2008). In addition, human studies have shown downregulation of local MMP activity in arterial vasculature in DM (Portik-Dobos et al., 2002). Despite the wide variation in reported MMP activity or expression in plasma or in tissue, which might reflect the complexity of ECM environment and the duration of hyperglycaemia, these studies have proved that DM induces an important dysregulation of MMP/TIMP system resulting in pathological vascular remodelling. In general, it is thought that hyperglycaemia tips the MMPs/TIMP balance towards the breakdown of ECM components (Kadoglou et al., 2005). However, the local enzyme activity in a specific tissue might be different. For instance, in renal tissue downregulation of MMP activity and expression is observed in diabetic microangiopathy and nephropathy (Song et al., 1999). Moreover, it has been observed that DM protects the aorta against aneurysm growth by modulating ECM synthesis/degradation in the vessel wall (Raffort et al., 2018). In contrast, in atherosclerotic plaques, the activity/level of MMPs has been reported to be increased in diabetic patients resulting in plaque destabilisation (Kadoglou et al., 2005). Therefore, it is plausible that the diabetic environment in the current study has resulted in ECM thickening, in particular, collagen by downregulation of MMPs in the aorta wall.

Another possible mechanism for ECM expansion in DM is via changing growth factor profiles, especially the profibrotic growth factor TGF- β . Enhanced TGF- β activity and/or expression has been associated with the development of macroangiopathy in DM. *In vitro* studies have shown that ECs and VSMCs release more TGF- β under high glucose conditions and this was associated with enhanced collagen production, while blocking TGF- β action by neutralising antibody abolished the effect of glucose on collagen matrix expression (Li et al., 2003a). In diabetic animals TGF- β 1 mRNA expression was elevated several fold in conjunction with ECM expansion in arterial vasculature for up to 8 months after T1DM induction (Rumble et al., 1997, Fukuda et al., 2005).

More importantly, in the current study, C-peptide administration retarded ECM remodelling in aorta of diabetic animals (Figure 6.3 and 6.4). There is apparently no previous report addressing the effect of C-peptide on collagen deposition in large blood vessels of diabetic animals. It has been reported that induction of T1DM in rats using STZ without diet modification requires long duration to achieve an observable increase in ECM mass of aorta (Searls et al., 2012, Miao et al., 2012, Groß et al., 2004). This might partially explain the limitation in data availability from other studies.

Experimental evidence has shown that C-peptide administration modulates several components in the fibrotic pathway. C-peptide treatment downregulates gene expression of TGF- β and type IV collagen in diabetic mice glomeruli (Li et al., 2018). *In vitro* treatment of murine podocytes with C-peptide blocks the stimulatory effect of exogenous TGF- β on collagen synthesis (Maezawa et al., 2006). In parallel, C-peptide protects human kidney PTCs against fibrosis by suppressing TGF- β induced phenotypic changes in these cells (Hills et al., 2009). Moreover, in a more recent study, it was demonstrated that C-peptide exerts an inhibitory effect on AGE-stimulated matrix protein production from mesangial cells (Xu et al., 2015).

On the other hand, several studies have demonstrated a modulatory effect for C-peptide on the MMP system. Inhibition of MMP-9 expression and secretion were detected in rat mesangial cells in response to high glucose exposure while C-peptide addition restored MMP-9 protein content thereby preventing excessive ECM protein accumulation and halting renal fibrosis (Wang et al., 2016).

Thus, by reviewing the previous reported studies, it is clear that the effect of C-peptide on fibrosis is of major interest in renal tissue. Furthermore, the beneficial effect of C-peptide on ECM composition has been demonstrated in other tissues. In retinal tissue, C-peptide protects against microangiopathy by modulating ECM protein production. C-peptide completely reversed DM-induced pathological changes in ECM protein deposition in rat retinas (Chakrabarti et al., 2004). Therefore, considering the fact that similar mediators are involved in regulating ECM composition in the vascular system, it is plausible that C-peptide attenuates the fibrotic response in aorta wall through manipulating TGF- β signalling and/or the MMP system.

Additionally, it is well established that both inflammation and oxidative damage are major causative factors for fibrotic defence in living tissue (Intengan and Schiffrin, 2001) and nowadays it is well-appreciated that inflammation represents a critical element in the progression of diabetic vascular complications (Cifarelli et al., 2011b). Experimental studies have reported anti-inflammatory effects for C-peptide in different types of tissue in response to various stimuli (Section 1.4.5.2). Therefore, it is conceivable that C-peptide improved the pathological vascular modification by suppressing the inflammatory response under DM conditions in the present study.

To conclude, DM resulted in ECM remodelling via collagen deposition in aorta wall thereby potentially increasing the incidence of cardiovascular diseases. However, more importantly, C-peptide administration hampered the progress of these structural changes in the blood vessel wall. Thus, by preventing the pathological aortic remodelling, C-peptide might have a therapeutic value in treating macrovascular complications in DM.

6.3.4 Effect of C-peptide on AGE accumulation in diabetic aorta

As shown in Figure 6.5 and 6.6, AGE accumulation in the diabetic aortas did not reach statistical significance compared to that of the control aortas. Consequently, C-peptide treatment did not show a remarkable change in AGE deposition in aorta wall.

Several lines of evidence have shown that AGEs accumulate in serum and tissues of diabetic patients at accelerated rate, and it is correlated with the development and progression of vascular injury (Nowotny et al., 2015). In a study performed by Wang et al (2014), it was demonstrated that compared to healthy control rat, induction of DM by STZ for 6 weeks resulted in a marked increase in AGE accumulation in the aorta wall of diabetic animals. Similarly, augmented AGE formation in vasculature of diabetic rats was observed in other studies (Rumble et al., 1997, Cheng et al., 2005).

Despite the fact that the immunohistochemical assay that has been used in this study offers the advantage of depicting AGE deposition loci in tissues, difficulties in using Anti-AGE antibodies for immunohistochemistry or ELISA have been reported (Nowotny et al., 2015). As AGEs represent a diverse group of compounds and only partially identified, anti-AGE antibodies are developed unspecifically against AGEs. In addition,

unfortunately, the immunohistochemical staining for RAGE expression in aorta tissue was unsuccessful in this study (- refer to section 6.3.6 study limitation).

The interest in evaluating the effect of C-peptide on the AGE-RAGE axis in the vascular wall in this study arises from previous findings which demonstrated that C-peptide inhibits the activity of the AGE-RAGE system and its downstream pathways. C-peptide treatment downregulates RAGE expression in renal tissue of diabetic rats and in cultured mesangial cells exposed to high glucose (Xu et al., 2015). Moreover, in a seven-month animal model of DM, Sima et al (2009) demonstrated that C-peptide replacement blocks RAGE overexpression in diabetic brain tissue; subsequently, it prevented NF κ B activation and its downstream pro-inflammatory mediators in diabetic tissues. Moreover, C-peptide (but not insulin) prevented AGE-induced ECM synthesis in cultured rat mesangial cells implying that C-peptide interferes with AGE signalling pathways (Xu et al., 2015).

As C-peptide does not affect hyperglycaemia, other mechanisms for C-peptide influence on AGE/RAGE axis have been proposed. C-peptide mediates suppression of RAGE expression in diabetic tissue possibly via correcting the defective I κ B insulin signalling pathways in diabetic tissue (Sima et al., 2009). However, Insulin supplementation to diabetic rats or to cultured mesangial cells exposed to high glucose concentration, did not prevent RAGE overexpression while C-peptide did (Xu et al., 2015). Alternatively, activation of PPAR γ by C-peptide might play a role (Al-Rasheed et al., 2004b). PPAR γ agonists interfere with the AGE/RAGE system, particularly RAGE expression (Yamagishi et al., 2009). Furthermore, there is mounting evidence of the beneficial effects of C-peptide on redox balance in vascular cells. Hyperglycaemia-induced oxidative stress is known to promote formation of AGEs (Yamagishi et al., 2012). Therefore, C-peptide may interfere with AGE/RAGE interaction in aorta wall by quenching ROS.

In summary, the present study did not detect an observable AGE accumulation in diabetic aorta tissue with or without C-peptide treatment. However by using different analytical techniques in future studies, the apparent small beneficial C-peptide-induced changes observed here might become more clearly visible.

6.3.5 Effect of C-peptide on oxidative stress level in diabetic aorta

By comparison with the controls, the level of 3-NT in aorta wall of diabetic rats did not reach statistical significance (Figure 6.7 and 6.8). Consequently, C-peptide treatment did not significantly affect 3-NT protein expression of aorta in comparison with that of diabetic rats. Nevertheless, other studies have reported a remarkable increase in 3-NT expression in rat diabetic aortas (Obrosova et al., 2007, Taguchi et al., 2007). Indeed, Miao et al (2012) observed that the 3-NT content in diabetic aorta after 6-months of DM was less than that after 3-months of DM. Thus, it is possible that the level of aortic 3-NT was significantly elevated at some points during the present study, but it decreased towards the end of the study. It has been observed that acute hyperglycaemia represents a more specific inducer for oxidative stress than prolonged chronic hyperglycaemia (Monnier et al., 2006). Additionally, the proteolytic degradation of nitrated protein has been observed *in vivo* (Radi, 2004). Moreover, it is possible that hyperglycaemia-induced impairment of NO production affects the availability of NO for protein nitration (Koo and Vaziri, 2003).

Apart from being as a marker of oxidative/nitrosative damage, the presence of nitrated proteins, such as proteins with 3-NT residues, in tissue might reflect impairment in functional activity. Reduction of NO availability is one of the expected consequences. Moreover, posttranslational modification of tyrosine residue in proteins can alter some key enzyme activities, change the cytoskeleton, and impair cellular signalling (Radi, 2004). Importantly, it was shown that these nitrate epitopes activate the innate immune system by forming anti-nitrotyrosine antibodies (Thomson, 2015).

To summarize, evaluating the immunoreactivity to 3-NT in aorta tissue as a marker of oxidative/nitrosative stress in aorta tissue did not reveal significant differences between any of the treatment groups. However, the inability to demonstrate an increase in oxidative stress magnitude at the end of the study does not exclude the possibility of its contribution to DM development throughout this long-term diabetic study.

It is noteworthy to mention that this animal study has limitations because further investigation was not feasible due to limited availability of frozen tissue samples. Moreover, additional immunohistochemical analysis was unsuccessful, involving

probing the tissue with several antibodies - probably due to fixation problems. Finally, the low number of animals in the control group impaired statistical analysis in these experiments. Despite that, future studies could be directed towards examining the ultrastructural changes using EM where thickening of endothelial basement membrane or changes at the level of the endoplasmic reticulum might be investigated. Furthermore, analysis of blood samples, for instance for vWF, might further confirm or support the present findings.

Chapter 7. General discussion and future work

The cardiovascular complications in diabetes are very common resulting in a major impact on human health. C-peptide deficiency in diabetic people may contribute to the progression of diabetic vasculopathy (Morrish et al., 2001). My thesis hypothesised that physiologically-relevant concentrations of C-peptide are important for maintaining normal vascular function especially in the endothelium.

C-peptide signalling in the endothelium has been an active area of research during the last two decades. Numerous reports from HUVEC culture studies and animal studies have shown that C-peptide is an effective tool for improving the condition of the endothelium during exposure to various injurious stimuli: by increasing NO production, cell proliferation and angiogenesis while quenching oxidative stress, inflammation and pathological apoptosis as reviewed in (Wahren and Larsson, 2015).

An important scientific contribution has been made in this thesis by identifying EA.hy926 cells for the first time as a responsive endothelial cell line for C-peptide. C-peptide activates key signalling pathways in EA.hy926 cells such as eNOS (Section 4.2.7.1). Diminished NO production and bioavailability is a characteristic feature of vascular dysfunction in diabetes which leads to a wide spectrum of vascular pathologies. Moreover, C-peptide activates a pivotal signalling molecule in EA.hy926 cells i.e. ERK1/2 (Section 4.2.1). This signalling cascade regulates numerous intracellular physiological processes such as cell growth and survival, while this enhanced cellular activity may counteract endothelial senescence which is common in diabetic vasculature (Munoz-Espin and Serrano, 2014). Endothelium-derived NO, on the other hand, plays a critical role in downregulation of senescence pathways in high-glucose treated ECs (Hayashi et al., 2006).

More importantly, the reactivity of EA.hy926 cells with C-peptide will open new avenues for elucidating the fashion of C-peptide interaction with cell membranes. Investigating the C-peptide receptor and its downstream signals in ECs will be a justifiable approach; since ECs are the chief initiator for diabetic vascular complications. When ECs lose their integrity, all the other vascular compartments as well as the underlying tissues become

easily accessible for harmful agents such as high glucose (De Caterina et al., 2007b). An important feature of EA.hy926 cells is that they are HUVEC-derived ECs but, unlike HUVECs, they are not fastidious in growth and preserve the main characteristic features of ECs even after a high number of passages (Edgell et al., 1983). The C-peptide-sensitive EA.hy926 cells may assist in unveiling the identity of the endothelial C-peptide receptor and verifying the potential significance of C-peptide in vascular biology.

During this project, I refined MP analysis by FCM extensively, optimising it for small-scale experiments which was an important practical purpose of this study (Chapter 3). A current limitation in FCM of nanoparticles is the unavailability of dedicated nano-scale flow cytometers, because the fluidic and optical systems of commercial flow cytometers are optimised for analysing cells (Shapiro, 2005). By using these optimised settings for MPs, a moderate stimulatory effect for C-peptide on MP release from ECs was delineated (Section 4.2.5). Previous studies have demonstrated that release of MPs from injured ECs is an important defence mechanism for disposing of redundant intracellular molecules; whereas, silencing this machinery impairs EC survival (Abid Hussein et al., 2007). Interestingly, the effect of C-peptide on MP release was dampened by treating the cells with PTX (Section 4.2.5.4) suggesting that the C-peptide signalling pathway is $G_{i/o}$ protein-dependent.

Of note, when NTA analysis was used to study the effect of C-peptide on MP generation; it did not reveal a significant difference compared to unstimulated cells. It might be that C-peptide enhanced the formation of a certain subset of EMPs. NTA methodology can detect vesicular or non-vesicular particles in suspension without preferences; in addition, the size range of particles included in the analysis was between 100-1000nm which was wider than the size range examined by FCM (Gardiner et al., 2013). The main idea from setting an analysis window for FCM relying on beads was to standardise the measurement and ensure that the same MP subset was analysed each time. Analysing MPs by FCM requires working close to the detection limit of the instrument, while day to day variation in the performance of flow cytometers is very common and negatively impacts the data obtained (Robert et al., 2012). In addition, the scatter signal (whether SSC or FSC) collected by any flow cytometer is an arbitrary unit; thus synthetic calibration beads of known size are used to infer the size of particles in biological

samples (Erdbrugger et al., 2014). Calibrating the flow cytometer by this approach is debatable but unavoidable due to absence of alternatives (van der Pol et al., 2018). As a result, the size range of MPs determined by FCM in my study should be regarded as relative rather than absolute (further details are presented in Chapter 3).

After confirming the suitability of EA.hy926 cells for performing C-peptide studies, I sought to investigate the potential protective effect of C-peptide on endothelial dysfunction evoked by high glucose with respect to MP shedding (Chapter 5). Unfortunately, these cells did not show an obvious sign of endothelial injury, at least in terms of survival, as might be expected for immortalised cells (Xu et al., 2018). Glucose is an indispensable energy source especially for cells with high proliferative capacity. The protein content of EA.hy926 cell monolayer was significantly increased during exposure to high glucose up to 45mM for 72h (Section 5.2.1.4), whereas, the level of MPs in the experimental medium did not significantly change (Sections 5.2.1.1 and 5.2.1.3), suggesting that high glucose might even be improving EA.hy926 cells' tolerance to serum deprivation (Section 5.3.3) and hence decreasing MP release expressed per mg of cell layer protein. However, it is well acknowledged that such observed effects of high glucose on EA.hy926 cells affecting the monolayer protein content and MP release do not necessarily mean that high glucose does not injure these cells. Furthermore, one of the main objectives of this project was to study MP generation as a novel measure of endothelial function, while other topics such as high glucose-induced oxidative stress or apoptosis have been previously addressed elsewhere (Karbach et al., 2012). Other researchers in the MP field have also noticed EA.hy926 cell resistance to MP release when stimulated with high glucose (D. Burger, personal communication). Thus, further investigation of the potential modulatory effect of C-peptide on MP shedding elicited by high glucose was not conducted.

MPs are increasingly recognised as a means of intercellular communication, while their autocrine/paracrine actions depend on the specific stimulus which generates the particles (Burger et al., 2017). Therefore, an attempt was made in this study to investigate the potential functional significance of endothelial MPs generated under conditions of high glucose with or without C-peptide (Section 5.3.4). As reported previously (Bammert et al., 2017), high glucose-derived EMPs increased the apoptosis

level in naïve endothelial cultures as presented in Section 5.2.3.2. However, MPs derived from cells stimulated with high glucose along with C-peptide showed similar effect to that derived from high glucose only (Section 5.2.3.2). In addition, evaluation of the inflammatory status of ECs during exposure to EMPs was also performed. The expression of key adhesion molecules on the endothelial surface (ICAM-1 and E-selectin) as well as secretion of the chemokine IL-8 were examined. However, neither high glucose- nor C-peptide-derived MPs altered these parameters (Section 5.2.3.1). Proteomic analysis of high glucose and C-peptide MPs demonstrated selective packaging of biomolecules within these vesicles; albeit, whether these proteins were functionally active remains to be determined. Alternatively, the identified proteins might be discarded by the cells via vesicles as a protective stratagem (Zu et al., 2015). Further proteomic studies on C-peptide-stimulated MPs are warranted to verify the present finding by using different manoeuvres to improve the protein yield from MP samples.

I tested another model of vascular injury by stimulating ECs with high extracellular Pi concentration similar to that seen in CKD patients. Pi-induced endothelial dysfunction has been widely confirmed in earlier studies, while the stimulatory effect of Pi on MP release was demonstrated recently in two independent studies (Di Marco et al., 2013, Abbasian et al., 2015). Pi impaired EC survival after long-exposure and increased MP formation (Sections 5.2.4 and 5.2.5). However, co-stimulation of ECs with Pi and C-peptide did not rescue ECs (Section 5.2.5). Although Pi-provoked oxidative stress and apoptosis has been proposed as a causative factor for Pi-mediated MP release (Di Marco et al., 2013), this was not confirmed in a later study in which Pi-induced alterations in phosphorylation status of cellular proteins was implicated in MP detachment from the cell membrane (Abbasian et al., 2015). Consequently, C-peptide does not seem to influence this particular pathway of Pi-enhanced MP shedding.

At the molecular level, high Pi level accelerated the onset of ERK phosphorylation in EA.hy926 cells stimulated by C-peptide (Section 4.2.8). Pi alters the phosphorylation status of intracellular proteins by inhibiting phosphoprotein phosphatases (Abbasian et al., 2015). These protein modifications might be involved in the early outset of ERK activation observed in this study. Notably, some responses to C-peptide are more

marked in rodent models than in humans (Lim et al., 2015, Wahren et al., 2016). Unlike humans, the normal serum Pi in rodents is in the range of 2-2.5mM (Haut et al., 1980). The importance of these novel findings is at present unknown, though it merits further investigation. The enhanced sensitivity to C-peptide in hyperphosphataemic conditions may have physiological significance in humans with advanced CKD. In addition, the inverse relationship between obesity estimated by BMI, and serum Pi, has been widely demonstrated in previous clinical studies (Lind et al., 1993, Haap et al., 2006). Theoretically, blunting of C-peptide signalling by the relatively low Pi levels in such obese individuals may have physiological consequences.

Further experiments were performed to investigate whether co-stimulation of ECs with high Pi and high glucose imposes an extra burden on EC function: but on the contrary, it appeared that glucose ameliorated Pi-induced MP release and improved the protein level in the cell monolayer (Section 5.3.6). Pi was probably sequestered within the metabolic intermediates of the glycolytic pathway diminishing the intracellular Pi level (Cox, 2002), thereby preventing further damage to ECs from high cytosolic Pi. A similar finding was recorded in a previous study in which stimulation of the glycolytic pathway by fructose retarded Pi-mediated MP generation (Abbasian et al., 2015).

The *in vivo* investigation presented in Chapter 6 revealed novel observations. For the first time the effect of C-peptide on diabetic rat aorta was investigated. In general, the vast majority of C-peptide studies has focused on the potential modulatory effect of C-peptide on microvasculopathy associated with diabetes; whereas, scarce data are available regarding its effects on the macrovascular complications. Apparently, there is only a single study reported by Vasic et al (2012) investigating the effect of a supra-physiological concentration (~13nM) of C-peptide on aorta of a non-diabetic mouse model of atherosclerosis. In the present study, STZ-induced diabetes in rats resulted in upregulation of vWF in the aortic intima; though, C-peptide administration prevented diabetes-induced overexpression of vWF protein (Section 6.2.2). The circulatory system of diabetic people is prone to accelerated atherosclerotic and thrombotic accidents (Morrish et al., 2001). A key mediator of vascular thrombosis and inflammation is vWF, while its deposition on the vascular collagen in contact with the bloodstream initiates thrombotic events (De Meyer et al., 1999). It is plausible that enhanced NO production

by C-peptide treatment exerted an inhibitory effect on vWF protein expression observed in diabetic aortas.

Another important finding in this diabetic animal study was that C-peptide blunted collagen deposition in the diabetic vascular wall (Section 6.3.3). Collagen is an abundant ECM protein, whilst its accumulation leads to ECM remodelling (Ban and Twigg, 2008). Increased collagen content in the aortic wall promotes vascular stiffness and potentially increases the incidence of cardiovascular diseases (Intengan and Schiffrin, 2001). (However, limitations of this animal study are presented in detail in the relevant chapter discussion).

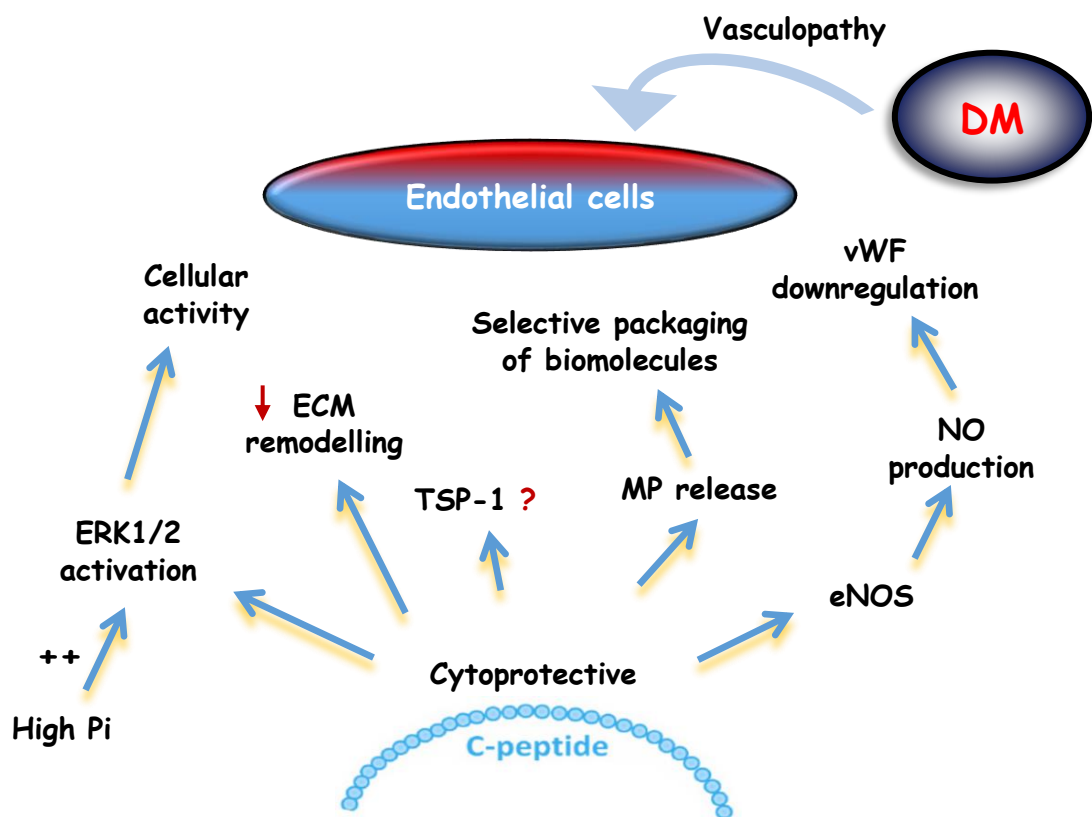


Figure 7.1 Schematic illustration of the mechanisms by which C-peptide modulates the biological activities in ECs. The available evidence is compatible with the hypothesis that C-peptide has cytoprotective effects via enhancing the expression of eNOS protein and possibly increasing NO production which downregulates vWF protein expression. There is also stimulation of the MAPK signalling pathway, resulting in augmented cellular activity while high Pi appears to enhance some C-peptide actions in ECs. In addition, ECM remodelling is inhibited, and TSP-1 expression is increased. C-peptide also elicits a moderate effect on MP generation from ECs suggesting a role for this peptide in cell-cell communication.

In summary, the findings presented in this thesis highlight the role of C-peptide as an active player in vascular biology and are shown in schematic form in Figure 7.1. C-peptide replacement in deficient people may therefore potentially restore normal EC function impaired by various injurious agents.

Future studies can be directed towards:

- Repeating the key observations from this project using other cultured endothelial models e.g. HUVECs or arterial EC models.
- Further characterisation of the functional properties of C-peptide-derived MPs by investigating potential modulation of signalling pathways or assessing EC function using different sets of markers.
- Characterisation of the molecular cargo within C-peptide-induced MPs especially the miRNA profile of these vesicles.
- Applying new approaches for MP isolation, purification or probably fractionation for LC-MS/MS analysis.
- Investigating the binding kinetics of C-peptide in EA.hy926 by using labelled C-peptide, or by overexpressing the candidate C-peptide receptor GPR146 to examine the resulting effect on (for example) eNOS or TSP-1 expression.

Appendix

Table of proteomics analysis (LC-MS/MS) of MPs derived from C-peptide- and glucose-treated EAhy926. Presence versus absence of particular protein is presented as analysed by Scaffold. Individual proteins within a cluster are not shown.

No.	Identified Proteins	Accession Number (Homo sapiens)	M. Wt.	Presence/Absence		
				Control MPs	C-peptide MPs	Glucose MPs
1	1,4-alpha-glucan-branching enzyme	Q04446	80 kDa	x	x	
2	4F2 cell-surface antigen heavy chain	F5GZS6	65 kDa	x	x	x
3	5'-nucleotidase	P21589	63 kDa	x	x	x
4	6-phosphogluconate dehydrogenase, decarboxylating	P52209	53 kDa	x	x	x
5	10 kDa heat shock protein, mitochondrial	P61604	11 kDa	x	x	x
6	Cluster of 14-3-3 protein zeta/delta	P63104	28 kDa	x	x	x
7	26S protease regulatory subunit 4	P62191	49 kDa			x
8	26S protease regulatory subunit 6A	E9PM69	44 kDa	x	x	x
9	26S protease regulatory subunit 7	P35998	49 kDa		x	
10	Cluster of 26S protease regulatory subunit 10B	A0A087X2I1	46 kDa	x	x	x
11	26S proteasome non-ATPase regulatory subunit 1	Q99460	106 kDa	x	x	x
12	26S proteasome non-ATPase regulatory subunit 2	Q13200	100 kDa	x	x	x
13	26S proteasome non-ATPase regulatory subunit 3	O43242	61 kDa	x	x	x
14	26S proteasome non-ATPase regulatory subunit 6	Q15008	46 kDa			x
15	26S proteasome non-ATPase regulatory subunit 11	O00231	47 kDa	x	x	x
16	26S proteasome non-ATPase regulatory subunit 13	A0A087WUL9	43 kDa	x		x
17	40S ribosomal protein S2 (Fragment)	H0YEN5	21 kDa	x	x	x
18	40S ribosomal protein S3	P23396	27 kDa	x	x	x
19	40S ribosomal protein S3a	P61247	30 kDa	x	x	x
20	40S ribosomal protein S4, X isoform	P62701	30 kDa	x	x	x
21	40S ribosomal protein S5 (Fragment)	M0R0F0	22 kDa	x	x	x
22	40S ribosomal protein S6	P62753	29 kDa	x	x	x
23	40S ribosomal protein S7	P62081	22 kDa	x	x	x
24	40S ribosomal protein S8	P62241	24 kDa	x	x	x
25	40S ribosomal protein S9	A0A024R4M0	23 kDa	x		
26	40S ribosomal protein S10	F6U211	20 kDa	x		
27	40S ribosomal protein S11	P62280	18 kDa	x		
28	40S ribosomal protein S12	P25398	15 kDa	x	x	x
29	40S ribosomal protein S13	P62277	17 kDa	x	x	x
30	40S ribosomal protein S14	P62263	16 kDa	x	x	x
31	40S ribosomal protein S15a	I3L3P7	11 kDa	x	x	x
32	40S ribosomal protein S16	M0R210	14 kDa	x	x	x
33	40S ribosomal protein S17	P08708	16 kDa	x	x	x
34	40S ribosomal protein S18	P62269	18 kDa	x	x	x

35	40S ribosomal protein S19	P39019	16 kDa	x		
36	40S ribosomal protein S20	P60866	13 kDa	x	x	x
37	40S ribosomal protein S23	P62266	16 kDa	x	x	x
38	40S ribosomal protein S24	A0A087WUS0	15 kDa	x	x	x
39	40S ribosomal protein S25	P62851	14 kDa	x		
40	40S ribosomal protein SA	A0A0C4DG17	33 kDa	x	x	x
41	60 kDa heat shock protein, mitochondrial	P10809	61 kDa	x	x	x
42	60S acidic ribosomal protein P0 (Fragment)	F8VU65	27 kDa	x	x	x
43	Cluster of 60S acidic ribosomal protein P1	P05386	12 kDa	x		x
44	60S ribosomal protein L3	P39023	46 kDa	x	x	x
45	60S ribosomal protein L4	P36578	48 kDa	x	x	x
46	60S ribosomal protein L5	P46777	34 kDa	x	x	x
47	60S ribosomal protein L6	Q02878	33 kDa	x		x
48	60S ribosomal protein L7	P18124	29 kDa	x	x	x
49	60S ribosomal protein L7a	P62424	30 kDa	x	x	x
50	60S ribosomal protein L8	P62917	28 kDa	x	x	x
51	60S ribosomal protein L10	P27635	25 kDa	x	x	
52	60S ribosomal protein L11	P62913	20 kDa	x	x	x
53	60S ribosomal protein L12	P30050	18 kDa	x	x	x
54	60S ribosomal protein L13	P26373	24 kDa	x	x	
55	60S ribosomal protein L13a (Fragment)	M0QYS1	24 kDa	x	x	
56	60S ribosomal protein L14	E7EPB3	15 kDa	x	x	x
57	60S ribosomal protein L15	P61313	24 kDa		x	x
58	60S ribosomal protein L17 (Fragment)	A0A087WXM6	20 kDa	x	x	x
59	60S ribosomal protein L18 (Fragment)	F8VUA6	15 kDa	x		
60	60S ribosomal protein L18a	M0R117	18 kDa	x	x	x
61	60S ribosomal protein L21	P46778	19 kDa	x		
62	60S ribosomal protein L22	P35268	15 kDa	x	x	x
63	60S ribosomal protein L23	P62829	15 kDa	x		x
64	60S ribosomal protein L23a	P62750	18 kDa	x	x	x
65	60S ribosomal protein L24	C9JNW5	18 kDa	x		
66	60S ribosomal protein L26	P61254	17 kDa	x	x	
67	60S ribosomal protein L27	P61353	16 kDa	x		
68	60S ribosomal protein L27a	E9PLL6	12 kDa	x	x	
69	60S ribosomal protein L30 (Fragment)	E5RI99	13 kDa	x		
70	72 kDa type IV collagenase	P08253	74 kDa	x	x	x
71	78 kDa glucose-regulated protein	P11021	72 kDa	x	x	x
72	116 kDa U5 small nuclear ribonucleoprotein component	Q15029	109 kDa	x	x	x
73	Cluster of ADP-ribosylation factor 3	P61204	21 kDa	x	x	x
74	Cluster of ADP/ATP translocase 2	P05141	33 kDa	x	x	x
75	AP-2 complex subunit alpha-1	O95782	108 kDa	x		
76	ATP synthase subunit alpha, mitochondrial	P25705	60 kDa	x	x	x
77	ATP synthase subunit beta, mitochondrial	P06576	57 kDa	x	x	x
78	ATP synthase subunit gamma, mitochondrial	P36542	33 kDa	x	x	

79	ATP-citrate synthase	P53396	121 kDa	x	x	x
80	Cluster of ATP-dependent 6-phosphofructokinase, platelet type	Q01813	86 kDa	x	x	x
81	ATP-dependent DNA helicase Q1	P46063	73 kDa	x	x	x
82	ATP-dependent RNA helicase A	Q08211	141 kDa	x	x	x
83	ATP-dependent RNA helicase DDX3X	A0A0D9SF53	81 kDa	x	x	x
84	Cluster of ATP-dependent RNA helicase DDX39A	O00148	49 kDa	x	x	x
85	Acetyl-CoA acetyltransferase, mitochondrial	P24752	45 kDa	x	x	
86	Actin-related protein 2/3 complex subunit 2	O15144	34 kDa		x	
87	Actin-related protein 3	P61158	47 kDa	x	x	x
88	Adenosylhomocysteinase	P23526	48 kDa	x	x	x
89	Adenylate kinase isoenzyme 1	P00568	22 kDa		x	
90	Adenylyl cyclase-associated protein 1	Q01518	52 kDa	x	x	x
91	Cluster of Adipocyte plasma membrane-associated protein	Q9HDC9	46 kDa	x	x	x
92	Alanine--tRNA ligase, cytoplasmic	P49588	107 kDa	x	x	x
93	Aldose reductase	E9PCX2	29 kDa	x		x
94	Alpha-2-HS-glycoprotein	P02765	39 kDa	x	x	x
95	Cluster of Alpha-actinin-4	O43707	105 kDa	x	x	x
96	Alpha-centractin	P61163	43 kDa	x	x	x
97	Cluster of Alpha-enolase	P06733	47 kDa	x	x	x
98	Alpha-fetoprotein	P02771	69 kDa			x
99	Aminopeptidase N	P15144	110 kDa	x	x	x
100	Amyloid beta A4 protein	P05067	87 kDa	x	x	x
101	Amyloid-like protein 2	Q06481	87 kDa			x
102	Annexin A1	P04083	39 kDa	x	x	x
103	Annexin A2	P07355	39 kDa	x	x	x
104	Annexin A4	P09525	36 kDa	x	x	x
105	Annexin A5	P08758	36 kDa	x	x	x
106	Cluster of Annexin A6	P08133	76 kDa	x	x	
107	Annexin A11	P50995	54 kDa	x	x	x
108	Anoctamin-6	Q4KMQ2	106 kDa		x	
109	Archain 1, isoform CRA_a	B0YIW6	62 kDa	x	x	
110	Arginine--tRNA ligase, cytoplasmic	P54136	75 kDa	x	x	x
111	Aspartate aminotransferase, mitochondrial	P00505	48 kDa	x	x	x
112	Aspartate--tRNA ligase, cytoplasmic	P14868	57 kDa	x	x	x
113	Aspartyl/asparaginyl beta-hydroxylase	Q12797	86 kDa	x		x
114	Cluster of Basement membrane-specific heparan sulfate proteoglycan core protein	P98160	469 kDa	x	x	x
115	Basigin (Fragment)	A0A087X2B5	24 kDa	x	x	x
116	Beta-2-microglobulin	P61769	14 kDa	x		
117	Cluster of Beta-actin-like protein 2	Q562R1 [4]	42 kDa	x	x	x
118	Brain acid soluble protein 1	P80723	23 kDa	x	x	x
119	C-1-tetrahydrofolate synthase, cytoplasmic	F5H2F4	111 kDa	x	x	x
120	CD44 antigen	H0YD13	23 kDa	x	x	x
121	CD59 glycoprotein	E9PNW4	12 kDa	x	x	x

122	CD63 antigen (Fragment)	F8VNT9	14 kDa	x		
123	CD109 antigen	Q6YHK3	162 kDa	x	x	x
124	Calnexin	P27824	68 kDa	x	x	x
125	Calpain-1 catalytic subunit	P07384	82 kDa	x	x	x
126	Calpain-2 catalytic subunit	P17655	80 kDa	x	x	x
127	Calreticulin	P27797	48 kDa	x	x	x
128	Calumenin	O43852	37 kDa	x	x	x
129	Capping protein (Actin filament) muscle Z-line, beta, isoform CRA_a	B1AK87	29 kDa	x	x	x
130	Cluster of Carbonyl reductase [NADPH] 1	P16152	30 kDa	x	x	x
131	Casein kinase II subunit alpha	E7EU96	45 kDa	x	x	x
132	Catenin (Cadherin-associated protein), alpha 1, 102kDa, isoform CRA_a	G3XAM7	93 kDa	x	x	x
133	Cathepsin B	P07858	38 kDa	x	x	x
134	Caveolin-1	Q03135	20 kDa	x	x	x
135	Cell division control protein 42 homolog	P60953	21 kDa	x	x	x
136	Charged multivesicular body protein 4b	Q9H444	25 kDa	x		
137	Chloride intracellular channel protein 1	O00299	27 kDa	x	x	x
138	Chloride intracellular channel protein 4	Q9Y696	29 kDa	x	x	x
139	Chromobox protein homolog 3	Q13185	21 kDa	x		
140	Citrate synthase	B4DJV2	50 kDa	x	x	x
141	Cluster of Clathrin heavy chain	A0A087WVQ6 [3]	192 kDa	x	x	x
142	Cluster of Clusterin	P10909	52 kDa	x	x	x
143	Coatomer subunit alpha	P53621	138 kDa	x	x	x
144	Coatomer subunit beta	P53618	107 kDa	x		
145	Cluster of Coatomer subunit gamma-1	Q9Y678	98 kDa	x	x	x
146	Cluster of Cofilin-1	P23528 [2]	19 kDa	x	x	x
147	Coiled-coil domain-containing protein 80	Q76M96	108 kDa	x	x	x
148	Collagen alpha-1(VIII) chain	P27658	73 kDa	x	x	x
149	Collagen alpha-1(XVIII) chain	P39060	178 kDa	x	x	x
150	Complement component 1 Q subcomponent-binding protein, mitochondrial	Q07021	31 kDa	x	x	x
151	Copine-1	A6PVH9	53 kDa	x	x	x
152	Cluster of Copine-2	Q96FN4 [2]	61 kDa	x	x	x
153	Core histone macro-H2A.1	O75367	40 kDa	x	x	
154	Coronin-1C	Q9ULV4	53 kDa	x	x	x
155	Cullin 4B, isoform CRA_e	K4DI93	103 kDa	x		x
156	Cystatin-C	P01034	16 kDa	x	x	x
157	Cluster of Cystatin-SN	P01037	16 kDa	x	x	x
158	Cysteine-rich protein 2 (Fragment)	H0YFA4	21 kDa	x	x	x
159	Cluster of Cytochrome b-c1 complex subunit 2, mitochondrial	H3BRG4 [2]	45 kDa	x		
160	Cytochrome c1, heme protein, mitochondrial	P08574	35 kDa	x		
161	Cytochrome c oxidase subunit 2	P00403	26 kDa	x		
162	Cytoplasmic FMR1-interacting protein 1	Q7L576	145 kDa	x		
163	Cytoplasmic dynein 1 heavy chain 1	Q14204	532 kDa	x		x

164	Cytoskeleton-associated protein 4	Q07065	66 kDa	x	x	x
165	Cytosolic acyl coenzyme A thioester hydrolase	O00154	42 kDa		x	
166	D-3-phosphoglycerate dehydrogenase	O43175	57 kDa	x		
167	DNA replication licensing factor MCM7	P33993	81 kDa		x	
168	DNA-dependent protein kinase catalytic subunit	P78527	469 kDa	x	x	
169	Destrin	F6RFD5	15 kDa		x	x
170	Dihydropyrimidinase-related protein 2	A0A1C7CYX9	74 kDa	x	x	x
171	Dihydropyrimidinase-related protein 3	Q14195	62 kDa	x	x	x
172	Dipeptidyl peptidase 1 (Fragment)	H0YCY8	28 kDa	x	x	x
173	DnaJ homolog subfamily A member 1	P31689	45 kDa	x		
174	DnaJ homolog subfamily B member 11	Q9UBS4	41 kDa			x
175	Dolichyl-diphosphooligosaccharide--protein glycosyltransferase 48 kDa subunit	A0A0C4DGS1	49 kDa	x	x	x
176	Dolichyl-diphosphooligosaccharide--protein glycosyltransferase subunit 1	P04843	69 kDa	x	x	x
177	Dolichyl-diphosphooligosaccharide--protein glycosyltransferase subunit 2	P04844	69 kDa	x	x	x
178	Cluster of Dual specificity mitogen-activated protein kinase kinase 2	P36507	44 kDa	x		
179	Dynamamin-1-like protein	G8JLD5	80 kDa	x	x	x
180	Dysferlin	O75923	237 kDa	x	x	x
181	EGF-containing fibulin-like extracellular matrix protein 1	Q12805	55 kDa	x	x	x
182	EGF-like repeat and discoidin I-like domain-containing protein 3	O43854	54 kDa	x	x	x
183	Cluster of EH domain-containing protein 1	A0A024R571	62 kDa	x	x	x
184	EH domain-containing protein 2	Q9NZN4	61 kDa	x	x	x
185	EH domain-containing protein 4	Q9H223	61 kDa	x	x	x
186	ELAV-like protein 1	Q15717	36 kDa	x		
187	ERO1-like protein alpha	Q96HE7	54 kDa	x	x	x
188	Elongation factor 1-alpha 1	P68104	50 kDa	x	x	x
189	Cluster of Elongation factor 1-delta	E9PRY8	77 kDa	x	x	x
190	Elongation factor 1-gamma	P26641	50 kDa	x	x	x
191	Elongation factor 2	P13639	95 kDa	x	x	x
192	Elongation factor Tu, mitochondrial	P49411	50 kDa	x	x	x
193	Endoglin	P17813	71 kDa	x	x	x
194	Endoplasmic reticulum resident protein 29	P30040	29 kDa	x	x	
195	Endoplasmin	P14625	92 kDa	x	x	x
196	Endothelial protein C receptor	Q9UNN8	27 kDa			x
197	Endothelin-converting enzyme 1	P42892	87 kDa	x	x	x
198	Enoyl-CoA hydratase, mitochondrial	P30084	31 kDa	x	x	x
199	Cluster of Ephrin type-A receptor 2	P29317	108 kDa	x	x	x
200	Cluster of Epididymis luminal protein 189	Q5HYB6 [2]	27 kDa	x	x	x
201	Erythrocyte band 7 integral membrane protein	P27105	32 kDa	x	x	x
202	Cluster of Eukaryotic initiation factor 4A-I	P60842	46 kDa	x	x	x
203	Eukaryotic initiation factor 4A-III	P38919	47 kDa	x	x	x
204	Eukaryotic translation initiation factor 2 subunit 1	P05198	36 kDa	x	x	x
205	Eukaryotic translation initiation factor 2 subunit 3	P41091	51 kDa	x	x	x

206	Eukaryotic translation initiation factor 3 subunit E	P60228	52 kDa			x
207	Eukaryotic translation initiation factor 3 subunit L	Q9Y262	67 kDa		x	
208	Eukaryotic translation initiation factor 3 subunit M	Q7L2H7	43 kDa	x		
209	Eukaryotic translation initiation factor 5A (Fragment)	I3L397	16 kDa	x	x	x
210	Eukaryotic translation initiation factor 6	P56537	27 kDa	x	x	x
211	Exportin-2	P55060	110 kDa	x	x	
212	Extended synaptotagmin-1	Q9BSJ8	123 kDa	x		
213	F-actin-capping protein subunit alpha-1	P52907	33 kDa	x	x	x
214	FACT complex subunit SSRP1	Q08945	81 kDa			x
215	Fascin	Q16658	55 kDa	x	x	x
216	Fibronectin	P02751	263 kDa	x	x	x
217	Cluster of Filamin-A	P21333 [4]	281 kDa	x	x	x
218	Follistatin-related protein 1	Q12841	35 kDa	x	x	x
219	Cluster of Fructose-bisphosphate aldolase A	P04075 [2]	39 kDa	x	x	x
220	GTP-binding nuclear protein Ran	B5MDF5	26 kDa	x	x	x
221	Galectin-1	P09382	15 kDa	x	x	x
222	Galectin-3	P17931	26 kDa	x		
223	Gap junction alpha-1 protein	P17302	43 kDa	x	x	x
224	Gelsolin	A0A0A0MS51	83 kDa	x	x	x
225	Glia-derived nexin	P07093	44 kDa	x	x	x
226	Glucose-6-phosphate 1-dehydrogenase	P11413	59 kDa	x	x	x
227	Glucose-6-phosphate isomerase (Fragment)	A0A0A0MTS2	65 kDa	x	x	x
228	Glucosidase 2 subunit beta	K7ELL7	60 kDa	x	x	x
229	Cluster of Glutamate dehydrogenase 1, mitochondrial	P00367	61 kDa	x	x	x
230	Glutathione S-transferase P	P09211	23 kDa	x	x	x
231	Glutathione S-transferase omega-1	P78417	28 kDa	x	x	
232	Glyceraldehyde-3-phosphate dehydrogenase	P04406	36 kDa	x	x	x
233	Glycine--tRNA ligase	P41250	83 kDa	x	x	x
234	Glycogen phosphorylase, brain form	P11216	97 kDa	x	x	
235	Granulins (Fragment)	K7EQI0	12 kDa	x		
236	Growth/differentiation factor 15	Q99988	34 kDa	x	x	x
237	Cluster of Guanine nucleotide-binding protein G(I)/G(S)/G(T) subunit beta-1	P62873 [2]	37 kDa	x	x	x
238	Cluster of Guanine nucleotide-binding protein G(i) subunit alpha-2	P04899 [3]	40 kDa	x	x	x
239	Cluster of Guanine nucleotide-binding protein subunit alpha-11	P29992	42 kDa		x	x
240	Cluster of HLA class I histocompatibility antigen, A-24 alpha chain	P05534 [2]	41 kDa	x	x	x
241	Heat shock 70 kDa protein 4	P34932	94 kDa	x	x	x
242	Cluster of Heat shock cognate 71 kDa protein	P11142 [6]	71 kDa	x	x	x
243	Heat shock protein 75 kDa, mitochondrial	I3L0K7	57 kDa	x		
244	Heat shock protein 105 kDa	Q92598	97 kDa	x	x	x
245	Cluster of Heat shock protein HSP 90-alpha	P07900 [4]	85 kDa	x	x	x
246	Heat shock protein beta-1	P04792	23 kDa	x	x	x
247	Heme-binding protein 1	Q9NRV9	21 kDa			x

248	Hemoglobin subunit alpha	P69905	15 kDa	x	x	x
249	Cluster of Heterogeneous nuclear ribonucleoprotein A1	F8W6I7 [2]	33 kDa	x	x	x
250	Heterogeneous nuclear ribonucleoprotein A3	P51991	40 kDa	x	x	x
251	Heterogeneous nuclear ribonucleoprotein A/B	D6R9P3	30 kDa	x	x	
252	Cluster of Heterogeneous nuclear ribonucleoprotein D0	Q14103	38 kDa	x	x	x
253	Heterogeneous nuclear ribonucleoprotein F	P52597	46 kDa	x	x	x
254	Cluster of Heterogeneous nuclear ribonucleoprotein H2	P55795 [2]	49 kDa	x	x	x
255	Heterogeneous nuclear ribonucleoprotein H3	P31942	37 kDa	x	x	x
256	Heterogeneous nuclear ribonucleoprotein K	P61978	51 kDa	x	x	x
257	Cluster of Heterogeneous nuclear ribonucleoprotein L (Fragment)	M0QXS5 [2]	58 kDa	x	x	x
258	Cluster of Heterogeneous nuclear ribonucleoprotein M	A0A087X0X3	78 kDa	x	x	x
259	Heterogeneous nuclear ribonucleoprotein Q	O60506	70 kDa	x	x	x
260	Heterogeneous nuclear ribonucleoprotein R	O43390	71 kDa	x	x	x
261	Heterogeneous nuclear ribonucleoprotein U	Q00839	91 kDa	x	x	x
262	Heterogeneous nuclear ribonucleoproteins A2/B1	P22626	37 kDa	x	x	x
263	Heterogeneous nuclear ribonucleoproteins C1/C2	B2R5W2	32 kDa	x	x	x
264	Hexokinase-1	P19367	102 kDa	x	x	
265	Cluster of High mobility group protein B1	P09429 [2]	25 kDa	x		
266	Histidine triad nucleotide-binding protein 1	P49773	14 kDa	x		
267	Cluster of Histone H1.2	P16403	21 kDa	x	x	x
268	Cluster of Histone H2A	A0A0U1RR32	18 kDa	x	x	x
269	Histone H2A.Z	P0C0S5	14 kDa	x	x	
270	Cluster of Histone H2B type 1-D	P58876 [11]	14 kDa	x	x	x
271	Cluster of Histone H3 (Fragment)	K7EK07 [6]	15 kDa	x	x	x
272	Histone H4	P62805	11 kDa	x	x	x
273	Hornerin	Q86YZ3	282 kDa		x	x
274	Hsc70-interacting protein	P50502	41 kDa	x	x	x
275	Hsp90 co-chaperone Cdc37	Q16543	44 kDa			x
276	Hypoxia up-regulated protein 1	A0A087X054	105 kDa	x	x	x
277	Importin subunit beta-1	Q14974	97 kDa	x	x	x
278	Inhibitor of nuclear factor kappa-B kinase-interacting protein	Q70UQ0	39 kDa	x		x
279	Cluster of Insulin-like growth factor 2 mRNA-binding protein 3	O00425	64 kDa	x	x	x
280	Insulin-like growth factor-binding protein 7	Q16270	29 kDa	x	x	x
281	Cluster of Integrin alpha-2	P17301 [2]	129 kDa	x	x	x
282	Integrin alpha-3	P26006	117 kDa	x	x	x
283	Integrin alpha-5	P08648	115 kDa	x	x	x
284	Integrin alpha-V	P06756	116 kDa	x	x	x
285	Integrin beta-1	P05556	88 kDa	x	x	x
286	Inter-alpha-trypsin inhibitor heavy chain H2	P19823	106 kDa	x	x	
287	Interleukin enhancer-binding factor 2	B4DY09	39 kDa	x	x	x
288	Interleukin enhancer-binding factor 3	Q12906	95 kDa	x	x	x
289	Interstitial collagenase	P03956	54 kDa	x	x	x
290	Keratin, type I cytoskeletal 9	P35527	62 kDa	x	x	x
291	Cluster of Keratin, type I cytoskeletal 10	P13645 [4]	59 kDa	x	x	x

292	Cluster of Keratin, type I cytoskeletal 13	P13646 [2]	50 kDa			x
293	Cluster of Keratin, type I cytoskeletal 18	P05783	48 kDa	x	x	x
294	Keratin, type II cytoskeletal 1	P04264	66 kDa	x	x	x
295	Cluster of Keratin, type II cytoskeletal 2 epidermal	P35908 [5]	65 kDa	x	x	x
296	Keratin, type II cytoskeletal 4	P19013	57 kDa			x
297	Cluster of Keratin, type II cytoskeletal 8	P05787	54 kDa	x	x	x
298	Kinesin-1 heavy chain	P33176	110 kDa	x		
299	Cluster of L-lactate dehydrogenase A chain	P00338 [2]	37 kDa	x	x	x
300	Lactadherin	Q08431	43 kDa	x	x	x
301	Lactotransferrin (Fragment)	E7EQB2	77 kDa	x		x
302	Lamin-B1	P20700	66 kDa	x	x	x
303	Lamin-B2	Q03252	70 kDa	x	x	
304	Laminin subunit alpha-4	A0A0A0MQS9	203 kDa		x	x
305	Laminin subunit beta-1	G3XA12	200 kDa	x	x	x
306	Laminin subunit gamma-1	P11047	178 kDa	x	x	x
307	Latent-transforming growth factor beta-binding protein 2	G3V3X5	190 kDa	x	x	x
308	Leucine--tRNA ligase, cytoplasmic	Q9P2J5	134 kDa	x		
309	Leucine-rich repeat-containing protein 59	Q96AG4	35 kDa	x	x	x
310	Leukocyte surface antigen CD47	Q08722	35 kDa	x	x	x
311	Long-chain-fatty-acid--CoA ligase 4	O60488	79 kDa	x	x	x
312	Lysine--tRNA ligase	Q15046	68 kDa		x	
313	Lysosomal protective protein	P10619	54 kDa	x	x	x
314	Lysosome-associated membrane glycoprotein 1	P11279	45 kDa	x	x	x
315	Lysosome-associated membrane glycoprotein 2	P13473	45 kDa	x	x	x
316	Major prion protein (Fragment)	A2A2V1	27 kDa	x	x	x
317	Major vault protein	Q14764	99 kDa	x	x	x
318	Malate dehydrogenase, cytoplasmic	B8ZZ51	19 kDa	x	x	x
319	Malate dehydrogenase, mitochondrial	P40926	36 kDa	x	x	x
320	Matrin-3	A0A0R4J2E8	95 kDa	x	x	x
321	Metalloproteinase inhibitor 1	P01033	23 kDa	x	x	x
322	Metalloproteinase inhibitor 2	P16035	24 kDa	x	x	x
323	Midkine	E9PLM6	17 kDa	x		x
324	Minor histocompatibility antigen H13	Q8TCT9	41 kDa	x		
325	Mitochondrial import receptor subunit TOM70	O94826	67 kDa		x	x
326	Cluster of Moesin	P26038 [4]	68 kDa	x	x	x
327	Monocarboxylate transporter 1	P53985	54 kDa		x	
328	Multifunctional protein ADE2	P22234	47 kDa	x	x	x
329	Myeloid-associated differentiation marker (Fragment)	C9J5M0	26 kDa	x		
330	Myoferlin	Q9NZM1	235 kDa	x	x	x
331	Myosin light polypeptide 6	B7Z6Z4	27 kDa	x	x	x
332	Myosin regulatory light chain 12A	J3QRS3	20 kDa	x	x	x
333	Cluster of Myosin-9	P35579 [2]	227 kDa	x	x	x
334	Myristoylated alanine-rich C-kinase substrate	P29966	32 kDa	x	x	x
335	NAD(P)H dehydrogenase [quinone] 1	B4DLR8	23 kDa	x	x	x

336	NADH-cytochrome b5 reductase 3	P00387	34 kDa	x	x	x
337	Nascent polypeptide-associated complex subunit alpha, muscle-specific form	E9PAV3	205 kDa	x	x	x
338	Neprilysin	P08473	86 kDa	x	x	x
339	Neuroblast differentiation-associated protein AHNAK	Q09666	629 kDa	x	x	x
340	Neutral alpha-glucosidase AB	Q14697	107 kDa	x	x	x
341	Neutral cholesterol ester hydrolase 1	A0A0A0MTJ9	50 kDa	x	x	x
342	Niban-like protein 1	Q96TA1	84 kDa	x	x	x
343	Noggin	Q13253	26 kDa	x		
344	Cluster of Non-POU domain-containing octamer-binding protein	Q15233	54 kDa	x	x	x
345	Cluster of Nucleobindin 2, isoform CRA_b	A0A087WSV8	50 kDa	x		
346	Nucleobindin-1	Q02818	54 kDa	x	x	x
347	Nucleolar protein 56	O00567	66 kDa	x	x	
348	Nucleolar protein 58	Q9Y2X3	60 kDa		x	
349	Nucleolin	P19338	77 kDa	x	x	x
350	Nucleophosmin	P06748	33 kDa	x	x	x
351	Cluster of Nucleoside diphosphate kinase	Q32Q12	33 kDa	x	x	x
352	Nucleosome assembly protein 1-like 1	F5H4R6	45 kDa	x	x	x
353	Nucleosome assembly protein 1-like 4	Q99733	43 kDa	x	x	x
354	PRA1 family protein 3	O75915	22 kDa	x		
355	Pentraxin-related protein PTX3	P26022	42 kDa	x	x	x
356	Cluster of Peptidyl-glycine alpha-amidating monooxygenase	P19021	108 kDa	x	x	x
357	Peptidyl-prolyl cis-trans isomerase A	P62937	18 kDa	x	x	x
358	Peptidyl-prolyl cis-trans isomerase B	P23284	24 kDa	x	x	x
359	Peptidyl-prolyl cis-trans isomerase FKBP1A	P62942	12 kDa	x	x	x
360	Peptidyl-prolyl cis-trans isomerase FKBP4	Q02790	52 kDa	x	x	x
361	Peroxiredoxin-1	Q06830	22 kDa	x	x	x
362	Peroxiredoxin-4	Q13162	31 kDa	x	x	x
363	Peroxiredoxin-5, mitochondrial	P30044	22 kDa	x	x	x
364	Peroxiredoxin-6	P30041	25 kDa	x	x	x
365	Peroxisomal multifunctional enzyme type 2	E7EWE5	78 kDa	x		
366	Cluster of Phosphate carrier protein, mitochondrial	F8VVM2	36 kDa	x	x	x
367	Phosphatidylethanolamine-binding protein 1	P30086	21 kDa	x		
368	Phosphoglycerate kinase 1	P00558	45 kDa	x	x	x
369	Phosphoglycerate mutase 1	P18669	29 kDa	x	x	x
370	Phospholipid transfer protein	P55058	55 kDa	x	x	x
371	Plasminogen activator inhibitor 1	P05121	45 kDa	x	x	x
372	Plasminogen activator inhibitor 1 RNA-binding protein	Q8NC51	45 kDa		x	
373	Cluster of Plastin-3	P13797	71 kDa	x	x	x
374	Platelet endothelial cell adhesion molecule	P16284	83 kDa		x	
375	Platelet-activating factor acetylhydrolase IB subunit beta	P68402	26 kDa		x	
376	Cluster of Plectin	Q15149	532 kDa	x	x	x
377	Podocalyxin	O00592	59 kDa	x	x	x
378	Poliovirus receptor	A0A0A0MSA9	43 kDa	x		

379	Cluster of Poly(rC)-binding protein 2 (Fragment)	F8VXH9 [5]	17 kDa	x	x	x
380	Polyadenylate-binding protein 2	Q86U42	33 kDa	x		
381	Cluster of Polyadenylate-binding protein	A0A087WTT1	59 kDa	x	x	x
382	Polymerase I and transcript release factor	Q6NZI2	43 kDa	x	x	x
383	Polypyrimidine tract-binding protein 1	A0A0U1RRM4	62 kDa	x	x	x
384	Pre-mRNA-splicing factor ATP-dependent RNA helicase DHX15	O43143	91 kDa	x	x	
385	Cluster of Prelamin-A/C	P02545 [2]	74 kDa	x	x	x
386	Preylcysteine oxidase 1	Q9UHG3	57 kDa		x	
387	Cluster of Probable ATP-dependent RNA helicase DDX5	J3KTA4 [3]	69 kDa	x	x	x
388	Procollagen galactosyltransferase 1	Q8NBJ5	72 kDa	x		
389	Procollagen-lysine,2-oxoglutarate 5-dioxygenase 1	Q02809	84 kDa	x	x	x
390	Cluster of Procollagen-lysine,2-oxoglutarate 5-dioxygenase 2	O00469 [2]	85 kDa	x	x	x
391	Cluster of Profilin-1	P07737	15 kDa	x	x	x
392	Programmed cell death 6-interacting protein	Q8WUM4	96 kDa	x	x	x
393	Programmed cell death protein 6	O75340	22 kDa	x	x	x
394	Prohibitin	P35232	30 kDa	x	x	x
395	Prohibitin-2	J3KPX7	33 kDa	x	x	x
396	Prolactin-inducible protein	P12273	17 kDa	x		
397	Proliferating cell nuclear antigen	P12004	29 kDa	x	x	x
398	Proliferation-associated protein 2G4	Q9UQ80	44 kDa	x	x	x
399	Prolyl 4-hydroxylase subunit alpha-1	P13674	61 kDa	x		
400	Prosaposin	P07602	58 kDa	x	x	x
401	Prostaglandin E synthase 3	A0A087WYT3	19 kDa	x	x	x
402	Proteasome activator complex subunit 1	Q06323	29 kDa		x	
403	Proteasome activator complex subunit 2	A0A087X1Z3	29 kDa	x		x
404	Proteasome subunit alpha type	G3V295	23 kDa	x		
405	Proteasome subunit alpha type-5	P28066	26 kDa	x		
406	Proteasome subunit alpha type-7	O14818	28 kDa	x	x	x
407	Protein ATP5J2-PTCD1	G3V325	84 kDa	x		
408	Protein CYR61	O00622	42 kDa	x	x	x
409	Protein S100-A10	P60903	11 kDa	x	x	x
410	Protein SET	A0A0C4DFV9	31 kDa	x		
411	Protein disulfide-isomerase A3	P30101	57 kDa	x	x	x
412	Protein disulfide-isomerase A4	P13667	73 kDa	x	x	x
413	Protein disulfide-isomerase A6	Q15084	48 kDa	x	x	x
414	Cluster of Protein disulfide-isomerase	P07237	57 kDa	x	x	x
415	Cluster of Protein kinase C beta type	P05771 [2]	77 kDa			x
416	Protein-glutamine gamma-glutamyltransferase 2	P21980	77 kDa	x	x	x
417	Proteolipid protein 2	Q04941	17 kDa	x	x	x
418	Cluster of Proto-oncogene tyrosine-protein kinase Src	P12931	60 kDa	x		
419	Cluster of Purine nucleoside phosphorylase	P00491	32 kDa	x	x	x
420	Cluster of Pyruvate kinase PKM	P14618	58 kDa	x	x	x
421	Cluster of RNA-binding motif protein, X chromosome (Fragment)	H0Y6E7 [3]	32 kDa	x	x	x

422	RNA-binding protein Raly	Q9UKM9	32 kDa	x	x	x
423	Cluster of Rab GDP dissociation inhibitor beta	P50395	51 kDa	x	x	x
424	Cluster of Ras GTPase-activating-like protein IQGAP1	P46940	189 kDa	x	x	x
425	Ras-related C3 botulinum toxin substrate 1	P63000	21 kDa	x	x	x
426	Cluster of Ras-related protein R-Ras	P10301 [2]	23 kDa	x	x	x
427	Cluster of Ras-related protein Rab-1A	P62820 [2]	23 kDa	x	x	x
428	Cluster of Ras-related protein Rab-2A	P61019	24 kDa	x	x	x
429	Cluster of Ras-related protein Rab-5C	P51148 [3]	23 kDa	x	x	x
430	Ras-related protein Rab-6B	Q9NRW1	23 kDa	x	x	
431	Ras-related protein Rab-7a	P51149	23 kDa	x	x	x
432	Ras-related protein Rab-8B (Fragment)	H0YNE9	22 kDa	x	x	x
433	Ras-related protein Rab-10	P61026	23 kDa	x	x	x
434	Ras-related protein Rab-11B	Q15907	24 kDa	x	x	x
435	Ras-related protein Rab-14	P61106	24 kDa	x	x	x
436	Cluster of Ras-related protein Ral-A	P11233	24 kDa	x	x	x
437	Ras-related protein Rap-1b	P61224	21 kDa	x	x	x
438	Cluster of Ras-related protein Rap-2b	P61225 [2]	21 kDa	x	x	
439	Cluster of Receptor of activated protein C kinase 1	P63244	35 kDa	x	x	x
440	Redox-regulatory protein FAM213A	Q9BRX8	26 kDa	x		
441	Cluster of Renin receptor	O75787 [8]	39 kDa			x
442	Reticulocalbin-1	Q15293	39 kDa	x	x	x
443	Reticulon	F8W914	37 kDa	x	x	x
444	Rho GDP-dissociation inhibitor 1 (Fragment)	J3KTF8	22 kDa	x	x	x
445	Rho GDP-dissociation inhibitor 2	P52566	23 kDa	x	x	x
446	Rho-related GTP-binding protein RhoG	P84095	21 kDa	x		
447	Ribonuclease inhibitor	P13489	50 kDa	x	x	x
448	Cluster of Ribose-phosphate pyrophosphokinase 1	P60891	35 kDa	x		
449	Ribosome-binding protein 1	A0A0A0MRV0	152 kDa	x		
450	RuvB-like 1	Q9Y265	50 kDa	x	x	x
451	RuvB-like 2	Q9Y230	51 kDa	x	x	x
452	SPARC (Fragment)	F5GY03	17 kDa		x	x
453	Sarcoplasmic/endoplasmic reticulum calcium ATPase 2	P16615	115 kDa	x	x	
454	Septin-2	B5MCX3	37 kDa	x	x	x
455	Septin-7	Q16181	51 kDa		x	
456	Serine hydroxymethyltransferase, mitochondrial	P34897	56 kDa	x	x	x
457	Serine protease 23	O95084	43 kDa	x	x	x
458	Serine--tRNA ligase, cytoplasmic	P49591	59 kDa		x	x
459	Serine/arginine-rich-splicing factor 1	J3KTL2	28 kDa	x	x	x
460	Serine/arginine-rich-splicing factor 3	A0A087X2D0	10 kDa	x		
461	Serine/threonine-protein phosphatase 2A 65 kDa regulatory subunit A alpha isoform	P30153	65 kDa	x	x	
462	Serine/threonine-protein phosphatase 2A catalytic subunit alpha isoform	P67775	36 kDa	x		x
463	Cluster of Serine/threonine-protein phosphatase PP1-alpha catalytic subunit	P62136	38 kDa			x
464	Serpin H1	P50454	46 kDa	x	x	x

465	Serum albumin	A0A0C4DGB6	69 kDa	x	x	x
466	Serum deprivation-response protein	O95810	47 kDa	x		x
467	Signal recognition particle 14 kDa protein	P37108	15 kDa	x		
468	Signal recognition particle receptor subunit beta	Q9Y5M8	30 kDa	x		
469	Slit homolog 2 protein	A0A087WYV5	160 kDa	x	x	x
470	Small nuclear ribonucleoprotein Sm D1	P62314	13 kDa			x
471	Small nuclear ribonucleoprotein Sm D2	P62316	14 kDa	x	x	x
472	Small nuclear ribonucleoprotein Sm D3	P62318	14 kDa	x	x	
473	Small nuclear ribonucleoprotein-associated protein N (Fragment)	J3QLE5	18 kDa	x		
474	Cluster of Sodium/potassium-transporting ATPase subunit alpha-1	P05023	113 kDa	x	x	x
475	Sodium/potassium-transporting ATPase subunit beta-3	P54709	32 kDa	x	x	x
476	Solute carrier family 2, facilitated glucose transporter member 1	P11166	54 kDa	x	x	x
477	Solute carrier family 2, facilitated glucose transporter member 3	P11169	54 kDa	x	x	x
478	Spectrin alpha chain, non-erythrocytic 1	A0A0D9SF54	283 kDa	x	x	x
479	Spectrin beta chain, non-erythrocytic 1	A0A087WUZ3	275 kDa	x		
480	Splicing factor 3B subunit 3	Q15393	136 kDa	x	x	x
481	Splicing factor U2AF 65 kDa subunit	K7ENG2	34 kDa	x		
482	Splicing factor, proline- and glutamine-rich	P23246	76 kDa	x	x	x
483	Stanniocalcin-1	P52823	28 kDa	x	x	x
484	Staphylococcal nuclease domain-containing protein 1	Q7KZF4	102 kDa	x	x	
485	Stress-70 protein, mitochondrial	P38646	74 kDa	x	x	x
486	Stress-induced-phosphoprotein 1	P31948	63 kDa	x	x	x
487	Stromelysin-2	P09238	54 kDa	x	x	x
488	Sulfhydryl oxidase 1	O00391	83 kDa	x	x	x
489	Superoxide dismutase [Cu-Zn]	P00441	16 kDa	x		
490	Surfeit locus protein 4	O15260	30 kDa		x	x
491	Sushi repeat-containing protein SRPX	P78539	52 kDa	x	x	x
492	Synaptic vesicle membrane protein VAT-1 homolog	Q99536	42 kDa	x	x	x
493	Cluster of Syntenin-1	O00560 [2]	32 kDa	x	x	x
494	T-complex protein 1 subunit alpha	P17987	60 kDa	x	x	x
495	T-complex protein 1 subunit beta	P78371	57 kDa	x	x	x
496	T-complex protein 1 subunit delta	P50991	58 kDa	x	x	x
497	T-complex protein 1 subunit epsilon	P48643	60 kDa	x	x	x
498	T-complex protein 1 subunit eta	Q99832	59 kDa	x	x	x
499	T-complex protein 1 subunit gamma	P49368	61 kDa	x	x	x
500	Cluster of T-complex protein 1 subunit theta	P50990	60 kDa	x	x	x
501	T-complex protein 1 subunit zeta	P40227	58 kDa	x	x	x
502	Talin-1	Q9Y490	270 kDa	x		x
503	Tenascin	F5H7V9	201 kDa	x	x	x
504	Cluster of Testican-1	Q08629	49 kDa	x	x	x
505	Tetraspanin GN=CD9 PE=1 SV=1	A6NNI4	18 kDa	x	x	x
506	Tetraspanin GN=CD81 PE=1 SV=1	A6NMH8	30 kDa	x		x

507	Thioredoxin domain-containing protein 5	Q8NBS9	48 kDa	x	x	x
508	Threonine--tRNA ligase, cytoplasmic	P26639	83 kDa	x	x	x
509	Thrombospondin-1	P07996	129 kDa	x	x	x
510	Tissue factor pathway inhibitor	P10646	35 kDa	x	x	x
511	Transaldolase	P37837	38 kDa	x	x	
512	Transcription intermediary factor 1-beta	Q13263	89 kDa	x	x	x
513	Transferrin receptor protein 1	P02786	85 kDa			x
514	Transforming growth factor-beta-induced protein ig-h3	Q15582	75 kDa	x	x	x
515	Cluster of Transforming protein RhoA	P61586 [3]	22 kDa	x	x	x
516	Transgelin-2	P37802	22 kDa	x	x	x
517	Transitional endoplasmic reticulum ATPase	P55072	89 kDa	x	x	x
518	Transketolase	P29401	68 kDa	x	x	x
519	Translocon-associated protein subunit delta	A6NLM8	16 kDa	x	x	
520	Transmembrane emp24 domain-containing protein 10	P49755	25 kDa	x	x	
521	Transmembrane protein 43	Q9BTV4	45 kDa	x	x	
522	Trifunctional enzyme subunit alpha, mitochondrial	P40939	83 kDa	x	x	x
523	Triosephosphate isomerase	P60174	31 kDa	x	x	x
524	Tripeptidyl-peptidase 1	O14773	61 kDa	x	x	x
525	Tropomyosin alpha-4 chain	P67936	29 kDa	x	x	x
526	Cluster of Tubulin alpha-1B chain	P68363 [4]	50 kDa	x	x	x
527	Cluster of Tubulin beta-6 chain	Q9BUF5 [9]	50 kDa	x	x	x
528	Tyrosine-protein phosphatase non-receptor type	B4DSN5	41 kDa	x		
529	U5 small nuclear ribonucleoprotein 200 kDa helicase	O75643	245 kDa		x	x
530	UDP-N-acetylhexosamine pyrophosphorylase	Q16222	59 kDa			x
531	UDP-glucose 6-dehydrogenase	O60701	55 kDa	x	x	x
532	UDP-glucose:glycoprotein glucosyltransferase 1	Q9NYU2	177 kDa	x		
533	UPF0568 protein C14orf166	Q9Y224	28 kDa		x	
534	Ubiquitin carboxyl-terminal hydrolase	D6RE83	23 kDa	x	x	x
535	Cluster of Ubiquitin-40S ribosomal protein S27a	P62979	18 kDa	x	x	x
536	Ubiquitin-conjugating enzyme E2 N	P61088	17 kDa	x		
537	Ubiquitin-like modifier-activating enzyme 1	P22314	118 kDa	x	x	x
538	Uncharacterized protein (Fragment)	H7C469	36 kDa	x	x	x
539	Unconventional myosin-Ic	F5H6E2	119 kDa	x	x	x
540	V-type proton ATPase catalytic subunit A	P38606	68 kDa	x		
541	Vacuolar protein sorting-associated protein 35	Q96QK1	92 kDa	x	x	x
542	Very-long-chain 3-oxoacyl-CoA reductase	Q53GQ0	34 kDa	x	x	x
543	Vesicle-trafficking protein SEC22b	O75396	25 kDa	x	x	x
544	Cluster of Vimentin	P08670	54 kDa	x	x	x
545	Vinculin	P18206	124 kDa	x	x	x
546	Vitamin D-binding protein	D6RF35	53 kDa	x	x	x
547	Voltage-dependent anion-selective channel protein 1	P21796	31 kDa	x	x	x
548	Voltage-dependent anion-selective channel protein 2 (Fragment)	A0A0A0MR02	30 kDa	x	x	x
549	WD repeat-containing protein 1	O75083	66 kDa	x	x	x
550	X-ray repair cross-complementing protein 6	B1AHC9	64 kDa	x	x	x

References

- AASS, H. C., OVSTEBO, R., TROSEID, A. M., KIERULF, P., BERG, J. P. & HENRIKSSON, C. E. 2011. Fluorescent particles in the antibody solution result in false TF- and CD14-positive microparticles in flow cytometric analysis. *Cytometry A*, 79, 990-9.
- ABBASIAN, N. 2015. *Microparticles as biomarkers of early changes leading to cardiovascular disease in chronic kidney disease*. PhD thesis, Department of Infection, Immunity and Inflammation. University of Leicester.
- ABBASIAN, N., BURTON, J. O., HERBERT, K. E., TREGUNNA, B.-E., BROWN, J. R., GHADERI-NAJAFABADI, M., BRUNSKILL, N. J., GOODALL, A. H. & BEVINGTON, A. 2015. Hyperphosphatemia, Phosphoprotein Phosphatases, and Microparticle Release in Vascular Endothelial Cells. *Journal of the American Society of Nephrology : JASN*, 26, 2152.
- ABID HUSSEIN, M. N., BÖING, A. N., STURK, A., HAU, C. M. & NIEUWLAND, R. 2007. Inhibition of microparticle release triggers endothelial cell apoptosis and detachment. *Thrombosis and haemostasis*, 98, 1096.
- AL-RASHEED, N., MEAKIN, F., ROYAL, E., LEWINGTON, A., BROWN, J., WILLARS, G. & BRUNSKILL, N. 2004a. Potent activation of multiple signalling pathways by C-peptide in opossum kidney proximal tubular cells. *Diabetologia*, 47, 987-997.
- AL-RASHEED, N. M., CHANA, R. S., BAINES, R. J., WILLARS, G. B. & BRUNSKILL, N. J. 2004b. Ligand-independent Activation of Peroxisome Proliferator-activated Receptor- γ by Insulin and C-peptide in Kidney Proximal Tubular Cells DEPENDENT ON PHOSPHATIDYLINOSITOL 3-KINASE ACTIVITY. *Journal of Biological Chemistry*, 279, 49747-49754.
- AL-RASHEED, N. M., WILLARS, G. B. & BRUNSKILL, N. J. 2006. C-Peptide Signals via Gai to Protect against TNF- α -Mediated Apoptosis of Opossum Kidney Proximal Tubular Cells. *Journal of the American Society of Nephrology*, 17, 986-995.
- ALICIC, R. Z., ROONEY, M. T. & TUTTLE, K. R. 2017. Diabetic Kidney Disease Challenges, Progress, and Possibilities. *Clinical Journal of the American Society of Nephrology*, 12, 2032-2045.
- AMABILE, N., GUÉRIN, A. P., TEDGUI, A., BOULANGER, C. M. & LONDON, G. M. 2012. Predictive value of circulating endothelial microparticles for cardiovascular mortality in end-stage renal failure: a pilot study. *Nephrology Dialysis Transplantation*, 27, 1873-1880.
- AMERICAN_DIABETES_ASSOCIATION 2014. Diagnosis and classification of diabetes mellitus. *Diabetes care*, 37, S81-S90.
- AMERICAN_DIABETES_ASSOCIATION 2018. 2. Classification and diagnosis of diabetes: standards of medical care in diabetes—2018. *Diabetes Care*, 41, S13-S27.
- ARRAUD, N., GOUNOU, C., TURPIN, D. & BRISSON, A. R. 2016. Fluorescence triggering: A general strategy for enumerating and phenotyping extracellular vesicles by flow cytometry. *Cytometry A*, 89, 184-95.
- AYERS, L., KOHLER, M., HARRISON, P., SARGENT, I., DRAGOVIC, R., SCHAAP, M., NIEUWLAND, R., BROOKS, S. A. & FERRY, B. 2011. Measurement of circulating cell-derived microparticles by flow cytometry: sources of variability within the assay. *Thromb Res*, 127, 370-7.

- BADAL, S. S. & DANESH, F. R. 2014. New insights into molecular mechanisms of diabetic kidney disease. *American Journal of Kidney Diseases*, 63, S63-S83.
- BAMMERT, T. D., HIJMANS, J. G., REIAKVAM, W. R., LEVY, M. V., BREWSTER, L. M., GOLDTHWAITE, Z. A., GREINER, J. J., STOCKELMAN, K. A. & DESOUZA, C. A. 2017. High glucose derived endothelial microparticles increase active caspase-3 and reduce microRNA-Let-7a expression in endothelial cells. *Biochem Biophys Res Commun*, 493, 1026-1029.
- BAN, C. R. & TWIGG, S. M. 2008. Fibrosis in diabetes complications: pathogenic mechanisms and circulating and urinary markers. *Vascular health and risk management*, 4, 575.
- BARANSKA, P., JERCZYNSKA, H., PAWLOWSKA, Z., KOZIOLKIEWICZ, W. & CIERNIEWSKI, C. S. 2005. Expression of Integrins and Adhesive Properties of Human Endothelial Cell Line EA.hy 926. *Cancer Genomics - Proteomics*, 2, 265-269.
- BD_LIFE_SCIENCES. 2017. *Relative Fluorochrome Brightness* [Online]. BD. Available: <http://static.bdbiosciences.com/documents/Fluorochrome-Chart-Relative-Brightness.pdf> [Accessed 5 June 2018].
- BELL, D. S. H. & OVALLE, F. 2006. Long-term glycaemic efficacy and weight changes associated with thiazolidinediones when added at an advanced stage of type 2 diabetes. *Diabetes, Obesity and Metabolism*, 8, 110-115.
- BEVINGTON, A., KEMP, G., GRAHAM, R. & RUSSEL, G. 1992. Phosphate-sensitive enzymes: a possible molecular basis for cellular disorders of phosphate metabolism. *Clinical chemistry and enzymology communications*, 4, 235-257.
- BEVINGTON, A., KEMP, G. & RUSSELL, R. 1990. Acquired disorders of phosphate metabolism. *The metabolic and molecular basis of acquired disease*. London, 8301, 1097-123.
- BHATT, M. P., LEE, Y.-J., JUNG, S.-H., KIM, Y. H., HWANG, J. Y., HAN, E.-T., PARK, W. S., HONG, S.-H., KIM, Y.-M. & HA, K.-S. 2016. C-peptide protects against hyperglycemic memory and vascular endothelial cell apoptosis. *Journal of Endocrinology*, JOE-16-0349.
- BHATT, M. P., LIM, Y.-C. & HA, K.-S. 2014. C-peptide replacement therapy as an emerging strategy for preventing diabetic vasculopathy. *Cardiovascular Research*, 104, 234-244.
- BHATT, M. P., LIM, Y.-C., HWANG, J., NA, S., KIM, Y.-M. & HA, K.-S. 2012. C-peptide prevents hyperglycemia-induced endothelial apoptosis through inhibition of reactive oxygen species-mediated transglutaminase 2 activation. *Diabetes*, DB_120293.
- BHATT, M. P., LIM, Y.-C., KIM, Y.-M. & HA, K.-S. 2013. C-peptide activates AMPK α and prevents ROS-mediated mitochondrial fission and endothelial apoptosis in diabetes mellitus. *Diabetes*, DB_130039.
- BINDEA, G., MLECNIK, B., HACKL, H., CHAROENTONG, P., TOSOLINI, M., KIRILOVSKY, A., FRIDMAN, W.-H., PAGÈS, F., TRAJANOSKI, Z. & GALON, J. 2009. ClueGO: a Cytoscape plug-in to decipher functionally grouped gene ontology and pathway annotation networks. *Bioinformatics*, 25, 1091-1093.
- BO, S., GENTILE, L., CASTIGLIONE, A., PRANDI, V., CANIL, S., GHIGO, E. & CICCONE, G. 2012. C-peptide and the risk for incident complications and mortality in type 2 diabetic patients. A retrospective cohort study after a 14-year follow-up. *European journal of endocrinology*, EJE-12-0085.

- BOERMA, M., KRUSE, J. J., VAN LOENEN, M., KLEIN, H. R., BART, C. I., ZURCHER, C. & WONDERGEM, J. 2004. Increased deposition of von Willebrand factor in the rat heart after local ionizing irradiation. *Strahlenther Onkol*, 180, 109-16.
- BOHREN, C. F. & HUFFMAN, D. R. 2008. *Absorption and scattering of light by small particles*, John Wiley & Sons.
- BORNSTEIN, P. 2009. Thrombospondins function as regulators of angiogenesis. *Journal of cell communication and signaling*, 3, 189-200.
- BROWNLEE, M. 2001. Biochemistry and molecular cell biology of diabetic complications. *Nature*, 414, 813.
- BROWNLEE, M. 2005. The pathobiology of diabetic complications: a unifying mechanism. *Diabetes*, 54, 1615-25.
- BRUNSKILL, N. 2017. C-peptide and diabetic kidney disease. *Journal of internal medicine*, 281, 41-51.
- BURGER, D., MONTEZANO, A. C., NISHIGAKI, N., HE, Y., CARTER, A. & TOUYZ, R. M. 2011. Endothelial microparticle formation by angiotensin II is mediated via Ang II receptor type I/NADPH oxidase/Rho kinase pathways targeted to lipid rafts. *Arteriosclerosis, thrombosis, and vascular biology*, 31, 1898-1907.
- BURGER, D., TURNER, M., XIAO, F., MUNKONDA, M. N., AKBARI, S. & BURNS, K. D. 2017. High glucose increases the formation and pro-oxidative activity of endothelial microparticles. *Diabetologia*, 60, 1791-1800.
- BURNSTOCK, G. 2014. Purinergic signalling: from discovery to current developments. *Experimental physiology*, 99, 16-34.
- BURTON, J. O., HAMALI, H. A., SINGH, R., ABBASIAN, N., PARSONS, R., PATEL, A. K., GOODALL, A. H. & BRUNSKILL, N. J. 2013. Elevated levels of procoagulant plasma microvesicles in dialysis patients. *PloS one*, 8, e72663.
- CAO, Y., GONG, Y., LIU, L., ZHOU, Y., FANG, X., ZHANG, C., LI, Y. & LI, J. 2017. The use of human umbilical vein endothelial cells (HUVECs) as an in vitro model to assess the toxicity of nanoparticles to endothelium: a review. *J Appl Toxicol*, 37, 1359-1369.
- CAPONNETTO, F., MANINI, I., SKRAP, M., PALMAI-PALLAG, T., DI LORETO, C., BELTRAMI, A. P., CEsSELLI, D. & FERRARI, E. 2017. Size-dependent cellular uptake of exosomes. *Nanomedicine: Nanotechnology, Biology and Medicine*, 13, 1011-1020.
- CASTAMAN, G., YU-FENG, L., BATTISTIN, E. & RODEGHIERO, F. 1997. Characterization of a novel bleeding disorder with isolated prolonged bleeding time and deficiency of platelet microvesicle generation. *British journal of haematology*, 96, 458-463.
- CELERMAJER, D. S., SORENSEN, K. E., GOOCH, V., SPIEGELHALTER, D., MILLER, O., SULLIVAN, I., LLOYD, J. & DEANFIELD, J. 1992. Non-invasive detection of endothelial dysfunction in children and adults at risk of atherosclerosis. *The lancet*, 340, 1111-1115.
- CERIELLO, A., MERCURI, F., QUAGLIARO, L., ASSALONI, R., MOTZ, E., TONUTTI, L. & TABOGA, C. 2001. Detection of nitrotyrosine in the diabetic plasma: evidence of oxidative stress. *Diabetologia*, 44, 834-838.
- CHAKRABARTI, S., KHAN, Z. A., CUKIERNIK, M., ZHANG, W. & SIMA, A. A. 2004. C-peptide and retinal microangiopathy in diabetes. *Exp Diabetes Res*, 5, 91-6.

- CHANDLER, W. L., YEUNG, W. & TAIT, J. F. 2011. A new microparticle size calibration standard for use in measuring smaller microparticles using a new flow cytometer. *J Thromb Haemost*, 9, 1216-24.
- CHARGAFF, E. & WEST, R. 1946. The biological significance of the thromboplastic protein of blood. *J Biol Chem*, 166, 189-197.
- CHAVAKIS, E. & DIMMELER, S. 2002. Regulation of endothelial cell survival and apoptosis during angiogenesis. *Arteriosclerosis, thrombosis, and vascular biology*, 22, 887-893.
- CHENG, G., WANG, L. L., QU, W. S., LONG, L., CUI, H., LIU, H. Y., CAO, Y. L. & LI, S. 2005. C16, a novel advanced glycation endproduct breaker, restores cardiovascular dysfunction in experimental diabetic rats. *Acta Pharmacol Sin*, 26, 1460-6.
- CHIMA, R. S., LAMONTAGNE, T., PIRAINO, G., HAKE, P. W., DENENBERG, A. & ZINGARELLI, B. 2011a. C-peptide, a novel inhibitor of lung inflammation following hemorrhagic shock. *Am J Physiol Lung Cell Mol Physiol*, 300, L730-9.
- CHIMA, R. S., MALTESE, G., LAMONTAGNE, T., PIRAINO, G., DENENBERG, A., O'CONNOR, M. & ZINGARELLI, B. 2011b. C-peptide ameliorates kidney injury following hemorrhagic shock. *Shock*, 35, 524-9.
- CHO, N., SHAW, J., KARURANGA, S., HUANG, Y., DA ROCHA FERNANDES, J., OHLROGGE, A. & MALANDA, B. 2018. IDF Diabetes Atlas: global estimates of diabetes prevalence for 2017 and projections for 2045. *Diabetes research and clinical practice*, 138, 271-281.
- CHONCHOL, M., DALE, R., SCHRIER, R. W. & ESTACIO, R. 2009. Serum phosphorus and cardiovascular mortality in type 2 diabetes. *The American journal of medicine*, 122, 380-386.
- CHRISTEN, A., L ARMENTANO, R., MIRANDA, A., GRAF, S., B SANTANA, D., ZOCCALO, Y., P BAGLIVO, H. & A SANCHEZ, R. 2010. Arterial wall structure and dynamics in type 2 diabetes mellitus methodological aspects and pathophysiological findings. *Current diabetes reviews*, 6, 367-377.
- CIFARELLI, V., GENG, X., STYCHE, A., LAKOMY, R., TRUCCO, M. & LUPPI, P. 2011a. C-peptide reduces high-glucose-induced apoptosis of endothelial cells and decreases NAD (P) H-oxidase reactive oxygen species generation in human aortic endothelial cells. *Diabetologia*, 54, 2702.
- CIFARELLI, V., LUPPI, P., TSE, H. M., HE, J., PIGANELLI, J. & TRUCCO, M. 2008. Human proinsulin C-peptide reduces high glucose-induced proliferation and NF-kappaB activation in vascular smooth muscle cells. *Atherosclerosis*, 201, 248-57.
- CIFARELLI, V., TRUCCO, M. & LUPPI, P. 2011b. Anti-inflammatory effects of C-peptide prevent endothelial dysfunction in type 1 diabetes. *Immunology, Endocrine & Metabolic Agents in Medicinal Chemistry (Formerly Current Medicinal Chemistry-Immunology, Endocrine and Metabolic Agents)*, 11, 59-70.
- CINES, D. B., POLLAK, E. S., BUCK, C. A., LOSCALZO, J., ZIMMERMAN, G. A., MCEVER, R. P., POBER, J. S., WICK, T. M., KONKLE, B. A. & SCHWARTZ, B. S. 1998. Endothelial cells in physiology and in the pathophysiology of vascular disorders. *Blood*, 91, 3527-3561.
- CLANCY, J. W., SEDGWICK, A., ROSSE, C., MURALIDHARAN-CHARI, V., RAPOSO, G., METHOD, M., CHAVRIER, P. & D'SOUZA-SCHOREY, C. 2015. Regulated delivery

- of molecular cargo to invasive tumour-derived microvesicles. *Nature communications*, 6, 6919.
- COINTE, S., JUDICONE, C., ROBERT, S., MOOBERRY, M. J., PONCELET, P., WAUBEN, M., NIEUWLAND, R., KEY, N. S., DIGNAT-GEORGE, F. & LACROIX, R. 2017. Standardization of microparticle enumeration across different flow cytometry platforms: results of a multicenter collaborative workshop. *J Thromb Haemost*, 15, 187-193.
- COMINACINI, L., FRATTA PASINI, A., GARBIN, U., DAVOLI, A., SANTIS, A., CAMPAGNOLA, M., RIGONI, A., ZENTI, M., MOGHETTI, P. & CASCIO, V. 1995. Elevated levels of soluble E-selectin in patients with IDDM and NIDDM: relation to metabolic control. *Diabetologia*, 38, 1122-1124.
- CONNOR, D. E., EXNER, T., MA, D. D. F. & JOSEPH, J. E. 2010. The majority of circulating platelet-derived microparticles fail to bind annexin V, lack phospholipid-dependent procoagulant activity and demonstrate greater expression of glycoprotein Ib. *Thrombosis and haemostasis*, 103, 1044.
- COTTER, M. A. & CAMERON, N. E. 2001. C-peptide effects on nerve conduction and blood flow in streptozotocin-induced diabetic rats: modulation by nitric oxide synthase inhibition. *Diabetes*, 50, A184.
- COX, T. M. 2002. The genetic consequences of our sweet tooth. *Nature Reviews Genetics*, 3, 481.
- CROMPOT, E., VAN DAMME, M., DUVILLIER, H., PIETERS, K., VERMEESCH, M., PEREZ-MORGA, D., MEULEMAN, N., MINEUR, P., BRON, D., LAGNEAUX, L. & STAMATOPOULOS, B. 2015. Avoiding false positive antigen detection by flow cytometry on blood cell derived microparticles: the importance of an appropriate negative control. *PLoS One*, 10, e0127209.
- DCCT_RESEARCH_GROUP 1993. The effect of intensive treatment of diabetes on the development and progression of long-term complications in insulin-dependent diabetes mellitus. *New England journal of medicine*, 329, 977-986.
- DE CATERINA, R., MASSARO, M. & LIBBY, P. 2007a. Endothelial Functions and Dysfunctions. In: DE CATERINA, P. & LIBBY, P. (eds.) *Endothelial Dysfunctions in Vascular Disease*. Blackwell Publishing.
- DE CATERINA, R., ZAMPOLLI, A., LAZZERINI, G. & LIBBY, P. 2007b. Endothelial Activation and the Initiation of Atherosclerosis. In: DE CATERINA, R. & LIBBY, P. (eds.) *Endothelial Dysfunctions in Vascular Disease*. Blackwell Publishing.
- DE JONG, O. G., VERHAAR, M. C., CHEN, Y., VADER, P., GREMMELS, H., POSTHUMA, G., SCHIFFELERS, R. M., GUCEK, M. & VAN BALKOM, B. W. 2012. Cellular stress conditions are reflected in the protein and RNA content of endothelial cell-derived exosomes. *Journal of extracellular vesicles*, 1, 18396.
- DE MEYER, G. R., HOYLAERTS, M. F., KOCKX, M. M., YAMAMOTO, H., HERMAN, A. G. & BULT, H. 1999. Intimal deposition of functional von Willebrand factor in atherosclerosis. *Arterioscler Thromb Vasc Biol*, 19, 2524-34.
- DEFRONZO, R. A., FERRANNINI, E., GROOP, L., HENRY, R. R., HERMAN, W. H., HOLST, J. J., HU, F. B., KAHN, C. R., RAZ, I. & SHULMAN, G. I. 2015. Type 2 diabetes mellitus. *Nature reviews Disease primers*, 1, 15019.
- DENG, F., WANG, S. & ZHANG, L. 2016. Endothelial microparticles act as novel diagnostic and therapeutic biomarkers of diabetes and its complications: a literature review. *BioMed research international*, 2016.

- DHINGRA, R., SULLIVAN, L. M., FOX, C. S., WANG, T. J., D'AGOSTINO, R. B., GAZIANO, J. M. & VASAN, R. S. 2007. Relations of serum phosphorus and calcium levels to the incidence of cardiovascular disease in the community. *Archives of internal medicine*, 167, 879-885.
- DI MARCO, G. S., HAUSBERG, M., HILLEBRAND, U., RUSTEMEYER, P., WITTKOWSKI, W., LANG, D. & PAVENSTÄDT, H. 2008. Increased inorganic phosphate induces human endothelial cell apoptosis in vitro. *American journal of physiology. Renal physiology*, 294, F1381.
- DI MARCO, G. S., KÖNIG, M., STOCK, C., WIESINGER, A., HILLEBRAND, U., REIERMANN, S., REUTER, S., AMLER, S., KÖHLER, G., BUCK, F., FÖBKER, M., KÜMPERS, P., OBERLEITHNER, H., HAUSBERG, M., LANG, D., PAVENSTÄDT, H. & BRAND, M. 2013. High phosphate directly affects endothelial function by downregulating annexin II. *Kidney International*, 83, 213-222.
- DICK, C. F., DOS-SANTOS, A. L. A. & MEYER-FERNANDES, J. R. 2011. Inorganic phosphate as an important regulator of phosphatases. *Enzyme research*, 2011.
- DISTLER, J., HUBER, L., HUEBER, A., REICH, C., GAY, S., DISTLER, O. & PISETSKY, D. 2005. The release of microparticles by apoptotic cells and their effects on macrophages. *Apoptosis*, 10, 731-741.
- DJEMLI-SHIPKOLYE, A., GALLICE, P., COSTE, T., JANNOT, M., TSIMARATOS, M., RACCAH, D. & VAGUE, P. 2000. The effects ex vivo and in vitro of insulin and C-peptide on Na/K adenosine triphosphatase activity in red blood cell membranes of type 1 diabetic patients. *Metabolism-Clinical and Experimental*, 49, 868-872.
- EDGEELL, C. J., MCDONALD, C. C. & GRAHAM, J. B. 1983. Permanent cell line expressing human factor VIII-related antigen established by hybridization. *Proceedings of the National Academy of Sciences of the United States of America*, 80, 3734.
- EDIC_RESEARCH_GROUP 2005. Intensive diabetes treatment and cardiovascular disease in patients with type 1 diabetes. *New England Journal of Medicine*, 353, 2643-2653.
- EDWIN, W. A., FRANCISCO, J. C., ROBERT, A. S., VELMA, G. G., SUSAN, S., DIANE, C. B. & THOMAS, J. L. 1992. HMEC-1: Establishment of an Immortalized Human Microvascular Endothelial Cell Line. *Journal of Investigative Dermatology*, 99, 683.
- EELLEN, G., DE ZEEUW, P., SIMONS, M. & CARMELIET, P. 2015. Endothelial cell metabolism in normal and diseased vasculature. *Circulation research*, 116, 1231-1244.
- EKBERG, K., BRISMAR, T., JOHANSSON, B. L., LINDSTROM, P., JUNTTI-BERGGREN, L., NORRBY, A., BERNE, C., ARNQVIST, H. J., BOLINDER, J. & WAHREN, J. 2007. C-Peptide replacement therapy and sensory nerve function in type 1 diabetic neuropathy. *Diabetes Care*, 30, 71-6.
- EL KHAWAND, C., JAMART, J., DONCKIER, J., CHATELAIN, B., LAVENNE, E., MORIAU, M. & BUYSSCHAERT, M. 1993. Hemostasis variables in type I diabetic patients without demonstrable vascular complications. *Diabetes Care*, 16, 1137-45.
- ELLAM, T. J. & CHICO, T. J. 2012. Phosphate: the new cholesterol? The role of the phosphate axis in non-uremic vascular disease. *Atherosclerosis*, 220, 310-318.

- ENGELMAN, J. A., LUO, J. & CANTLEY, L. C. 2006. The evolution of phosphatidylinositol 3-kinases as regulators of growth and metabolism. *Nature Reviews Genetics*, 7, 606.
- ERDBRUGGER, U., RUDY, C. K., ETTER, M. E., DRYDEN, K. A., YEAGER, M., KLIBANOV, A. L. & LANNIGAN, J. 2014. Imaging flow cytometry elucidates limitations of microparticle analysis by conventional flow cytometry. *Cytometry A*, 85, 756-70.
- EWENCE, A. E., BOOTMAN, M., RODERICK, H. L., SKEPPER, J. N., MCCARTHY, G., EPPLE, M., NEUMANN, M., SHANAHAN, C. M. & PROUDFOOT, D. 2008. Calcium phosphate crystals induce cell death in human vascular smooth muscle cells: a potential mechanism in atherosclerotic plaque destabilization. *Circulation research*, 103, e28-e34.
- FENG, B., CHEN, Y., LUO, Y., CHEN, M., LI, X. & NI, Y. 2010. Circulating level of microparticles and their correlation with arterial elasticity and endothelium-dependent dilation in patients with type 2 diabetes mellitus. *Atherosclerosis*, 208, 264-269.
- FENG, L., MA, X., WANG, J. & TIAN, Q. 2017. Up-regulation of 14-3-3 β plays a role in intimal hyperplasia following carotid artery injury in diabetic Sprague Dawley rats by promoting endothelial cell migration and proliferation. *Biochemical and Biophysical Research Communications*, 490, 1237-1243.
- FENG, Q., STORK, C. J., XU, S., YUAN, D., XIA, X., LAPENNA, K. B., GUO, G., SUN, H., XU, L. C. & SIEDLECKI, C. A. 2019. Increased circulating microparticles in streptozotocin-induced diabetes propagate inflammation contributing to microvascular dysfunction. *The Journal of physiology*.
- FIORDALISO, F., CUCCOVILLO, I., BIANCHI, R., BAI, A., DONI, M., SALIO, M., DE ANGELIS, N., GHEZZI, P., LATINI, R. & MASSON, S. 2006. Cardiovascular oxidative stress is reduced by an ACE inhibitor in a rat model of streptozotocin-induced diabetes. *Life Sci*, 79, 121-9.
- FLATT, P. R., SWANSTON-FLATT, S. K., HAMPTON, S. M., BAILEY, C. J. & MARKS, V. 1986. Specific binding of the C-peptide of proinsulin to cultured B-cells from a transplantable rat islet cell tumor. *Bioscience Reports*, 6, 193-199.
- FLAUMENHAFT, R. 2006. Formation and fate of platelet microparticles. *Blood Cells, Molecules, and Diseases*, 36, 182-187.
- FONG, D. S., AIELLO, L., GARDNER, T. W., KING, G. L., BLANKENSHIP, G., CAVALLERANO, J. D., FERRIS, F. L. & KLEIN, R. 2004. Retinopathy in diabetes. *Diabetes care*, 27 Suppl 1, S84.
- FORST, T., DUFAYET DE LA TOUR, D., KUNT, T., PFÜTZNER, A., GOITOM, K., POHLMANN, T., SCHNEIDER, S., JOHANSSON, B. L., WAHREN, J., LÖBIG, M., ENGELBACH, M., BEYER, J. & VAGUE, P. 2000. Effects of proinsulin C-peptide on nitric oxide, microvascular blood flow and erythrocyte Na⁺,K⁺-ATPase activity in diabetes mellitus type I. *Clinical Science*, 98, 283-290.
- FORST, T., HACH, T., KUNT, T., WEBER, M. M. & PFÜTZNER, A. 2009. Molecular effects of C-Peptide in microvascular blood flow regulation. *The review of diabetic studies: RDS*, 6, 159.
- FOURCADE, O., SIMON, M.-F., VIODÉ, C., RUGANI, N., LEBALLE, F., RAGAB, A., FOURNIÉ, B., SARDA, L. & CHAP, H. 1995. Secretory phospholipase A2

- generates the novel lipid mediator lysophosphatidic acid in membrane microvesicles shed from activated cells. *Cell*, 80, 919-927.
- FREEMAN, D. W., HOOTEN, N. N., EITAN, E., GREEN, J., MODE, N. A., BODOGAI, M., ZHANG, Y., LEHRMANN, E., ZONDERMAN, A. B. & BIRAGYN, A. 2018. Altered extracellular vesicle concentration, cargo, and function in diabetes. *Diabetes*, 67, 2377-2388.
- FUKUDA, G., KHAN, Z. A., BARBIN, Y. P., FARHANGKHOEE, H., TILTON, R. G. & CHAKRABARTI, S. 2005. Endothelin-mediated remodeling in aortas of diabetic rats. *Diabetes Metab Res Rev*, 21, 367-75.
- GALUSKA, D., PIRKMAJER, S., BARRÈS, R., EKBERG, K., WAHREN, J. & CHIBALIN, A. V. 2011. C-Peptide Increases Na,K-ATPase Expression via PKC- and MAP Kinase-Dependent Activation of Transcription Factor ZEB in Human Renal Tubular Cells. *PLOS ONE*, 6, e28294.
- GAPIZOV, S. S., PETROVSKAYA, L. E., SHINGAROVA, L. N., SVIRSCHEVSKAYA, E. V., DOLGIKH, D. A. & KIRPICHNIKOV, M. P. 2018. The Effect of TNF and VEGF on the Properties of Ea.hy926 Endothelial Cells in a Model of Multi-Cellular Spheroids. *Acta Naturae*, 10, 34-42.
- GARDINER, C., FERREIRA, Y. J., DRAGOVIC, R. A., REDMAN, C. W. & SARGENT, I. L. 2013. Extracellular vesicle sizing and enumeration by nanoparticle tracking analysis. *J Extracell Vesicles*, 2.
- GARDINER, C., VIZIO, D. D., SAHOO, S., THERY, C., WITWER, K. W., WAUBEN, M. & HILL, A. F. 2016. Techniques used for the isolation and characterization of extracellular vesicles: results of a worldwide survey. *Journal of extracellular vesicles*, 5, 32945.
- GAVIN III, J. R., ALBERTI, K., DAVIDSON, M. B. & DEFRONZO, R. A. 1997. Report of the expert committee on the diagnosis and classification of diabetes mellitus. *Diabetes care*, 20, 1183.
- GERALDES, P. & KING, G. L. 2010. Activation of protein kinase C isoforms and its impact on diabetic complications. *Circulation research*, 106, 1319-1331.
- GERÖ, D. & SZABO, C. 2016. Glucocorticoids suppress mitochondrial oxidant production via upregulation of uncoupling protein 2 in hyperglycemic endothelial cells. *PloS one*, 11, e0154813.
- GIEBINK, A. W., VOGEL, P. A., MEDAWALA, W. & SPENCE, D. M. 2013. C-peptide-stimulated nitric oxide production in a cultured pulmonary artery endothelium is erythrocyte mediated and requires Zn²⁺. *Diabetes/metabolism research and reviews*, 29, 44-52.
- GRAGNANO, F., SPERLONGANO, S., GOLIA, E., NATALE, F., BIANCHI, R., CRISCI, M., FIMIANI, F., PARIGGIANO, I., DIANA, V., CARBONE, A., CESARO, A., CONCILIO, C., LIMONGELLI, G., RUSSO, M. & CALABRO, P. 2017. The Role of von Willebrand Factor in Vascular Inflammation: From Pathogenesis to Targeted Therapy. *Mediators Inflamm*, 2017, 5620314.
- GROSS, P., SIX, I., KAMEL, S. & MASSY, Z. A. 2014. Vascular toxicity of phosphate in chronic kidney disease. *Circulation Journal*, 78, 2339-2346.
- GROß, M.-L., HEISS, N., WECKBACH, M., HANSEN, A., EL-SHAKMAK, A., SZABÓ, A., MÜNTER, K., RITZ, E. & AMANN, K. 2004. ACE-inhibition is superior to endothelin A receptor blockade in preventing abnormal capillary supply and fibrosis of the heart in experimental diabetes. *Diabetologia*, 47, 316-324.

- GRUNBERGER, G., QIANG, X., LI, Z., MATHEWS, S., SBRISSA, D., SHISHEVA, A. & SIMA, A. 2001. Molecular basis for the insulinomimetic effects of C-peptide. *Diabetologia*, 44, 1247-1257.
- GYORGY, B., MODOS, K., PALLINGER, E., PALOCZI, K., PASZTOI, M., MISJAK, P., DELI, M. A., SIPOS, A., SZALAI, A., VOSZKA, I., POLGAR, A., TOTH, K., CSETE, M., NAGY, G., GAY, S., FALUS, A., KITTEL, A. & BUZAS, E. I. 2011. Detection and isolation of cell-derived microparticles are compromised by protein complexes resulting from shared biophysical parameters. *Blood*, 117, e39-48.
- GYÖRGY, B., SZABÓ, T. G., PÁSZTÓI, M., PÁL, Z., MISJÁK, P., ARADI, B., LÁSZLÓ, V., PÁLLINGER, E., PAP, E. & KITTEL, A. 2011. Membrane vesicles, current state-of-the-art: emerging role of extracellular vesicles. *Cellular and molecular life sciences*, 68, 2667-2688.
- HAAP, M., HELLER, E., THAMER, C., TSCHRITTER, O., STEFAN, N. & FRITSCH, A. 2006. Association of serum phosphate levels with glucose tolerance, insulin sensitivity and insulin secretion in non-diabetic subjects. *European journal of clinical nutrition*, 60, 734.
- HACH, T., FORST, T., KUNT, T., EKBERG, K., PFÜTZNER, A. & WAHREN, J. 2008. C-peptide and its C-terminal fragments improve erythrocyte deformability in type 1 diabetes patients. *Experimental diabetes research*, 2008.
- HAIDET, J., CIFARELLI, V., TRUCCO, M. & LUPPI, P. 2009. Anti-inflammatory properties of C-Peptide. *Rev Diabet Stud*, 6, 168-79.
- HAUSER, S., JUNG, F. & PIETZSCH, J. 2017. Human Endothelial Cell Models in Biomaterial Research. *Trends in Biotechnology*, 35, 265-277.
- HAUT, L. L., ALFREY, A. C., GUGGENHEIM, S., BUDDINGTON, B. & SCHRIER, N. 1980. Renal toxicity of phosphate in rats. *Kidney international*, 17, 722-731.
- HAYASHI, T., MATSUI-HIRAI, H., MIYAZAKI-AKITA, A., FUKATSU, A., FUNAMI, J., DING, Q.-F., KAMALANATHAN, S., HATTORI, Y., IGNARRO, L. J. & IGUCHI, A. 2006. Endothelial cellular senescence is inhibited by nitric oxide: implications in atherosclerosis associated with menopause and diabetes. *Proceedings of the National Academy of Sciences*, 103, 17018-17023.
- HILLS, C. E., AL-RASHEED, N., AL-RASHEED, N., WILLARS, G. B. & BRUNSKILL, N. J. 2009. C-peptide reverses TGF-beta1-induced changes in renal proximal tubular cells: implications for treatment of diabetic nephropathy. *Am J Physiol Renal Physiol*, 296, F614-21.
- HILLS, C. E. & BRUNSKILL, N. J. 2008. Intracellular signalling by C-peptide.
- HILLS, C. E. & BRUNSKILL, N. J. 2009. Cellular and physiological effects of C-peptide. *Clinical science*, 116, 565-574.
- HOEBEN, A., LANDUYT, B., HIGHLEY, M. S., WILDIERS, H., VAN OOSTEROM, A. & DE BRUIJN, E. 2004. Vascular endothelial growth factor and angiogenesis. *Pharmacological Reviews*, 56, 549-580.
- HOFFMAN, R. A. & WOOD, J. C. 2007. Characterization of flow cytometer instrument sensitivity. *Curr Protoc Cytom*, Chapter 1, Unit1 20.
- HOGAS, S. M., VORONEANU, L., SERBAN, D. N., SEGALL, L., HOGAS, M. M., SERBAN, I. L. & COVIC, A. 2010. Methods and potential biomarkers for the evaluation of endothelial dysfunction in chronic kidney disease: a critical approach. *J Am Soc Hypertens*, 4, 116-27.

- HOLNTHONER, W., BONSTINGL, C., HROMADA, C., MUEHLEDER, S., ZIPPERLE, J., STOJKOVIC, S., REDL, H., WOJTA, J., SCHÖCHL, H., GRILLARI, J., WEILNER, S. & SCHLIMP, C. J. 2017. Endothelial Cell-derived Extracellular Vesicles Size-dependently Exert Procoagulant Activity Detected by Thromboelastometry. *Scientific Reports*, 7.
- HONG, S.-H., PARK, S.-J., LEE, S., KIM, S. & CHO, M.-H. 2015. Biological effects of inorganic phosphate: potential signal of toxicity. *The Journal of toxicological sciences*, 40, 55-69.
- HSU, Y.-J., HSU, S.-C., HUANG, S.-M., LEE, H.-S., LIN, S.-H., TSAI, C.-S., SHIH, C.-C. & LIN, C.-Y. 2015. Hyperphosphatemia induces protective autophagy in endothelial cells through the inhibition of Akt/mTOR signaling. *Journal of vascular surgery*, 62, 210-221. e2.
- HUANG, Y., LEI, L., LIU, D., JOVIN, I., RUSSELL, R., JOHNSON, R. S., DI LORENZO, A. & GIORDANO, F. J. 2012. Normal glucose uptake in the brain and heart requires an endothelial cell-specific HIF-1 α -dependent function. *Proceedings of the National Academy of Sciences*, 201209281.
- HULSPAS, R. 2010. Titration of fluorochrome-conjugated antibodies for labeling cell surface markers on live cells. *Curr Protoc Cytom*, Chapter 6, Unit 6 29.
- HULSPAS, R., O'GORMAN, M. R., WOOD, B. L., GRATAMA, J. W. & SUTHERLAND, D. R. 2009. Considerations for the control of background fluorescence in clinical flow cytometry. *Cytometry B Clin Cytom*, 76, 355-64.
- HUNDAL, H. S., MARETTE, A., RAMLAL, T., LIU, Z. & KLIP, A. 1993. Expression of β subunit isoforms of the Na⁺, K⁺-ATPase is muscle type-specific. *FEBS letters*, 328, 253-258.
- HUNT, B. J. & JURD, K. M. 2002. The endothelium in health and disease. In: HUNT, B., POSTON, L., SCHACHTER, M. & HALLIDAY, A. (eds.) *An Introduction to Vascular Biology : From Basic Science to Clinical Practice*. 2 ed.: Cambridge University Press.
- HUNTER, M. P., ISMAIL, N., ZHANG, X., AGUDA, B. D., LEE, E. J., YU, L., XIAO, T., SCHAFER, J., LEE, M.-L. T. & SCHMITTGEN, T. D. 2008. Detection of microRNA expression in human peripheral blood microvesicles. *PloS one*, 3, e3694.
- ILSE, M. R., JEROEN, K. J. D., MICHAEL, L. M., WIM, P. M. T., DANIEL, W. W., JACK, F. M. W. & JON, B. K. 2010. Comparison of three methods for isolation of urinary microvesicles to identify biomarkers of nephrotic syndrome. *Kidney International*, 78, 810.
- INGLIS, H. C., DANESH, A., SHAH, A., LACROIX, J., SPINELLA, P. C. & NORRIS, P. J. 2015. Techniques to improve detection and analysis of extracellular vesicles using flow cytometry. *Cytometry A*, 87, 1052-63.
- INTENGAN, H. D. & SCHIFFRIN, E. L. 2001. Vascular Remodeling in Hypertension. *Hypertension*, 38, 581-587.
- INTERNATIONAL_DIABETES_FEDERATION. 2017. *IDF Diabetes Atlas* [Online]. Brussels, Belgium. Available: <http://www.diabetesatlas.org> [Accessed 2 December 2018].
- INZUCCHI, S. E., BERGENSTAL, R. M., BUSE, J. B., DIAMANT, M., FERRANNINI, E., NAUCK, M., PETERS, A. L., TSAPAS, A., WENDER, R. & MATTHEWS, D. R. 2012. Management of hyperglycaemia in type 2 diabetes: a patient-centered approach. Position statement of the American Diabetes Association (ADA) and

- the European Association for the Study of Diabetes (EASD). *Diabetologia*, 55, 1577-1596.
- ISLAM, M. S. & WILSON, R. D. 2012. Experimentally induced rodent models of type 2 diabetes. *Animal Models in Diabetes Research*. Springer.
- JANABI, A. M. H. 2017. *Proinsulin C-peptide-mediated signalling and the search for its receptor*. PhD thesis, Department of Molecular and Cell Biology. University of Leicester.
- JANSEN, F., LI, Q., PFEIFER, A. & WERNER, N. 2017. Endothelial- and Immune Cell-Derived Extracellular Vesicles in the Regulation of Cardiovascular Health and Disease. *JACC: Basic to Translational Science*, 2, 790-807.
- JANSEN, F., WANG, H., PRZYBILLA, D., FRANKLIN, B. S., DOLF, A., PFEIFER, P., SCHMITZ, T., FLENDER, A., ENDL, E., NICKENIG, G. & WERNER, N. 2016. Vascular endothelial microparticles-incorporated microRNAs are altered in patients with diabetes mellitus. *Cardiovasc Diabetol*, 15, 49.
- JANSEN, F., YANG, X., BAUMANN, K., PRZYBILLA, D., SCHMITZ, T., FLENDER, A., PAUL, K., ALHUSSEINY, A., NICKENIG, G. & WERNER, N. 2015. Endothelial microparticles reduce ICAM-1 expression in a microRNA-222-dependent mechanism. *Journal of Cellular and Molecular Medicine*, 19, 2202-2214.
- JANSEN, F., YANG, X., FRANKLIN, B. S., HOELSCHER, M., SCHMITZ, T., BEDORF, J., NICKENIG, G. & WERNER, N. 2013. High glucose condition increases NADPH oxidase activity in endothelial microparticles that promote vascular inflammation. *Cardiovasc Res*, 98, 94-106.
- JANSEN, F., YANG, X., HOYER, F. F., PAUL, K., HEIERMANN, N., BECHER, M. U., ABU HUSSEIN, N., KEBSCHULL, M., BEDORF, J., FRANKLIN, B. S., LATZ, E., NICKENIG, G. & WERNER, N. 2012. Endothelial microparticle uptake in target cells is annexin I/phosphatidylserine receptor dependent and prevents apoptosis. *Arterioscler Thromb Vasc Biol*, 32, 1925-35.
- JENSEN, M. E. & MESSINA, E. J. 1999. C-peptide induces a concentration-dependent dilation of skeletal muscle arterioles only in presence of insulin. *American Journal of Physiology-Heart and Circulatory Physiology*, 276, H1223-H1228.
- JEON, H.-Y., LEE, Y.-J., KIM, Y.-S., KIM, S.-Y., HAN, E.-T., PARK, W. S., HONG, S.-H., KIM, Y.-M. & HA, K.-S. 2018. Proinsulin C-peptide prevents hyperglycemia-induced vascular leakage and metastasis of melanoma cells in the lungs of diabetic mice. *The FASEB Journal*, fj. 201800723R.
- JIMENEZ, J. J., JY, W., MAURO, L. M., SODERLAND, C., HORSTMAN, L. L. & AHN, Y. S. 2003. Endothelial cells release phenotypically and quantitatively distinct microparticles in activation and apoptosis. *Thromb Res*, 109, 175-80.
- JIMÉNEZ, B., VOLPERT, O. V., CRAWFORD, S. E., FEBBRAIO, M., SILVERSTEIN, R. L. & BOUCK, N. 2000. Signals leading to apoptosis-dependent inhibition of neovascularization by thrombospondin-1. *Nature medicine*, 6, 41.
- JING, T., YA-SHU, K., XUE-JUN, W., HAN-JING, H., YAN, L., YI-AN, Y., FEI, C. & XUE-BO, L. 2017. Sirt6 mRNA-incorporated endothelial microparticles (EMPs) attenuates DM patient-derived EMP-induced endothelial dysfunction. *Oncotarget*, 8, 114300-114313.
- JOHANSSON, B.-L., LINDE, B. & WAHREN, J. 1992. Effects of C-peptide on blood flow, capillary diffusion capacity and glucose utilization in the exercising forearm of type 1 (insulin-dependent) diabetic patients. *Diabetologia*, 35, 1151-1158.

- JOHANSSON, B.-L., WAHREN, J. & PERNOW, J. 2003. C-peptide increases forearm blood flow in patients with type 1 diabetes via a nitric oxide-dependent mechanism. *American Journal of Physiology-Endocrinology and Metabolism*, 285, E864-E870.
- JOHANSSON, J., EKBERG, K., SHAFQAT, J., HENRIKSSON, M., CHIBALIN, A., WAHREN, J. & JÖRNVALL, H. 2002. Molecular effects of proinsulin C-peptide. *Biochemical and biophysical research communications*, 295, 1035-1040.
- JOLIVALT, C., RODRIGUEZ, M., WAHREN, J. & CALCUTT, N. 2015. Efficacy of a long-acting C-peptide analogue against peripheral neuropathy in streptozotocin-diabetic mice. *Diabetes, Obesity and Metabolism*, 17, 781-788.
- KADOGLOU, N. P., DASKALOPOULOU, S. S., PERREA, D. & LIAPIS, C. D. 2005. Matrix Metalloproteinases and Diabetic Vascular Complications. *Angiology*, 56, 173-189.
- KAISER, N., SASSON, S., FEENER, E. P., BOUKOBZA-VARDI, N., HIGASHI, S., MOLLER, D. E., DAVIDHEISER, S., PRZYBYLSKI, R. J. & KING, G. L. 1993. Differential regulation of glucose transport and transporters by glucose in vascular endothelial and smooth muscle cells. *Diabetes*, 42, 80-89.
- KAMIKAWA, A., ISHII, T., SHIMADA, K., MAKONDO, K., INANAMI, O., SAKANE, N., YOSHIDA, T., SAITO, M. & KIMURA, K. 2008. Proinsulin C-peptide abrogates type-1 diabetes-induced increase of renal endothelial nitric oxide synthase in rats. *Diabetes/metabolism research and reviews*, 24, 331-338.
- KARBACH, S., JANSEN, T., HORKE, S., HEEREN, T., SCHOLZ, A., COLDEWEY, M., KARPI, A., HAUSDING, M., KROLLER-SCHON, S., OELZE, M., MUNZEL, T. & DAIBER, A. 2012. Hyperglycemia and oxidative stress in cultured endothelial cells--a comparison of primary endothelial cells with an immortalized endothelial cell line. *J Diabetes Complications*, 26, 155-62.
- KATSAROU, A., GUDBJÖRNSDOTTIR, S., RAWSHANI, A., DABELEA, D., BONIFACIO, E., ANDERSON, B. J., JACOBSEN, L. M., SCHATZ, D. A. & LERNMARK, Å. 2017. Type 1 diabetes mellitus. *Nature reviews Disease primers*, 3, 17016.
- KIM, S.-T., KIM, B.-J., LIM, D.-M., SONG, I.-G., JUNG, J.-H., LEE, K.-W., PARK, K.-Y., CHO, Y.-Z., LEE, D.-H. & KOH, G.-P. 2011. Basal C-peptide level as a surrogate marker of subclinical atherosclerosis in type 2 diabetic patients. *Diabetes & metabolism journal*, 35, 41-49.
- KING, A. & BOWE, J. 2016. Animal models for diabetes: Understanding the pathogenesis and finding new treatments. *Biochem Pharmacol*, 99, 1-10.
- KITADA, M., ZHANG, Z., MIMA, A. & KING, G. L. 2010. Molecular mechanisms of diabetic vascular complications. *Journal of diabetes investigation*, 1, 77-89.
- KITAMURA, T., KIMURA, K., JUNG, B. D., MAKONDO, K., OKAMOTO, S., CAÑAS, X., SAKANE, N., YOSHIDA, T. & SAITO, M. 2001. Proinsulin C-peptide rapidly stimulates mitogen-activated protein kinases in Swiss 3T3 fibroblasts: requirement of protein kinase C, phosphoinositide 3-kinase and pertussis toxin-sensitive G-protein. *Biochemical Journal*, 355, 123-129.
- KITAMURA, T., KIMURA, K., JUNG, B. D., MAKONDO, K., SAKANE, N., YOSHIDA, T. & SAITO, M. 2002. Proinsulin C-peptide activates cAMP response element-binding proteins through the p38 mitogen-activated protein kinase pathway in mouse lung capillary endothelial cells. *Biochemical Journal*, 366, 737-744.

- KITAMURA, T., KIMURA, K., MAKONDO, K., FURUYA, D., SUZUKI, M., YOSHIDA, T. & SAITO, M. 2003. Proinsulin C-peptide increases nitric oxide production by enhancing mitogen-activated protein-kinase-dependent transcription of endothelial nitric oxide synthase in aortic endothelial cells of Wistar rats. *Diabetologia*, 46, 1698-1705.
- KOBAYASHI, Y., NARUSE, K., HAMADA, Y., NAKASHIMA, E., KATO, K., AKIYAMA, N., KAMIYA, H., WATARAI, A., NAKAE, M., OISO, Y. & NAKAMURA, J. 2005. Human proinsulin C-peptide prevents proliferation of rat aortic smooth muscle cells cultured in high-glucose conditions. *Diabetologia*, 48, 2396-401.
- KOGA, H., SUGIYAMA, S., KUGIYAMA, K., WATANABE, K., FUKUSHIMA, H., TANAKA, T., SAKAMOTO, T., YOSHIMURA, M., JINNOUCHI, H. & OGAWA, H. 2005. Elevated levels of VE-cadherin-positive endothelial microparticles in patients with type 2 diabetes mellitus and coronary artery disease. *Journal of the American College of Cardiology*, 45, 1622-1630.
- KOO, J. R. & VAZIRI, N. D. 2003. Effects of diabetes, insulin and antioxidants on NO synthase abundance and NO interaction with reactive oxygen species. *Kidney Int*, 63, 195-201.
- KOWAL, J., ARRAS, G., COLOMBO, M., JOUVE, M., MORATH, J. P., PRIMDAL-BENGTSON, B., DINGLI, F., LOEW, D., TKACH, M. & THÉRY, C. 2016. Proteomic comparison defines novel markers to characterize heterogeneous populations of extracellular vesicle subtypes. *Proceedings of the National Academy of Sciences*, 113, E968-E977.
- KOWALTOWSKI, A. J., CASTILHO, R. F. & VERCESI, A. E. 2001. Mitochondrial permeability transition and oxidative stress. *FEBS Letters*, 495, 12-15.
- KOZIEL, A., SOBIERAJ, I. & JARMUSZKIEWICZ, W. 2015. Increased activity of mitochondrial uncoupling protein 2 improves stress resistance in cultured endothelial cells exposed in vitro to high glucose levels. *Am J Physiol Heart Circ Physiol*, 309, H147-56.
- KULP, A. & KUEHN, M. J. 2010. Biological functions and biogenesis of secreted bacterial outer membrane vesicles. *Annual review of microbiology*, 64, 163-184.
- LACROIX, R., ROBERT, S., PONCELET, P., KASTHURI, R. S., KEY, N. S., DIGNAT-GEORGE, F. & WORKSHOP, I. S. 2010. Standardization of platelet-derived microparticle enumeration by flow cytometry with calibrated beads: results of the International Society on Thrombosis and Haemostasis SSC Collaborative workshop. *J Thromb Haemost*, 8, 2571-4.
- LACROIX, R., SABATIER, F., MIALHE, A., BASIRE, A., PANNELL, R., BORGHI, H., ROBERT, S., LAMY, E., PLAWINSKI, L. & CAMOIN-JAU, L. 2007. Activation of plasminogen into plasmin at the surface of endothelial microparticles: a mechanism that modulates angiogenic properties of endothelial progenitor cells in vitro. *Blood*, 110, 2432-2439.
- LANSDOWN, A., ELLINS, E. & HALCOX, J. 2014. The Vascular Endothelium in Diabetes. In: BETTERIDGE, D. J. & NICHOLLS, S. (eds.) *Managing Cardiovascular Complications in Diabetes*. Hoboken, UNITED KINGDOM: John Wiley & Sons, Incorporated.

- LATHAM, S. L., TIBERTI, N., GOKOOLPARSADH, N., HOLDAWAY, K., COURAUD, P. O., GRAU, G. E. & COMBES, V. 2015. Immuno-analysis of microparticles: probing at the limits of detection. *Scientific reports*, 5, 16314.
- LAURINDO, F. R. M., LIBERMAN, M., FERNANDES, D. C. & LEITE, P. F. 2018. Chapter 8 - Endothelium-Dependent Vasodilation: Nitric Oxide and Other Mediators. *In: DA LUZ, P. L., LIBBY, P., CHAGAS, A. C. P. & LAURINDO, F. R. M. (eds.) Endothelium and Cardiovascular Diseases*. Academic Press.
- LEAHY, J. L. 2005. Pathogenesis of Type 2 Diabetes Mellitus. *Archives of Medical Research*, 36, 197-209.
- LEE, T. H., CHENNAKRISHNAIAH, S., MEEHAN, B., MONTERMINI, L., GARNIER, D., D'ASTI, E., HOU, W., MAGNUS, N., GAYDEN, T. & JABADO, N. 2016. Barriers to horizontal cell transformation by extracellular vesicles containing oncogenic H-ras. *Oncotarget*, 7, 51991.
- LEIGHTON, E., SAINSBURY, C. A. & JONES, G. C. 2017. A practical review of C-peptide testing in diabetes. *Diabetes therapy*, 8, 475-487.
- LENZEN, S. 2008. The mechanisms of alloxan-and streptozotocin-induced diabetes. *Diabetologia*, 51, 216-226.
- LI, J. H., HUANG, X. R., ZHU, H. J., JOHNSON, R. & LAN, H. Y. 2003a. Role of TGF-beta signaling in extracellular matrix production under high glucose conditions. *Kidney Int*, 63, 2010-9.
- LI, Y., ZHONG, Y., GONG, W., GAO, X., QI, H., LIU, K. & QI, J. 2018. C-peptide prevents SMAD3 binding to alpha promoters to inhibit collagen type IV synthesis. *J Mol Endocrinol*, 61, 47-56.
- LI, Z. G., ZHANG, W. & SIMA, A. A. 2003b. C-peptide enhances insulin-mediated cell growth and protection against high glucose-induced apoptosis in SH-SY5Y cells. *Diabetes/metabolism research and reviews*, 19, 375-385.
- LIM, Y.-C., BHATT, M. P., KWON, M.-H., PARK, D., LEE, S., CHOE, J., HWANG, J., KIM, Y.-M. & HA, K.-S. 2013. Prevention of VEGF-mediated microvascular permeability by C-peptide in diabetic mice. *Cardiovascular research*, 101, 155-164.
- LIM, Y.-C., BHATT, M. P., KWON, M.-H., PARK, D., NA, S., KIM, Y.-M. & HA, K.-S. 2015. Proinsulin C-peptide prevents impaired wound healing by activating angiogenesis in diabetes. *Journal of Investigative Dermatology*, 135, 269-278.
- LIND, L., LITHELL, H., HVARFNER, A., POLLARE, T. & LJUNGHALL, S. 1993. On the relationships between mineral metabolism, obesity and fat distribution. *European journal of clinical investigation*, 23, 307-310.
- LINDAHL, E., NYMAN, U., MELLES, E., SIGMUNDSSON, K., STÅHLBERG, M., WAHREN, J., ÖBRINK, B., SHAFQAT, J., JOSEPH, B. & JÖRNVALL, H. 2007. Cellular internalization of proinsulin C-peptide. *Cellular and molecular life sciences*, 64, 479.
- LINDSTRÖM, K., JOHANSSON, C., JOHNSON, E. & HARALDSSON, B. 1996. Acute effects of C-peptide on the microvasculature of isolated perfused skeletal muscles and kidneys in rat. *Acta Physiologica Scandinavica*, 156, 19-25.
- LING, Z. L., COMBES, V., GRAU, G. E. & KING, N. J. C. 2011. Microparticles as immune regulators in infectious disease—an opinion. *Frontiers in immunology*, 2, 67.
- LIU, J., MAK, T. C.-P., BANIGESH, A., DESAI, K., WANG, R. & WU, L. 2012. Aldolase B Knockdown Prevents High Glucose-Induced Methylglyoxal Overproduction and

- Cellular Dysfunction in Endothelial Cells.(Research Article). *PLoS ONE*, 7, e41495.
- LIU, Y., CHEN, C., SUMMERS, S., MEDAWALA, W. & SPENCE, D. M. 2015. C-peptide and zinc delivery to erythrocytes requires the presence of albumin: implications in diabetes explored with a 3D-printed fluidic device. *Integrative Biology*, 7, 534-543.
- LOWRY, O. H., ROSEBROUGH, N. J., FARR, A. L. & RANDALL, R. J. 1951. Protein measurement with the Folin phenol reagent. *The Journal of biological chemistry*, 193, 265.
- LU, L., ZHANG, Q., PU, L. J., PENG, W. H., YAN, X. X., WANG, L. J., CHEN, Q. J., ZHU, Z. B., MICHEL, J. B. & SHEN, W. F. 2008. Dysregulation of matrix metalloproteinases and their tissue inhibitors is related to abnormality of left ventricular geometry and function in streptozotocin-induced diabetic minipigs. *Int J Exp Pathol*, 89, 125-37.
- LU, Z. & XU, S. 2006. ERK1/2 MAP kinases in cell survival and apoptosis. *IUBMB life*, 58, 621-631.
- LUPPI, P., CIFARELLI, V., TSE, H., PIGANELLI, J. & TRUCCO, M. 2008. Human C-peptide antagonises high glucose-induced endothelial dysfunction through the nuclear factor-kappaB pathway. *Diabetologia*, 51, 1534-43.
- LUPPI, P. & DRAIN, P. 2014. Autocrine C-peptide mechanism underlying INS1 beta cell adaptation to oxidative stress. *Diabetes/Metabolism Research and Reviews*, 30, 599-609.
- MACISAAC, R. J., EKINCI, E. I. & JERUMS, G. 2014. Markers of and risk factors for the development and progression of diabetic kidney disease. *American journal of kidney diseases*, 63, S39-S62.
- MAECKER, H. T., FREY, T., NOMURA, L. E. & TROTTER, J. 2004. Selecting fluorochrome conjugates for maximum sensitivity. *Cytometry A*, 62, 169-73.
- MAENG, Y.-S., MIN, J.-K., KIM, J. H., YAMAGISHI, A., MOCHIZUKI, N., KWON, J.-Y., PARK, Y.-W., KIM, Y.-M. & KWON, Y.-G. 2006. ERK is an anti-inflammatory signal that suppresses expression of NF- κ B-dependent inflammatory genes by inhibiting IKK activity in endothelial cells. *Cellular signalling*, 18, 994-1005.
- MAEZAWA, Y., YOKOTE, K., SONEZAKI, K., FUJIMOTO, M., KOBAYASHI, K., KAWAMURA, H., TOKUYAMA, T., TAKEMOTO, M., UEDA, S., KUWAKI, T., MORI, S., WAHREN, J. & SAITO, Y. 2006. Influence of C-peptide on early glomerular changes in diabetic mice. *Diabetes Metab Res Rev*, 22, 313-22.
- MAGENTA, A., GRECO, S., CAPOGROSSI, M. C., GAETANO, C. & MARTELLI, F. 2014. Nitric oxide, oxidative stress, and p66Shc interplay in diabetic endothelial dysfunction. *Biomed Res Int*, 2014, 193095.
- MALLAT, Z. & TEDGUI, A. 2000. Apoptosis in the vasculature: mechanisms and functional importance. *British journal of pharmacology*, 130, 947-962.
- MARTIN, A., KOMADA, M. R. & SANE, D. C. 2003. Abnormal angiogenesis in diabetes mellitus. *Medicinal research reviews*, 23, 117-145.
- MARX, N., SILBERNAGEL, G., BRANDENBURG, V., BURGMAIER, M., KLEBER, M. E., GRAMMER, T. B., WINKELMANN, B. R., BOEHM, B. O. & MÄRZ, W. 2013. C-peptide levels are associated with mortality and cardiovascular mortality in patients undergoing angiography: the LURIC study. *Diabetes care*, 36, 708-714.

- MIAO, X., BAI, Y., SUN, W., CUI, W., XIN, Y., WANG, Y., TAN, Y., MIAO, L., FU, Y., SU, G. & CAI, L. 2012. Sulforaphane prevention of diabetes-induced aortic damage was associated with the up-regulation of Nrf2 and its down-stream antioxidants. *Nutr Metab (Lond)*, 9, 84.
- MONNIER, L., MAS, E., GINET, C., MICHEL, F., VILLON, L., CRISTOL, J. P. & COLETTE, C. 2006. Activation of oxidative stress by acute glucose fluctuations compared with sustained chronic hyperglycemia in patients with type 2 diabetes. *Jama*, 295, 1681-7.
- MOREL, O., JESEL, L., FREYSSINET, J.-M. & TOTI, F. 2011. Cellular mechanisms underlying the formation of circulating microparticles. *Arteriosclerosis, thrombosis, and vascular biology*, 31, 15-26.
- MORRISH, N. J., WANG, S. L., STEVENS, L. K., FULLER, J. H. & KEEN, H. 2001. Mortality and causes of death in the WHO Multinational Study of Vascular Disease in Diabetes. *Diabetologia*, 44 Suppl 2, S14-21.
- MUGHAL, R. S., SCRAGG, J. L., LISTER, P., WARBURTON, P., RICHES, K., O'REGAN, D. J., BALL, S. G., TURNER, N. A. & PORTER, K. E. 2010. Cellular mechanisms by which proinsulin C-peptide prevents insulin-induced neointima formation in human saphenous vein. *Diabetologia*, 53, 1761-71.
- MUNOZ-ESPIN, D. & SERRANO, M. 2014. Cellular senescence: from physiology to pathology. *Nature reviews Molecular cell biology*, 15, 482.
- MURAKAMI, T., HORIGOME, H., TANAKA, K., NAKATA, Y., OHKAWARA, K., KATAYAMA, Y. & MATSUI, A. 2007. Impact of weight reduction on production of platelet-derived microparticles and fibrinolytic parameters in obesity. *Thrombosis research*, 119, 45-53.
- MURALIDHARAN-CHARI, V., CLANCY, J., PLOU, C., ROMAO, M., CHAVRIER, P., RAPOSO, G. & D'SOUZA-SCHOREY, C. 2009. ARF6-regulated shedding of tumor cell-derived plasma membrane microvesicles. *Current Biology*, 19, 1875-1885.
- NATARELLI, L., RANALDI, G., LEONI, G., ROSELLI, M., GUANTARIO, B., COMITATO, R., AMBRA, R., CIMINO, F., SPECIALE, A., VIRGILI, F. & CANALI, R. 2015. Nanomolar Caffeic Acid Decreases Glucose Uptake and the Effects of High Glucose in Endothelial Cells. *PLoS One*, 10, e0142421.
- NOLAN, J. P. & DUGGAN, E. 2018. Analysis of individual extracellular vesicles by flow cytometry. *Flow Cytometry Protocols*. Springer.
- NOLAN, J. P. & STONER, S. A. 2013. A trigger channel threshold artifact in nanoparticle analysis. *Cytometry A*, 83, 301-5.
- NORDQUIST, L., PALM, F. & ANDRESEN, B. T. 2008. Renal and vascular benefits of C-peptide: Molecular mechanisms of C-peptide action. *Biologics: targets & therapy*, 2, 441.
- NOWOTNY, K., JUNG, T., HOHN, A., WEBER, D. & GRUNE, T. 2015. Advanced glycation end products and oxidative stress in type 2 diabetes mellitus. *Biomolecules*, 5, 194-222.
- OBROSOVA, I. G., DREL, V. R., OLTMAN, C. L., MASHTALIR, N., TIBREWALA, J., GROVES, J. T. & YOREK, M. A. 2007. Role of nitrosative stress in early neuropathy and vascular dysfunction in streptozotocin-diabetic rats. *Am J Physiol Endocrinol Metab*, 293, E1645-55.

- OHTOMO, Y., APERIA, A., SAHLGREN, B., JOHANSSON, B.-L. & WAHREN, J. 1996. C-peptide stimulates rat renal tubular Na⁺, K⁺-ATPase activity in synergism with neuropeptide Y. *Diabetologia*, 39, 199-205.
- OLIVEIRA, G. A. & KOWALTOWSKI, A. J. 2004. Phosphate Increases Mitochondrial Reactive Oxygen Species Release. *Free Radical Research*, 2004, Vol.38(10), p.1113-1118, 38, 1113-1118.
- PARK, C. W. 2014. Diabetic kidney disease: from epidemiology to clinical perspectives. *Diabetes & metabolism journal*, 38, 252-260.
- PAROLINI, I., FEDERICI, C., RAGGI, C., LUGINI, L., PALLESCHI, S., DE MILITO, A., COSCIA, C., IESSI, E., LOGOZZI, M. & MOLINARI, A. 2009. Microenvironmental pH is a key factor for exosome traffic in tumor cells. *Journal of Biological Chemistry*, 284, 34211-34222.
- PATLAK, M. 2002. New weapons to combat an ancient disease: treating diabetes. *The FASEB Journal*, 16, 1853e-1853e.
- PAULUS, P., JENNEWEIN, C. & ZACHAROWSKI, K. 2011. Biomarkers of endothelial dysfunction: can they help us deciphering systemic inflammation and sepsis? *Biomarkers*, 16 Suppl 1, S11-21.
- PEARSON, J. 2000. Normal endothelial cell function. *Lupus*, 9, 183-188.
- PFEIFER, P., WERNER, N. & JANSEN, F. 2015. Role and Function of MicroRNAs in Extracellular Vesicles in Cardiovascular Biology. *Biomed Res Int*, 2015, 161393.
- POBER, J. S. & MIN, W. 2006. Endothelial Cell Dysfunction, Injury and Death. In: MONCADA, S. & HIGGS, A. (eds.) *The Vascular Endothelium II*. Berlin, Heidelberg: Springer Berlin Heidelberg.
- POLONSKY, K. S. 2012. The past 200 years in diabetes. *New England Journal of Medicine*, 367, 1332-1340.
- PONCELET, P., ROBERT, S., BAILLY, N., GARNACHE-OTTOU, F., BOURICHE, T., DEVALET, B., SEGATCHIAN, J. H., SAAS, P. & MULLIER, F. 2015. Tips and tricks for flow cytometry-based analysis and counting of microparticles. *Transfus Apher Sci*, 53, 110-26.
- PONCELET, P., ROBERT, S., BOURICHE, T., BEZ, J., LACROIX, R. & DIGNAT-GEORGE, F. 2016. Standardized counting of circulating platelet microparticles using currently available flow cytometers and scatter-based triggering: Forward or side scatter? *Cytometry A*, 89, 148-58.
- POPOV, D. 2010. Endothelial cell dysfunction in hyperglycemia: Phenotypic change, intracellular signaling modification, ultrastructural alteration, and potential clinical outcomes. *International Journal of Diabetes Mellitus*, 2, 189-195.
- PORTIK-DOBOS, V., ANSTADT, M. P., HUTCHINSON, J., BANNAN, M. & ERGUL, A. 2002. Evidence for a matrix metalloproteinase induction/activation system in arterial vasculature and decreased synthesis and activity in diabetes. *Diabetes*, 51, 3063.
- PRIES, A. R. & KUEBLER, W. M. 2006. Normal Endothelium. In: MONCADA, S. & HIGGS, A. (eds.) *The Vascular Endothelium I*. Berlin, Heidelberg: Springer Berlin Heidelberg.
- PUGSLEY, M. & TABRIZCHI, R. 2000. The vascular system: An overview of structure and function. *Journal of pharmacological and toxicological methods*, 44, 333-340.
- PÉREZ-CASAL, M., DOWNEY, C., CUTILLAS-MORENO, B., ZUZEL, M., FUKUDOME, K. & TOH, C. H. 2009. Microparticle-associated endothelial protein C receptor and

- the induction of cytoprotective and anti-inflammatory effects. *haematologica*, haematol. 13547.
- QI, H., CASALENA, G., SHI, S., YU, L., EBEFORS, K., SUN, Y., ZHANG, W., D'AGATI, V., SCHLONDORFF, D. & HARALDSSON, B. 2017. Glomerular endothelial mitochondrial dysfunction is essential and characteristic of diabetic kidney disease susceptibility. *Diabetes*, 66, 763-778.
- RADI, R. 2004. Nitric oxide, oxidants, and protein tyrosine nitration. *Proc Natl Acad Sci U S A*, 101, 4003-8.
- RAFFORT, J., LAREYRE, F., CLEMENT, M., HASSEN-KHODJA, R., CHINETTI, G. & MALLAT, Z. 2018. Diabetes and aortic aneurysm: current state of the art. *Cardiovasc Res*.
- REINILA, A. 1981. Long-term effects of untreated diabetes on the arterial wall in rat. An ultrastructural study. *Diabetologia*, 20, 205-12.
- RIBAU, J. C., SAMIS, J. A., SENIS, Y. A., MAURICE, D. H., GILES, A. R., DERESKE, M., ABSHER, P. M., HATTON, M. W. & RICHARDSON, M. 2000. Aortic endothelial cell von Willebrand factor content, and circulating plasminogen activator inhibitor-1 are increased, but expression of endothelial leukocyte adhesion molecules is unchanged in insulin-dependent diabetic BB rats. *Atherosclerosis*, 149, 331.
- RICHARDS, J. P., BOWLES, E. A., GORDON, W. R., ELLSWORTH, M. L., STEPHENSON, A. H. & SPRAGUE, R. S. 2015. Mechanisms of C-peptide-mediated rescue of low O₂-induced ATP release from erythrocytes of humans with Type 2 diabetes. *American Journal of Physiology-Heart and Circulatory Physiology*.
- RIDLEY, A. J. 2001. Rho family proteins: coordinating cell responses. *Trends in Cell Biology*, 11, 471-477.
- RIGLER, R., PRAMANIK, A., JONASSON, P., KRATZ, G., JANSSON, O., NYGREN, P.-Å., STÅHL, S., EKBERG, K., JOHANSSON, B.-L. & UHLEN, S. 1999. Specific binding of proinsulin C-peptide to human cell membranes. *Proceedings of the National Academy of Sciences*, 96, 13318-13323.
- ROBERT, S., LACROIX, R., PONCELET, P., HARHOURI, K., BOURICHE, T., JUDICONE, C., WISCHHUSEN, J., ARNAUD, L. & DIGNAT-GEORGE, F. 2012. High-sensitivity flow cytometry provides access to standardized measurement of small-size microparticles--brief report. *Arterioscler Thromb Vasc Biol*, 32, 1054-8.
- RUMBLE, J. R., COOPER, M. E., SOULIS, T., COX, A., WU, L., YOUSSEF, S., JASIK, M., JERUMS, G. & GILBERT, R. E. 1997. Vascular hypertrophy in experimental diabetes. Role of advanced glycation end products. *The Journal of clinical investigation*, 99, 1016-1027.
- SAAD, M. J. A. 2018. Chapter 44 - Obesity, Diabetes, and Endothelium: Molecular Interactions. In: DA LUZ, P. L., LIBBY, P., CHAGAS, A. C. P. & LAURINDO, F. R. M. (eds.) *Endothelium and Cardiovascular Diseases*. Academic Press.
- SABATIER, F., CAMOIN-JAU, L., ANFOSSO, F., SAMPOL, J. & DIGNAT-GEORGE, F. 2009. Circulating endothelial cells, microparticles and progenitors: key players towards the definition of vascular competence. *Journal of cellular and molecular medicine*, 13, 454-471.
- SABATIER, F., DARMON, P., HUGEL, B., COMBES, V., SANMARCO, M., VELUT, J.-G., ARNOUX, D., CHARPIOT, P., FREYSSINET, J.-M., OLIVER, C., SAMPOL, J. & DIGNAT-GEORGE, F. 2002. Type 1 and type 2 diabetic patients display different patterns of cellular microparticles. *Diabetes*, 51, 2840.

- SAENZ-CUESTA, M., ARBELAIZ, A., OREGI, A., IRIZAR, H., OSORIO-QUEREJETA, I., MUNOZ-CULLA, M., BANALES, J. M., FALCON-PEREZ, J. M., OLASCOAGA, J. & OTAEGUI, D. 2015. Methods for extracellular vesicles isolation in a hospital setting. *Front Immunol*, 6, 50.
- SAGE, A. P., LU, J., TINTUT, Y. & DEMER, L. L. 2011. Hyperphosphatemia-induced nanocrystals upregulate the expression of bone morphogenetic protein-2 and osteopontin genes in mouse smooth muscle cells in vitro. *Kidney international*, 79, 414-422.
- SALUM, E., BUTLIN, M., KALS, J., ZILMER, M., EHA, J., AVOLIO, A. P., AREND, A., AUNAPUU, M. & KAMPUS, P. 2014. Angiotensin II receptor blocker telmisartan attenuates aortic stiffening and remodelling in STZ-diabetic rats. *Diabetol Metab Syndr*, 6, 57.
- SAPET, C., SIMONCINI, S., LORIOD, B., PUTHIER, D., SAMPOL, J., NGUYEN, C., DIGNAT-GEORGE, F. & ANFOSSO, F. 2006. Thrombin-induced endothelial microparticle generation: identification of a novel pathway involving ROCK-II activation by caspase-2. *Blood*, 108, 1868-1876.
- SARI, R. & BALCI, M. K. 2005. Relationship between C peptide and chronic complications in type-2 diabetes mellitus. *Journal of the National Medical Association*, 97, 1113.
- SCALIA, R., COYLE, K. M., LEVINE, B. J., BOOTH, G. & LEFER, A. M. 2000. C-peptide inhibits leukocyte-endothelium interaction in the microcirculation during acute endothelial dysfunction. *Faseb j*, 14, 2357-64.
- SCHLEGEL, R. & WILLIAMSON, P. 2001. Phosphatidylserine, a death knell. *Cell death and differentiation*, 8, 551.
- SCHRIJVERS, B. F., DE VRIESE, A. S. & FLYVBJERG, A. 2004. From hyperglycemia to diabetic kidney disease: the role of metabolic, hemodynamic, intracellular factors and growth factors/cytokines. *Endocrine reviews*, 25, 971-1010.
- SEARLS, Y., SMIRNOVA, I. V., VANHOOSE, L., FEGLEY, B., LOGANATHAN, R. & STEHNO-BITTEL, L. 2012. Time-dependent alterations in rat macrovessels with type 1 diabetes. *Exp Diabetes Res*, 2012, 278620.
- SEBBAGH, M., RENVOIZÉ, C., HAMELIN, J., RICHÉ, N., BERTOGLIO, J. & BRÉARD, J. 2001. Caspase-3-mediated cleavage of ROCK I induces MLC phosphorylation and apoptotic membrane blebbing. *Nature cell biology*, 3, 346.
- SERGE, A., DE KEIJZER, S., VAN HEMERT, F., HICKMAN, M. R., HERELD, D., SPAINK, H. P., SCHMIDT, T. & SNAAR-JAGALSKA, B. E. 2011. Quantification of GPCR internalization by single-molecule microscopy in living cells. *Integrative Biology*, 3, 675-683.
- SHAFQAT, J., JUNTTI-BERGGREN, L., ZHONG, Z., EKBERG, K., KÖHLER, M., BERGGREN, P.-O., JOHANSSON, J., WAHREN, J. & JÖRNVALL, H. 2002. Proinsulin C-peptide and its analogues induce intracellular Ca²⁺ increases in human renal tubular cells. *Cellular and Molecular Life Sciences CMLS*, 59, 1185-1189.
- SHANNON, P., MARKIEL, A., OZIER, O., BALIGA, N. S., WANG, J. T., RAMAGE, D., AMIN, N., SCHWIKOWSKI, B. & IDEKER, T. 2003. Cytoscape: a software environment for integrated models of biomolecular interaction networks. *Genome research*, 13, 2498-2504.

- SHAO, H., IM, H., CASTRO, C. M., BREAKEFIELD, X., WEISSLEDER, R. & LEE, H. 2018. New technologies for analysis of extracellular vesicles. *Chemical reviews*, 118, 1917-1950.
- SHAPIRO, H. M. 2005. *Practical flow cytometry*, John Wiley & Sons.
- SHEIBANI, N. & FRAZIER, W. 1999. Invited Reviews-Thrombospondin-1, PECAM-1, and regulation of angiogenesis. *Histology and histopathology*, 14, 285-294.
- SHEIBANI, N., SORENSON, C. M., CORNELIUS, L. A. & FRAZIER, W. A. 2000. Thrombospondin-1, a natural inhibitor of angiogenesis, is present in vitreous and aqueous humor and is modulated by hyperglycemia. *Biochemical and biophysical research communications*, 267, 257-261.
- SHI, Y. & VANHOUTTE, P. M. 2017. Macro- and microvascular endothelial dysfunction in diabetes. *J Diabetes*, 9, 434-449.
- SHIN, E. S., SORENSON, C. M. & SHEIBANI, N. 2014. Diabetes and retinal vascular dysfunction. *Journal of ophthalmic & vision research*, 9, 362.
- SHUTO, E., TAKETANI, Y., TANAKA, R., HARADA, N., ISSHIKI, M., SATO, M., NASHIKI, K., AMO, K., YAMAMOTO, H. & HIGASHI, Y. 2009. Dietary phosphorus acutely impairs endothelial function. *Journal of the American Society of Nephrology*, 20, 1504-1512.
- SIMA, A. A., ZHANG, W., KREIPKE, C. W., RAFOLS, J. A. & HOFFMAN, W. H. 2009. Inflammation in Diabetic Encephalopathy is Prevented by C-Peptide. *Rev Diabet Stud*, 6, 37-42.
- SONG, R. H., SINGH, A. K. & LEEHEY, D. J. 1999. Decreased glomerular proteinase activity in the streptozotocin diabetic rat. *Am J Nephrol*, 19, 441-6.
- STALL, A. M. 2010. *Using BD FACSDiva™ CST to Evaluate Cytometer Performance, Create Custom Assay Setting and Implement* [Online]. Available: http://static.bdbiosciences.com/documents/webinar_2010_09_facsddiva.pdf [Accessed 5 June 2018].
- STEHOUWER, C. D., LAMBERT, J., DONKER, A. J. & VAN HINSBERGH, V. W. 1997. Endothelial dysfunction and pathogenesis of diabetic angiopathy. *Cardiovascular research*, 34, 55.
- STEINER, D. F., CUNNINGHAM, D., SPIGELMAN, L. & ATEN, B. 1967. Insulin biosynthesis: evidence for a precursor. *Science*, 157, 697-700.
- STEPANIAN, A., BOURGUIGNAT, L., HENNOU, S., COUPAYE, M., HAJAGE, D., SALOMON, L., ALESSI, M. C., MSIKA, S. & DE PROST, D. 2013. Microparticle increase in severe obesity: not related to metabolic syndrome and unchanged after massive weight loss. *Obesity*, 21, 2236-2243.
- SZOTOWSKI, B., ANTONIAK, S., GOLDIN-LANG, P., TRAN, Q.-V., PELS, K., ROSENTHAL, P., BOGDANOV, V. Y., BORCHERT, H.-H., SCHULTHEISS, H.-P. & RAUCH, U. 2007. Antioxidative treatment inhibits the release of thrombogenic tissue factor from irradiation- and cytokine-induced endothelial cells. *Cardiovascular Research*, 73, 806-812.
- TAGUCHI, K., KOBAYASHI, T., HAYASHI, Y., MATSUMOTO, T. & KAMATA, K. 2007. Enalapril improves impairment of SERCA-derived relaxation and enhancement of tyrosine nitration in diabetic rat aorta. *Eur J Pharmacol*, 556, 121-8.
- TAHERGORABI, Z. & KHAZAEI, M. 2012. Imbalance of angiogenesis in diabetic complications: the mechanisms. *International journal of preventive medicine*, 3, 827-838.

- TANG, V. A., RENNER, T. M., FRITZSCHE, A. K., BURGER, D. & LANGLOIS, M. A. 2017. Single-Particle Discrimination of Retroviruses from Extracellular Vesicles by Nanoscale Flow Cytometry. *Sci Rep*, 7, 17769.
- TARALLO, S., BELTRAMO, E., BERRONE, E., DENTELLI, P. & PORTA, M. 2010. Effects of high glucose and thiamine on the balance between matrix metalloproteinases and their tissue inhibitors in vascular cells. *Acta Diabetol*, 47, 105-11.
- THOMSON, L. 2015. 3-nitrotyrosine modified proteins in atherosclerosis. *Dis Markers*, 2015, 708282.
- THÉRY, C., WITWER, K. W., AIKAWA, E., ALCARAZ, M. J., ANDERSON, J. D., ANDRIANTSITOHAINA, R., ANTONIOU, A., ARAB, T., ARCHER, F., ATKIN-SMITH, G. K., AYRE, D. C., BACH, J.-M., BACHURSKI, D., BAHARVAND, H., BALAJ, L., BALDACCHINO, S., BAUER, N. N., BAXTER, A. A., BEBAWY, M., BECKHAM, C., BEDINA ZAVEC, A., BENMOUSSA, A., BERARDI, A. C., BERGESE, P., BIELSKA, E., BLENKIRON, C., BOBIS-WOZOWICZ, S., BOILARD, E., BOIREAU, W., BONGIOVANNI, A., BORRÀS, F. E., BOSCH, S., BOULANGER, C. M., BREAKFIELD, X., BREGGIO, A. M., BRENNAN, M. Á., BRIGSTOCK, D. R., BRISSON, A., BROEKMAN, M. L. D., BROMBERG, J. F., BRYL-GÓRECKA, P., BUCH, S., BUCK, A. H., BURGER, D., BUSATTO, S., BUSCHMANN, D., BUSSOLATI, B., BUZÁS, E. I., BYRD, J. B., CAMUSSI, G., CARTER, D. R. F., CARUSO, S., CHAMLEY, L. W., CHANG, Y.-T., CHEN, C., CHEN, S., CHENG, L., CHIN, A. R., CLAYTON, A., CLERICI, S. P., COCKS, A., COCUCCI, E., COFFEY, R. J., CORDEIRO-DA-SILVA, A., COUCH, Y., COUMANS, F. A. W., COYLE, B., CRESCITELLI, R., CRIADO, M. F., D'SOUZA-SCHOREY, C., DAS, S., DATTA CHAUDHURI, A., DE CANDIA, P., DE SANTANA, E. F., DE WEVER, O., DEL PORTILLO, H. A., DEMARET, T., DEVILLE, S., DEVITT, A., DHONDT, B., DI VIZIO, D., DIETERICH, L. C., DOLO, V., DOMINGUEZ RUBIO, A. P., DOMINICI, M., DOURADO, M. R., DRIEDONKS, T. A. P., DUARTE, F. V., DUNCAN, H. M., EICHENBERGER, R. M., EKSTRÖM, K., EL ANDALOUSSI, S., ELIE-CAILLE, C., ERDBRÜGGER, U., FALCÓN-PÉREZ, J. M., FATIMA, F., FISH, J. E., FLORES-BELLVER, M., FÖRSÖNITS, A., FRELET-BARRAND, A., et al. 2018. Minimal information for studies of extracellular vesicles 2018 (MISEV2018): a position statement of the International Society for Extracellular Vesicles and update of the MISEV2014 guidelines. *Journal of Extracellular Vesicles*, 7, 1535750.
- TIAN, T., WANG, Y., WANG, H., ZHU, Z. & XIAO, Z. 2010. Visualizing of the cellular uptake and intracellular trafficking of exosomes by live-cell microscopy. *Journal of cellular biochemistry*, 111, 488-496.
- TONELLI, M., SACKS, F., PFEFFER, M., GAO, Z. & CURHAN, G. 2005. Relation between serum phosphate level and cardiovascular event rate in people with coronary disease. *Circulation*, 112, 2627-2633.
- TOOKE, J. E., GOH, K. L. & SHORE, A. C. 2002. The vasculature in diabetes. In: HUNT, B., POSTON, L., SCHACHTER, M. & HALLIDAY, A. (eds.) *An Introduction to Vascular Biology : From Basic Science to Clinical Practice*. Cambridge University Press.
- TORTORA, G. J. & DERRICKSON, B. 2014. *Principles of anatomy and physiology*, New York, Wiley-Blackwell.
- TRAMONTANO, A. F., O'LEARY, J., BLACK, A. D., MUNIYAPPA, R., CUTAIA, M. V. & EL-SHERIF, N. 2004. Statin decreases endothelial microparticle release from human coronary artery endothelial cells: implication for the Rho-kinase pathway. *Biochemical and biophysical research communications*, 320, 34-38.

- TSILIBARY, E. C. 2003. Microvascular basement membranes in diabetes mellitus. *J Pathol*, 200, 537-46.
- UKPDS_GROUP 1998. Effect of intensive blood-glucose control with metformin on complications in overweight patients with type 2 diabetes (UKPDS 34). *The Lancet*, 352, 854-865.
- UNGER, R. E., KRUMP-KONVALINKOVA, V., PETERS, K. & KIRKPATRICK, C. J. 2002. In Vitro Expression of the Endothelial Phenotype: Comparative Study of Primary Isolated Cells and Cell Lines, Including the Novel Cell Line HPMEC-ST1.6R. *Microvascular Research*, 64, 384-397.
- VAGUE, P., COSTE, T. C., JANNOT, M., RACCAH, D. & TSIMARATOS, M. 2004. C-peptide, Na⁺,K⁺-ATPase, and diabetes. *Experimental Diabetes Research*, 5, 37-50.
- VALKONEN, S., VAN DER POL, E., BÖING, A., YUANA, Y., YLIPERTTULA, M., NIEUWLAND, R., LAITINEN, S. & SILJANDER, P. 2017. Biological reference materials for extracellular vesicle studies. *European Journal of Pharmaceutical Sciences*, 98, 4-16.
- VAN DER POL, E., COUMANS, F. A., GROOTEMAAT, A. E., GARDINER, C., SARGENT, I. L., HARRISON, P., STURK, A., VAN LEEUWEN, T. G. & NIEUWLAND, R. 2014. Particle size distribution of exosomes and microvesicles determined by transmission electron microscopy, flow cytometry, nanoparticle tracking analysis, and resistive pulse sensing. *J Thromb Haemost*, 12, 1182-92.
- VAN DER POL, E., STURK, A., VAN LEEUWEN, T., NIEUWLAND, R., COUMANS, F. & GROUP, I.-S.-V. W. 2018. Standardization of extracellular vesicle measurements by flow cytometry through vesicle diameter approximation. *J Thromb Haemost*.
- VAN DER POL, E., VAN GEMERT, M. J., STURK, A., NIEUWLAND, R. & VAN LEEUWEN, T. G. 2012. Single vs. swarm detection of microparticles and exosomes by flow cytometry. *J Thromb Haemost*, 10, 919-30.
- VANWIJK, M. J., VANBAVEL, E., STURK, A. & NIEUWLAND, R. 2003. Microparticles in cardiovascular diseases. *Cardiovascular research*, 59, 277-287.
- VASIC, D., MARX, N., SUKHOVA, G., BACH, H., DURST, R., GRUB, M., HAUSAUER, A., HOMBACH, V., ROTTBAUER, W. & WALCHER, D. 2012. C-peptide promotes lesion development in a mouse model of arteriosclerosis. *J Cell Mol Med*, 16, 927-35.
- VASIC, D. & WALCHER, D. 2012. Proinflammatory effects of C-Peptide in different tissues. *Int J Inflam*, 2012, 932725.
- VERMA, S. & ANDERSON, T. J. 2002. Fundamentals of endothelial function for the clinical cardiologist. *Circulation*, 105, 546-549.
- VISH, M. G., MANGESHKAR, P., PIRAINO, G., DENENBERG, A., HAKE, P. W., O'CONNOR, M. & ZINGARELLI, B. 2007. Proinsulin c-peptide exerts beneficial effects in endotoxic shock in mice. *Crit Care Med*, 35, 1348-55.
- VISTICA, D. T., SKEHAN, P., SCUDIERO, D., MONKS, A., PITTMAN, A. & BOYD, M. R. 1991. Tetrazolium-based assays for cellular viability: a critical examination of selected parameters affecting formazan production. *Cancer research*, 51, 2515-2520.
- VON MERING, J. & MINKOWSKI, O. 1889. Diabetes mellitus after pancreas extirpation. *Arch Exp Pathol Pharmacol*, 26, 111.

- VOZIYAN, P., BROWN, K. L., CHETYRKIN, S. & HUDSON, B. 2014. Site-specific AGE modifications in the extracellular matrix: a role for glyoxal in protein damage in diabetes. *Clin Chem Lab Med*, 52, 39-45.
- WAHREN, J. 2017. C-peptide and the pathophysiology of microvascular complications of diabetes. *Journal of internal medicine*, 281, 3-6.
- WAHREN, J., EKBERG, K. & JÖRNVALL, H. 2007. C-peptide is a bioactive peptide. *Diabetologia*, 50, 503.
- WAHREN, J., FOYT, H., DANIELS, M. & AREZZO, J. C. 2016. Long-acting C-peptide and neuropathy in type 1 diabetes: a 12-month clinical trial. *Diabetes care*, dc152068.
- WAHREN, J. & LARSSON, C. 2015. C-peptide: New findings and therapeutic possibilities. *Diabetes Research and Clinical Practice*, 107, 309-319.
- WAHREN, J., SHAFQAT, J., JOHANSSON, J., CHIBALIN, A., EKBERG, K. & JORNVALL, H. 2004. Molecular and cellular effects of C-peptide--new perspectives on an old peptide. *Exp Diabesity Res*, 5, 15-23.
- WALCHER, D., BABIAK, C., POLETEK, P., ROSENKRANZ, S., BACH, H., BETZ, S., DURST, R., GRUB, M., HOMBACH, V., STRONG, J. & MARX, N. 2006. C-Peptide induces vascular smooth muscle cell proliferation: involvement of SRC-kinase, phosphatidylinositol 3-kinase, and extracellular signal-regulated kinase 1/2. *Circ Res*, 99, 1181-7.
- WALCHER, D. & MARX, N. 2009. C-Peptide in the vessel wall. *Rev Diabet Stud*, 6, 180-6.
- WALLERATH, T., KUNT, T., FORST, T., CLOSS, E. I., LEHMANN, R., FLOHR, T., GABRIEL, M., SCHÄFER, D., GÖPFERT, A. & PFÜTZNER, A. 2003. Stimulation of endothelial nitric oxide synthase by proinsulin C-peptide. *Nitric Oxide*, 9, 95-102.
- WANG, C. H., CHANG, R. W., KO, Y. H., TSAI, P. R., WANG, S. S., CHEN, Y. S., KO, W. J., CHANG, C. Y., YOUNG, T. H. & CHANG, K. C. 2014. Prevention of arterial stiffening by using low-dose atorvastatin in diabetes is associated with decreased malondialdehyde. *PLoS One*, 9, e90471.
- WANG, J., LI, Y., XU, M., LI, D., WANG, Y., QI, J. & HE, K. 2016. C-peptide exhibits a late induction effect on matrix metalloproteinase-9 in high glucose-stimulated rat mesangial cells. *Exp Ther Med*, 12, 4142-4146.
- WARRELL, D. A., COX, T. M. & FIRTH, J. D. 2010. *Oxford textbook of medicine*, Oxford, Oxford University Press.
- WEI, M., ONG, L., SMITH, M. T., ROSS, F. B., SCHMID, K., HOEY, A. J., BURSTOW, D. & BROWN, L. 2003. The streptozotocin-diabetic rat as a model of the chronic complications of human diabetes. *Heart Lung & Circulation*, 12, 44-50.
- WELSH, J. A., HOLLOWAY, J. A., WILKINSON, J. S. & ENGLYST, N. A. 2017. Extracellular Vesicle Flow Cytometry Analysis and Standardization. *Front Cell Dev Biol*, 5, 78.
- WHITE, K. E., BILOUS, R. W. & GROUP, C. S. 2000. Type 2 diabetic patients with nephropathy show structural—functional relationships that are similar to type 1 disease. *Journal of the American Society of Nephrology*, 11, 1667-1673.
- WINN, R. & HARLAN, J. 2005. The role of endothelial cell apoptosis in inflammatory and immune diseases. *Journal of Thrombosis and Haemostasis*, 3, 1815-1824.
- WIROSTKO, B., WONG, T. Y. & SIMÓ, R. 2008. Vascular endothelial growth factor and diabetic complications. *Progress in retinal and eye research*, 27, 608-621.
- WOLF, P. 1967. The nature and significance of platelet products in human plasma. *British journal of haematology*, 13, 269-288.

- WU, J. & YAN, L.-J. 2015. Streptozotocin-induced type 1 diabetes in rodents as a model for studying mitochondrial mechanisms of diabetic β cell glucotoxicity. *Diabetes, metabolic syndrome and obesity: targets and therapy*, 8, 181.
- WU, K. K. & HUAN, Y. 2007. Diabetic atherosclerosis mouse models. *Atherosclerosis*, 191, 241-249.
- XIANG, Y., CHENG, J., WANG, D., HU, X., XIE, Y., STITHAM, J., ATTEYA, G., DU, J., TANG, W. H., LEE, S. H., LESLIE, K., SPOLLETT, G., LIU, Z., HERZOG, E., HERZOG, R. I., LU, J., MARTIN, K. A. & HWA, J. 2015. Hyperglycemia repression of miR-24 coordinately upregulates endothelial cell expression and secretion of von Willebrand factor. *Blood*, 125, 3377-87.
- XU, R., GREENING, D. W., ZHU, H.-J., TAKAHASHI, N. & SIMPSON, R. J. 2016. Extracellular vesicle isolation and characterization: toward clinical application. *The Journal of clinical investigation*, 126, 1152-1162.
- XU, S., JIANG, Y., WANG, H., WANG, Z., LIU, H., PENG, L., FANG, Q., DENG, T., YOU, J., ZHOU, X., ZHANG, W. & LOU, J. 2015. C-peptide ameliorates renal injury in type 2 diabetic rats through protein kinase A-mediated inhibition of fibronectin synthesis. *Biochem Biophys Res Commun*, 458, 674-80.
- XU, Y. X., HUANG, C., LIU, M., CHEN, N., CHEN, W., YANG, C., ZHAO, Y., LI, X., DUAN, J., LIU, S. & YANG, S. 2018. Survivin regulated by autophagy mediates hyperglycemia-induced vascular endothelial cell dysfunction. *Exp Cell Res*, 364, 152-159.
- YAMAGISHI, S., MAEDA, S., MATSUI, T., UEDA, S., FUKAMI, K. & OKUDA, S. 2012. Role of advanced glycation end products (AGEs) and oxidative stress in vascular complications in diabetes. *Biochim Biophys Acta*, 1820, 663-71.
- YAMAGISHI, S., NAKAMURA, K. & MATSUI, T. 2009. Regulation of advanced glycation end product (AGE)-receptor (RAGE) system by PPAR-gamma agonists and its implication in cardiovascular disease. *Pharmacol Res*, 60, 174-8.
- YOSTEN, G. L., KOLAR, G. R., REDLINGER, L. J. & SAMSON, W. K. 2013. Evidence for an interaction between proinsulin C-peptide and GPR146. *Journal of Endocrinology*, JOE-13-0203.
- YOUNG, L. H., IKEDA, Y., SCALIA, R. & LEFER, A. M. 2000. C-peptide exerts cardioprotective effects in myocardial ischemia-reperfusion. *Am J Physiol Heart Circ Physiol*, 279, H1453-9.
- YU, M., XIE, R., ZHANG, Y., LIANG, H., HOU, L., YU, C., ZHANG, J., DONG, Z., TIAN, Y., BI, Y., KOU, J., NOVAKOVIC, V. A. & SHI, J. 2018. Phosphatidylserine on microparticles and associated cells contributes to the hypercoagulable state in diabetic kidney disease. *Nephrol Dial Transplant*.
- ZHANG, R., WANG, X., HONG, M., LUO, T., ZHAO, M., SHEN, H., FANG, J., LI, X., ZANG, S., CHEN, P., NIE, D., ZHENG, P., WU, Q. & XIA, L. 2017. Endothelial microparticles delivering microRNA-155 into T lymphocytes are involved in the initiation of acute graft-versus-host disease following allogeneic hematopoietic stem cell transplantation. *Oncotarget*, 8, 23360-23375.
- ZHOU, R., KANG, X., TANG, B., MOHAN, C., WU, T., PENG, A. & LIU, J.-Y. 2016. Ornithine is a key mediator in hyperphosphatemia-mediated human umbilical vein endothelial cell apoptosis: Insights gained from metabolomics. *Life sciences*, 146, 73-80.

- ZU, L., NIU, C., LI, J., SHAN, L., LI, L., ZHANG, D., WILLARD, B. & ZHENG, L. 2015. Proteomic research of high-glucose-activated endothelial microparticles and related proteins to Alzheimer's disease. *Diab Vasc Dis Res*, 12, 467-70.
- ZUCKER, R. M., ORTENZIO, J. N. & BOYES, W. K. 2016. Characterization, detection, and counting of metal nanoparticles using flow cytometry. *Cytometry A*, 89, 169-83.